Development and Application of a Novel Crystal Growth Inhibition (CGI) Method for Evaluation of Kinetic Hydrate Inhibitors

by

Houra Mozaffar

Submitted for the degree of Doctor of Philosophy in

Petroleum Engineering

Heriot-Watt University

Institute of Petroleum Engineering

October 2013

Abstract

Gas hydrates can cause serious economic/safety concerns in oil and gas production operations. Recently, low dosage polymeric Kinetic Hydrate Inhibitors (KHIs) have seen increasing industry use as alternatives to traditional thermodynamic inhibitors (e.g. methanol, glycol). To date, KHIs have been primarily understood to work by delaying/interfering with the hydrate nucleation process, inhibiting the onset of hydrate growth for a significant 'induction time' (t_i) period. If the induction time exceeds fluid residence time in the hydrate region, then hydrate formation/plugging is avoided. However, due to nucleation being probabilistic, induction time data measured in standard laboratory KHI evaluation studies are often highly stochastic, making KHI assessment problematic and time-consuming

To address this problem, the primary aim of this project was to develop a crystal growth inhibition (CGI) based approach to KHI evaluation. In this technique gas hydrate growth and dissociation patterns in the presence of KHI polymers were carefully inspected to evaluate repeatability of features and the existence of any consistency between runs and transferability between set ups within KHI systems. Extensive studies using this method show that KHIs - rather than being solely 'nucleation delayers' - induce a number of highly repeatable, well-defined hydrate crystal growth inhibition regions as a function of subcooling, ranging from complete inhibition, through reduced growth rates to ultimate failure with increasing subcooling. These crystal growth inhibition properties, in addition to offering further protection against hydrate formation/plugging (e.g. if hydrate nucleation does occur), provide a means to evaluate formulations much more rapidly and reliably. These measured CGI regions have shown good correlation with traditional induction time data, meaning CGI methods can be used to both rapidly approximate t_i patterns and support/confirm t_i test results, speeding up the KHI evaluation process while giving greatly increased operator confidence in inhibitor performance.

Furthermore in this project, the new approach has been applied for evaluating the performance of different types of kinetic hydrate inhibitors as well as assessing the influence of various other components (e.g. liquid hydrocarbons, salts and thermodynamic inhibitors) on KHI performance. Moreover, studies have been conducted on KHI evaluation in different hydrate structure systems (i.e., Structure I,

structure II and structure H) systems in the presence of several different single, binary and multi-component gases.

For this purpose in all experiments undertaken throughout this thesis, with the application of the newly developed CGI technique, crystal growth inhibition regions have been measured for different systems and from the extent of these regions, hydrate inhibition properties of each KHI system has been evaluated and analysed.

Results of these studies proved that the pendant group of a polymer plays a major role on the KHI inhibition properties. Also investigations of different guest gas/hydrate structure systems using the new CGI technique indicated that guest/cage occupancy plays an important role in hydrate inhibition and different hydrate structure systems (e.g. s-I, s-II and s-H) are inhibited differently by the same KHI. For instance, PVCap performance was considerably superior in s-II and s-H forming systems compared to s-I forming systems (e.g. methane), supporting stronger polymer adsorption on s-II or s-H hydrate crystal surfaces.

Also through the newly developed CGI studies, it was found that while the presence of NaCl enhances PVCap methane hydrate inhibition, a carbonate salt like K_2CO_3 can have a generally negative effect on PVCap performance.

In addition to that, test on liquid hydrocarbons proved that the presence of these compounds can slightly deteriorate PVCap performance.

Moreover, results indicated that the combination of thermodynamic inhibitors and PVCap show better performance than thermodynamic inhibitors alone although glycols generally acted as ‘top-up’ thermodynamic inhibitor with PVCap which was a much better compared to the performance of alcohols with PVCap.

This thesis is dedicated to my dear parents.

For their endless love, support and encouragement, not only in this work but all the way throughout my life.

Acknowledgements

In the Name of God, the Compassionate, the Merciful

This thesis is submitted in partial fulfilment of the requirements for the Ph.D. degree at Heriot-Watt University. This work has been conducted at the Institute of Petroleum Engineering under the supervision of Professor Bahman Tohidi and Mr Ross Anderson.

The project has been financed by grants by a Joint Industrial Project (JIP) conducted at the Institute of Petroleum Engineering, Heriot-Watt University. The JIP is supported by Baker Hughes, Champion Technologies, Clariant Oil Services UK Ltd, DONG Energy, Petronas, OMV, Shell/NAM, Statoil and TOTAL, which is gratefully acknowledged.

I would like to thank my first supervisor, Professor Bahman Tohidi for offering me the opportunity to work in this challenging environment at the Centre for Gas Hydrate Research. I would also like to appreciate his genuine support throughout this project. Thanks to you, these years will be years to remember and I will look back at my thesis with pride.

Thanks are also due to my second supervisor, Mr Ross Anderson, for his help and devotion during these years. In encouraging as well as constructively guiding my work, you have contributed to the development of this thesis as well as to my personal development as a researcher. Your intense enthusiasm during the time we worked together provided me with inspiration I wouldn't have gained elsewhere.

Also, and in relation to the reviewing my thesis as well as supporting me over the years, I would like to thank Mr Rod Burgess. Your constant help is much appreciated. Additionally, I am grateful for the help and valuable discussions of Dr Antonin Chapoy and Dr Jinhai Yang during my period of study. . Moreover, I wish to express my thanks to the Institute of Petroleum Engineering, Heriot-Watt University.

Moreover, I greatly appreciate the examiners and reviewers of this thesis, Dr Robin Westacott and Dr Ulfert Klomp for their precious time and valuable suggestions.

I would also like to acknowledge the colleagues as well as friends in the Centre for Gas Hydrate Research for making my stay in Edinburgh very pleasant. Also thanks to my family in Edinburgh, my two sisters and brother in laws, for being there for me all the time, while I was away from home.

Last, but not least, I would like to express my gratefulness to my parents and my amazing brother. Thanks to my mother, who constantly encouraged me to stay concentrated on my studies, no matter the predicaments she may have experienced while her daughter was miles away. I deeply admire her great strength in adversity. And thanks to my dearest father, who inspired me to learn and achieve high goals throughout my life. Without his support and encouragement, this wouldn't have been possible.

Houra Mozaffar

ACADEMIC REGISTRY

Research Thesis Submission

Name*:*	Houra Mozaffar		
School/PGI:	Institute of Petroleum Engineering		
Version: *(i.e. First, Resubmission, Final)*	Final	Degree Sought (Award **and** Subject area)	PhD Petroleum Engineering

Declaration

In accordance with the appropriate regulations I hereby submit my thesis and I declare that:

1) the thesis embodies the results of my own work and has been composed by myself
2) where appropriate, I have made acknowledgement of the work of others and have made reference to work carried out in collaboration with other persons
3) the thesis is the correct version of the thesis for submission and is the same version as any electronic versions submitted*.
4) my thesis for the award referred to, deposited in the Heriot-Watt University Library, should be made available for loan or photocopying and be available via the Institutional Repository, subject to such conditions as the Librarian may require
5) I understand that as a student of the University I am required to abide by the Regulations of the University and to conform to its discipline.

* *Please note that it is the responsibility of the candidate to ensure that the correct version of the thesis is submitted.*

Signature of Candidate*:*		Date:	

Submission

Submitted By *(name in capitals):*	HOURA MOZAFFAR
Signature of Individual Submitting:	
Date Submitted:	

For Completion in the Student Service Centre (SSC)

Received in the SSC by *(name in capitals):*			
1.1 Method of Submission *(Handed in to SSC; posted through internal/external mail):*			
1.2 **E-thesis Submitted (**mandatory for final theses)			
Signature:		Date:	

Table of Contents

Table of Figures

Table of Tables

List of important symbols

ΔP_h	Pressure change due to hydrate formation
ΔT_{s-I}	Subcooling from structure-I hydrate phase boundary
ΔT_{s-II}	Subcooling from structure-II hydrate phase boundary
ΔT_{sub}	Subcooling from hydrate phase boundary
AA	Anti-Agglomerant
AMW	Average Molecular Weight
1,4-BDO	1,4-butanediol
n-BOH	Normal Butanol
C1	Methane
C2	Ethane
C3	Propane
iC4	Iso butane
nC4	Normal butane
iC5	Iso pentane
nC5	Normal pentane
cC5	Cyclopentane
mC6	Methylcyclohexane
CGI	Crystal Growth Inhibition
CIR	Complete Crystal Growth Inhibition Region
CO_2	Carbon dioxide
DSC	Differential Scanning Calorimeter

EG	Ethylene glycol
EtOH	Ethanol
EO	Ethylene Oxide
His	History (hydrate history)
HSZ	Hydrate Stability Zone
K_2CO_3	Potassium Carbonate
KHI	Kinetic Hydrate Inhibitor
HMW	High Molecular Weight
LCST	Lower Critical Solution Temperature
LDHI	Low Dosage Hydrate Inhibitor
LMW	Low Molecular Weight
M	Moderate (Growth Rate)
MEG	Mono Ethylene Glycol
MeOH,	Methanol
MW	Molecular Weight
NaCl	Sodium Chloride
NG	Natural Gas
NHis	No History (no hydrate history)
P	Pressure
1,3-PDO	1,3-propanediol
PEO	Poly Ethylene Oxide
i-POH	Iso Propanol

n-POH	Normal Propanol
PVCap	Poly-*n*VinylCaprolactam
PVP	Poly-*n*-VinylPyrrolidone
RFR	Rapid Failure Region
RGR	Restricted Growth Rate Region
S	Slow (Growth Rate)
s-H	Structure-H hydrate
s-I	Structure-I hydrate
s-II	Structure-II hydrate
SDR	Slow Dissociation Rate Region
T	Temperature
THF	Tetrahydrofuran
ti	Induction time
V	Volume
VS	Very Slow (Growth Rate)
x	Composition of liquid/vapour phases

1. INTRODUCTION

1.1. Background on Hydrate Inhibitors

The very first documentation of natural gas hydrates was done in 1810 by Sir Humphrey Davy when he discovered chlorine (oxymuriatic gas) hydrate in his lab (Davy, 1811). However, it was only until mid-1930's that Hammerschmidt found that the cause of blockage in gas transmission lines above ice point was related to natural gas hydrates (Hammerschmidt, 1934). This discovery turned gas hydrates from just a scientific curiosity to a challenging topic in petroleum industry, resulting in a new era of research on this topic.

Gas hydrates, or clathrate hydrates, are ice-like crystalline compounds that form from hydrogen bonding of water molecules and suitably sized gas (guest) molecules under favourable pressure and temperature conditions. For this molecular complex to be stable, gas molecules should occupy a minimum number of cavities in the water lattice structure.

Depending on the size of gas (guest) molecules in the water lattice structure and the number of filled cavities required for a stable structure, different hydrate structures are formed. Most common clathrate hydrate structures to date are cubic structure I (s-I) (formed by guest molecules with diameters between 4.2 and 6Å, like methane, ethane and carbon dioxide), cubic structure II (s-II) (formed from both small molecules with $d<4.2$Å like nitrogen and larger molecules with $6Å<d<7Å$ such as propane or iso-butane) and hexagonal structure H (s-H) which requires the cooperation of two guest gases (large with $7Å<d<9Å$ such as butane or iso-pentane and small with $d<6Å$ such as methane or nitrogen) to be stable. (Sloan, 1997)

With the application of definitive X-ray diffraction, Jeffrey and McMullan (1965) found that the unit cell of structure I consists of 46 water molecules which form two types of cages, two small against six large. In this structure small cages have 12 pentagonal faces (5^{12}) while larger cages are made up of 12 pentagonal and 2 hexagonal faces ($5^{12}6^2$). The pictorial view of a unit crystal of structure I hydrate presented by these researchers is illustrated in Figure 1-1

Also, using the same technique Mak and McMullan (1965) published that 136 water molecules form a unit cell of Structure II hydrate constructing 16 small cavities and 8 large ones. In this structure, small cages are largely similar to structure I hydrate with 12 pentagonal faces (5^{12}) whereas large cages are of a different shape having 12 pentagonal and 4 hexagonal faces ($5^{12}6^4$). The pictorial view of structure II hydrate unit crystal is illustrated in Figure 1-2.

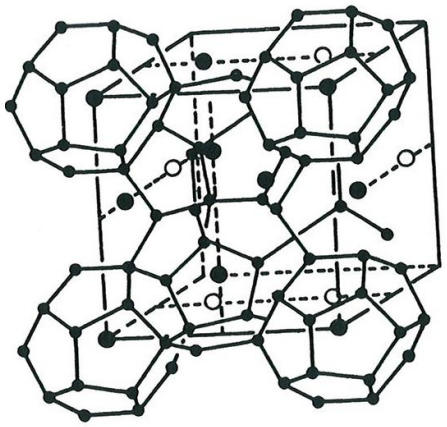

Figure 1-1 Hydrate Crystal Unit Structure I (Sloan, E.D., 2008)

Both structures I and II are known as simple hydrates indicating that they can be stabilized by a single guest gas filling either the large or the small cavities. However, the later discovered structure H hydrate is known to require both a large molecule and a small molecule in collaboration with one another, a double hydrate, to have a stable structure.

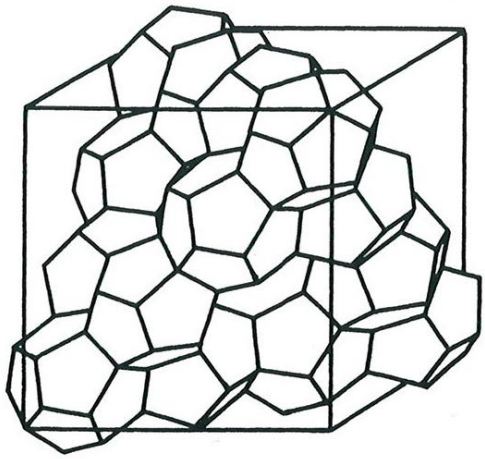

Figure 1-2 Hydrate Crystal Unit Structure II (Sloan, E.D., 2008)

Structure H was only discovered in 1987 by Ripmeester et al. using NMR spectroscopy together with X-Ray and power diffraction. It was reported that the unit cell of type H structure consists of 34 water molecules forming 3 different types of cages, two smaller and one very large. Overall the structure H hydrate is made up of three small cavities with 12 pentagonal faces (5^{12}), two medium sized cavities with 3 square faces, 6 pentagonal faces, and 3 hexagonal faces ($4^3 5^6 6^3$) and one very large cavity with 12 pentagonal faces and 8 hexagonal faces ($5^{12}6^8$). The reported structure is illustrated in Figure 1-3.

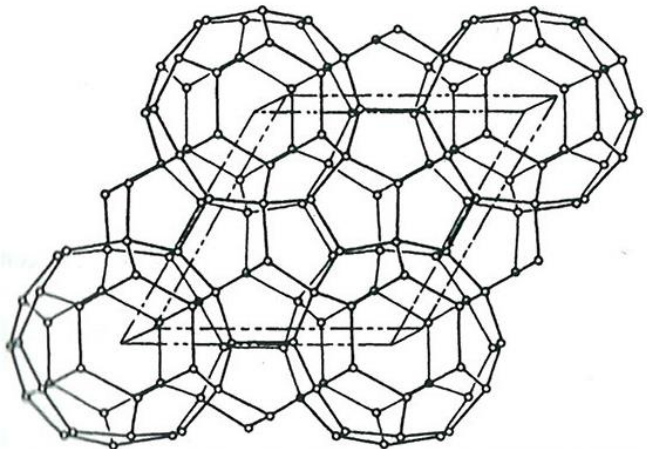

Figure 1-3 Hydrate Crystal Unit Structure H (Sloan, E.D., 2008)

Crystal properties of s-I, s-II and s-H are given in more detail in Table 1-1.

Table 1-1 Geometry of Cages and crystal properties of different hydrate crystal structures. (Sloan, E.D., 2008)

Hydrate Crystal Structure	I		II		H		
Cavity	Small	Large	Small	Large	Small	Medium	Large
Description	5^{12}	$5^{12}6^2$	5^{12}	$5^{12}6^4$	5^{12}	$4^3 5^6 6^3$	$5^{12}6^8$
Number of Cavities/Unit Cell	2	6	16	8	3	2	1
Average Cavity Radius, A°	3.95	4.33	3.91	4.73	3.91[c]	4.06[c]	5.71[c]
Variation in Radiusa , %	3.4	14.4	5.5	1.73	Not Available		
Coordination Number[b]	20	24	20	28	20	20	36

a. Variation in distance of oxygen atoms from centre of cage

b. Number of oxygens at the periphery of each cavity.

c. Estimates of structure H cavities from geometric models.

The very first step of hydrate formation is the nucleation of hydrate. In the process of hydrate nucleation, the old phase gains a higher free energy than the new emerging phase (Hohenberg and Halperin 1977; Chaikin and Lubensky 1995). During this process small water and gas clusters form inside the large volume of the old phase which has become metastable. However, it should be considered that although the free energy per molecule in the bulk of the new phase is less than that of the solvent phase, it is the opposite for the molecules on the surface of the two phases. Therefore, for this transformation to occur, passage over a free energy barrier called the interfacial free energy is required (Kashchiev 1999). Interfacial free energy which is also defined as the difference between the free energy per molecule of the bulk and that of the surface is a positive term and therefore acts towards destabilizing the nucleus. Consequently when the nucleus is very small, addition of more molecules just increases the free energy of the system and makes the nucleus even more unstable. Hence, on average such a nucleus will dissolve rather than grow. However, once the nucleus becomes large enough the surface free energy becomes unimportant in comparison to the drop of free energy from the formation of the bulk phase and the addition of each molecule to the lattice lowers the free energy of the system. The intermediate nucleus size at which the free energy of the system is decreased whether the nucleus grows or dissolves is known as the critical size (De Yoreo, 2003).

For hydrate crystals to nucleate and form, a system should be sitting at the right temperature and pressure conditions. Based on this property, thermodynamic curves can be drawn. Figure 1-4 shows a normal crystallization curve with a metastable (CD) and equilibrium curves (AB). Sloan et al. (2007) describes the crystallization regions in this figure as: 1- The stable zone (any point like P) to the right of line AB where solution is superheated and nucleation and crystal growth will not occur. 2- The metastable (supersaturated) zone (any point like Q) between lines AB and CD where nuclei and crystals may or may not form. 3- The unstable or labile (supersaturated) zone (any point like S), where nucleation is more likely due to the high degree of spersaturation, or driving force.

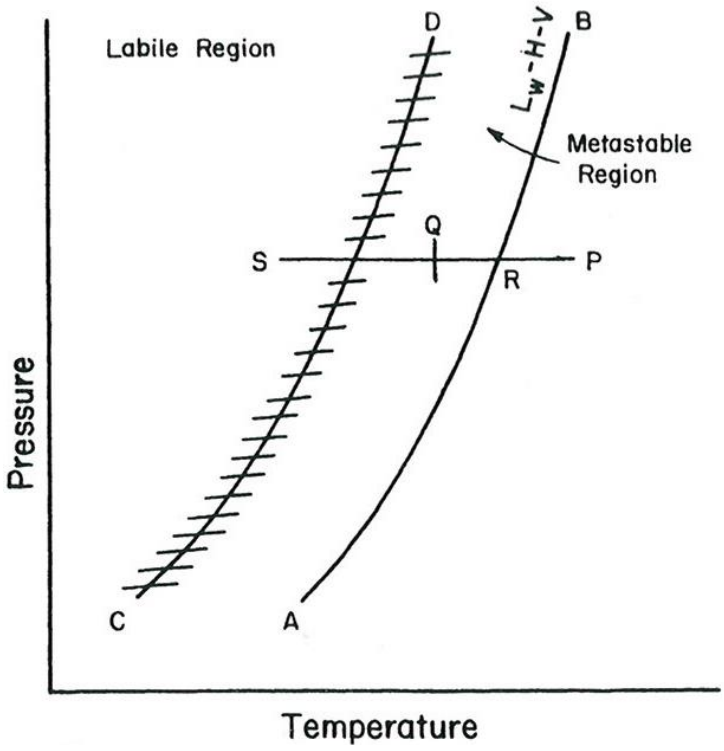

Figure 1-4 Hydrate Formation as a Function of Subcooling Relative to the Equilibrium Line (AB) and the Metastable Line Region (CD). (Sloan, E.D., 2008)

When a system is set at unstable supersaturation conditions, for hydrates to nucleate and grow, hydrate nuclei which are made up of small water and gas clusters grow and disperse in a way to reach the critical size for them to become stable and continue growth. Lederhos et al. (1996) has detailed this process in 4 stages which is illustrated in Figure 1-5. This figure shows the progress of molecular species from water [A] through metastable species [B] and [C], to stable nuclei [D] which can grow to large species. Point [A] which is the beginning of the process shows the presence of liquid water and gas in the system. After the interaction of these two phases both large and small clusters are formed which is shown as point [B]. The cages formed at this stage are relatively long-lived but unstable hence may either disappear or grow to hydrate unite cell or agglomerate to unit cells thus forming metastable nuclei presented in Point [C]. Since these unit cells have not yet reached the critical size they may either grow or shrink in a stochastic process. The metastable nuclei are in quasi-equilibrium with the liquid-like cages until the nuclei reach the critical size shown as point [D], after which the crystals can grow rapidly and hydrate is said to form and grow (Lederhos et al., 1996). Using this hypothesis it can be explained that if hydrate is formed in a system and then heated until hydrate dissociation point is reached or passed only a couple of degrees higher than the dissociation point, there will be still be microscopic species in

the water ranging from multiple hydrate unit cells [C] to metastable nuclei [B]. These residual structures are also known as hydrate history which can promote hydrate formation if cooled again (e.g. Lederhos et al., 1996, Greaves et al., 2008; Duchateau et al., 2009).

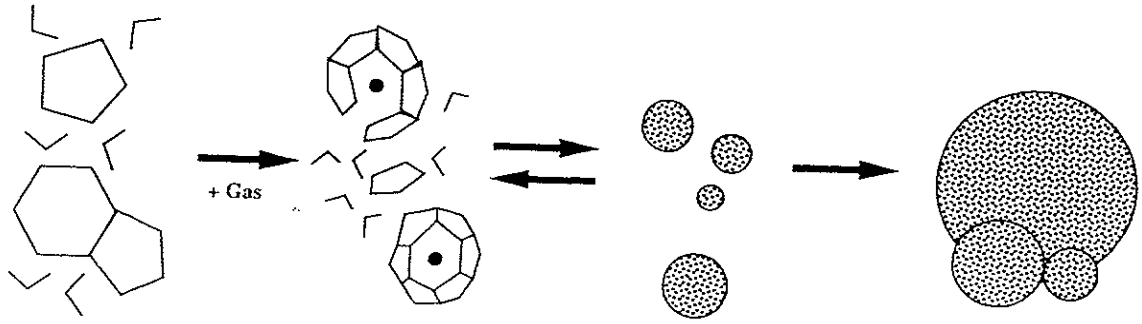

A. Initial Condition
Pressure and temperature in hydrate forming region, but no gas molecules dissolved in water.

D. Labile Clusters
Upon dissolution of gas in water, labile clusters form immediately.

C. Agglomeration
Labile clusters agglomerate by sharing faces, thus increasing disorder.

B. Primary Nucleation and Growth
When the size of the cluster agglomerates reaches a critical value, growth begins.

Figure 1-5 Schematic Model of Hydrate Cluster Growth. (Sloan, E.D., 2008)

1.2. Problems Associated with Hydrate Inhibitors

Gas hydrate discussions and studies can be classified into two categories. One category is related to concerns in association with natural gas hydrates which have been in existence long before the technogenic ones, and presumably have been of considerable importance in the formation of planets and other space bodies (Makagon, 1997). Wherever methane and water are in close proximity at low temperature and elevated pressures there is a high chance of occurrence for these natural hydrates. These methane clathrates in subsea continental slope sediments and in the subsurface of Arctic permafrost regions can be of great importance in their potential for use as a strategic energy reserve.

The second category of gas hydrates is related to hydrate formation in industrial operations such as petroleum exploration and production operations. In contrast to considering hydrates as an opportunity as in natural hydrates these gas hydrates can cause major and potentially hazardous flow assurance problems making them a serious economic and safety concern.

In the process of deep water drilling for instance, due to the relatively low seabed temperature and the hydrostatic pressure of the drilling fluid column, there is a high chance of hydrate formation in the event of a gas kick. Hence, one solution for avoiding this is to use a combination of salts and chemicals in the drilling fluid.

The other major area of concern is the formation of gas hydrates in multiphase transfer lines from well-head to the production platform. In such pipelines due to low seabed temperatures and high operation pressures, the risk of gas hydrate blockage increases. A great amount of experience has been built to prevent hydrate formation in these systems.

In this regards, various methods have been introduced towards removing conditions necessary for hydrate formation.

The most impractical method for hydrate inhibition in this process is to remove the guest molecule. However, in most production operations removing the guest gas results in eliminating the purpose of the operation.

One of the possible methods is to operate at pressures below hydrate formation pressure at fixed temperature. However, decreasing the pressure to these quantities could result in the decrease of energy density to a point where the process is no longer economical.

A more practical method for hydrate prevention is heating and/or insulating the system to prevent it from entering the hydrate stability zone. However, this method can also be uneconomical for long pipeline systems. Moreover, for insulated systems which are being continually heated using hot production fluids, during shut-down situations in which production fluid cool down there is high risk of hydrate formation.

Another hydrate prevention technique is to dry the gas by removing the free water and vaporized water, one of the hydrate formers. By doing so, the dew point is lowered and chemical potential of water molecules in gas decrease in a way that they can no longer enclathrate gas molecules and form hydrate.

The most common method for hydrate inhibition to date is the use of chemical inhibitors. Chemical inhibitors are mainly categorized into two main types: thermodynamic and low dosage hydrate inhibitors (LDHIs).

Thermodynamic inhibitors (typically methanol and mono ethylene glycol) control hydrate formation through changing intermolecular interactions, braking hydrate

hydrogen bonds and competing for available water molecules. By adding this type of inhibitors, thermodynamic equilibrium between water and gas molecules change so that the thermodynamic equilibrium phase boundary (L_w-H-V equilibrium curve) of the system will be shifted to a lower temperature at a certain pressure. This will provide a wider operating pressure and temperature range. However, the main problem with using these inhibitors is that adding large quantities may sometimes be required which will make them economically unfavourable.

On the other hand, low dosage hydrate inhibitors, as evident from their name, are only added in very small quantities and have been shown to be active at much lower concentrations than thermodynamic inhibitors, that is about 0.5-2.0 wt% compared to 40-60 wt%. Hence these inhibitors can potentially eliminate some economic and environmental issues associated with thermodynamic inhibitors. LDHIs are typically subdivided into two groups; kinetic hydrate inhibitors (KHIs) and antiagglomerants (AAs).

AAs are surface active agents that do not stop hydrate formation, but reduce particle adhesion so that plugs will not form. Chemicals that act as AAs are generally surfactants that can be categorized into two types: (1) The type that typically provides a relatively stable water-in oil emulsion (Kelland et al., 2006) and (2) the type that have hydrate-philic head group(s) and long hydrophobic tail(s) (Jager et al.,2000 and TenBroek et al., 1993). The second type AA can be either water soluble, with one long hydrocarbon tail, or oil soluble, with two long hydrocarbon tails. Both these are illustrated in Figure 1-6. A typical water soluble AA is a quaternary salt (QAS), in which two or three of the four ammonium branches are short (e.g., a butyl compound that might be a candidate for inclusion within hydrate cavities) and one or two branch(es) are much longer (e.g., C_8 to C_{18}) so that it might be soluble within the oil phase. The exact mechanism of AAs is yet uncertain but clearly they are closely related to the chemical structure of the AA. Sloan and Koh (2007) mentioned that since the butyl-ammonium end of the AA is very attractive to both hydrate and water, it will remain strongly attached either to water droplets or hydrates after hydrate formation. Also, the long carbon end of the AA will stabilize the QAS in the liquid hydrocarbon and hence spherical hydrates with long protruding chemical strands will remain separated and agglomeration does not occur for the suspension in the oil phase.

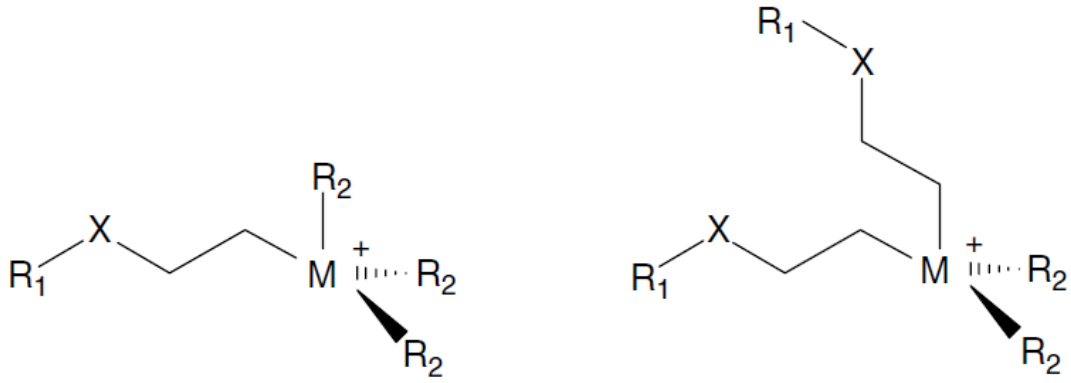

Figure 1-6 The two Shell-types of antiagglomerant. On the left is the water-soluble type, with one branch (R1) containing 8–18 carbons. On the right is the oil-soluble type with two branches (R1) with 8–18 carbons. The central atom is nitrogen or phosphorus, and the shorter branches (R2) are butyl- or pentyl-groups. (Sloan, E.D., 2000)

KHIs are typically low molecular weight polymers that are dissolved in a carrier solvent which were first discovered in the early 1990s. Since then a large number of compounds have been developed (and patented) as supposed kinetic hydrate inhibitors. However amongst all these different compounds, the most well-known, studied and arguably best performing (when combined with synergist chemicals/solvents) are the poly-*n*vinylamides, including poly-*n*vinylcaprolactam (PVCap), poly-*n*-vinylpyrrolidone (PVP) and their co-polymers (Kelland, 2006). While the precise mechanisms by which these (and other) KHIs inhibit hydrate nucleation/growth is still poorly understood, the generally accepted mechanism is crystal surface adsorption. Larsen et al. (1998) concluded that when polymers adsorb to the crystal surface, adsorbed molecules act as barrier for further growth. When the concentration is high enough, polymer molecules will sit closer on the surface than twice the critical radius for crystal growth at the corresponding temperature, and the crystal will not be able to grow between the polymer strands. The adsorption process is fairly rapid, as no measurable growth takes place after a crystal is transferred to an inhibited solution. However, there is certainly some time involved in diffusion and orientation of the inhibitor, the polymer molecules clearly being the slowest diffusing component in the system (Larsen et al., 1998)

Moreover, molecular dynamic simulations suggest that PVCap/PVP adsorb onto growing hydrate crystal surfaces, with the general agreement that this occurs through partial enclathration of the pendant group (into large $5^{12}6^2$ or $5^{12}6^4$ cavities) coupled with hydrogen bonding of the amide group oxygen with the water lattice (e.g. Freer and Sloan, 2000; Makogon and Sloan, 2002; Chapoy et al., 2007; Kvamme, 2005).

There is a widespread understanding within the industry and academia that KHIs delay/slow down/interfere the process of hydrate nucleation which will lead to an increase in 'induction time', *ti*; the period between the moment the system enters the hydrate stability zone (HSZ) and the moment critical nuclei are achieved and hydrate formation and growth takes place. In theory, if at ΔT_{sub}, P the KHI-induced induction time is greater than the pipeline fluid residence time at that condition, then the KHI should be able to prevent hydrate nucleation/growth and therefore plugging in avoided.

With regards to the fact that KHIs delay/interfere with hydrate nucleation, this property has remained the primary focus for the evaluation of KHIs. Therefore, induction/hold time studies have typically been the main technique employed for developing and testing of most KHI and formulations (Kelland, 2006). Also, determining the effects of various parameters including pressure, presence of synergists, salts, liquid hydrocarbons (condensate, oil) and other oilfield chemicals (e.g. corrosion and scale inhibitors) on KHI performance have been done using results of induction/hold time studies. However, since induction time depends largely on the process of nucleation which is a stochastic property in nature, results from this method are inevitably quite stochastic, poorly repeatable and commonly non-transferable (e.g. Kelland, 2006; Sloan and Koh, 2008; Duchateau et al., 2009). This problem has caused lack of confidence for the use of KHIs in production operations. In contrast, traditional thermodynamic inhibitors, while requiring much larger volumes at a higher cost, offer an absolute equilibrium 'hydrate-free' zone which is relatively simple to determine reliably. If such readily measurable, repeatable, time-independent data existed for KHIs, then their application in production operations could be greatly increased, offering potentially enormous cost savings.

In this project, the primary aim is to develop a reliable, repeatable and ideally rapid technique for KHI evaluation which is based on the inspection of gas hydrate growth and dissociation patterns in the presence of KHI polymers. The new approach is developed through examining the repeatability of features and the existence of any consistency between runs and transferability between set ups within KHI systems. In Chapter 2 of this work, by careful examination of polymer-controlled hydrate growth and dissociation behaviours, some crystal growth inhibition (CGI) regions for KHI inhibited systems are defined based on hydrate growth rate. These regions are tested and established once more in different experimental set ups to confirm the transferability of results. Determination of these CGI regions offers a reliable technique to compare the relative performance of different KHIs and also evaluate the effect of various

parameters. In addition to that it is important to understand and determine the presence of any correlation or trend between induction time measurements and results of the new CGI technique. Through this finding, expected induction time patterns can be approximated ahead of such tests where appropriate. For this purpose, at the end of this chapter, the evaluation of the possibility of induction time within different crystal growth inhibition regions based on crystal growth rates are also presented.

After having developed this technique in the following chapters of this work the newly developed crystal growth inhibition method has been applied on different systems to compare the relative performance of these systems and evaluate the effect of various parameters. In all experiments undertaken throughout these chapters, crystal growth inhibition regions are measured using the CGI technique and based on the extent of these regions, hydrate inhibition properties of each KHI system is evaluated; the larger these boundaries, the better and more effective the KHI system is in inhibiting hydrate formation and growth.

Chapter 3 has concentrated on the evaluation of the effect and performance of different KHI polymer types and concentration. In this chapter while the effect of different polymer concentrations are presented, CGI regions are determined for most popular KHI polymers (PVCap and PVP) to understand the efficiency of each polymer and the degree of subcooling offered by them to determine safe operation conditions in the presence of each. Also, the performance of the combination of these polymers was evaluated and is presented in this chapter. In addition to these two popular polymers, other KHIs such as commercial KHIs and biodegradable polymers were tested and are reported as part of this chapter.

Due to the lack of a reliable technique, so far only a very small number of studies have been done on KHI evaluation in different hydrate structure systems which are mainly performed with semiclathrate hydrate formers, such as THF and EO, at atmospheric pressures. However, evaluating KHI behaviour under these conditions will be distanced from actual KHI performance under pressure in the presence of a real gas. Therefore, it is important to perform experiments under real conditions for true evaluation of KHIs. Applying the newly developed CGI technique to these systems provide a means to truly assess the effect of guest gases on KHI-induced hydrate crystal growth inhibition patterns. Chapter 4 will be focused on the study of KHI performance in the presence of several different systems with single, binary and multi component gases. The purpose is

to gradually build up more complex gas systems toward natural gas to better understand and examine the influence of each individual component and its presence with other gases on KHI performance.

The performance of kinetic hydrate inhibitors is evidently influenced by the presence of various components in reservoir fluids. The performance of a same inhibitor can be widely varied in the presence of heavy oil or lighter condensate systems. To date studies on the effect of liquid hydrocarbons on KHI performance have shown contrasting data for single alkanes such as n-heptane and real condensate. However, due to uncertainty in results from induction time method, findings have not been reliable. Hence, in chapter 5 the new crystal growth inhibition (CGI) approach is applied to systems with a liquid hydrocarbon phase present to gain more definitive information on the role of the latter.

Given that reservoir produced waters commonly contain varying concentrations of dissolved salts and also the fact that presence of salt commonly reduce polymer (e.g. PVCap) solubility in aqueous solutions, understanding the effect of this component on KHI performance can be of high importance. In chapter 6 of this work crystal growth inhibition studies are primarily performed on the effect of NaCl as the major salt component in reservoir produced waters. However, since results of the effect of NaCl do not necessarily apply for all other salts particularly carbonate salts that have a completely different structure some preliminary tests on the effect of K_2CO_3, a carbonate salt, are also undertaken.

Chapter 7 concentrates on the effect of alcohols, one main type of thermodynamic inhibitors, on the performance of kinetic hydrate inhibitors. Commonly thermodynamic inhibitors are used in KHI formulations as solvents and also to increase the subcooling to which KHIs can be used. Hence understanding the behaviour and performance of these two inhibitors together can be very valuable. For this purpose as will be presented in chapter 7, a number of popular thermodynamic inhibitor alcohols such as methanol and ethanol in the presence of KHIs were examined with the application of the newly developed CGI technique. Also for a fairer understanding of the mechanism of this interference and the role of alcohol structure on this process, a number of other alcohols with similar properties/molecular structures but different number of carbons in the alkyl ‘tail’ and also alcohols with the same molecular formula but different structure were tested using the same technique.

Finally in chapter 8, study on the effect of glycols, one other popular type of thermodynamic inhibitor, on KHI performance using the new CGI technique is revealed. Similar to alcohols, some glycols are also commonly used in KHI formulations to increase the subcooling to which KHIs can be used by acting as a 'top-up' inhibitor and also by increasing the solubility of these polymers. Despite this important role and application of glycols, studies on the performance of the combination of these inhibitors with KHIs have been limited. Therefore, in-depth studies on the effect of mono-ethylene-glycol, the most commonly used thermodynamic inhibitor, were set as the primary aim of this chapter to evaluate KHI behaviour in its presence using the new technique. In addition to that, as the second part of this chapter, some other glycols have been tested and will be presented to help conclude on the performance of glycols more comprehensively and suggest a more reliable explanation for any behaviour observed.

References

Atilhan, M., S. Aparicio, et al., 2005, *"Natural Gas Hydrates."* Advances in Natural Gas Technology 7: 193-206.

Chaikin, P. and T. Lubensky, 1995, *"Principles of condensed matter physics"*, Cambridge University Press, Cambridge (GB).

Chapoy, A., R. Anderson, et al., 2007, *"Low-pressure molecular hydrogen storage in semi-clathrate hydrates of quaternary ammonium compounds."*, Journal of the American Chemical Society 129(4): 746-747.

Davy, H., 1811, "*The Bakerian Lecture: On some of the combinations of oxymuriatic gas and oxygene, and on the chemical relations of these principles, to inflammable bodies."*, Philosophical Transactions of the Royal Society of London 101: 1-35.

De Yoreo, J. J. and P. G. Vekilov, 2003, *"Principles of crystal nucleation and growth."*, Reviews in mineralogy and geochemistry 54(1): 57-93.

Duchateau, C., Peytavy, J.-L., Glénat, P., Pou, T.-E., Hidalgo, M., and Dicharry, C., 2009, *"Laboratory Evaluation of Kinetic Hydrate Inhibitors: A Procedure for*

Enhancing the Repeatability of Test Results", Energy and Fuels 23 (2): 962–966.

Duchateau, C., P. Glenat, et al., 2009, *"Hydrate precursor test method for the laboratory evaluation of kinetic hydrate inhibitors."*, Energy & Fuels 24(1): 616-623.

Greaves, D., J. Boxall, et al., 2008, *"Measuring the particle size of a known distribution using the focused beam reflectance measurement technique."*, Chemical Engineering Science 63(22): 5410-5419.

Hammerschmidt, E.G., *1934 "Formation of Gas Hydrates in Natural Gas Transmission Lines,"*, Industrial and Engineering Chemistry 26(8), 851-855

Hohenberg, P. C. and B. I. Halperin, 1977, *"Theory of dynamic critical phenomena",* Reviews of Modern Physics 49(3): 435-479

Jager, T., F. A. A. Sanchez, et al., 2000, *"Toxicokinetics of polycyclic aromatic hydrocarbons in Eisenia andrei (Oligochaeta) using spiked soil."*, Environmental Toxicology and Chemistry 19(4): 953-961.

Kashchiev, D. and D. Exerowa, 2001, *"Structure and surface energy of the surfactant layer on the alveolar surface."*, European Biophysics Journal 30(1): 34-41.

Kelland, M. A., 2006, *"History of the development of low dosage hydrate inhibitors."*, Energy & Fuels 20(3): 825-847.

Kelland, M. A., T. M. Svartaas, et al., 2006, "*Studies on some alkylamide surfactant gas hydrate anti-agglomerants*", Chemical Engineering Science, 61(13): 4290‑4298.

Kvamme, B., T. Kuznetsova, et al., 2005, *"Molecular dynamics simulations for selection of kinetic hydrate inhibitors."*, Journal of Molecular Graphics and Modelling 23(6): 524-536

Larsen, R., Knight, C. A., and Sloan, E. D., 1998, *"Clathrate Hydrate Growth and Inhibition"*, Fluid Phase Equilibria, 150-151, 353-360

Lederhos, J.P., Long, J.P., Sum, A., Christiansen, R.L., Sloan, E.D., 1996, *"Effective kinetic inhibitors for natural gas hydrates"*, Chemical Engineering Science, 51, 1221–1229

Makagon, Y., 1997, *"Hydrates of Hydrocarbons"*, Pennwell publishing company, Tulsa, Oklahoma

Makogon, T. Y. and E. D. Sloan, 2002, *"Mechanism of kinetic hydrate inhibitors"*, Proceedings of the 4th International Conference on Gas Hydrates, Yokohama, Japan

Mc Mullan, R. K. and G. Jeffrey, 1965, *"Polyhedral clathrate hydrates. IX. Structure of ethylene oxide hydrate."*, The Journal of Chemical Physics 42(8): 2725-2732

Mak, T. C. W. and R. K. McMullan, 1965, *"Polyhedral clathrate hydrates. X. Structure of the double hydrate of tetrahydrofuran and hydrogen sulfide."*, The Journal of Chemical Physics 42: 2732

Ripmeester, J. A., S. T. John, et al., 1987, *"A new clathrate hydrate structure."*, Nature 325(6100): 135-136

Sloan Jr, E. D. and C. Koh, 2007, *"Clathrate Hydrates of Natural Gases"*, Third Edition, CRC Press, New York

TenBroek, E. M., P. D. Lampe, et al., 2001, *"Ser364 of connexin43 and the upregulation of gap junction assembly by cAMP."*, The Journal of cell biology 155(7): 1307-1318

2. DEVELOPMENT OF THE CGI TECHNIQUE

2.1. Previous Method: Induction Time

While our understanding of LDHIs – both KHIs and AAs – has grown considerably over the past decade, there are still many things to be investigated such as the actual inhibition mechanism for these chemicals. Because of increasing interest in LDHIs as promising alternatives to other inhibitors, the major effort has been put into producing ever 'better' proprietary formulations, utilising combinations of active chemicals (e.g. KHI polymers, AA surfactants) and synergists. This development has mainly been carried out through the screening of many chemical/combinations with the aim of (ideally) discovering a new/superior active component and/or synergist combination. However, as yet not much effort and time has been devoted to establishing the actual mechanism of these KHIs for hydrate inhibition and how different parameters can affect this property. Therefore, even when testing inhibitors for use in a particular pipeline or field development the same screening technique is used to ensure system suitability/compatibility. However, such an approach for LDHI evaluation is very time consuming and since it does not fully appreciate the mechanism by which these inhibitors work, can be genuinely risky. Consequently, even if this method reveals good performance for a particular inhibitor under laboratory conditions it will have difficulty to foresee problems which may occur once used in a real pipeline/field condition and thus results may differ greatly once used in the field.

Moreover, while the precise mechanisms by which KHIs inhibit hydrate nucleation/growth are still poorly understood, it is generally accepted that they delay/interfere with the process of hydrate nucleation. This interference will cause a delay in the formation of a stable hydrate nuclei and the onset of hydrate growth for a specific period which is the 'induction/hold time'. If at conditions within the hydrate stability zone, the pipeline fluid has a residence time shorter than the induction time, then it is assumed that the inhibitor will be able to prevent hydrate formation and thus blockage. Since the ability to define a fixed (or at least minimum) induction time for a particular system has offered an attractive 'benchmark' means, determining this parameter has remained the most popular technique for KHI evaluation and also development of many KHI formulations (Kelland, 2006). Moreover, there has been

great deal of effort put into identifying the relationship between induction time and various operating parameters (e.g. pressure, temperature and composition). However, even with some consistency being detected with general trends, there has not been a great deal of success in these studies. Findings in one study are commonly in disagreement with those of another due to the probabilistic nature of nucleation. Moreover, data are often neither transferable nor repeatable. (e.g. Englezos et al., 1987; Christiansen et al., 1994; Kelland, 2006; Sloan and Koh, 2008; Duchateau et al., 2009).

Problems with this technique are explained in more detail below.

2.1.1. Induction Time Definition

For the purposes of further discussion, 'induction time' (or 'hold time') is here defined by the accepted scientific definition as the nucleation time period which passes at a specific subcooled PVTx (Pressure, Volume, Temperature and Composition of liquid and vapour phases) condition before a new growing crystalline hydrate phase emerges.

As mentioned in the introduction, classical nucleation theory defines the activation barrier to nucleation as the sum of the increase in free energy arising from the creation of a new interface and the decrease from creation of a more thermodynamically stable phase (Kashchiev, 2000).

The interfacial free energy is proportional to the square of the crystal radius (assuming a sphere), with the free energy associated with the phase change being proportional to the cube of the crystal radius. This yields an energy maximum relative to radius for the emerging daughter phase crystal; this corresponds to the critical radius. When − though random molecular interactions − a nucleus reaches the critical radius, further growth is energetically favourable, and nucleation proceeds to growth (Kashchiev, 2000). It is at this point that induction time ends. In a constant volume system such as those used in experiments throughout this thesis, at isobaric conditions, the end of induction time is indicated by a reduction in pressure due to the increase in bulk system density associated with enclathration of free gas.

Nucleation generally occurs homogeneously or heterogeneously. Homogeneous nucleation takes place when a critical nucleus emerges directly from the parent phase. As the critical nucleus size is large at low subcoolings, the probability of one forming is small. As subcooling increases, the difference in free energy between the parent and

daughter phase increases, reducing the critical nucleus to smaller radii. At sufficiently high subcoolings, the critical radius is reduced to such a small size that homogeneous nucleation will ultimately take place spontaneously; this condition is known as the spinodal.

In heterogeneous nucleation, molecular clusters gather in contact with a third phase, which lowers the interfacial energy cost of further growth. This means considerably smaller critical nuclei may allow energetically favourable growth at a given PVTX condition. This lowers the energy barrier associated with heterogeneous nucleation in comparison with homogeneous nucleation, allowing crystallisation to occur more readily at lower subcoolings in the presence of impurities. Due to the inevitable presence of the latter in typical laboratory and real pipeline systems, hydrate nucleation will be almost invariably heterogeneous under these conditions.

2.1.2. Problem of Data Stochasticity in Induction Time Method

While, as described, the critical radius for an ideal system can be defined as a function of subcooling by established thermodynamics, the 'induction time' itself is ultimately governed primarily by statistical probability; i.e. the likelihood of a sufficient molecules gathering and structuring to form a critical nucleus. This means that there is typically no 'fixed' induction time for a system at a given ΔT and P, but rather the likelihood of a critical nucleus appearing will be described by a probability distribution function with a 'mean' value. Thus there will always be some 'scatter' in data; this merely reflecting the probability function. This stochastic nature of nucleation typically leads to large variations in the induction time measured for hydrate formation (e.g. Englezos et al., 1987; Christiansen et al., 1994; Duchateau et al., 2009). However, in theory, if a large number of repeat runs are carried out under identical conditions, then the distribution of function for induction times − and so the mean − should be measurable.

There are two major problems with this approach: (1) a very large sample size may be required, particularly at low subcoolings (low probability, so large induction time range), and (2) reliable measurement is dependent on very rigorous criteria, including:

- Systems are 'clean', i.e. completely free of all (except inert) additional components which might alter results by encouraging or discouraging nucleation
- System parameters are identical in each case (PT, mixing rate, cooling rate to that condition, phase volumes)

- The system is hydraulically equilibrated, i.e. all phases are evenly mixed with no dead volume
- Instrumentation is sufficient to detect the exact point in time where growth begins; i.e. if growth is very slow in the beginning it may be difficult to discern it

Clearly, achieving the above is very difficult, and even if such conditions are successfully created, it is hard to argue that results will be applicable to real pipeline systems which are far from ideal.

With respect to testing KHIs, in this study using the new approach (detailed in Section 2.2) show that polymers such as PVCap and PVP may be better described as crystal growth inhibitors/modifiers, rather than as 'nucleation delayers' per se. In this sense, we may consider that the apparent increase in induction times they cause is merely one of the 'symptoms' of their activity, and one which is inherently difficult to quantify due to its stochastic nature. Results also suggest that for many laboratory experimental conditions, measurement of a 'real' induction time, as defined above, is not physically possible, as detailed in Section 2.5.

2.1.3. Other Problems associated with Induction Time Method

In addition to the problem with the stochastic nature of induction time, the other problem that could lead to unreliable results is that methods and equipment used for measuring this parameter vary greatly between laboratories.

Some of the different apparatuses used for testing KHI performance are stirred or rocking autoclave cell chambers (Arjmandi et al.,2003; Lederhos et al., 1996) , flow loops (Peytavy et al., 2008) and high pressure differential scanning calorimeter (DSC) (Koh et al., 2002; Sivaraman , 2003).

In all these different apparatuses as indicated the parameter used for evaluating the performance of KHIs is the induction time of hydrate nucleation. Between all the different methods used for the measurement of induction time, one of the most typical ones particularly employed for experimental set ups without visual windows such as stirred cells, rocking cells and flow loops is to interpret the curve of pressure drop with the elapsed time. Figure 2-1 shows an example of a typical pressure versus time curve. As evident from the curve, changes in the pressure undergo three stages: the first stage

with rapid pressure drop which corresponds to dissolving of gas in the liquid phase; the second stage during which pressure is stable, represents the induction time for hydrate nucleation; and the third stage with another rapid pressure drop denoting rapid growth of hydrate crystals. However, in this method there are usually two problems. In some cases, changes in the pressure are such that the stable pressure stage is not so clear and hence it is not possible to define an induction time by this. Moreover, in cases where the stable region is detectable it is very difficult to define an exact start and end point for this region and in many cases the very first hydrate formation point is not easily detectable. Therefore, there can be different readings of induction time from a single figure (Chen et al. 2010). In addition to that, in this technique long test times and high number of replicate runs are required which will result is loss of time and build-up of waste chemicals.

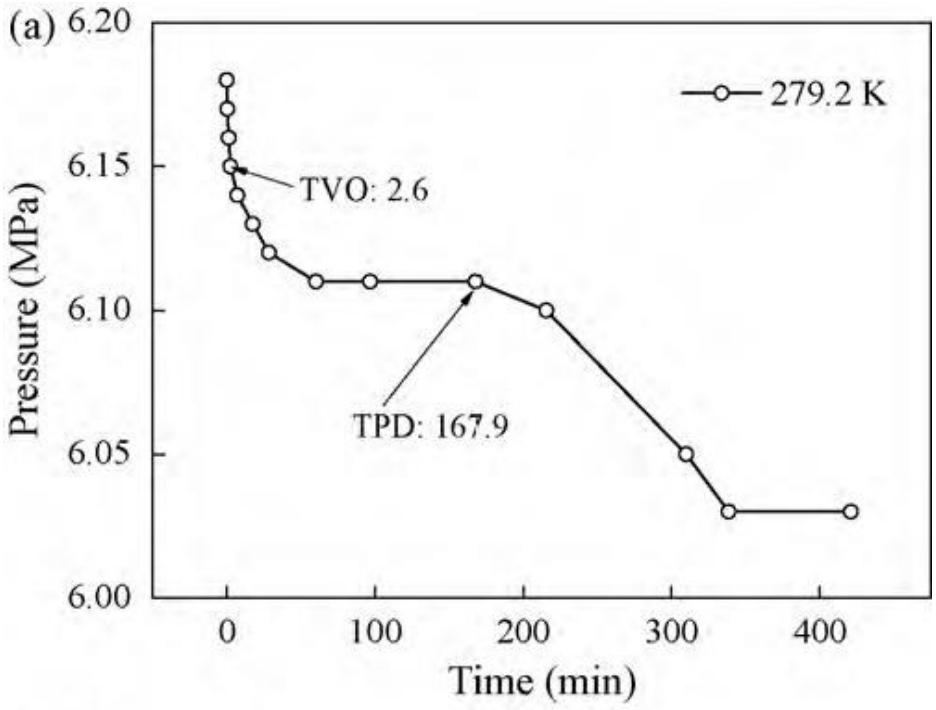

Figure 2-1 Changes of pressure with time during hydrate formation at a specific subcooling (Li-Tao Chen , et al. 2010)

As a result of all these obstacles, the new DSC technique was developed. This technique was first applied on hydrate studies by Koh et al. (2002) to compare effects of the addition of 3 different chemical hydrate inhibitors at the surface and in bulk solution. Differential scanning calorimetry is a thermoanalytical technique in which the difference in the amount of heat required to increase the temperature of a sample and reference is measured as a function of temperature. The result of a DSC experiment is a curve of heat flux/ temperature versus time. A sample DSC curve is illustrated in Figure

2-2 (Dalmazzone et al 2006). In a complete run of each experiment, the system is cooled to a specific subcooling at a fast rate. Then the system is kept at that subcooling for a certain period of time for hydrate to form. And finally the sample is heated until complete dissociation of hydrate. Each step is detectable on the mentioned heat flow/temperature versus time curve. On this curve, first heat flow peak is simply the response of the DSC sensor to the fast cooling. The second one is the exothermic heat released during the isothermal hydrate formation at the specific subcooling. Finally the last signal reveals the dissociation of methane hydrate upon warming. Although very useful, there are again problems with this method that have cause unreliability of results. One problem is that at temperatures close to equilibrium (low subcoolings), the shape of the hydrate formation peak gets wider and smoother and becomes less symmetrical, and in some cases barely distinguishable from the baseline. (Dalmazzone et al 2006). Furthermore, in cases where there is a distinct and symmetric exothermic peak, detection of the start and end point of this peak is not easily noticeable.

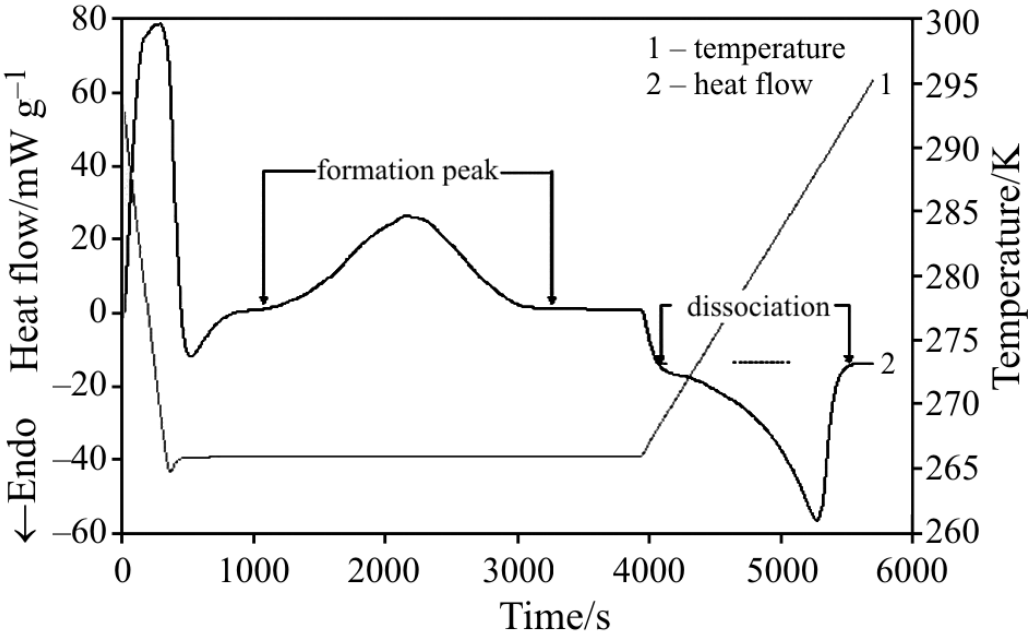

Figure 2-2 Curve of formation and dissociation of methane hydrate in Fluid #2. P(CH4)=30 MPa (Dalmazzone et al. 2006)

In addition to all mentioned problems with each individual technique, as mentioned earlier, due to the stochastic nature of nucleation, data are often neither transferable nor repeatable. This inherent and widespread stochasticity in KHI results raises serious questions as to the reliability of current test protocols and the validity of generated data. Due to the unsatisfactory results, trust in KHIs is limited and there has been uncertainty in the industry regarding employment of these chemical as hydrate inhibitors in real field operations.

Thus, if industry is to trust the use of LDHIs in hydrates control processes as a standard flow assurance solution, the aforementioned problems should be resolved. For this purpose it is necessary to develop a method that yields reliable and rapid results which are repeatable and transferable between different laboratories/experimental set-ups. This requires a better understanding of the actual mechanism by which LDHIs inhibit hydrate formation and the effect of different factors on it, such as system type (gas, condensate, oil), PT conditions, and the presence of other chemicals (e.g. salts, thermodynamic inhibitors, scale, corrosion inhibitors).

2.2. Development of the New Approach: Background

The primary aim of this project was to develop a reliable, repeatable and ideally rapid technique to evaluate the performance of KHIs. To this aim a new approach was developed by initially examining whether any truly repeatable features which have both high consistency between runs and transferability between set ups exist within KHI systems.

Within the literature, two main clues were identified that indicated the high chance of the presence of such repeatable features in KHI systems. The first clue was related to the significant reduction of hydrate dissociation rate outside hydrate phase boundary (e.g. Habetinova et al., 2002; Svartaas et al., 2008). The second one was from single crystal studies on KHI systems that suggested complete inhibition of hydrate crystals at certain degrees of subcooling. (e.g. Makogon et al., 1997; Larsen et al., 1998, 1999).

Studies on hydrate dissociation under the influence of KHIs by Habetinova concluded that kinetic hydrate inhibitors can cause difference between the observed dissociation temperatures and the equilibrium temperature for pure hydrate. Also he found that hydrate dissociation rate is connected to the efficiency of the KHI and also the temperature difference from the hydrate phase boundary (Habetinova et al., 2002). Moreover, Svartass's extensive work on the dissociation properties of structure II hydrates in the presence of one main structure of KHIs (namely PVCap) revealed that in PVCap present systems, the final dissociation temperature was significantly displaced towards higher temperatures. This displacement was found to be dependent on system pressure, concentration and molecular weight of the polymer. Also, it was established that the dissociation temperature was a function of both heating rate and the sub-cooling during hydrate formation. (Svartaas et al., 2008).

A number of studies have been done to observe how KHIs could possibly inhibit hydrate nucleation and monitor hydrate growth habits using single crystal studies. In these studies, single hydrate or ice crystals are grown at the tip of a pipette which is then immersed into a subcooled aqueous liquid containing a water soluble hydrate former (e.g. THF for structure-II and ethylene oxide for structure-I) with and without KHI present. In these experiments the shape of the single crystal, its growth pattern and growth rate were visually observed as a function of subcooling. These studies have revealed some very important properties of KHI polymers (e.g. PVCap, PVP). It has been found that these inhibitors can apparently inhibit crystal growth completely. To achieve this full inhibition, there is a minimum concentration of hydrate required which strongly depends on the subcooling, polymer type and molecular weight of the inhibitor. Furthermore, these tests showed that crystals which had been exposed to inhibited solutions remain inhibited for a couple of hours even when transferred back to an uninhibited solution. While tests are somewhat unrealistic with respect to real pipeline conditions (conducted at atmospheric pressure with water soluble hydrate formers and little or no mixing), findings are very useful for understanding the real behaviour of KHIs. One very important conclusion from these studies is that complete growth inhibition is a result of KHI polymer adsorption to the crystal surface, with the adsorbed molecules acting as barriers for further growth. (Makogon et al., 1997; Larsen et al., 1998, 1999).

In addition to these two clues, other workers confirmed that in systems where the aqueous phase has been ‘seeded’ with nuclei of some sort, KHIs can still significantly inhibit hydrate nucleation and/or growth (Peytavy et al. 2008; Duchateau et al. 2008, 2009, 2010).

In these studies Paytavy et al. reported that in a KHI exposed system, after one hydrate formation run, when complete decomposition of hydrates is done at a small ΔT of supercooling, dispersion of induction time data in a hydrate reformation run reduces significantly compared to a situation in which decomposition is done at higher supercoolings. Also in such systems, temperature at which hydrate formation was detected was at lower subcoolings. Therefore, it was concluded that the presence of precursory hydrate structures in the water phase provided templates for faster hydrate formation and therefore reduced the stochastic character of hydrate nucleation. (Peytavy et al. 2008). Moreover, Duchateau et al. observed that hydrate formation in a system containing fresh water leads to highly scattered results due to the stochastic nature of

hydrate crystallization. On the other hand, in a system that has already formed hydrates, if the first hydrate dissociation is done at temperatures not too far from the thermodynamic hydrate temperature, it is far easier and quicker to form hydrates and on top of that, the onset of hydrate formation was far more reproducible from test to test. It was suggested that the basic phenomenon behind this could be related to the hydrate clusters remaining in the system after the first hydrate formation. These clusters will then act as the heterogeneous germs that are present in real systems which will cause a reduction in the stochastic behaviour of the second nucleation run. Utilizing this new procedure for laboratory evaluation of KHIs' efficiency it was found that, inhibited systems exhibit higher protection against hydrate formation and increasing KHI concentration improves hydrate prevention.

All the above studies show that the effect of KHIs is not limited to nucleation of hydrate. The first group of workers clearly illustrated that dissociation temperature of KHI exposed hydrates is clearly displaced. Therefore, these hydrates become metastable at temperatures where they would normally dissociate. Moreover, as indicated above the second set of workers discovered that KHI polymers can apparently completely inhibit further hydrate crystal growth indefinitely up to a certain subcooling. Work undertaken by the third group of researchers suggested that that if so called 'hydrate history' – a condition where the aqueous phase has recently hosted a solid hydrate phase – does represent hydrate 'nuclei' of some form, then this could potentially be construed as KHIs strongly inhibiting after nucleation, adding further support to previous findings by Makogon et al. and Larsen et al.

While individually each of these findings have their own specific implications – as discussed above – clearly, taken together they provide very strong evidence that KHI interaction with hydrate crystals occur throughout the hydrate nucleation-growth-dissociation cycle by polymer crystal surface adsorption and since this is a thermodynamic process it must be controlled to a large extent by thermodynamics and so quantifiable in a repeatable way. The fact that hydrates can not only inhibit hydrate formation but also prevent further growth of an already present hydrate inside the phase boundary where it might be considered that KHI has failed is particularly important. If KHIs perform similarly in real systems (e.g. with saline waters, hydrocarbon gases, condensate) and show similar thermodynamic effects, this will raise hope for the use of KHIs in the industry. Therefore, it is important to understand if this behaviour is

repeatable and consistent between different set-ups and if there are limits in terms of the subcooling achieved for this hydrate inhibition in the presence of KHIs.

This chapter focuses on the work undertaken in this project to investigate gas hydrate growth and dissociation patterns in the presence of KHI polymers. As already mentioned induction time studies are not a promising method for evaluating KIHs thus it is important to develop a new approach for this evaluation. Consequently, in an intentional divergence from induction time studies, work has focussed on determining fundamental polymer-controlled hydrate growth and dissociation phase behaviour. By carefully examining these behaviours some crystal growth inhibition (CGI) regions for KHI inhibited systems are defined based on rate of hydrate growth. Determination of CGI data can then provide a robust means to compare the relative performance of different KHIs, evaluate the effect of various parameters, and approximate expected induction time patterns ahead of such tests where appropriate.

2.3. Experimental Equipment and Procedures

2.3.1. Experimental equipment and set-up

In any experiment, it is vital that the equipment and procedures are designed to ensure that results reflect what was actually intended, rather than being an unintentional artefact of experimental design. If care is not taken to appreciate/account for all processes involved, both induced (e.g. T, P, mixing rate, initial phase volumes) and reactive (e.g. exothermic/endothermic behaviour, growth of hydrates, emulsification, dissolution of gas…), it is quite possible that even in what might be judged a simple system, data may not actually reflect what was intended, resulting in inconclusive or incorrect interpretation. Therefore, while no specialized equipment was required, particular care was taken in the design and layout of the equipment to maintain repeatable, reliable and transferrable data in determining crystal growth inhibition regions for the development of the CGI technique.

Figure 2-3 shows the apparatus used to determine crystal growth inhibition regions by detecting hydrate growth rate based on changes of pressure and temperature. The figure shows a standard autoclave cylindrical cell which can be made of stainless steel or titanium (salt compatible). Cell volume required to ideally suit the purpose, based on experience gained throughout this study, can range between 100-500 ml but the typical volume used in most of the experiment is 280 ml. The cell can be operated up to 410 bar

between 233 K and 323 K. For these set-ups, cell temperature is controlled by circulating coolant from a programmable cryostat through a jacket surround the cell. The cryostat can maintain the cell temperature to within 0.1 °C. To achieve good temperature stability, the jacket is insulated with polystyrene board and the pipes that connect it to the cryostat are covered with plastic foam. Temperature is determined by a platinum resistance thermometer (PRT, ± 0.1 °C) which is connected to a computer for direct acquisition. In these CGI experiments it is particularly important to ensure that the temperature data actually represent that of fluid, so it should be noted that ideally the temperature sensitive region of the probe should be within or regularly wetted by cell liquid. The pressure is measured by either strain gauge pressure transducer (± 0.4 bar) or precision Quartzdyne (± 0.07 bar) transducer; these being regularly calibrated against a dead weight tester. The pressure transducer is mounted directly on the cell and connected to the same data acquisition unit as the temperature. This will allow real time monitoring and recording of cell temperature and pressure throughout different temperature cycles.

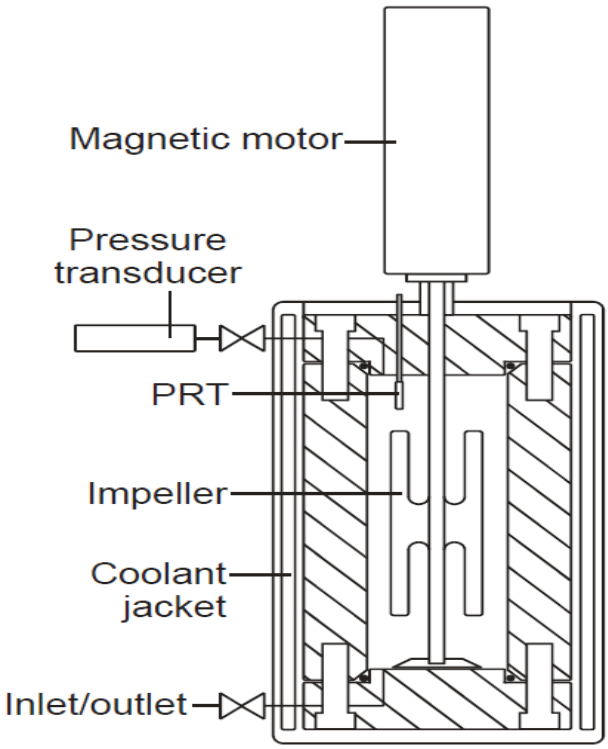

Figure 2-3 Schematic illustration of the 280 ml high pressure (max 410 bar) autoclave cells used in experiments.

To achieve a fast thermodynamic equilibrium and create a state where all phases have an equal as possible ability to interact with each other, a stirrer with a magnetic motor was used to agitate the test fluid. It is crucial to consider that for data to show good repeatability, irrespective of whether the process is kinetically and/or

thermodynamically driven, fluids should be well mixed and there should be no/minimal dead (unmixed) volume within the experimental cell. The primary problem with the presence of a dead volume is that hydrate might be able to grow slowly from polymer-free condensed water in these places. Hence, rather than results representing the behaviour of one system, they may represent two (or more) systems with varying degrees of physical interaction. To minimise this problem, it is vital to design the setup so that the entire internal surface of the test cell is regularly wetted with the KHI aqueous phase. For this purpose, a paddle type stirrer was used together with the cell placed horizontally. At moderate rpm (e.g. 500+), the paddle will lift and throw liquid to the top of the cell, facilitating complete wetting of internal surfaces, so eliminating the dead volume problem. Accordingly, to aid further mass transfer/reaction rates were maximised by typically setting the impeller speed at 750 rpm, giving good shearing/co-mingling of aqueous and gaseous phases.

In the constant volume standard autoclaves used in our experiments, changes in the pressure due to gas consumption through hydrate formation will strongly depend on the volumetric ratio of gas to liquids (water, liquid hydrocarbon) in the cell. At low gas volumes (thus low total moles gas) relative to liquids, then pressure will be much more sensitive to gas hydrate formation than will be the case for high gas volumes (high total moles of gas). In light of this, the volume fraction of hydrate represented by a certain pressure drop due to hydrate formation for low gas volume fractions is much smaller than that for high gas volume fractions. Therefore, it is much more accurate and simpler to calculate and control the percentage of hydrate in low gas volume fractions and so in CGI tests, experiment were designed in a way that large liquid volumes were preferably used. If cell and liquid volumes (thus gas volume) are accurately known, from changes in pressure due to hydrate formation the fraction of hydrate present in the system can be calculated to a reasonable degree of accuracy using simple PVT relationships. If the same liquid volumes are used in different tests, for a given pressure, at low ΔP_h, hydrate fractions will generally be similar. The most suitable liquid volume fractions for CGI tests were found to be around 0.80-0.85. At these volume fractions there will be both high sensitivity for detection of hydrate and minimised dead volume. In this work, hydrate fractions were calculated based on P, T and phase volumes using a thermodynamic model, HydraFLASH® 2.2, developed by Hydrafact.

The main KHI polymer used in mostly these tests, unless stated otherwise, is poly-nvinylcaprolactam (PVCap) which is one of the most well-known and arguably best

performing amongst different KHIs (Kelland, 2006). The PVCap used in experiments was Luvicap-EG base polymer (average molecular weight / AMW =~7000) with the ethylene glycol solvent removed by vacuum oven drying (supplied by BASF).

Ultra high purity grade methane gas (99.995% pure) supplied by BOC was used. Solutions were prepared using deionized water throughout the experimental work with aqueous PVCap solutions prepared gravimetrically.

2.3.2. Experimental procedures

Determining Baseline KHI-Free Reference Phase Boundary

The first step in the experiments is to establish a reference 'baseline' condition which is the actual hydrate formation phase boundary of the tested gas in a KHI free system. In most experiments this line is established both experimentally and predicted using a thermodynamic model such as HydraFLASH® 2.2. In CGI experiments, a baseline test should be identical to KHI tests in terms of all parameters such as mixing rate, phase volumetric ratios, composition and initial PT except of course with no KHI present.

To determine the thermodynamic hydrate phase boundary experimentally, the employed method was the isochoric step-heating used by Deaton and Frost in the 1940s. In this technique, after initial hydrate formation by temperature decrease at constant volume, hydrate is dissociated by increasing the temperature in steps, allowing sufficient time for equilibrium to be reached at each step. By determining the equilibrium pressure at each temperature, heating curves are generated. Only equilibrium (stable P at set T) points are used to create heating curves for interpolation to determine dissociation points (Tohidi, 2000).

For single component gas systems (e.g. methane), where the hydrate phase boundary is well established and there will be only one degree of freedom (a typical Hydrate + Liquid + Gas condition), determining the baseline is much simpler and there is no need to measure heating curves/dissociation points. Thus, if the system is well mixed and not component limited (which should generally not be at the recommended 80% initial cell volume as liquid phase), PT conditions upon hydrate formation should rapidly fall to the phase boundary and closely track back and forth along this in response to temperature changes. To record normal hydrate growth rates in the absence of the KHI and determine the maximum pressure drop due to hydrate formation at a given temperature,

the system is once more cooled but with hydrate present. Figure 2-4 illustrates an example for a methane-water system in a standard autoclave system.

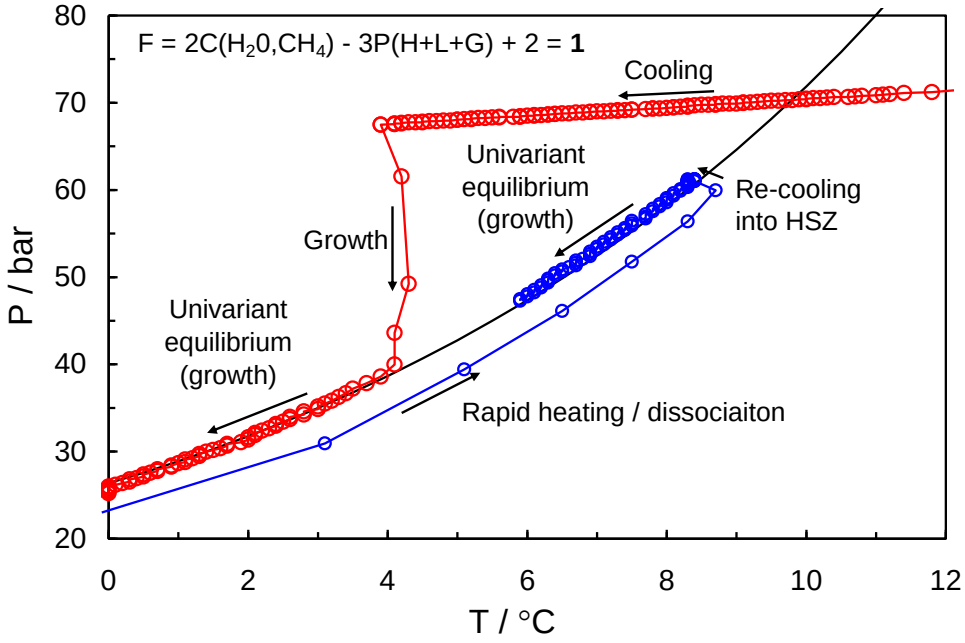

Figure 2-4 PT plot showing cooling-heating curves for a simple methane-water system (univariant hydrate + liquid + gas equilibrium). Raw data points are every 5 minutes. Upon cooling at 1 °C/hr with no history present, hydrate nucleates at ~−5.5 °C subcooling. As soon as hydrate forms there is only 1 degree of freedom.

However for binary and multicomponent systems, since there is more than one degree of freedom and also the possibility of two hydrate structures forming (s-I and s-II), the system is more complex and both heating curves and dissociation points should be determined for the KHI-free system. An example of a binary (5 mole% ethane / 95 mole% methane) gas mixture is illustrated in Figure 2-5 which was measured as part of this project for evaluating the effect of KHIs in gas mixtures presented in detail in Chapter 4. Figure 2-5 shows raw PT data (points every 5 minutes), determined equilibrium points and interpolations for dissociation conditions. Phase boundaries (HydraFLASH® 2.2 predictions) for methane and 5 mole% ethane in methane are shown for comparison. As can be seen, due to the fact that ethane-methane mixtures can form both s-I and s-II hydrates, the complete heating curve is very complex in this case.

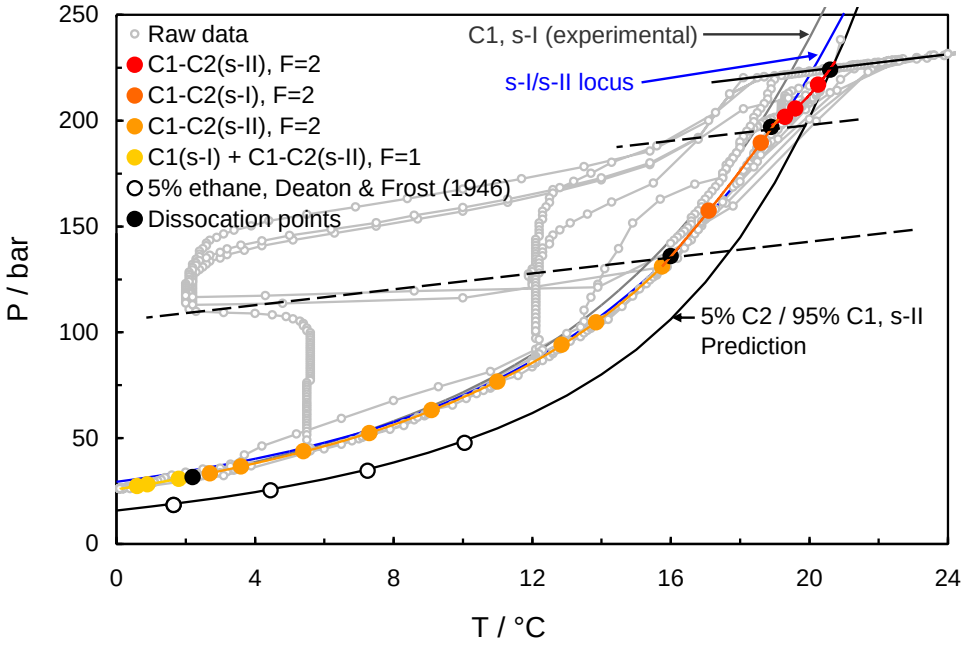

Figure 2-5 PT plot showing raw data and derived equilibrium points for measurement of hydrate dissociation conditions by isochoric equilibrium step-heating methods for a 5 mole% ethane/ 95 mole% methane system. Raw data points are every 5 minutes. Hydrate growth occurs readily within the hydrate region at low subcoolings and initial growth rates for the first small volume fractions of hydrate (e.g. first 50 bar pressure drop from the linear no hydrate Liquid + Gas baseline) are rapid.

Description of the CGI approach

Once KHI-free behaviour is established to an appropriate degree, the CGI procedure is performed by detecting hydrate growth and dissociation patterns in the presence of KHI (e.g. PVCap). For this purpose experiments were carried under three different scenarios:

1. No hydrate history
2. Hydrate history present
3. Hydrate present

No History: The phenomenon of hydrate 'history' - i.e. where the aqueous phase has recently hosted a solid hydrate phase - is known to cause hydrate to grow at lower degrees of subcooling when re-entering the hydrate stability zone (e.g. Sloan and Koh, 2008; Duchateau et al., 2009). While the real cause of history is yet to be fully understood, it is believed to be related to the presence of remnant crystalline water structures and/or excess gas solubility potentially associated with the latter. As found by Duchateau et al.(2009) history can be a very important factor in KHI behaviour as its presence can clearly reduce scatter in measured induction times.

Thus experiments have been conducted on 'history free' systems to compare with results for history and hydrate present (see below). To achieve this, systems are warmed to a high temperature (typically 20 °C above the phase boundary) for at least 2 hours before cooling to form hydrates. Based on experience and literature (Duchateau et al. 2008), this has been found to be more than sufficient to eliminate any history effects in previous induction time studies.

History Present: To determine hydrate growth patterns with history present, hydrates are typically formed initially at high degrees of subcooling, before the cell temperature is increased to induce complete dissociation. However, temperature conditions for dissociation are kept quite close to the phase boundary for the system (typically 3-6 °C higher at most, depending on hydrate structure), and the system is then re-cooled into the hydrate stability zone (HSZ) within 2 hours of complete disappearance of a detectable (from pressure drop) hydrate phase.

Hydrate Present: Testing KHIs with a hydrate phase already present represents the most challenging condition. In theory, under such conditions, there is no induction time as the critical nucleus has been exceeded and crystals with the potential to grow are already present. However, contrary to widespread belief, this does not mean a KHI will fail. To test for hydrate present scenarios, hydrates are similarly formed initially, typically at a high degree of subcooling, before the cell temperature is warmed to outside the HSZ to induce dissociation. However, prior to complete dissociation, with only a small fraction of hydrate remaining (<1 mass% of the aqueous phase, small pressure drop still remaining), the cell temperature is again reduced, bringing conditions back into the hydrate stability zone in preparation for a cooling run.

To circumvent the stochasticity associated with hydrate nucleation, the first step in CGI approach is to seed the system with hydrate ahead of cooling/hydrate formation tests runs which is very similar to the method used by Duchateau et al. (2009; 2010). For this purpose, hydrate is first formed at high subcooling, then the system is heated to dissociate the hydrate so that only a small but measurable fraction of water as hydrate (generally <0.5 mass% of water phase) is left in the system before cooling again into the hydrate region to observe growth conditions for various scenarios (e.g. constant rate cooling). Tests can also be performed with only 'history' present in the system through complete dissociation of hydrates while holding dissociation conditions close to the hydrate phase boundary to preserve hydrate history. However, as mentioned above since

having hydrate present in the system is the most challenging condition and also a hydrate present scenario has been found to give similar, but generally more repeatable growth patterns than hydrate history alone on re-cooling into the hydrate region, most of the tests are done under this scenario.

Figure 2-6 shows a liquid + gas (methane with 0.5 mass% Luvicap Bio + 1.5 mass% 2-butoxyethanol) initial cooling run with no hydrate present in the system. As illustrated in the figure, a linear 'no hydrate' PT relationship is observed upon cooling until hydrate formation which is detected at ~ 1 °C / 70 bar through the sudden pressure drop. This linear relationship forms the baseline for calculation of the pressure change due to hydrate formation, ΔP_h, and from that the amount of hydrate present during various test stages. The small pressure rise after some hydrate formation is related to ice formation which can occur when working near the ice point and is best to be avoided as it can cause blockage of/put strain on stirrers etc.

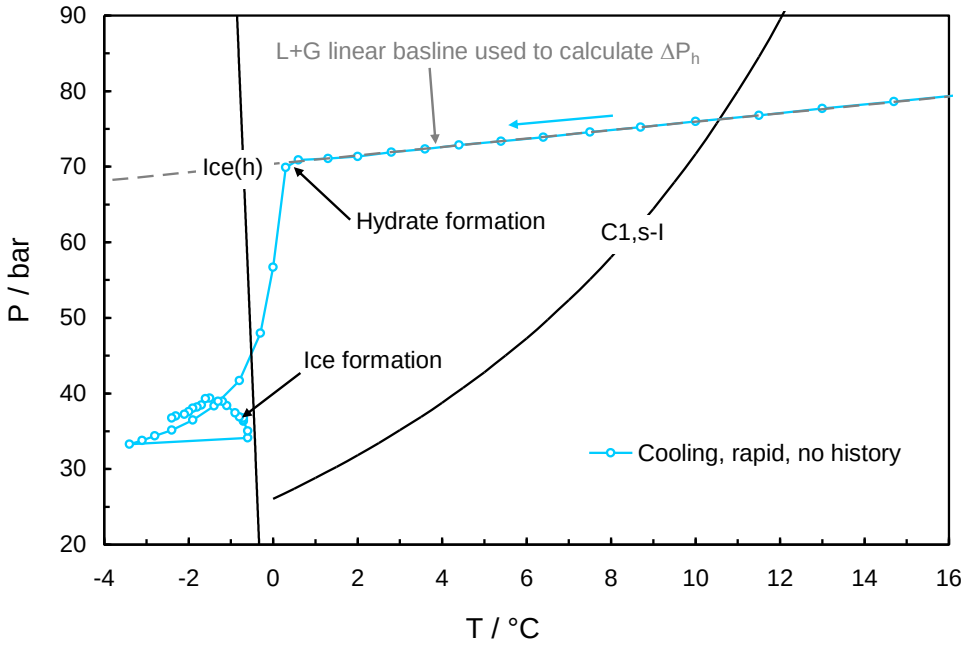

Figure 2-6 An example (methane with 0.5 mass% Luvicap Bio + 1.5 mass% 2-butoxyethanol) CGI method initial cooling run without any hydrate. Points are every 5 minutes.

After hydrate formation in the initial run, the system should be heated so that most of the hydrate is dissociated until only a very small fraction remains in the system (typically < 0.5% of water converted but this will be discussed in more detail in Chapter 3 as some KHIs are highly sensitive to the fraction of aqueous phase converted to hydrate). As found by Habetinova et al. (2002) and Svartaas et al. (2008) KHI exposed hydrates dissociate at slower rates and the dissociation temperature is clearly displace hence in KHI present systems one can define a slow dissociation region (SDR). So

while dissociating the hydrate the other goal is to establish the extent of this region. Finding this region is important both with respect to KHI usage in production operations (e.g. if plugging does occur) and with respect to CGI lab test planning as it can govern what temperature can be set to reduce the time needed to dissociate most of the hydrate whilst ensuring not all hydrate (or history) is lost.

Figure 2-7 shows a step by step heating of the previously formed hydrate which clearly demonstrates the abnormally slow dissociation (heavy clustering of points) at each step, confirming SDR conditions. Based on this information, the extent of the slow dissociation region can be determined.

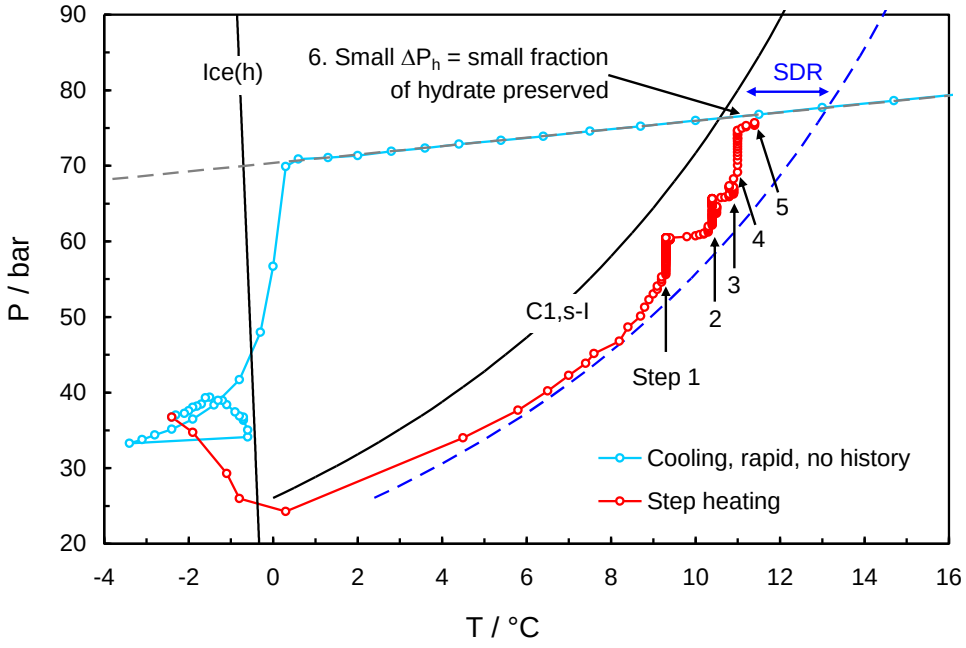

Figure 2-7 An example (methane with 0.5 mass% Luvicap Bio + 1.5 mass% 2-butoxyethanol) CGI method dissociating hydrate to preserve a small fraction of hydrate and establish the SDR region. Points are every 5 minutes.

Once the target for remaining hydrate fraction is achieved, the cell temperature is cooled again, this time at a constant rate (1 °C / hr experienced to be as a very productive cooling rate for detecting all changes) to follow the hydrate growth behaviour inside the hydrate phase boundary in a KHI present system. By comparing this system to a KHI free system (Figure 2-5) it is clearly evident that phase behaviour is quite different in the presence of aqueous KHI polymers. Figure 2-8 shows four repeat constant cooling rate 'with hydrate' present runs for methane with 0.5 mass% Luvicap Bio + 1.5 mass% 2-butoxyethanol. As can be seen, both runs show very good repeatability and interpretation is relatively straightforward. Unlike the simple methane-water system in which crystal growth on re-cooling into the HSZ immediately starts and follows the

phase boundary, it seems completely inhibited up to a certain ΔT_{sub} before crystal growth is clearly detectable from the deviation of the cooling curve from the linear 'no hydrate' baseline. The figure illustrates that at a subcooling of ~−4.2 °C, growth begins in earnest. The growth rate then increases as subcooling increases before picking up markedly at a subcooling of ~−5.2 °C (a common subcooling for CGI boundaries relative to s-I stability). Following this, PT conditions return to and follow the obvious CGI boundary at ~−4.2 °C. From these runs we can thus determine a rapid failure region(RFR) where obvious polymer controlled growth can no longer be observed as growth rate acceleration is observed as soon as PT conditions reach the boundary of this region. Also a region in which slow but detectable hydrate growth occurs can be defined as the reduced (slow/medium) growth rate region (RGR). Data clearly suggest that in this system the KHI shows very good performance up to the RGR at ΔT_{sub} = ~–4.2 °C (from the s-I methane boundary) and moderate performance up to RFR at ΔT_{sub} = ~–5.2 °C. However, the exact nature of the region preceding the boundary at ~−4.2 °C subcooling cannot be fully understood (whether there is very slow growth or complete inhibition) and needs to be examined in more depth.

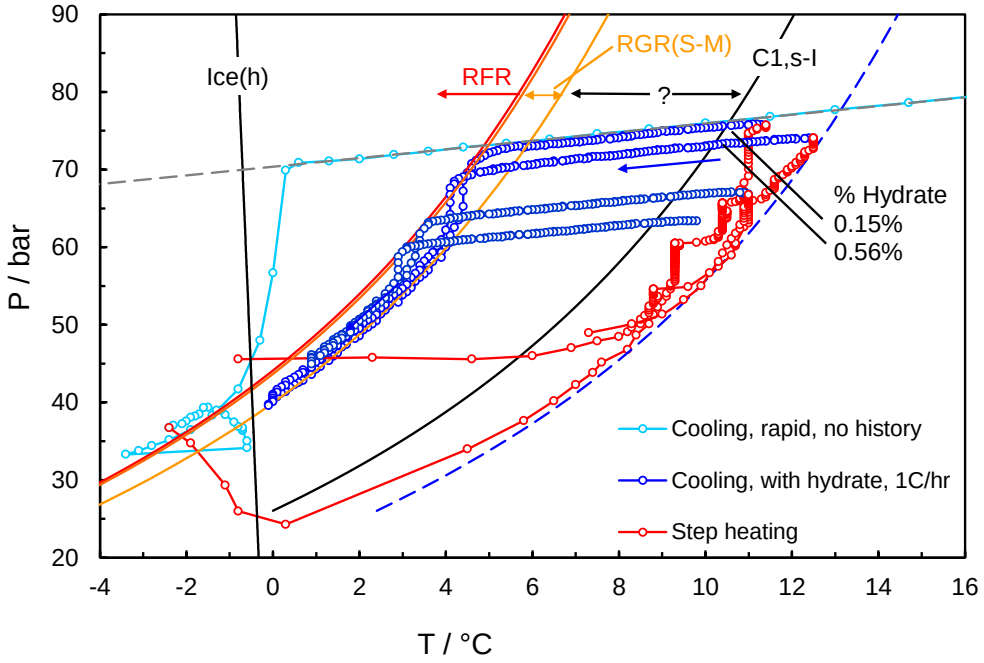

Figure 2-8 An example (methane with 0.5 mass% Luvicap Bio + 1.5 mass% 2-butoxyethanol) CGI method cooling curve at constant cooling rate 'with hydrate' present to determine RGR and RFR. Points are every 5 minutes.

Therefore, although as will be discussed in more detail there are other features in system behaviour observed during constant cooling (ΔP_h reduction) and heating (abnormally early dissociation) runs that can indicate complete hydrate inhibition in this region, for definitive confirmation of this behaviour cooling run is done stepwise rather than

continuous cooling at constant rate. The procedure for preparing for a step-cooling run is identical to that for constant cooling in that hydrate is first formed – typically as part of a previous constant cooling run – then mostly dissociated by step-heating to leave only a small fraction remaining (< 0.5% of water as usual). The temperature is then reduced in steps, with the system held at a particular subcooling/temperature step for 24 hours (although for definite interpretation, in preliminary experiments hydrate had been kept at temperatures inside the hydrate phase boundary for up to 3 weeks) and behaviour observed.

Figure 2-9 shows step cooling data for the example system compared to CGI regions established so far. Figure 2-10 shows temperature difference from the hydrate phase boundary (ΔT_{sub}) subcooling from the hydrate phase boundary and change in pressure due to hydrate formation (ΔP_h) as a function of time for the step cooling run.

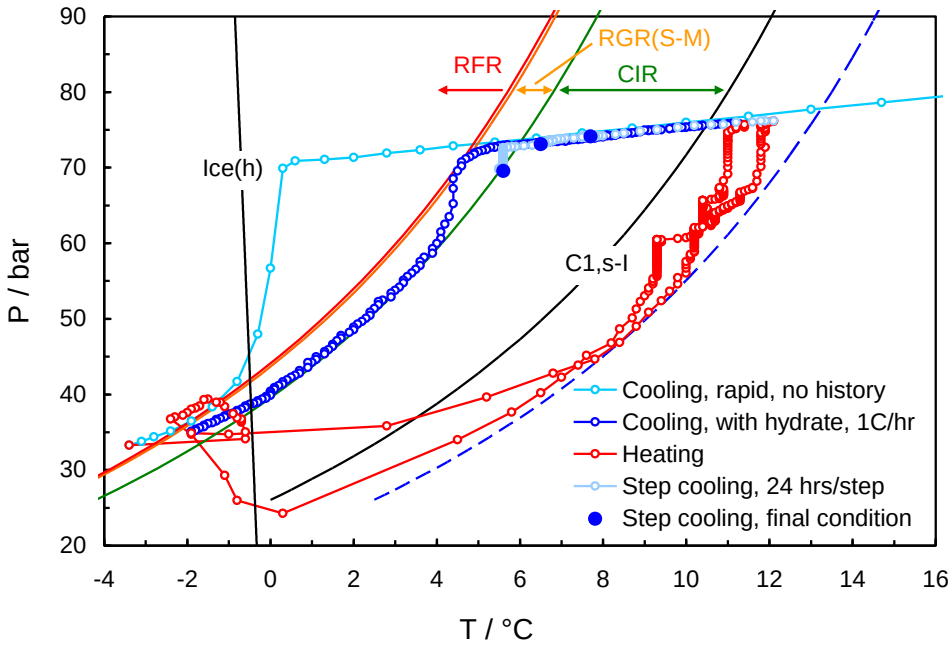

Figure 2-9 An example (methane with 0.5 mass% Luvicap Bio + 1.5 mass% 2-butoxyethanol) CGI method step-cooling 'with hydrate' present to determine CIR. Points are every 5 minutes.

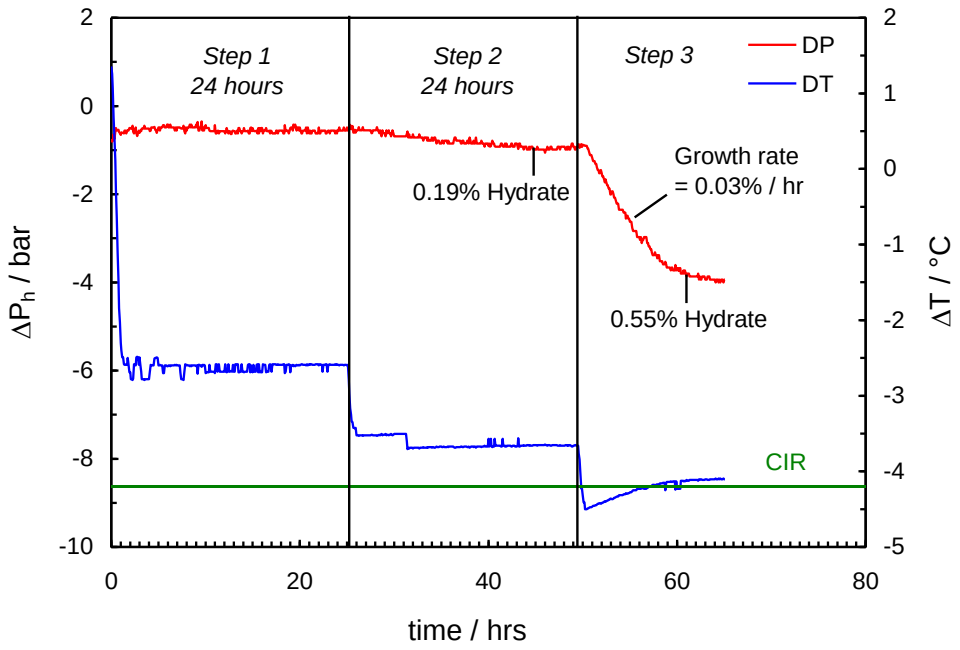

Figure 2-10 Changes of pressure and temperature with time in an example (methane with 0.5 mass% Luvicap Bio + 1.5 mass% 2-butoxyethanol) CGI method step-cooling 'with hydrate' to determine CIR.

As can be seen in Figure 2-10, the final PT point conditions after 24 hours at each step suggest pressure remained apparently constant until the temperature/subcooling was greater than the clear CGI boundary identified in constant rate cooling runs at ΔT_{sub} = ~–4.2 °C. After that, quite slow growth is seen. This pattern is clearly observable in Figure 2-9 and Figure 2-10. At step 1 (ΔT_{sub} = ~–2.6 °C), no increase in the amount of hydrate present (as indicated by ΔP_h) in the system was observed for 24 hours. At step 2 (ΔT_{sub} = ~–3.7 °C), as occasionally occurs, a very slight increase in ΔP_h suggests hydrate might have attempted to grow/reconfigure due to the sudden change in temperature, but then this clearly stops and pressure again stabilises, with even a slight possible increase (indicating slight dissociation) around the time the next step is initiated. At the final step (ΔT_{sub} = ~–4.5 °C initially), growth is clear and continuous, as shown by a steady increase in ΔP_h with time. Thus, data support that for the first two steps, inhibition is complete, with growth only occurring when the CGI boundary at ΔT_{sub} = ~–4.2 °C is surpassed. This is further supported by behaviour at the last step; as hydrate grows and pressure falls, so does the degree of subcooling. This brings conditions back towards the ΔT_{sub} = ~–4.2 °C boundary. As shown in Figure 2-10, this causes growth to slow down and stop as the CIR is re-entered, supporting the conclusion that in this inhibition zone (CIR), irrespective of whether there is history or hydrate already present in the system, no hydrate growth occurs apparently indefinitely.

Subsequent to detecting this behaviour of hydrates in the presence of KHIs, it is necessary to interpret and define each of the mentioned regions to develop a standardised CGI region description.

Interpretation of CGI Data for CGI Regions: Further Discussion

Different crystal growth inhibition regions are described in more detail in the following section.

Defining CGI Regions

While CGI boundaries are quite commonly clear, behaviour within some regions is more difficult to define as they are based on *relative growth rates*, i.e. in comparison with a KHI free system. The primary problem lies with the reduced growth rate region (RGR) as the CIR and RFR are not in theory rate dependent; the CIR means zero growth while the RFR means growth rates are effectively the same as they would be if no KHI was present. However, for the RGR, growth rates might be mixing rate dependent for example.

Based on studies undertaken throughout this thesis particularly the emerging close correlation between growth rates and exponential-type induction time trends a simple logarithmic-type definition for RGR regions was defined (see Table 2-1) and subsequently employed throughout the project. The important thing to note is that growth rates in Table 2-1 assume good mixing of fluids.

Table 2-1 CGI regions and respective growth rates times. RGR rates are based on the assumption the system is non-static and well mixed.

Region	Hydrate Growth Rate	%Aqueous Phase Conversion Rate
CIR	Completely inhibited	Completely inhibited
RGR(VS)	Very slow growth (VS)	$\leq$ 0.1% / hr
RGR(S)	Slow growth (S)	> 0.1% to $\leq$1.0% / hr
RGR(M)	Moderate growth (M)	> 1.0% $\leq$10.0% / hr
RFR	Rapid/fast	> 10.0% / hr or as for no KHI present

Throughout this thesis percentage of water converted into hydrate is calculated through the pressure drop due to hyrate formation. Changes of pressure at a certain temperature represents the number of moles of gas transferred from the gas phase into the liquid phase which mainly happens due to the formation of hydrate (changes of pressure due

to gas solubility are negligible in a system at constant temperature). Moles of water converted into hydrate can be calculated through moles of gas converted (stoichiometry of moles of water and gas in a single hyrate crystal are known based on the type of hydrate structure formed). Hence, in all the tests percentage of the total initial water converted into hydrate can be easily calculated through detection of pressure changes.

For a clear understanding and distinction of these regions, each region is explained and described in more detail.

Distinguishing the CIR

The Complete Inhibition Region (CIR) – a key region of KHI performance – can be the sometimes the easiest or the most difficult to definitely distinguish. The CIR is defined by three basic properties:

- Infinite induction time (at least up to the tested periods)
- No crystal growth (up to a hydrate fraction related to KHI type and concentration)
- Potential abnormal hydrate dissociation within the normal thermodynamic stability region

In terms of induction time, the problem with using such an approach to define KHIs is the probabilistic nature of nucleation; it is impossible to predict *t*i. For example, in the case of a sample which shows a very long induction time during a test, the tester has no idea whether if they stop the experiment, they may being doing so just a moment before growth begins/*t*i ends. Furthermore, the large scatter commonly seen in *t*i data raises the concern that while three repeats might give, e.g. 12, 18 and 24 hours *t*i, the next could be only 2 hours; the chance is low, but there is still in theory a probability that this will occur (Section 2.5). In the case of the CIR, the first of the above points means it is impossible to determine from *t*i data; the tester has no idea how long to wait as the possibility that growth might occur at some point if enough time is given can't be ruled out.

As for no crystal growth detection alone – no sign of growth of existing hydrates – of course suffers somewhat the same problem as induction time measurements; maybe the growth is very slow and if the tester waits long enough, it will be observed. However, for the CGI test approach recommended here, with hydrate already present in a system

(e.g. at < 0.5% of water converted) and high sensitivity (e.g. 0.05% water conversion detectable), if a long time limit – e.g. ~24 hours is set – then it is almost irrelevant as to whether slow growth occurs in the longer term as for practical purposes a < 0.05% change in water as hydrate over one day is hardly likely to present a problem given the generally much shorter residence times of pipeline fluids in the hydrate region. Furthermore, there should be on most occasions (given that line fluids typically cool from high temperatures so have no hydrate history) a very long induction time (e.g. > 24 hours) before this slow growth rate is even permitted. Thus, even though there may be cases where a true CIR is difficult to completely confirm, this can be safely assumed for practical purposes based on CGI results.

The most obvious feature which can definitely distinguish the complete inhibition region is when hydrate dissociation is observed within the thermodynamic stability region. An example is shown in Figure 2-11 for methane with aqueous PVCap; after forming hydrate, upon heating, rather than pressure continuing to fall towards the phase boundary, on re-entry to the CIR, a large proportion of the hydrate present dissociates. This behaviour does not always occur and is most often observed upon heating following initial rapid hydrate formation at high subcoolings, although it is not uncommon when subsequently re-cooling at a constant rate as part of the CGI general test procedure. Figure 2-12 illustrates a condition in which the pressure drop associated with hydrates (ΔP_{hyd} for hydrate present runs) actually reduces on cooling within the CIR region, showing that hydrate (preserved from a previous growth-dissociation cycle) can actually dissociate within the CIR zone, even though it should be thermodynamically stable. Clearly, if hydrate is dissociating at a specific PT condition, then growth would not be favoured and such behaviour has been found as ubiquitously supportive of CIR conditions in tests performed in this project. (Reasons speculated for this behaviour will be discussed in more detail in Chapter 3).

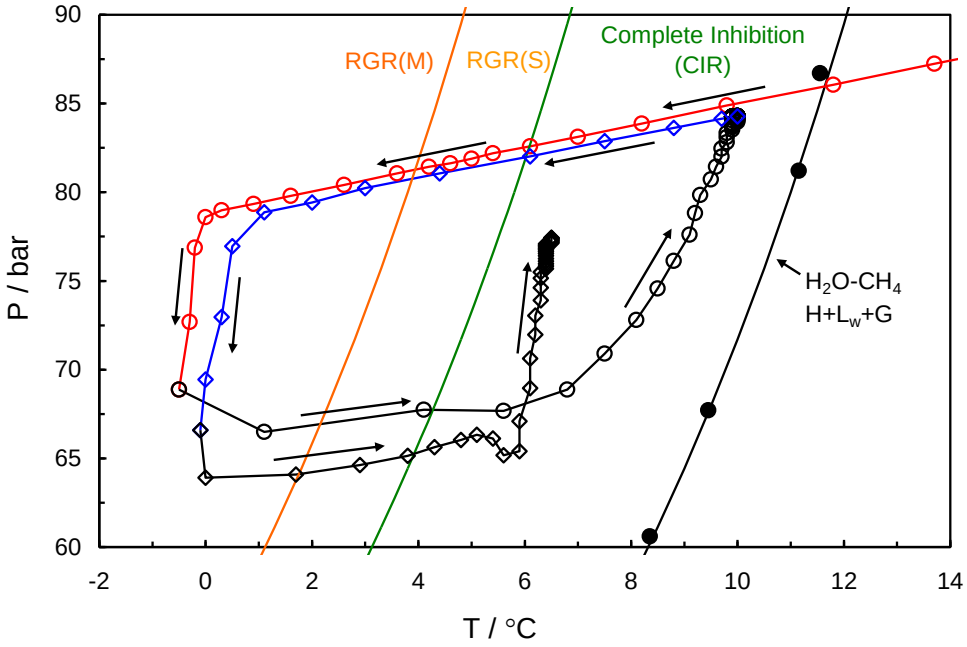

Figure 2-11 plot showing example of polymer induced hydrate dissociation within the hydrate stability zone under KHI complete inhibition conditions CIR). System is methane with 0.5 mass% PVCap aqueous.

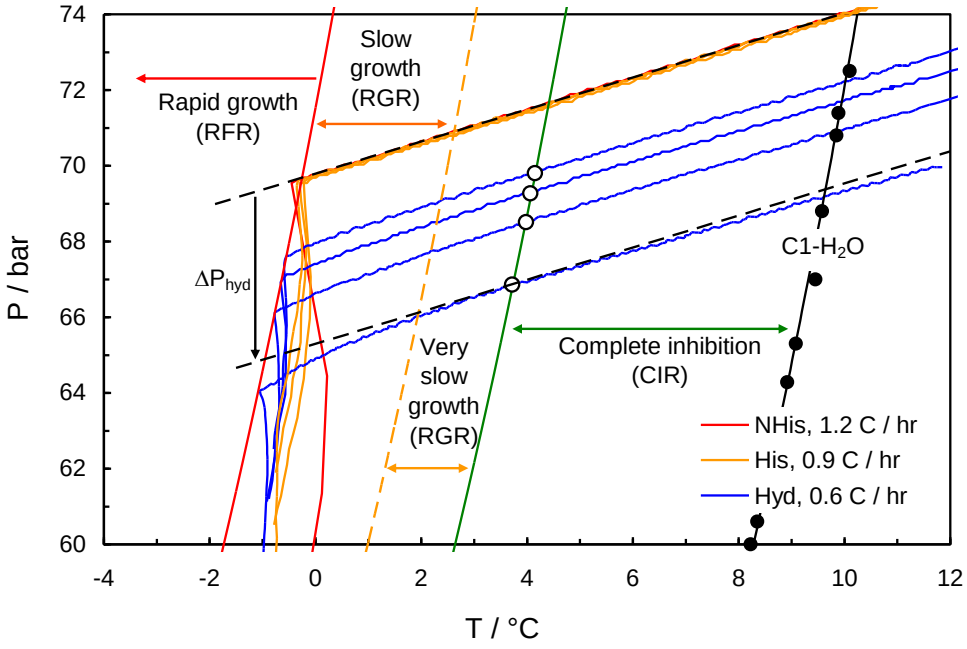

Figure 2-12 PT plot showing example of polymer induced hydrate dissociation within the hydrate stability zone during 'with hydrate' constant rate cooling run under KHI complete inhibition conditions CIR). System is methane with 1.0 mass% PVCap aqueous.

Distinguishing the RGR and RFR

Reduced Growth Rate region (RGR) and Rapid Failure Region (RFR) are relatively straightforward to identify from repeat constant cooling rate runs with small fractions of hydrate present. In the RGR, hydrate crystals can grow, but at a rate measurably slower than they would in the absence of a KHI whereas in the RFR, growth rates are close to

or the same as they would be in the absence of a KHI, which at high subcoolings (e.g. for well performing inhibitors) is generally rapid.

The RFR line essentially delineates the region where an 'induction time' may occur, but as soon as hydrate forms, growth is rapid/catastrophic until the RGR/CIR are re-entered. As can be seen, for hydrate or hydrate history present, immediate and rapid failure (rapid pressure drop as gas is consumed) occurs as soon as conditions reach this line on cooling (Figure 2-12). If no history is present, and cooling rates are rapid (e.g. > 1.0 °C / hr), failure may occur at a subcooling (few °C) within the RFR (thus a short induction time could potentially be measured). However, as shown in Figure 2-12, if cooling is moderate or very slow, even with no history, sudden and rapid hydrate growth always occurs at this line for this system. Figure 2-12 clearly demonstrates that this feature, the RFR, is consistent and repeatable no matter the fluid history, the region boundary being at apparently fixed subcooling as a function of pressure (will be further confirmed in future chapters). Also as illustrated in Figure 2-13 and will be discussed further in Section 2.5 the RFR is clear from behaviour following an induction time; growth is rapid until the RGR/CIR are re-entered.

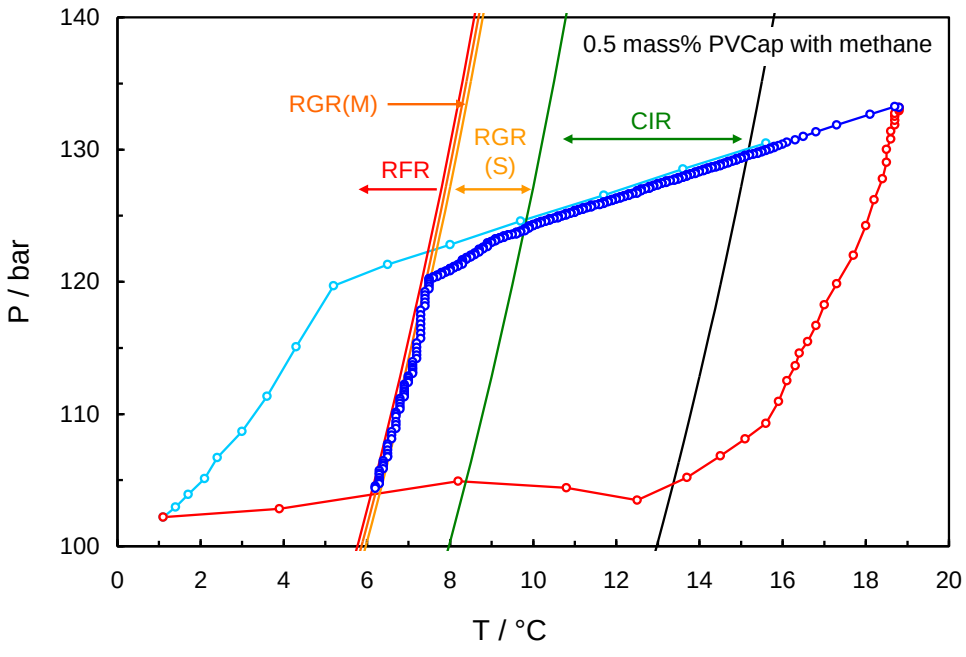

Figure 2-13 Pressure versus temperature data for methane with 0.5 mass% PVCap showing identification of the RFR/RGR(S)/RGR(M) from a constant cooling rate run. Points are every 5 minutes.

The transition from CIR to RFR is marked by ΔP_{hyd} starting to increase in the RGR, i.e. hydrate growth is beginning in earnest. In Figure 2-12, this is most apparent in the cases where hydrate is present, although if cooling rates are slow enough, detectable growth

will also occur in the RGR if only history is present. As can be seen in Figure 2-12, the growth rate within the RGR is dependent on the fraction of hydrate already present; the run with the largest initial fraction of hydrate (largest initial ΔP_{hyd}) on cooling showing the greatest increase in ΔP_{hyd} upon cooling through the RGR. Based on hydrate growth rates in the RGR it may be further subdivided, into very slow growth RGR (VS), slow RGR(S), and moderate RGR (M), growth rate zones (will be discussed in more detail in Chapter 3).

As shown in Figure 2-13, the onset of slow growth RGR(S), then subsequent change to medium growth rates RGR(M) is clear from constant cooling rate curves with hydrate present.

In Figure 2-14, RGR(S) and RFR conditions can be detected from constant cooling rate curves, however a step cooling run was required to distinguish very slow growth RGR(VS) from complete inhibition (CIR).

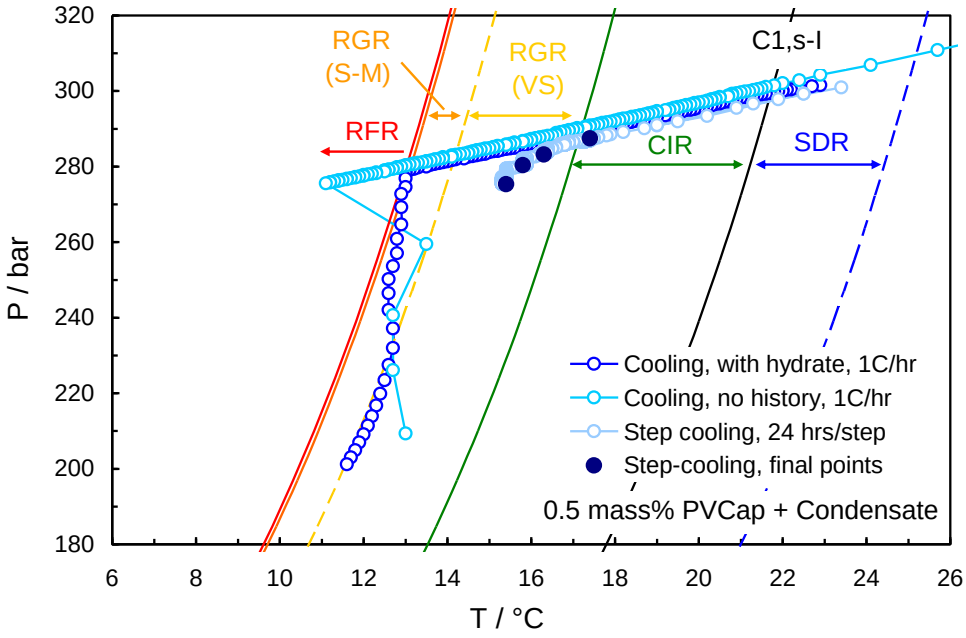

Figure 2-14 Pressure versus temperature data for methane with 0.5 mass% PVCap and real condensate showing identification of the RFR/RGR(S-M) from constant cooling rate runs and the CIR/RGR(VS) from step cooling. Points are every 5 minutes.

Moreover, in the RGR region, various evolutions in growth rates and patterns may be observed. For example, in Figure 2-14, as hydrate forms initially at the RGR(M)/RFR boundary, PT conditions then retreat to lower subcoolings as the hydrate fraction increases before following a further CGI boundary at a lower subcooling as illustrated. KHI systems are very complex and as such subtle differences will always mean a degree

of flexibility in definition is required for the RGR, i.e. the goal should be to describe behaviour as well as possible from what is observed, e.g. “slow growth up to X% hydrate, then rapid growth”, “slow growth up to X% hydrate then moderate growth”.

Ultimately, in terms of performance at operating conditions, results have suggested that operating within the CIR can be considered ‘safe’, operating within the RGR for time periods which are less than the induction time should also be safe, but operating within the RFR is likely to pose a significant risk as if hydrate nucleates; growth is apparently largely polymer-uncontrolled with growth rates similar to KHI free systems.

As a result, to evaluate the performance of KHIs each of these boundaries has to be measured and based on the extent of these regions, the hydrate inhibition properties of KHIs can be evaluated. The larger these boundaries, specially the CIR, the better and more effective KHIs are in inhibiting hydrate growth.

2.4. Confirming Repeatability of Results with the New Approach Using Different Set-ups: Rocking Cell & Autoclave Comparison

As described in Section 2.3 experimental set-ups used to develop the new CGI approach and employ to assess the effects of various parameters on KHI performance have been high-pressure stirred autoclaves. However, previous literature studies have reported quite different KHI performance results for different set-ups at least in terms of induction times (e.g. Klomp, 2008).

However, using the new approach it was found that results were completely repeatable in different autoclave set-ups. Also, based on the current understanding that crystal growth inhibition (CGI) patterns are thermodynamically driven (by polymer crystal surface adsorption), it was assumed that results using the new method should be no different in totally different set-ups like rocking cells than they are in autoclaves so long as the correct methodology is followed.

Therefore, to confirm suitability of other set –ups such as rocking cells for applying the new CGI approach, CGI studies for methane with aqueous PVCap were carried out in a standard rocking cell to compare with autoclave results.

2.4.1. Experimental equipment and set-up

Experiments were carried out on a 300 ml, high pressure (up to 690 bar), titanium rocking cell illustrated in Figure 2-15. Temperature control and pressure measurements were done using very similar apparatuses and techniques to high pressure stirred autoclaves explained in Section 2.3.1. Similar to an autoclave system temperature measurements were determined by a platinum resistance thermometer (PRT, ± 0.1 °C) which was connected to a computer for direct acquisition, but this time due to the equipment design could not be in direct contact with cell fluid and was placed inside the cooling jacket surrounding the cell.

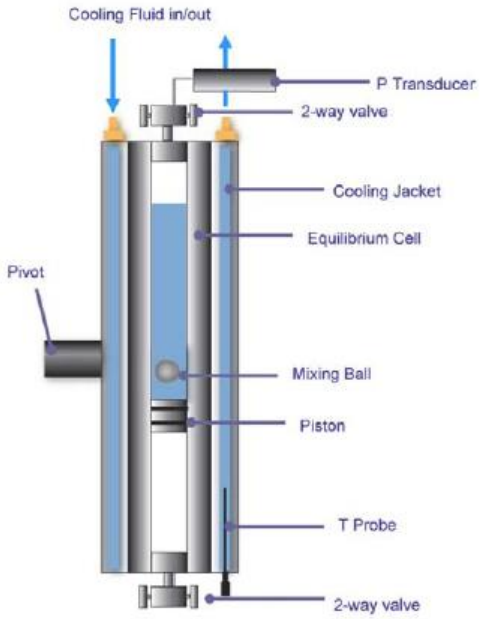

Figure 2-15 Schematic Illustration of the high pressure (max 690 bar), 300 ml (when piston fully retracted) high pressure rocking cell used in experiments. The cell is rocked fully through 180°, typically once every 30 seconds or more.

The main difference between a high pressure autoclave and rocking cell is the mixing. In a rocking cell, mixing is done using mixing balls with the cell rocked fully through 180°, typically once every 30 seconds or more.

As mentioned earlier in this chapter ultra high purity grade methane gas used was 99.995%. Also deionised water was used in all tests. The PVCap used was a lower molecular weight Luvicap-MEG base polymer (average MW = 4000-8000) supplied by Champion Technologies, with the mono-ethylene-glycol solvent removed by oven drying. For these experiments, 0.5 mass% PVCap aqueous was prepared in deionised water. In line with the autoclave CGI methodology, aqueous phase was ~80% of cell volume.

The experimental procedure explained as the new CGI technique was employed in these tests. Hence after determining the KHI free phase boundary, each step was performed to establish different CGI regions for this system. Results for this system are then compared to the same system tested in an autoclave to conclude on the repeatability of results in different experimental set-ups using this technique. Results presented here for 0.5 mass% PVCap aqueous tested in an autoclave are from experiments described in detail in Chapter 3.

2.4.2. Results and Discussion

Figure 2-16 shows example CGI method cooling curves and interpreted CGI regions for 0.5 mass% PVCap aqueous with methane in the rocking cell in comparison with autoclave data for the same pressure. Also, Table 2-2 details average PVCap induced inhibition region subcooling extents for 0.5 mass% PVCap (same PVCap sample / AMW) with methane systems in the rocking cell and stirred autoclave at ~85 bar (average of more than 5 runs for measuring CGI regions in each set-up with ±0.5°C deviation). As can be seen from both the figure and data in the table, the results for the rocking cell and autoclave are almost identical within experimental error (±0.5 °C). In both systems, CIR which is the key for evaluating KHI properties in CGI studies is ~–5.2 °C. Also for both systems, for RGR(S-M) ΔT_{sub}= ~ –7.3°C , for RGR(M)-RFR ΔT_{sub} = ~ –9.6°C and for SDR ΔT_{sub} = ~ 4.0 °C.

Table 2-2 Comparison of experimentally determined CGI region ΔT extents for methane with 0.5 mass% PVCap aqueous at ~85 bar in autoclave and rocking cell experiments. Regions are indistinguishable within experimental error.

	ΔT_{sub} RGR(M) -RFR / °C	ΔT_{sub} RGR(S-M) / °C	ΔT_{sub} CIR -RGR(S) / °C	ΔT_{sub} SDR / °C
Rocking Cell	−9.5	−7.9	−5.2	4.2
Autoclave	−9.6	−7.3	−5.2	3.9

The only difference observed in data is due to an experimental artefact; namely that the rocking cell probe is in the cell jacket, rather than fluids. This means that the recorded temperature can deviate from actual fluid temperature during fast heating/cooling. This is evident for example at the beginning of rocking cell heating steps in Figure 2-16; while they show slow dissociation patterns just like the autoclave data; the latter track the SDR boundary more closely as ‘true’ cell temperature is being recorded. In the rocking cell case, the jacket temperature outpaces cell temperature, resulting in the

observed lag. This also can occur on rapid cooling, giving an apparent non-linear convex liquid + gas relationship, but is wholly equipment related. Such an issue is generally eliminated simply by lowering heating/cooling rates if required.

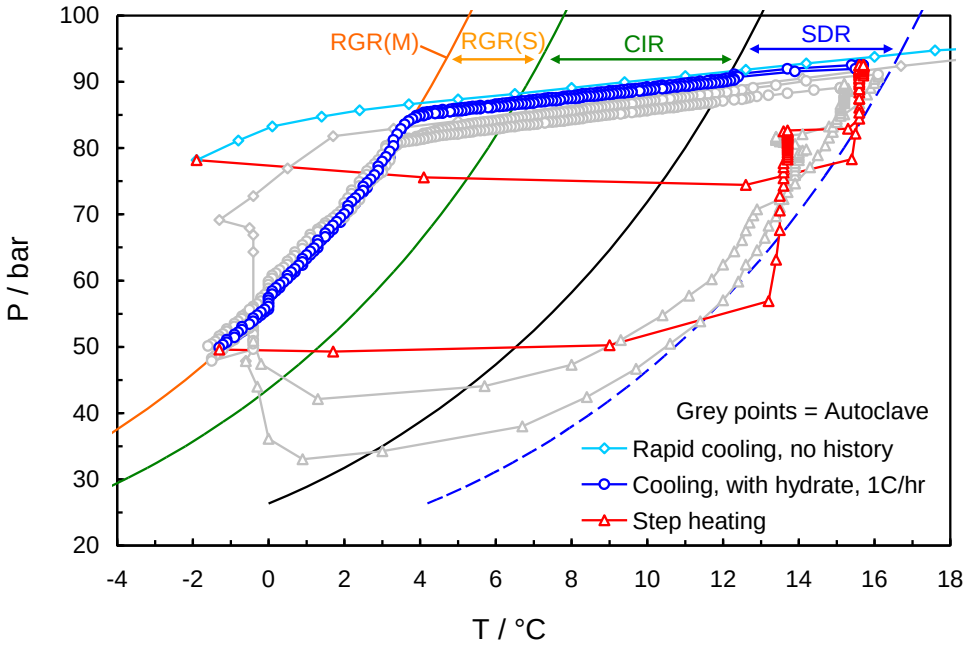

Figure 2-16 Comparison of example CGI cooling and heating runs for 0.5 mass% PVCap aqueous with methane in the rocking cell and standard autoclave.

Results are identical with the exception of some temperature probe positioning artefacts.This result supports the theory that CGI regions are primarily thermodynamically driven and thus results are fully repeatable and transferrable between different types of equipment assuming good mixing and appropriate methodology as outlined in Section 2.3.

2.5. Correlation of Crystal Growth Inhibition Patterns with Induction Times

As mentioned at the beginning of this chapter, induction time, t_i, has remained the industry standard for evaluation of KHIs and has been central to the concept of how KHIs prevent gas hydrate problems, i.e. by inhibiting nucleation longer than the residence time of pipeline fluids within the HSZ. However, due to the inherent stochastic nature of nucleation, robustly quantifying KHI performance with confidence through t_i measurements is time consuming and, without a large quantity of data, confidence may not be high.

Moreover, from CGI studies, KHI polymers - rather than being solely 'nucleation delayers' - induce a number of highly repeatable, well-defined hydrate crystal growth inhibition regions as a function of subcooling, hence may be better described as crystal growth inhibitors/modifiers.

Results also suggest that for many laboratory experimental conditions, measurement of a 'real' induction time is not physically possible, as will be detailed in this section.

2.5.1. Experimental Methods and Materials

All experiments were carried out on 300-500 ml standard high-pressure stirred autoclaves, identical to the ones described for CGI tests, lying horizontally with 80% volume filled with aqueous phase. Rate of mixing was also set to a similar speed as the experiments described for CGI technique at around 750 rpm. To remove hydrate history, following each run, cell temperature was raised to at least 20 °C above the thermodynamic phase boundary for the system and held there for minimum 2 hours. Temperature was then reduced as rapidly as possible to the set point; typically at a rate of ~12 °C/hr. The induction time, t_i, was defined as the length of time when the temperature was at within ±0.2 °C of the set point temperature during which no detectable (from pressure drop at constant volume) hydrate growth was detected.

Similar to previous experiments, the KHI used in these tests is poly-nvinylcaprolactam (PVCap) supplied by BASF as Luvicap-EG base polymer (average molecular weight / AMW =~7000) with the ethylene glycol solvent removed by vacuum oven drying. Also, other chemicals used in these experiments were methanol (MeOH) with 99.5% purity, mono-ethylene glycol (MEG) with 99.5% purity and NaCl salt which was 99.5% pure. PVCap solutions were prepared gravimetrically using deionised water in all experiments. Ultra high purity grade methane gas (99.995% pure) supplied by BOC was used.

Evaluating the possibility of induction time within different crystal growth inhibition regions based on crystal growth rates was briefly carried out using a 0.5 mass% PVCap aqueous with methane which is tested in detail using the CGI technique (presented in Section 2.1)

Detailed induction time, *t*i, measurements were done for three different systems that were also examined using the new CGI approach (results of the CGI approach are

reported in relevant chapters) to develop a correlation between CGI patterns and induction time data. These were:

- 0.5 mass% PVCap aqueous with 5 mass% methanol (relative to water + PVCap)
- 0.5 mass% PVCap aqueous with 5 mass% NaCl (relative to water + PVCap)
- 0.5 mass% PVCap aqueous with 20 mass% MEG (relative to water + PVCap)

2.5.2. Possibility of Induction Time within Crystal Growth Inhibition Regions

In addition to determining polymer-induced crystal growth/inhibition regions for different systems it is important to focus on determining whether a 'real' induction time can be measured within each region depending on system properties; specifically whether there is hydrate or hydrate history present or not.

It is generally believed that while hydrates may form spontaneously even at very small degrees of subcooling, this may be delayed for very long periods even at high degrees of subcooling. However, the probability of having formed hydrates at a given time decreases with decreasing degrees of subcooling (Sloan and Koh, 2007). Also, studies have shown that due to the fact that at higher a subcooling there is a higher driving force for hydrate formation, induction time generally becomes smaller (Duchateau et al, 2009). As previously mentioned, in the presence of KHIs this trend is believed to remain the same but with an increase in the values of induction time. A simple illustration of this trend is shown in Figure 2-17.

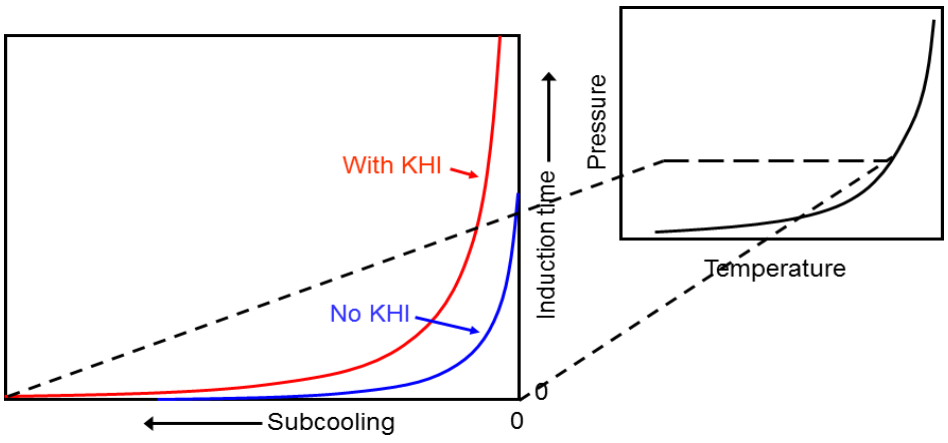

Figure 2-17 General understanding of induction time behaviour in relation to subcooling from the phase boundary in KHI free and KHI present system.

Prior to in depth experimental investigation of induction time in each region, interpretations on this data can be made based on the mentioned system properties and

also crystal growth rates in each region. Table 2-3 summarizes these results according to identified crystal growth inhibition regions which will be explained in more detail below.

Table 2-3 Results of investigations into whether an induction/hold time (t_i) can be observed in identified crystal growth regions depending on system properties for PVCap systems.

Initial condition	Zone	ti?	Reason
Hydrate	CIR	No	Crystal growth inhibited indefinitely
History	CIR	No	Crystal growth inhibited indefinitely
No history	CIR	No	Crystal growth inhibited indefinitely
Hydrate	RGR (All)	No	Growth begins immediately but rates slow due to polymer inhibition
History	RGR (All)	No	Growth begins immediately but rates slow due to polymer inhibition
No history	RGR (All)	Yes	But stochastic and behaves as for history/hydrate present when growth does begin
Hydrate	RFR	No	Growth occurs immediately, typically rapidly
History	RFR	No	Growth occurs immediately, typically rapidly
No history	RFR	Yes	Possible stochastic short ti just inside this region for rapid cooling rates. At higher subcoolings, fails instantly

As mentioned earlier in this chapter, in a well-equilibrated/mixed system, within the complete crystal growth inhibition region (CIR) hydrate growth is inhibited apparently indefinitely. Whether there is a history of hydrate or not, no new crystal growth occurs. Even if a small fraction of hydrate is present, further crystal growth is completely inhibited (no further growth of a small fraction of hydrate has been observed for over 21 days for systems tested to date). This means that an 'induction time' cannot be measured as a property of the system - hydrate never grows/'failure' never occurs. Effectively, t_i is infinite, thus is not measurable for a wide range of subcooling. It may

be that critical nuclei are formed; however these are apparently prevented from growing into viable crystals by the polymer.

Upon cooling into the RGR/reduced growth rate region, if hydrate or hydrate history is present, growth begins immediately though they may be very slow. This is shown in Figure 2-18 which illustrates changes in pressure due to hydrate formation (ΔP_{hyd}) as a function of time for 'no history' induction time measurement runs compared to a 'history present' run for a 0.5 mass% PVCap aqueous with methane system at −~6.2 °C subcooling (which lays within RGR(S) as will be shown in Section 3.1) and 70.3 bar. As can be seen, pressure drops of 1 psi / 0.07 bar over a number of hours are not unusual for higher polymer concentrations. Thus, under such conditions, induction time is again not a measurable property of the system, being effectively zero (or at least so small as to be considered so for practical purposes).

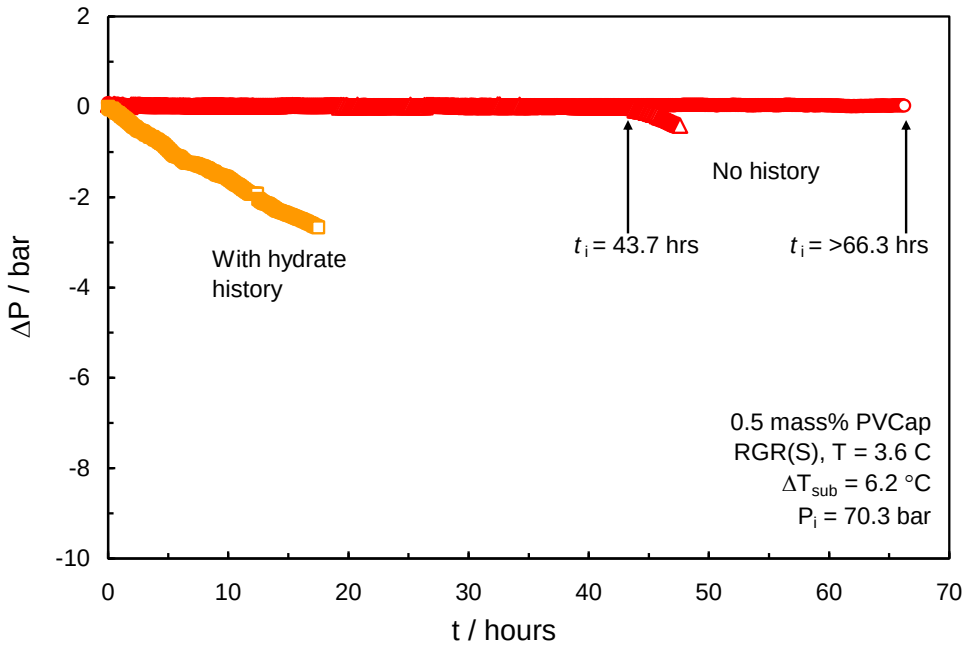

Figure 2-18 Plot of change in pressure due to hydrate formation (ΔP) as a function of time for 'no history' induction time measurement runs (red points) compared to a 'history present' run (yellow points) for a 0.5 mass% PVCap aqueous with methane system at 6.2 °C subcooling (RGR(S)) and 70.3 bar.

If no history of hydrate is present, initial results suggest a 'real' induction time is apparently possible in the RGR region and the RFR. However, as shown in Figure 2-18 and Figure 2-19 for a 0.5 mass% PVCap aqueous with methane at different subcoolings (offering both RGR and RFR conditions), results are, as is typical, quite stochastic; without history to provide nuclei, the system is subject to statistical probability and thus inevitable stochasticity (as found by Duchateau et al. 2009). In any event, when hydrate

growth finally begins, growth patterns are essentially identical to those seen for hydrate or history present conditions; these being proscribed by the current inhibition region (note very slow growth rates in Figure 2-18 and Figure 2-19 which are typical for these regions, as will be discussed in detail in Section 3.1).

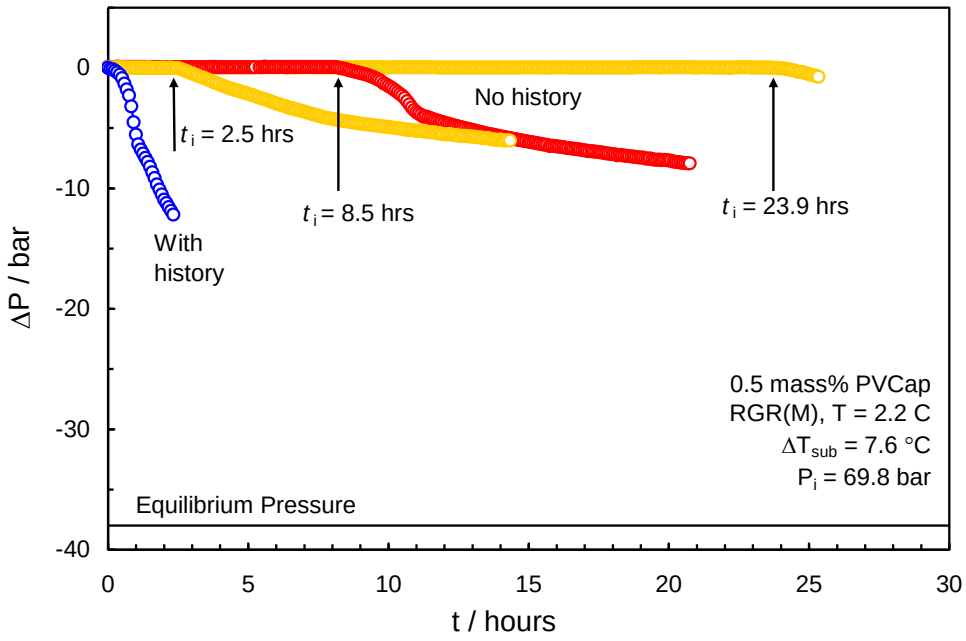

Figure 2-19 Plot of change in pressure due to hydrate formation (ΔP) as a function of time for 'no history' induction time measurement runs (orange/red points) compared to a 'history present' run (blue points) for a 0.5 mass% PVCap aqueous with methane system at 7.6 °C subcooling (RGR(M)) and 69.8 bar.

Based on the above interpretations it is concluded that the general belief that "the higher the subcooling the smaller the induction time", is true however in a system with KHI present the trend shown in Figure 2-17 is no longer valid since induction time inside CIR is indefinite. Hence there has to be a ΔT_{CIR} shift in the induction time verses subcooling curve in Figure 2-17 to represent this property of the system. This correction is applied and displayed in Figure 2-20.

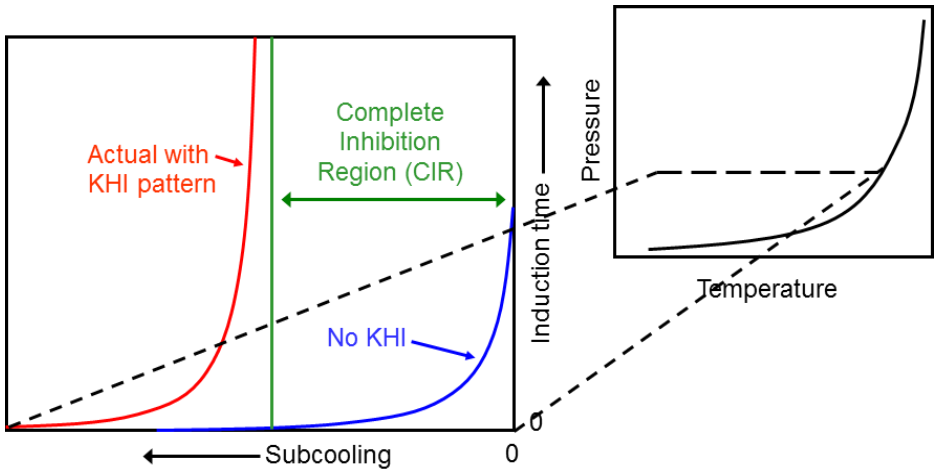

Figure 2-20 Real behaviour of induction time in relation to subcooling from the phase boundary in KHI free and KHI present systems.

In addition to these findings, appropriate induction time measurements were required to determine whether a true correlation can be established between crystal growth inhibition patterns and induction time data. For this propose, in this section, experiments were performed and analysed for three different systems (0.5 mass% PVCap aqueous + 5 mass% MeOH, 0.5 mass% PVCap aqueous + 5 mass% NaCl and 1.0 mass% PVCap aqueous + 20 mass% MEG) which are detailed below.

2.5.3. Detailed Induction Time Measurements

As detailed above, it was found that where an induction time does occur, the growth rate following nucleation reflects that expected for the CGI region; i.e. if nucleation occurs following an induction time in the RGR, growth will be slow. Likewise, growth following a *t*i in the RFR region will be rapid. Thus all evidence supports the fact that induction times/nucleation inhibition patterns are primary related to underlying crystal growth inhibition patterns, meaning the widespread assumption that *t*i is primarily related to subcooling (e.g. through the size of the critical radius) from the thermodynamic phase boundary is incorrect.

Figure 2-21 shows typical CGI pressure versus temperature data for *t*i measurement runs on a methane with 0.5 mass% Luvicap Bio + 1.5 mass% 2-butoxyethanol system (CGI regions illustrated in this graph are taken from experimental data measurements shown in Table 3.8). In this figure, induction time measurement runs within the RFR region are clearly displayed. As can be seen in this figure, PT data for *t*i runs support previously interpreted CGI region boundaries; once growth does occur, growth rates are rapid in the RFR, as expected then immediately slow down/begin to stall as PT

conditions re-enter the RGR/CIR region, i.e. the KHI begins to severely inhibit growth again (complete inhibition is not necessarily guaranteed as the volume fraction of hydrate is quite large following rapid growth).

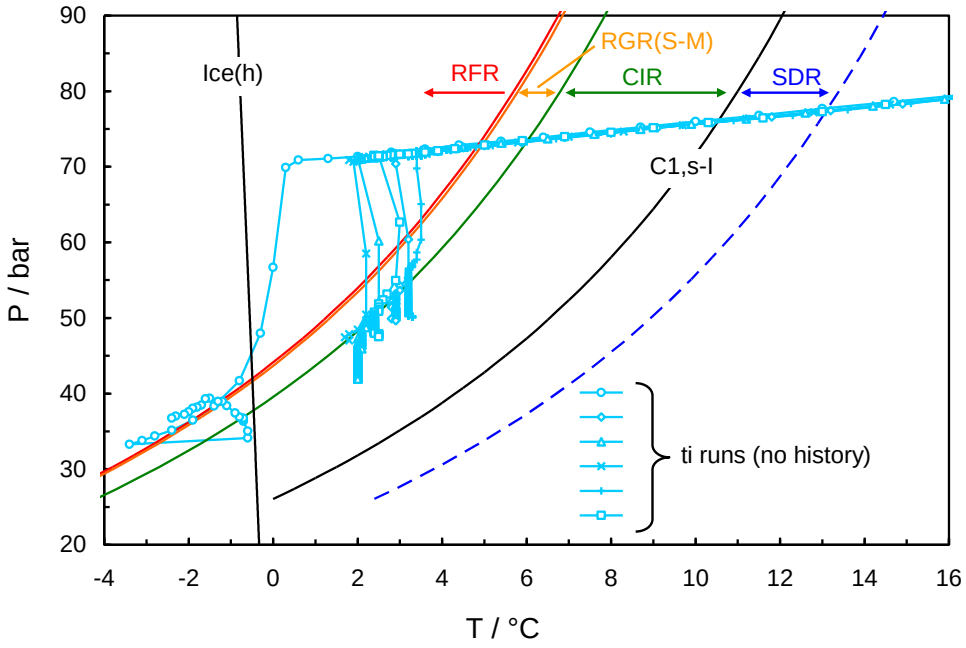

Figure 2-21 An example (methane with 0.5 mass% Luvicap Bio + 1.5 mass% 2-butoxyethanol) pressure versus temperature data for ti measurement runs (methane with 0.5 mass% Luvicap Bio + 1.5 mass% 2-butoxyethanol). Points are every 5 minutes.

Induction time data for three systems (0.5 mass% PVCap aqueous + 5 mass% MeOH, 0.5 mass% PVCap aqueous + 5 mass% NaCl and 1.0 mass% PVCap aqueous + 20 mass% MEG) are plotted as a function of subcooling in Figure 2-22 to Figure 2-24 respectively. In each figure, for better interpretation of the correlation between induction time data and CGI patterns, each CGI region is also indicated on the graph based on findings for each composition from CGI studies revealed in future chapters.

As Figure 2-22 to Figure 2-24 show, for all systems tested, induction times approach zero a few degrees inside the rapid failure region (RFR) and rise exponentially towards infinity over a very short temperature range in the reduced growth rate region (RGR). Approximate exponential lines have been drawn through *t*i points. It is also interesting to note that the closer these points get to the RGR or the further into the RGR they get, the more scattered they become. Hence, while not all points will sit exactly on this curve an approximate expected t_i trend can be pencilled, rising from zero towards infinity as the CIR is approached. Thus, from CGI regions alone it can be decided whether this KHI will be suitable for operating conditions. Also, the exponential rise towards infinity within the RGR clearly confirms CGI findings in that PVCap

completely inhibits hydrate nucleation/growth within the complete inhibition region (CIR); induction times being apparently infinite/not a system property in this region. These finding clearly match the interpretations in Figure 2-20 and confirms the ΔT_{CIR} shift of the exponential curve.

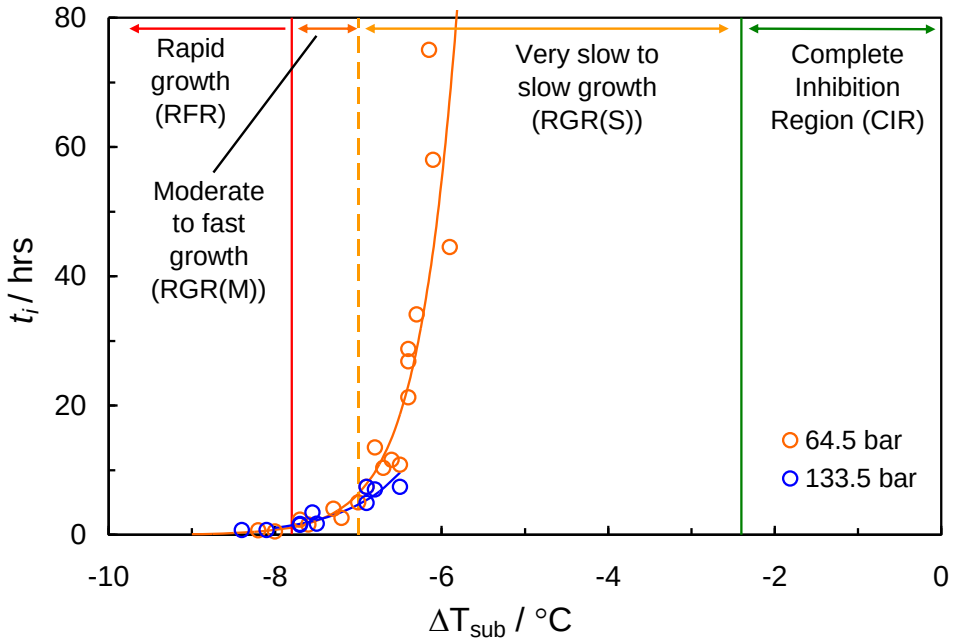

Figure 2-22 Plot of methane hydrate induction time versus subcooling data for 0.5 mass% PVCap aqueous with 5 mass% methanol (relative to water + PVCap) aqueous.

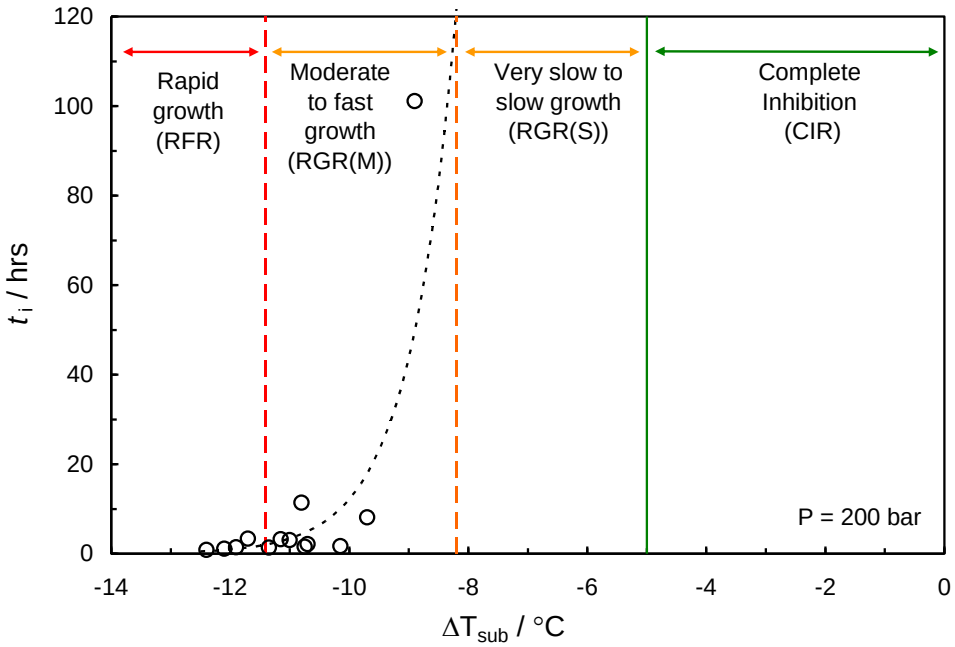

Figure 2-23 Plot of methane hydrate induction time versus subcooling data for 0.5 mass% PVCap aqueous with 5 mass% NaCl (relative to water + PVCap) aqueous.

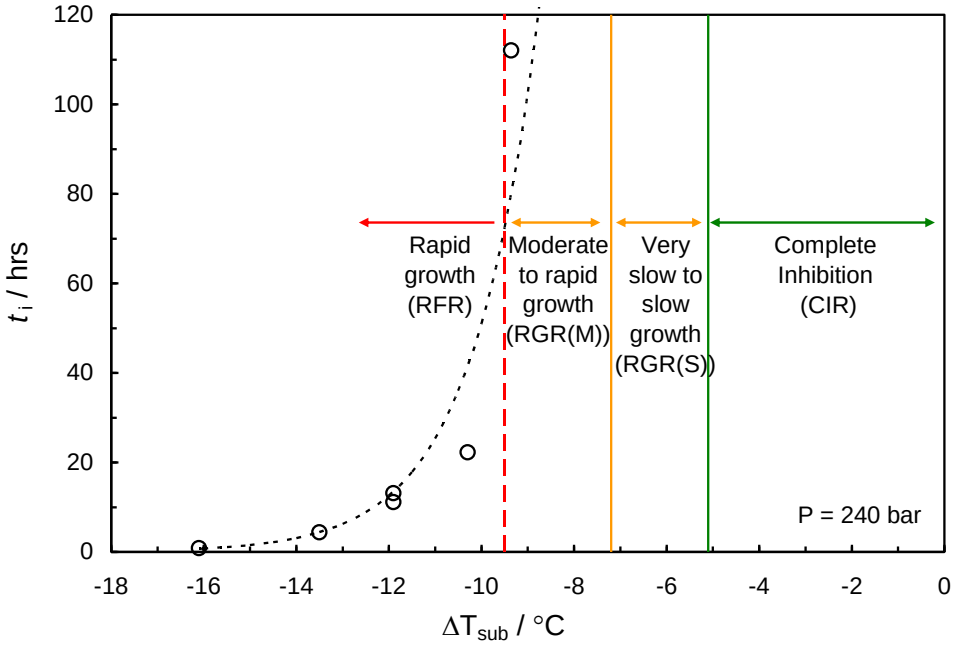

Figure 2-24 Plot of methane hydrate induction time versus subcooling data for 1.0 mass% PVCap aqueous with 20 mass% MEG (relative to water + PVCap) aqueous.

The fact that that t_i rapidly drops to zero within a few degrees of the RFR boundary proves that while a t_i is possible in this region, growth is always rapid when it does occur, hence operating in this region should be avoided.

To conclude, induction time measurements on a number of systems undertaken in addition to CGI region studies revealed good correlations between these parameters. These correlations can be summarized as:

- A true induction time can only be measured for a relatively short range of subcooling within the KHI-induced reduced growth rate (RGR) and rapid failure regions (RFR)
- It is impossible (at least within 21 days tested) to measure an aqueous phase hydrate nucleation induction time in the complete inhibition region, supporting CGI studies which show that hydrate growth seems inhibited in this subcooling range
- Evidence suggest that induction times/nucleation inhibition patterns are most likely related to underlying CGI regions, proposing that the widespread assumption that *t*i is simply related to subcooling (e.g. through the size of the critical radius) may not necessarily be correct (at least whithin our experimental period).

2.6. Conclusions

Results demonstrate that through simple, carefully controlled PVT experiments, different regions of polymer-controlled hydrate crystal growth inhibition can be readily identified from changes in crystal growth rates (as detected by changes in pressure due to gas consumption/release at constant volume). These regions are entirely repeatable and transferable between different set-ups, in contrast the inherently scattered data yielded by induction time studies. Hence, by using these boundaries or in other words the crystal growth inhibited (CGI) regions a reliable, repeatable and ideally rapid technique was developed to evaluate the performance of KHIs.

These KHI controlled crystal growth-inhibition patterns are

- The subcooling to initial formation/rapid failure (RGR and RFR)
- An apparent complete crystal inhibition zone (CIR)
- The slow dissociation region, as found by other workers (SDR)

Results indicated that even with hydrate already present in the system it is not possible to further grow hydrates within the CIR (in the region of subcooling available within the CIR before ice formation).

Within the RGR whether there is history or hydrate present in the system, pressure drop on cooling is observed, indicating hydrate growth. This region can be subdivided into smaller regions based on hydrate growth rates. Also, the growth rate within the RGR is dependent on the fraction of hydrate already present.

The RFR line essentially delineates the region where an ‘induction time’ may occur, but as soon as hydrate forms, growth is rapid/catastrophic until the RGR/CIR is re-entered.

No special equipment is required in this technique; only a well-mixed system with good temperature control and sufficient instrument sensitivity (to detect small pressure changes) is required. Also it was found that results are fully repeatable and transferrable between different types of equipment assuming good mixing and appropriate methodology (e.g. rocking cell and autoclaves), thus this supports the theory that CGI regions are primarily thermodynamically driven.

Comparison of induction time measurements and results of the new CGI technique reveals that a good correlation exists between these two methods. Induction

times/nucleation inhibition patterns are primary related to underlying CGI regions such that a true induction time can only be measured for a relatively short range of subcooling within the KHI-induced reduced growth rate (RGR) and rapid failure regions (RFR). Likewise, it is apparently impossible to measure an aqueous phase hydrate nucleation induction time in the complete inhibition region, supporting CGI studies which show that hydrate growth is completely/indefinitely inhibited in this subcooling range.

References

Arjmandi, M., Ren, S., Tohidi, B., 2003, *"Progress in Design and Asessment of Low Dosage Hydrate Inhibitors",* 6th Offshore Mediterranean Conference, Italy, Ravenna.

Chen,L.T., Sun, C.Y., Chen, G.J., Zuo, J.Y., Ng, H.G., 2010, *"Assessment of hydrate kinetic inhibitors with visual observations"*, Fluid Phase Equilibria, 298, 143–149

Christiansen, R. L., Bansal, V., and Sloan, E. D., 1994, *"Avoiding Hydrates in the Petroleum Industry: Kinetics of Formation"*, University of Tulsa Centennial Petroleum Engineering Symposium, Tulsa, Oklahoma

Dalmazzone, D., Hamed, N., Dalmazzone, Christine and Rousseau L., 2006, "*Application of high pressure DSC to the kinetics of formation of methane hydrate in water-in-oil emulsion*", Journal of Thermal Analysis and Calorimetry, 85, 361–368

Duchateau C, Dicharry C, Peytavy J-L, Glénat P, Pou T-E, Hidaldo E., 2008, "*Laboratory evaluation of kinetic hydrate inhibitors: a new procedure for improving the reproducibility of measurements"*, Proceedings of the 6th International Conference on Gas hydrates, Vancouver, Canada

Duchateau C, Peytavy J-L, Glénat P, Pou TE, Hidalgo M, Dicharry C., 2009, *"Laboratory evaluation of kinetic hydrate inhibitors: A procedure for enhancing the repeatability of test results"*, Energy and Fuels, 23, 962-966

Duchateau C, Glénat P, Pou, T-E, Hidalgo M, Dicharry C., 2010, *"Hydrate precursor test method for the laboratory evaluation of kinetic hydrate inhibitors"*, Energy Fuels, 24, 616–623

Englezos, P., Kalogerakis, N., Dholabhai, P. D., Bishnoi, P. R., 1987, *"Kinetics of Formation of Methane and Ethane Gas Hydrates"*, Chemical Engineering Science, 42, 2647–2658

Habetinova, E., Lund, A., and Larsen, R., 2002, *"Hydrate Dissociation under the Influence of Low-Dosage Kinetic Inhibitors"*, Proceedings of the 4th International Conference on Gas Hydrates, Yokohama, Japan

Kashchiev, D., 2000, *"Nucleation"*, First Edition, Butterworth-Heinemann, Oxford

Kelland, M. A., 2006, "History of the Development of Low Dosage Hydrate Inhibitors", Energy Fuels, 20, 825-847

Klomp, U., 2008, *"The World of LDHI: From Conception to Development to Implementation"*, Proceedings of the 6th International Conference on Gas hydrates, Vancouver, Canada

Koh, C.A., Westacott, R.E., Zhang, W., Hirachand, K., Creek, J.L., Soper, A.K., 2002, *"Mechanisms of gas hydrate formation and inhibition"*, Fluid Phase Equilibria, 194, 143–151

Larsen, R., Knight, C. A., and Sloan, E. D., 1998, *"Clathrate Hydrate Growth and Inhibition"*, Fluid Phase Equilibria, 150-151, 353-360

Larsen, R., Knight, C. A., Rider, K. T., and Sloan, E. D., 1999, *"Melt Growth and Inhibition of Ethylene Oxide Clathrate Hydrate"*, Journal of Crystal Growth, 204, 376- 381

Lederhos, J.P. and Sloan, E.D., 1996, *"Transferability of Kinetic Inhibitors between Laboratory and Pilot Plant"*, Presented at SPE Annual Technical Conference and Exhibition, U.S.A, Colorado, Denver, 173-179

Makogon, T. Y., Larsen, R., Knight, C. A., and Sloan, E. D., 1997, *"Melt Growth of Tetrahydrofuran Clathrate Hydrate and its Inhibition: Method and First Results"*, Journal of Crystal Growth, 179, 258-262

Peytavy, J.L., Glenat, P., Bourg, P., 2008, *"Qualification of low dose hydrate inhibitors (LDHIs): field cases studies demonstrate the good reproducibility of the results obtained from flow loops"*, Proceedings of 6th International Conference on Gas Hydrates, Canada, Vancouver.

Sivaraman, R., 2003, *"Understanding the mechanisms of hydrate nucleation and Inhibition"*, Gas TIPS, 9(2): 28–33

Sloan Jr, E. D. and C. Koh, 2007, *"Clathrate Hydrates of Natural Gases"*, Third Edition, CRC Press, New York.

Svartaas, T. M., Gulbrandsen, A. C., Huseboe, S. B. R., and Sandved, O., 2008, *"An experimental study on "un-normal" dissociation properties of structure II hydrates formed in presence of PVCAP at pressures in the region 30 to 175 bars – dissociation by temperature increase"*, Proceedings of the 6th International Conference on Gas Hydrates, Vancouver, Canada

Tohidi, B., Burgass, R.W., Danesh, A., Todd, A.C., and Østergaard, K.K., 2000, *"Improving the Accuracy of Gas Hydrate Dissociation Point Measurements*", Annals of the New York Academy of Sciences, 912, 924-931

3. APPLICATION: KHI POLYMER TYPE AND CONCENTRATION

3.1. Polymer Type

It has long been believed that kinetic hydrate inhibitors (KHIs) primarily act as gas hydrate anti-nucleators, although most of them also delay the growth of gas hydrate crystals (Kelland, 2006). These hydrate inhibitors are generally water-soluble polymers used in the industry to manage the risk of hydrate formation.

The most important discovery in KHI technology was found at Colorado School of Mines (CSM) in 1991. Through construction of a THF hydrate ball-stop rig they began screening a large number of commercial products (Kelland, 2006). Studies revealed that a suitable KHI should generally comprise of a polar cyclic chemical group in its molecular structure. This polymer preferably has a molecular weight greater than about 3,000, more preferably of molecular weight greater than about 20,000, and most preferably of molecular weight greater than about 40,000. An effective polymer with these descriptions was found to be Poly(vinylpyrrolidone), (PVP), which is a five-ring member of the series of polyvinyllactams with its cyclic groupings extending from a polymer backbone, Figure 3-1 (Sloan.E.D, May 1995). This polymer was found to show good KIH performance by delaying hydrate formation.

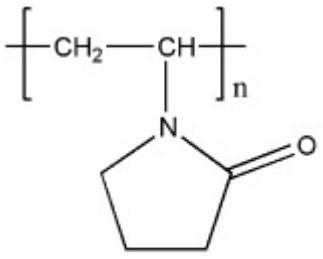

Figure 3-1 Structure of poly(vinylpyrrolidone)

In addition to that, a second polymer identified by CSM that clearly outperformed PVP in the ball-stop test was a polymer comprising a seven member cyclic grouping called Poly(vinylcaprolactam) (Figure 3-2) (Sloan.E.D, July 1995). Because of its impressive performance, PVCap became a standard by which other KHIs would be compared. The

early high molecular weight version of PVCap gave a 24hr induction time at subcooling of 8-9°C at a concentration of 0.5wt% (Kelland, 2006).

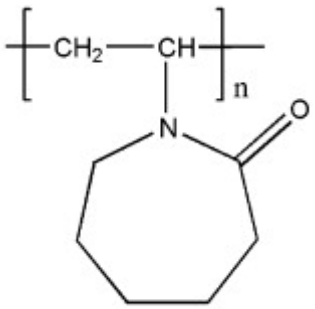

Figure 3-2 Structure of polyvinylcaprolactam

Other types of polymers which can be used as KHIs suggested by CSM are copolymers which comprise at least two cyclic chemical groups with one group preferably having a different number of atoms in its ring than a second cyclic chemical group. One effective copolymer would be one that has both a five member cyclic chemical group like vinylpyrrolidone and a seven member cyclic chemical group like vinylcaprolactam (VCap) (Sloan.E.D, 1997). Other workers have also suggested other VCap copolymers to compare with the performance of PVCap alone. Colle et al. (1999), patented his work on the performance of a copolymer called N-methyl-N-vinylacetamide:VCap 1:1 copolymer (VIMA:VCap 1:1) (Figure 3-3). This copolymer performed better than PVCap by 2-3 °C subcooling in a sapphire cell test (Kelland, 2006).

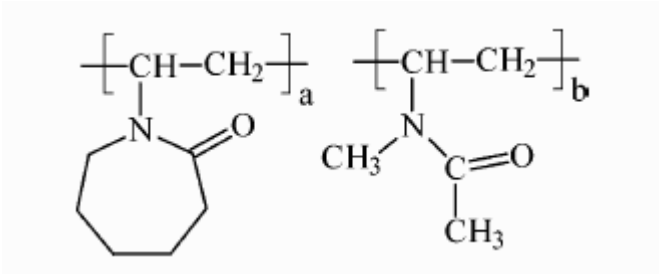

Figure 3-3 Structure of *N*-methyl-*N*-vinylacetamide:vinyl caprolactam 1:1 copolymer (VIMA:VCap) where a = b

Up until now, different workers have performed a large number of experiments to evaluate the performance of these KHI polymers in gas hydrate inhibition. Larsen et al. (1998, 1999) examined the effect of PVCap, PVP and a terpolymer of VP, VCap and dimethylaminoethylmethacrylate (VC-713) in two different system; water plus tetrahydrofuran (THF) and ethylene oxide (EO) aqueous solutions which form structure II (s-II) and structure I (s-I) hydrates respectively. Results of their experiments showed

that in a THF system although lower concentrations (<0.1wt%) of PVCap and VC-713 only changed the growth patterns and shape of the crystals, at slightly higher concentrations these polymers completely inhibited further crystal growth. On the other hand, presence of PVP in this system even at high concentrations can only change shape and direction of hydrate growth and cannot completely inhibit its growth. Furthermore experiments in an EO system indicated that low concentrations of PVCap or VC-173 again cause changes in the shape of the crystal by producing rapid, small scale branching of the crystals. Higher concentrations can inhibit hydrate formation completely, although these concentrations are somewhat higher than concentrations required for s-II hydrate inhibition. On the contrary, similar to the THF system, PVP in EO aqueous solution will only cause crystal growth rate reduction and change crystal morphology. The reason for the behaviour of these polymers was believed to be mainly due to different pendant groups of each polymer which can cause dissimilar stabilizing effects on partial cavities of the hydrate crystals that can in turn provide different strength of adsorption on hydrate surface (Larsen et al., 1998; Larsen et al., 1999).

Habetinova et al. (2002) also observed the effect of three polymers (PVCap, PVP and VC-713) in THF-water aqueous solution at atmospheric pressure. Results of their experiments established a connection between the efficiency of the inhibitor and the dissociation rates and temperatures and hence used these parameters for comparison of the effectiveness of these inhibitors. Tests concluded that all three inhibitors clearly shifted the dissociation temperature of hydrates to higher temperatures. However this shift in the dissociation temperature was largest for PVCap, then VC-173 and had only a very slight shift for PVP. Moreover, PVCap hydrates gave the longest dissociation periods double that of VC-173 whereas PVP's dissociation time was found to be the shortest. These findings clearly conclude that between these three polymers, PVCap was the most effective hydrate inhibitor while PVP was the least (Habetinova et al., 2002).

Sakaguchi et al. (2003) used a structure II hydrate former, HCFC-141b (CH_3CCl_2F), at hydrate forming temperatures under atmospheric pressure to evaluate the performance of two popular hydrate inhibitor polymers, PVP and PVCap. The major finding obtained in their study was that PVCap shows stronger inhibition effect on hydrate growth along the interface than PVP polymer. However, PVP greatly changes the morphology of the hydrate crystal along the interface whereas PVCap causes only slight changes in this (Sakaguchi et al., 2003).

The influence of PVP on the formation of hydrate methane/ propane in pre-saturated liquid water has also been studied by Kumar et al. (2008). Results demonstrated that at low concentrations of PVP (0.1 wt%) hydrate formation started as a film at the gas/liquid interface similar to the crystal behaviour without inhibitor. However, in the presence of PVP morphology of crystals grown within the liquid pool differed significantly from that without this polymer. On the other hand, at higher PVP concentrations (0.5 wt% and 1 wt%) growth did not start at the interface layer but rather at the walls above gas liquid interface and from within the liquid phase respectively. Moreover, at these higher concentrations or at 3.2 °C subcooling there was no hydrate growth within the liquid pool showing complete inhibition (Kumar et al., 2008).

More recently O'Reilly et al. (2011) examined crystal growth inhibition of THF hydrate in the presence of a synthesized 6-ring lactam polymer called poly (N-vinyl piperidone) (PVPip) as a kinetic inhibitor and compared it to the performance of PVP and PVCap polymers. In their previous studies, it was observed that PVP could not completely inhibit hydrate formation up to concentrations as high as 50,000 ppm (5.0 wt%) and total inhibition was only achievable in saline THF solutions as long as PVP polymer molecular weight was high. For PVCap it was observed that at high concentrations system could be totally inhibited while at low PVCap concentrations when the system was under-inhibited the shape and amount of hydrate crystals formed depended on the concentration of the polymer. Comparing these behaviours with results gained from tests on PVPip concluded that the performance of this synthesized polymer lies between that of PVP and PVCap at all subcoolings. Likewise, at ~3.8°C subcooling the concentration of polymer needed for complete inhibition approximately doubled going from PVCap to PVPip to PVP. However, as the subcooling increases the concentration of low molecular weight PVP needed to totally prevent THF hydrate formation increases sharply whereas for PVPip and PVCap there is only a very gradual increase (O'Reilly et al., 2011).

All the above studies have shown that different polymers can perform differently for the purpose of hydrate inhibition and it was generally found that PVCap is a better crystal growth inhibitor than PVP. However, in most of these studies changes in the morphology of hydrates were examined visually which can help understand the mechanism of inhibition of each polymer rather than providing reliable information for their application in the industry. Investigating crystal growth inhibition regions of different inhibitor polymers using the newly developed crystal growth inhibition

technique can offer consistent information in this regard. Hence, for each polymer, CGI boundaries can be measured and based on the extent of these regions, the hydrate inhibition properties of each KHI polymer can be evaluated. As mentioned in the previous chapter the larger these boundaries, the better and more effective KHIs are in inhibiting hydrate growth. Accordingly, since the CIR is considered to be the region where hydrate formation and growth is completely inhibited, polymers with a large CIR are most effective and reliable for use as inhibitors. Furthermore, as operating within the RGR for time periods which are less than the induction time are also known to be safe, KHIs with larger RGRs are also preferable and safe to use if laid under conditions within the RGR.

Consequently, in this chapter CGI regions have been determined for most popular KHI polymers (PVCap and PVP) to investigate which polymer is more effective and what degree of subcooling each polymer provides to determine safe operation conditions in the presence of each polymer.

In addition to that, while PVCap is known (and will be confirmed later in this chapter) to be a much better KHI than PVP, the former has much poorer solubility in water with a considerably lower critical solution temperature (LCST). As a result, PVCap presents concerns with respect to polymer precipitation, particularly at higher temperatures, which may be experienced at wellhead injection points. Precipitation risks can be reduced through the addition of PVP; however this would be expected to result in a reduction in overall KHI performance, meaning a balance must be struck. Therefore, it was suggested to test a combination of both polymers (PVCap-PVP) and determine whether this combination could offer good inhibition while having less solubility problem.

Furthermore, in this chapter the effect of Poly Ethylene Oxide (PEO), a polymer made up of repeating EO monomers, as an inhibitor has been investigated (Figure 3-4). The ethylene oxide monomer is nothing more than an epoxide ring. Two corners of the molecule consist of -CH2- linkages while the third corner is oxygen, -O-. In the presence of a catalyst the monomer forms a chain having the repeat unit -CH2-CH2-O-. As mentioned by Larsen et al. (1998), ethylene oxide (EO) is a structure I hydrate former as molecules of this chemical are of a suitable size to fit into cavities of this hydrate structure. Accordingly, it was suspected that PEO may also have the right structure and size to fit into cavities on the surface of a structure I hydrate and prevent

further growth similar to a kinetic hydrate inhibitor. Also, PEO is a non-toxic, non-irritant, high molecular weight polymer with good water solubility. All these properties can make it a potential favourable kinetic hydrate inhibitor if of course it has hydrate inhibition properties. Hence, CGI regions where determined for PEO to evaluate its KHI properties.

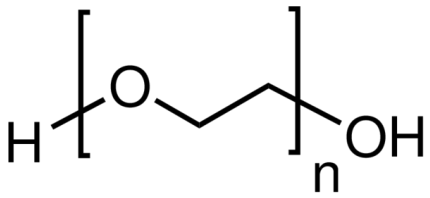

Figure 3-4 Structure of polyethylene oxide

Furthermore in this chapter, two commercial polymers called T1441 and HYTREAT 10-588K, supplied from Champion Technologies and Clarient, Inc. respectively, were tested using the developed CGI technique. Evaluating these inhibitors using this technique proves the application and reliability of this method for KHI evaluation and also determines a safety margin up to which hydrate in inhibited and operators can safely operate in when using each inhibitor.

Finally, hydrate inhibition properties of a biodegradable KHI polymer called Luvicap Bio, produced by BASF, was studied. The main purpose of this experiment was due to the fact that active polymers are typically poorly biodegradable which will result in some environmental issues for the use of normal KHIs. This poor polymer biodegradability is due to both typical low reactivity, and, in particular, very large molecular sizes which restrict breakdown by microorganisms. As a result, conventional formulations often perform poorly in biodegradability tests.

While environmental controls on chemical use/release vary considerably globally, there is a general trend towards tightening of restrictions, with chemicals having to meet increasingly stricter biodegradability standards. In some regions, such as Norwegian waters, conventional KHIs generally cannot be used at all due to very strict environmental regulations on offshore chemical use.

In light of the above, there is a growing interest in ‘green’ KHIs, although historically, development has not met with great success; the balance between good biodegradability and good KHI properties being difficult to achieve. However, in recent years, R&D

within the industry has resulted in the emergence of new hybrid polymers which apparently do offer good KHI properties combined with improved biodegradability (e.g. Kelland et al., 2010). A common approach to achieve this is through bond substitution in backbone chains of conventional KHI polymers; e.g. partial substitution of C-C bonds with more reactive/easily broken linkages, facilitating more rapid breakdown in the natural environment.

Given the increasing interest in this field and the emergence of some potentially promising biodegradable base polymers, some evaluation on bio KHIs for hydrate inhibition using the new CGI method was done. For this purpose test on a biodegradable polymer, Luvicap Bio, were performed and are reported in this chapter.

3.1.1. PVCap−Water−Methane System

Due to the good performance Poly (vinylcaprolactam) (PVCap) observed by a number of researchers (Section 3.1) this polymer was mainly used in most of the experiments throughout this project. Hence, it was necessary to study the crystal growth inhibition (CGI) properties of this polymer thoroughly, define each CGI region precisely and understand the inhibition properties of PVCap based on this new technique. Therefore in this section, crystal growth inhibition region data have been generated for a range of PVCap concentrations (0.25, 0.5, 1.0 and 5.0 mass% PVCap aqueous) in the presence of 99.995% pure methane gas, which forms structure I hydrate, at pressures up to 300 bar (4350 psi). The PVCap used in all the experiments, as mentioned in Section 2.3.1, was Luvicap-EG base polymer (K-value = 25-8, average MW = 7000), as supplied by BASF, with the ethylene glycol solvent removed by vacuum oven drying.

The basics of the method used to determine CGI regions are discussed in Chapter 2.For each system careful, controlled PVT studies have revealed that aqueous PVCap induces a number of well-defined hydrate growth / inhibition / dissociation regions which have been observed for all PVCap concentrations tested, including:

1. A slow dissociation rate region (SDR) outside the hydrate stability zone (HSZ)
2. A complete crystal growth inhibition region (CIR) within the HSZ to quite high subcoolings
3. A following restricted/reduced hydrate growth rate region (RGR), which can be further subdivided based on relative crystal growth rates
4. And a final rapid/immediate failure region (RFR)

Results and Discussion

Crystal growth inhibition regions found for each system are illustrated in Figure 3-5, Figure 3-6, Figure 3-7 and Figure 3-8 for 0.25, 0.5, 1.0 and 5.0 mass% PVCap aqueous respectively.

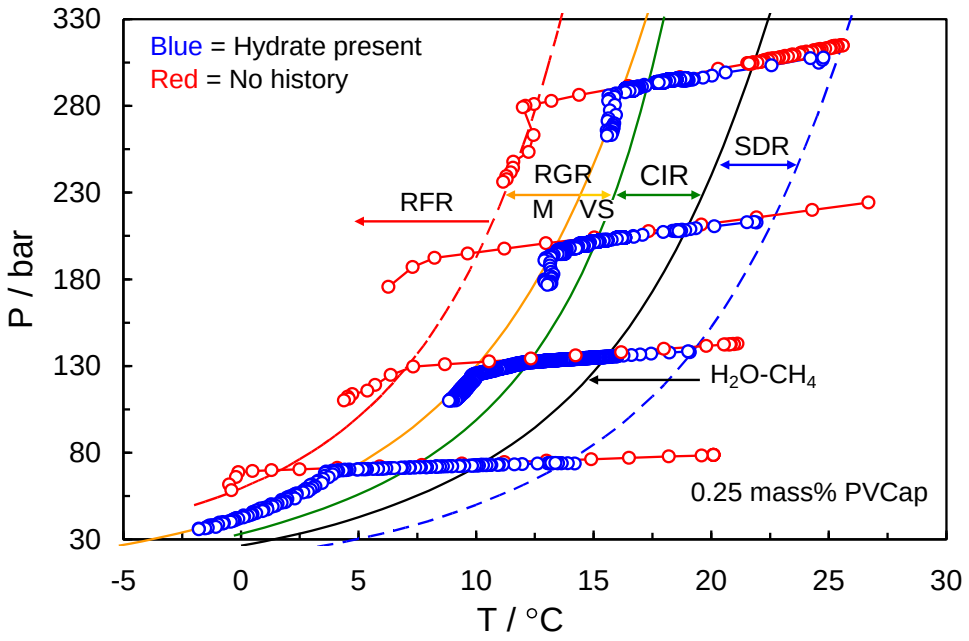

Figure 3-5 PT plot showing measured experimental points delineating the various crystal growth inhibition regions for 0.25 mass% PVCap (Luvicap-EG base polymer). Solid and dashed lines are interpolations.

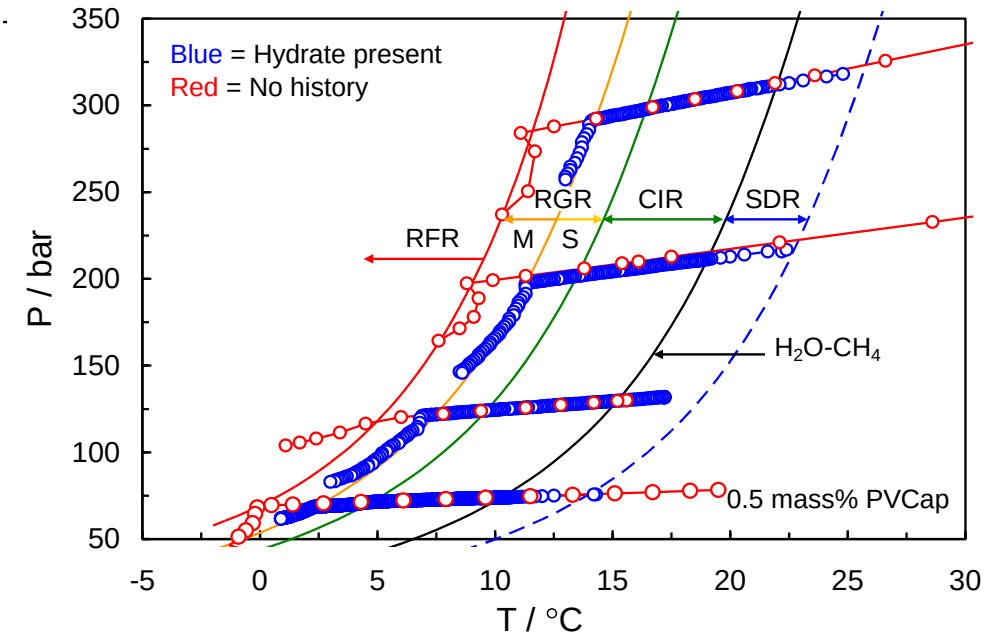

Figure 3-6 PT plot showing measured experimental points delineating the various crystal growth inhibition regions for 0.5 mass% PVCap (Luvicap-EG base polymer). Solid and dashed lines are interpolations.

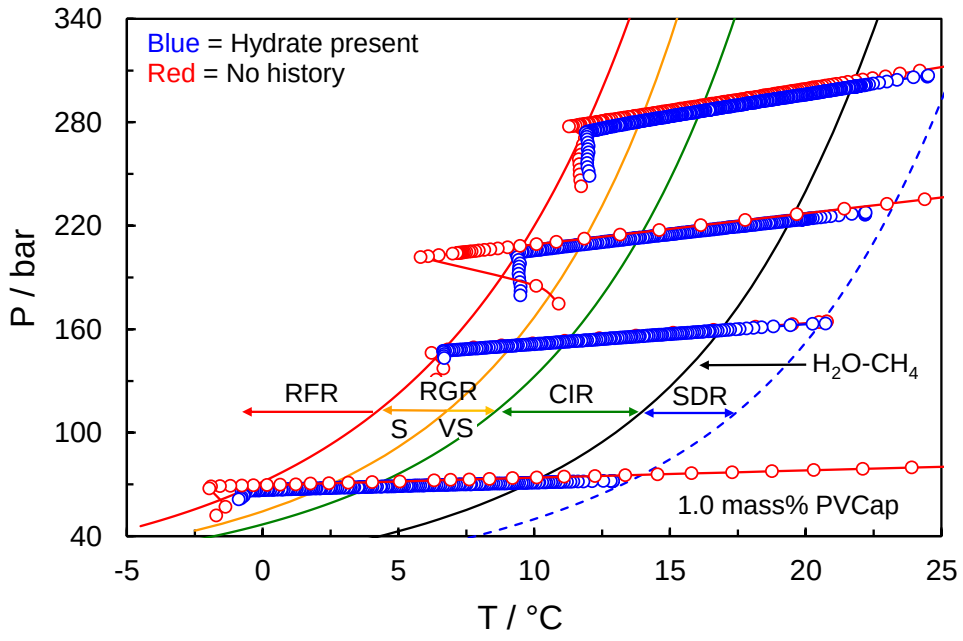

Figure 3-7 Experimentally determined points on crystal growth inhibition region boundary lines for 1.0 mass% PVCap (Luvicap-EG base polymer) aqueous with methane. Solid and dashed lines are interpolations.

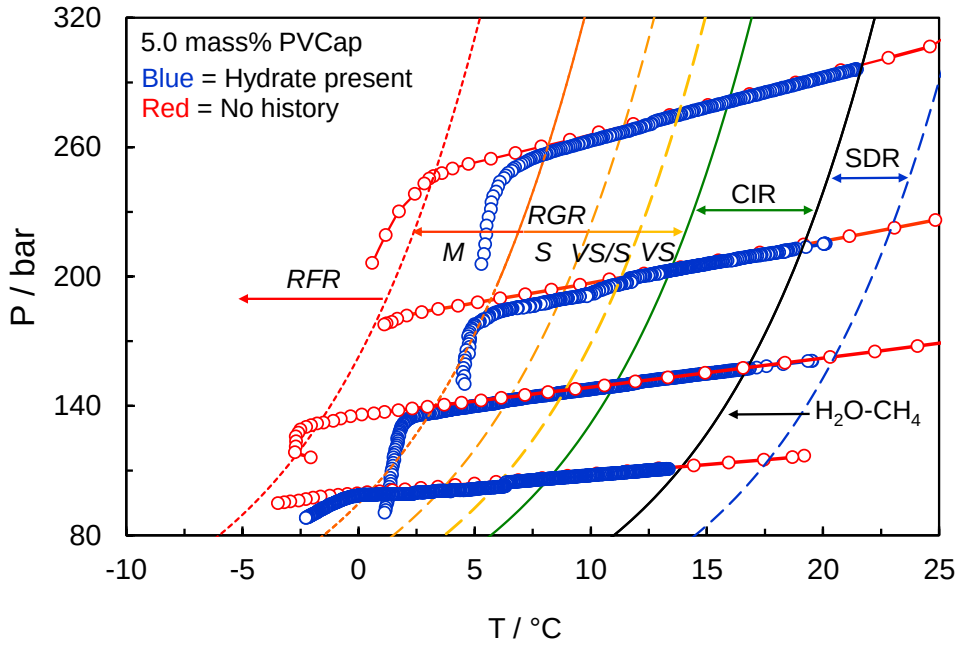

Figure 3-8 Experimentally determined points on crystal growth inhibition region boundary lines for 5.0 mass% PVCap (Luvicap-EG base polymer) aqueous with methane. Solid and dashed lines are interpolations.

Table 3-1 details the average subcooling range and observed relative growth rates for each region. Experimental points for region boundaries, as determined from changes in relative growth rates for both continuous and step-cooling runs, are reported in Table 3-2 to Table 3-5.

Table 3-1 Experimentally determined hydrate growth inhibition regions for PVCap-water-methane systems. Growth rates are relative. For comparison, approximations to convert initial 1% of aqueous phase to hydrates are as follows: very slow = 48 hours+, slow = 24-48 hours, moderate = 1-24 hours, fast = <1 hour. ΔT_{sub} ranges are absolute width of the regions over all experiments with ±0.5 ºC deviation. See Section 2.3.1for growth rate definitions.

Mass% PVCap	0.25	0.50	1.00	5.00
CIR (No Growth) ΔT_{sub} range / ºC	~0.0 − 3.5	~0.0 − 5.2	~0.0 − 5.3	~0.0 − 5.3
RGR (very slow , VS) ΔT_{sub} range / ºC	~3.5 − 5.2	N.A.	~5.3 − 7.3	~5.3 − 7.3
RGR (Very Slow-Slow, VS/S) ΔT_{sub} range / ºC	N.A.*	N.A.	N.A.	~7.3 − 9.5
RGR (Slow, S) ΔT_{sub} range / ºC	N.A.	~5.2 − 7.3	~7.3 − 9.5	~9.5 −12.5
RGR (Moderate, M) ΔT_{sub} range / ºC	~5.2 − 8.4	~7.3 − 9.6	N.A.	~12.5 −17.0
RFR (Fast) ΔT_{sub} range / ºC	~8.4+	~9.6+	~9.5+	~17.0+

*N.A. Not Available.

Table 3-2 Experimentally determined points (avegare of at least 3 runs) on crystal growth inhibition region boundary lines for 0.25 mass% PVCap (Luvicap-EG base polymer) aqueous with methane.

CGR boundary	*Growth rate	T / ºC (± 0.5)	P / bar (± 0.2)	ΔT_{s-I} / ºC (± 0.5)
CIR–RGR(VS)	No growth	7.3	72.2	−2.8
		12.2	129.0	−3.0
		15.0	201.2	−3.7
		16.9	275.5	−4.1
RGR(VS-M)	Very slow to moderate	2.4	55.9	−5.2
		4.6	69.9	−5.1
		10.0	130.3	−5.2
		16.1	286.3	−5.2
RGR(M)–RFR	Moderate	7.0	129.0	−8.1
		10.2	196.1	−8.3
		11.8	247.4	−8.4
		12.6	281.8	−8.6

*Growth rate is for ΔT CGI region preceding the associated boundary

Table 3-3 Experimentally determined points (avegare of at least 3 runs) on crystal growth inhibition region boundary lines for 0.5 mass% PVCap (Luvicap-EG base polymer) aqueous with methane.

CGR boundary	*Growth rate	T / ºC (± 0.5)	P / bar (± 0.2)	ΔT_{s-I} / ºC (± 0.5)
CIR–RGR(S)	No growth	4.7	71.0	−5.2
		10.2	131.6	−5.1
		13.6	204.8	−5.2
		16.4	297.6	−5.2
RGR(S-M)	Slow to moderate	2.4	68.3	−7.4
		7.9	129.6	−7.3
		11.4	201.3	−7.3
		14.3	291.8	−7.3
RGR(M)–RFR	Moderate	0.2	69.2	−9.6
		5.5	128.4	−9.6
		9.0	196.9	−9.4
		11.5	283.8	−9.7

*Growth rate is for ΔT CGI region preceding the associated boundary

Table 3-4 Experimentally determined points (avegare of at least 3 runs) on crystal growth inhibition region boundary lines for 1.0 mass% PVCap (Luvicap-EG base polymer) aqueous with methane.

CGR boundary	*Growth rate	T / ºC (± 0.5)	P / bar (± 0.2)	ΔT_{s-I} / ºC (± 0.5)
CIR–RGR(VS)	No growth	3.7	66.9	−5.6
		11.2	152.5	−5.4
		13.8	210.5	−5.2
		16.1	285.0	−5.2
RGR(VS-S)	Very slow to slow	1.9	66.0	−7.3
		9.2	150.2	−7.2
		11.6	206.3	−7.2
		13.8	279.2	−7.3
RGR(S)–RFR	Slow	−1.1	64.0	−9.5
		6.7	147.3	−9.5
		9.4	206.9	−9.5
		11.8	274.9	−9.1

*Growth rate is for ΔT CGI region preceding the associated boundary

Table 3-5 Experimentally determined points (avegare of at least 3 runs) on crystal growth inhibition region boundary lines for 5.0 mass% PVCap (Luvicap-EG base polymer) aqueous with methane.

CGR boundary	*Growth rate	T / ºC (± 0.5)	P / bar (± 0.2)	ΔT_{s-I} / ºC (± 0.5)
CIR–RGR(VS)	No growth	15.9	280.9	−5.2
RGR(VS-VS/S)	Very slow to Very slow/Slow	13.2	273.2	−7.3
RGR(VS/S-S)	Very slow/Slow to slow	11.2	266.3	−9.5
RGR(S-M)	Slow to moderate	7.9	256.2	−12.5
RGR(M)–RFR	moderate	3.1	245.3	−17.0

*Growth rate is for ΔT CGI region preceding the associated boundary

Moreover Figure 3-9 represents methane hydrate CGI regions as a function of mass% PVCap aqueous for better comparison and interpretation of results.

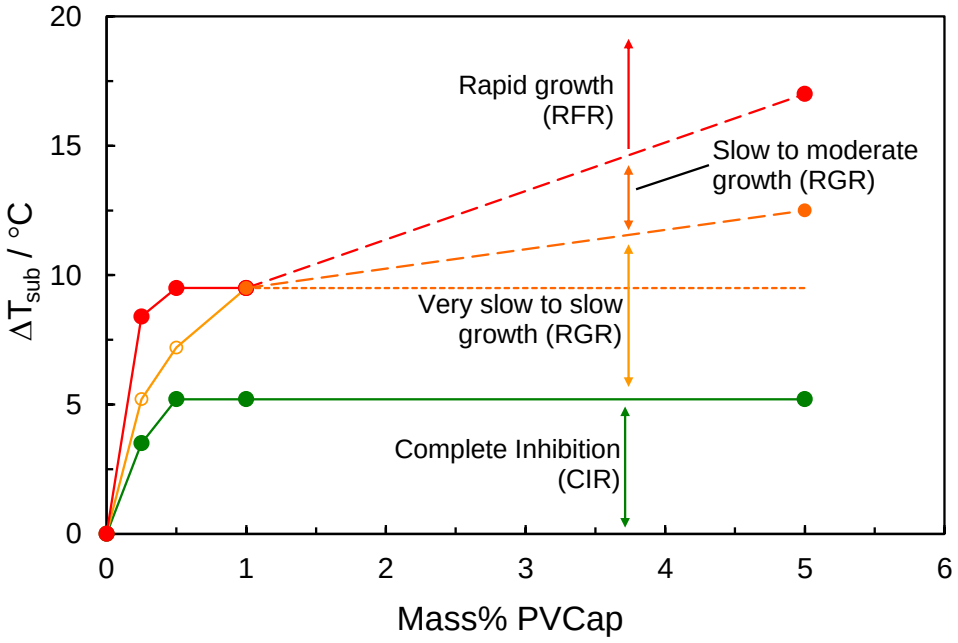

Figure 3-9 Methane hydrate CGI regions as a function of mass% PVCap aqueous.

Slow Dissociation Rate Region (SDR): As discussed in Chapter 2, the phenomenon of very slow hydrate dissociation rates outside the thermodynamic stability zone in the presence of KHI polymers has been previously reported in the literature (Habetinova, et al., 2002; Svartaas et al., 2008). This behaviour is testament to the fact that polymer effects extend well beyond the nucleation process which was clearly confirmed with CGI studies.

It is difficult to define the SDR region precisely as it does not appear to be delineated by a clear sudden change in dissociation rate, rather rates increase back to the 'normal' rate (everything being relative) as ΔT outside the thermodynamic hydrate phase boundary is increased. It is also a function of both the rate of temperature change (very rapid rises in temperature can cause faster temporary dissociation rates, presumably as readjustment of the polymer in response is quite slow due to its large size and thus low diffusion rate/mobility) as concluded by Svartaas et al. (2008), but also potentially the conditions at which the clathrates were formed. For hydrates grown rapidly at high subcoolings then quickly warmed to the SDR, dissociation can be quite rapid initially, presumably because there is insufficient time (during rapid growth) for strong, stable, organised polymer adsorption to take place; the rate of growth likely exceeding the rate at which the polymer can diffuse to growing crystal faces. In contrast, if hydrate is grown slowly (e.g. in the RGR region), it classically shows very slow dissociation rates in the SDR; i.e. a stable hydrate-polymer complex has been formed.

Heating curves generated as part of inhibition zone studies (when preparing for a 'history' or 'hydrate' present cooling run) suggests that for all concentrations of PVCap tested, the size of the SDR did not seem to change significantly. In PVCap-methane (structure-I) systems 3-4 °C is a good approximation for the SDR. The similar SDR at all concentrations suggest that there is some stoichiometry (presumably in terms of fraction of polymer per unit surface area of hydrate) to the complexes formed.

Complete Crystal Growth Inhibition Region (CIR): A major discovery of this method was the existence of the CIR region (see Figure 3-5- Figure 3-8). All results have suggested that in a well-equilibrated/ mixed system, within the CIR hydrate growth from the aqueous phase is inhibited apparently indefinitely.

Whether there is a history of hydrate or not, no new crystal growth occurs. Even if a small fraction of hydrate is already present on cooling into the HSZ, further crystal growth is completely inhibited. In all of the systems tested throughout this project (including s-II systems) no further growth (of a small fraction of hydrate) within this region has been observed for over 21 days (experiments stopped intentionally). The region is very well defined – lowering the temperature a fraction of a degree into the RGR causes hydrate growth to commence immediately. Such behaviour has been observed for single crystal studies on THF and ethylene oxide hydrates in the presence

of KHI polymers (e.g. Makogon et al., 1997; Larsen et al., 1998, 1999). Thus our findings confirm that this phenomenon also occurs in real systems.

A further fascinating feature of the CIR region which has also been mentioned in Section 2.3.1 is that hydrate dissociation can occur within it (see Figure 3-10 for an example). As described in Chapter 2 for a 'hydrate present' run, a volume of hydrate is first formed by cooling into the RGR or RFR. This is then mostly dissociated by heating to the outer edge of the SDR until only a small fraction is left. Cooling back towards the phase boundary into the SDR reduces the dissociation rate so much that it becomes negligible. A small fraction of hydrate is thus preserved in readiness for a cooling run to determine inhibition regions. However, on numerous occasions it has been found that hydrate which is very meta-stable just outside the phase boundary actually dissociates when it is cooled back into the hydrate zone; i.e. the polymer is inducing hydrate dissociation.

This behaviour is speculated to be due to crystal regrowth patterns. Hydrates formed at high subcoolings may have crystal morphologies which are only favourable (e.g. high surface to volume dendrites) with a large driving force (Larsen et al., 1998). When these crystals are taken to low subcooling conditions, the high surface free energy component is not favourable, so regrowth into more stable, lower surface/volume morphologies is attempted. However, regrowth requires both a dissociation and growth component on different faces. The polymer permits the dissociation, but not the growth, so effectively causes the hydrate to 'self-dissociate'. This is a simple explanation for this intriguing phenomenon which agrees with crystal growth inhibition patterns.

For 0.5, 1.0 and 5.0 mass% PVCap, the CIR consistently extends to a subcooling of around −5.2 °C while for the lower concentration of hydrate, 0.25 mass%, the CIR is clearly smaller, ΔT_{sub} at ~−3-−4 °C (Table 3-1). Data thus suggest a concentration dependence in terms of the extent of the CIR, with an optimal concentration of >0.25 and ≤ 0.5 mass% aqueous. Interestingly, the ΔT_{sub} width of the CIR in the case of 0.25 mass% PVCap actually grows with pressure, increasing from around −3 °C at 100 bar to ~−4 °C at 300 bar. This suggests that, contrary to what might be expected, PVCap performance is apparently enhanced with pressure in this case. Based on the trends observed in Figure 3-5, it is speculated that the CIR for 0.25 mass% may reach that common to 0.5 and 1.0 mass% PVCap (ΔT_{sub} ~−5.2 °C) at higher pressures (> 400 bar).

While ~−5.2 °C is not a particularly large degree of subcooling for complete inhibition, it is equivalent to the same degree of thermodynamic inhibition offered by ~18.5 mass% MEG, i.e. 0.5 mass% PVCap offers the same degree of complete inhibition as 37 times its mass of MEG (will be discussed in more detail in Chapter 8). This is a very substantial reduction in inhibitor mass/volume, yet still offering time-independent complete aqueous phase hydrate inhibition. The extent of the CIR may potentially be increased through the addition of small fractions of synergists. Furthermore, the ~−5.2 °C CIR applies for structure-I forming methane systems. As will be discussed in Chapter 4, PVCap performance is much greater for structure-II forming (e.g. natural gas) systems, giving a much larger CIR (ΔT_{sub} > 15 °C).

Restricted Growth Rate Region (RGR): Upon cooling into the RGR region, if hydrate or hydrate history is present, growth begins immediately (e.g. see Figure 3-10). Growth rates may be very slow however, depending on the polymer concentration. Rates may even be so slow as to be almost imperceptible; for example a pressure drop of 0.07 bar (1 psi) over a number of hours is not unusual. To confirm this slow growth, we employed high-precision *Quartzdyne* pressure transducers, which can detect pressure changes of 0.001 psi (0.00007 bar).

For 0.25 mass% PVCap, the RGR can be subdivided into 2 regions based on crystal growth rates (measured through pressure drop in time), here termed RGR(VS) and RGR(M). RGR(VS) lies between ΔT_{sub} ~−3-−4 and ~−5.2 °C. As shown in Figure 3-10 and Figure 3-11, growth is very slow in RGR(VS), with a pressure drop of only 0.07 bar / hr (1 psi / hr) being observed for over 12 hours. The increase in growth rate on cooling into RGR(M) is clear in both Figures, with the pressure change rising to 1.34 bar / hr. As can be seen in Figure 3-10and Figure 3-11, on entering RGR(M), PT conditions closely follow the RGR(VS-M) boundary line. This behaviour is very common and demonstrates the consistency in inhibition regions. In the absence of PVCap, hydrate growth would rapidly drive conditions to the univariant phase boundary for the system. However, presumably, as crystal growth is not favoured in the CIR, this forces only modest growth in response to reducing temperature as PT conditions track the CIR boundary line.

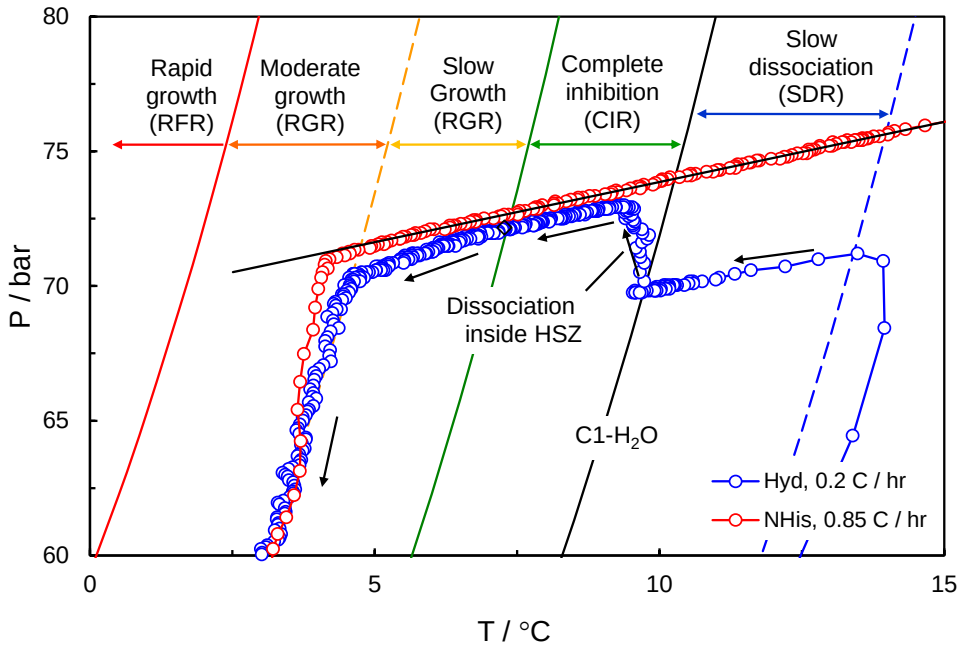

Figure 3-10 PT plot showing cooling curves for determination of complete inhibition and (CIR) reduced growth rate region (RGR) boundary lines for 0.25 mass% PVCap (Luvicap-EG base polymer) aqueous for no history (NHis) and hydrate (Hyd) present. Note pressure rise within the CIR indicating hydrate dissociation.

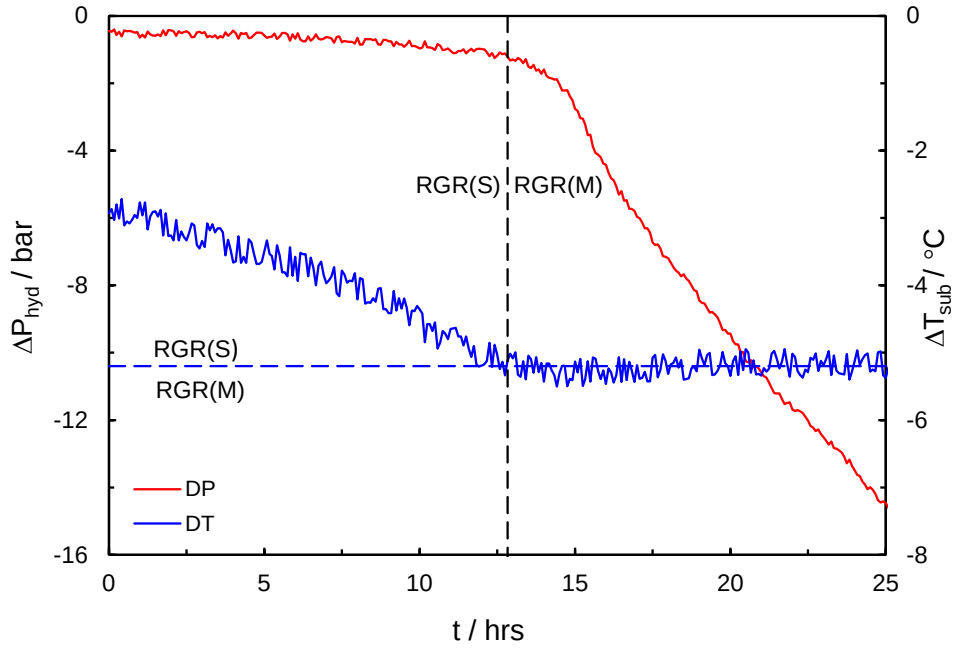

Figure 3-11 Plot of change in pressure due to hydrate formation (ΔP_{hyd}) and subcooling (ΔT_{sub}) as a function of time for a hydrate present cooling run with 0.25 mass% PVCap (PT data shown in Figure 3-10). The increase in growth rate (pressure drop as function of time) when conditions move from RGR(VS) into RGR(M) is clear.

Figure 3-12 shows example cooling curves for determination of the CIR, RGR and RFR boundary lines for 0.5 mass% PVCap aqueous for no history, history and hydrate present. As noted, the CIR extends to ΔT_{sub} ~−5.2 °C for this PVCap concentration; this

is clearly defined in Figure 3-12 where pressure is seen to begin dropping on leaving this region. RGR (S) extends from this to ΔT_{sub} = ~−7.2 °C, with RGR(M) extending to the RFR boundary at ΔT_{sub} = ~−9.5 °C. In a similar case for 0.25 mass%, PT conditions in the RGR closely follow a crystal growth region boundary line, although in this case the RGR(S-M) line is at higher subcooling, which is consistent with polymer concentration dependence for inhibition and typical of 0.5 mass% PVCap.

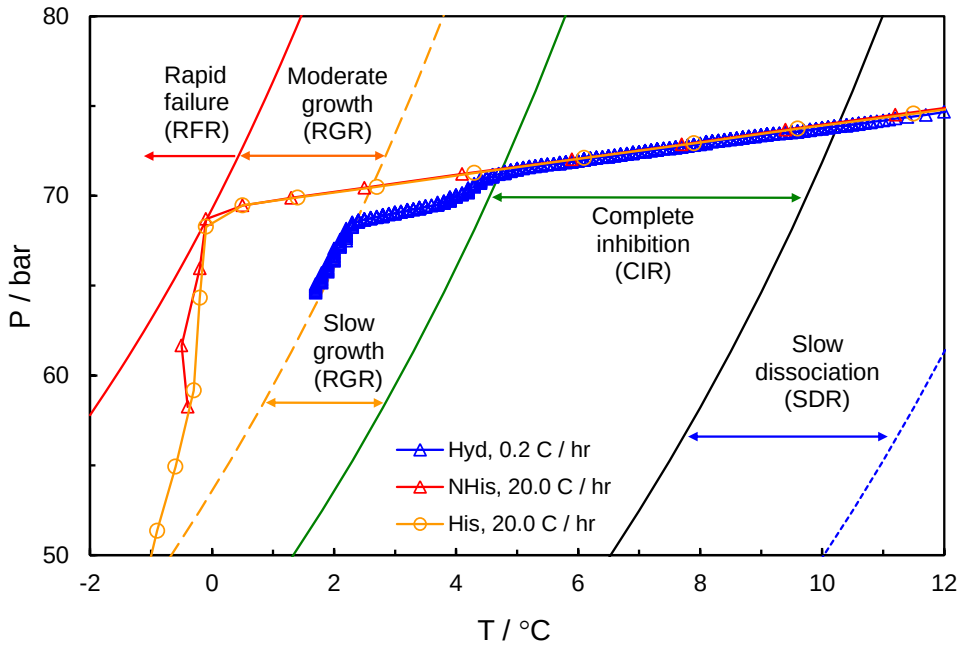

Figure 3-12 PT plot showing cooling curves for determination of complete inhibition (CIR) and reduced growth rate region (RGR) boundary lines for 0.5 mass% PVCap (Luvicap-EG base polymer) aqueous for no history (NHis), history (His) and hydrate (Hyd) present.

Figure 3-13 shows the change in pressure due to hydrate formation as a function of time for a hydrate present run in RGR(S) and RGR(VS) for 0.5 and 1.0 mass% PVCap aqueous with methane respectively. As can be seen, there is apparently little difference in growth rates for these concentrations in this region. In both cases, growth is extremely slow initially (slightly faster in the case of 0.5 mass%), and may stop if PT conditions are driven (by pressure drop during growth) back towards the CIR before a significant volume of hydrate is formed. Typically, growth patterns show an exponential type rise leading to ultimate failure; the beginnings of this rise apparent in Figure 3-13 for the 1 mass% test. However, as can be seen, very little growth takes place for over 60 hours inside this region, with only a very small fraction of water being converted to hydrate.

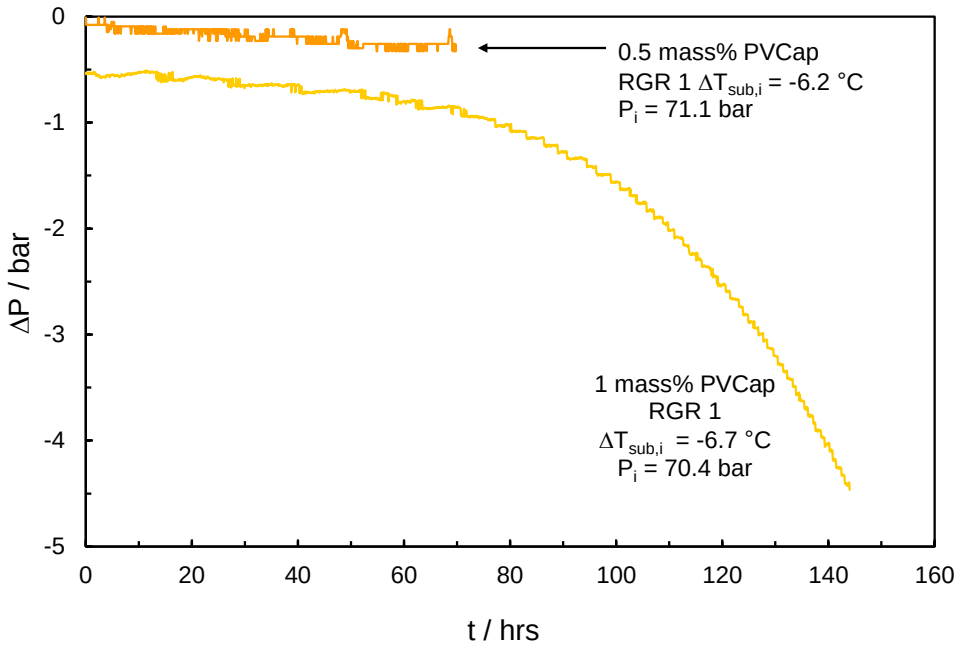

Figure 3-13 Plot of change in pressure due to hydrate formation (ΔP_{hyd}) as a function of time for hydrate present in RGR(S) and RGR(VS) for 0.5 and 1.0 mass% PVCap aqueous with methane

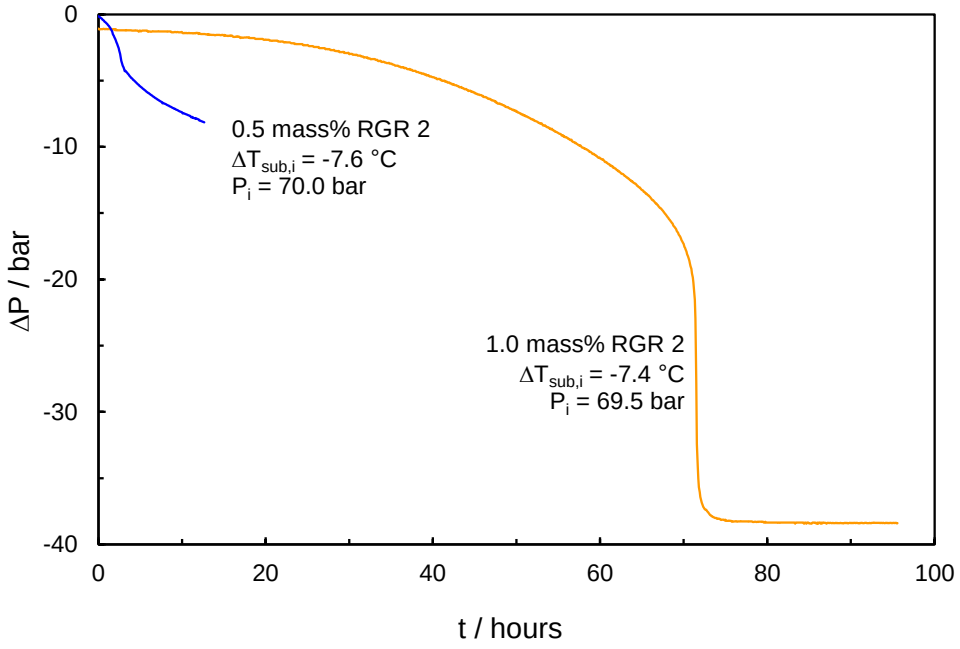

Figure 3-14 Plot of change in pressure due to hydrate formation (ΔP_{hyd}) as a function of time for hydrate present in RGR(M) and RGR(S) for 0.5 and 1.0 mass% PVCap aqueous with methane respectively.

Figure 3-14 shows the change in pressure due to hydrate formation as a function of time for hydrate present runs in RGR(M) and RGR(S) for 0.5 and 1.0 mass% PVCap aqueous with methane respectively. As can be seen, concentration dependence means growth rates are considerably faster for 0.5 mass% in around the same subcooling range (ΔT_{sub} = ~−7.3-−9.6°C). Thus, while increasing the PVCap concentration from 0.5 to 1.0 mass% aqueous apparently creates a reduced growth rate region in the same

subcooling range, it does change growth rates within this boundary; 1.0 mass% inhibiting growth considerably more in ΔT_{sub} = ~−7.3-−9.6°C.

Figure 3-15 shows a plot of change in pressure due to hydrate formation as a function of time for hydrate present cooling runs in different inhibition regions for 1.0 mass% PVCap (see Figure 3-7); the differences in growth rates for different regions are very clear. In RGR(VS), the growth rate is extremely slow, although as noted, it typically rises to eventual failure. Increasing the subcooling by only 0.7 °C into RGR(S) causes a very obvious change in growth rate; rates are still very slow initially, but growth accelerates more rapidly, showing the classic exponential rise to eventual rapid failure which is characteristic of the RGR region. The highest growth rate is seen when the boundary for the RFR region is reached.

Moreover, as can be observed from Figure 3-9 and Table 3-1 for 5mass% PVCap, similar to 0.5 and 1.0 mass% aqueous, hydrate growth rate in the subcooling range of ~−5.3-−7.3°C is extremely slow (named RGR(VS) for 1mass% and 5mass% and RGR (S) for 0.5mass%) . However, at higher subcoolings in the range of ~−7.3-−9.6°C (RGR(VS/S) for 1mass % PVCap) growth rate is much slower than that for both 0.5 and 1.0 mass% PVCap aqueous. Furthermore, slow growth rate of hydrate (RGR(S)) occurs at subcoolings between ~−9.5-−12.5°C and even more interestingly at higher subcoolings up to ~−17.0°C there is only moderate growth of hydrate detected.

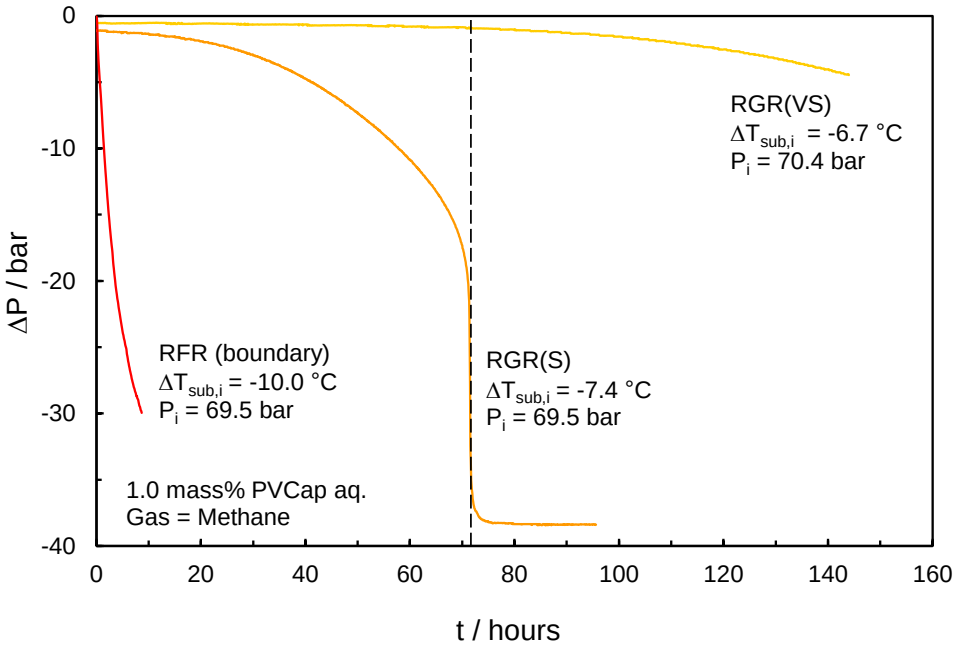

Figure 3-15 Plot of change in pressure due to hydrate formation (ΔP_{hyd}) as a function of time for hydrate present cooling runs in different inhibition regions for 1.0 mass% PVCap (see Figure 3-7).

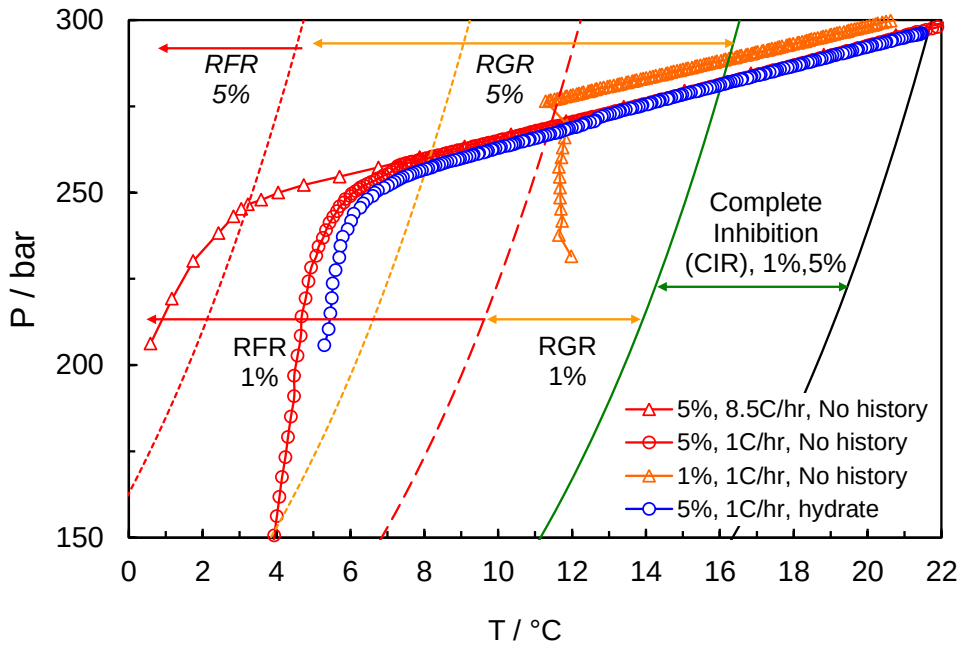

Figure 3-16 Example cooling curves for determination of CGI regions for 1.0 and 5.0 mass% PVCap aqueous with methane. Even with no history present, at 1% PVCap, rapid-moderate growth initiates at the RGR-RFR boundary ΔT_{sub} = ~−9.5 °C. In contrast, for 5 mass%, the reduced growth rate region (RGR) extends to ~−17 °C subcooling.

Figure 3-16 illustrates the differences of the extent of CGI regions between 1 mass% and 5 mass% PVCap aqueous in methane. As can be detected, at 5 mass% PVCap growth rates are slow to moderate up to ~−17 °C of subcooling, whereas rapid failure consistently occurs at ΔT_{sub} = ~−9.5 °C for 1 mass% (and 0.5 mass%). This clearly shows that the extent of the reduced growth rate region (very slow to moderate growth rates) continues to expand to considerably greater subcoolings with increasing PVCap concentrations up to 5mass%. Thus, as the complete inhibition region (CIR) remains relatively constant at ~−5.2 °C for PVCap concentrations higher than 0.5mass%, the benefit of adding further PVCap is to reduce growth rates at higher subcoolings.

Rapid Failure Region (RFR): In the RFR region, quite rapid failure occurs ubiquitously once the growth process begins; which is immediate in the case of history or hydrate present, but may be subject to a short delay for no history (typically only in the order of minutes). Hydrate growth rates in the RFR typically show a classical exponential decay type pattern (see Figure 3-14 for 1 mass% PVCap), i.e. initiation of growth is abrupt, with a rapid formation rate in the early stages, before rates increasingly reduce as thermodynamic equilibrium is approached. This RFR can thus be considered the danger zone – the polymer can apparently no longer prevent growth nor effectively control the growth rate, with blockage (stirrer blocked) often occurring within a short time period.

As evident from Figure 3-5-Figure 3-8, for 5 mass% PVCap aqueous with methane the RFR boundary line is at ΔT_{sub} of ~−17.0 °C. However as mentioned earlier, for both 0.5 and 1 mass%, this boundary is apparently equal and lies at a smaller subcooling of ~−9.5 °C. For 0.25 mass%, RFR is considerably less at ~−8-−8.5 °C, in agreement with the concentration dependence discussed for CIR and RGR regions.

3.1.2. PVP−Water−Methane System

From many of the studies mentioned Poly-*n*-vinylpyrrolidone (PVP), like PVCap is known as a kinetic hydrate inhibitor, although it is understood to be much less effective than the latter (Larsen et al., 1998 & 1999; Habetinova et al., 2002; Sakaguchi et al., 2003; O'Reilly et al., 2011). However in most of these studies, experiments were done using methods based on visual observations. Hence, to better understand the performance of PVP as an inhibitor it is necessary to measure its different CGI boundaries.

Simple CGI tests have been performed to assess different crystal growth inhibition regions for PVP−water−methane system for comparison with data for PVCap. Tests have been undertaken at pressures around 70 bar with 99.995% pure methane gas. Concentration of PVP used was 0.5 mass% PVP-40 (average molecular weight = 400, supplied by Sigma-Aldrich) aqueous solution.

Results and Discussion

Figure 3-17 shows cooling curve data (hydrate present) for a 0.5 mass% PVP aqueous with methane. As can be seen, the performance of PVP is very poor; 0.5 mass% only inducing a CIR region of ~−1.4 °C which it is almost a quarter of that compared to that for PVCap at ~−5.2 °C.

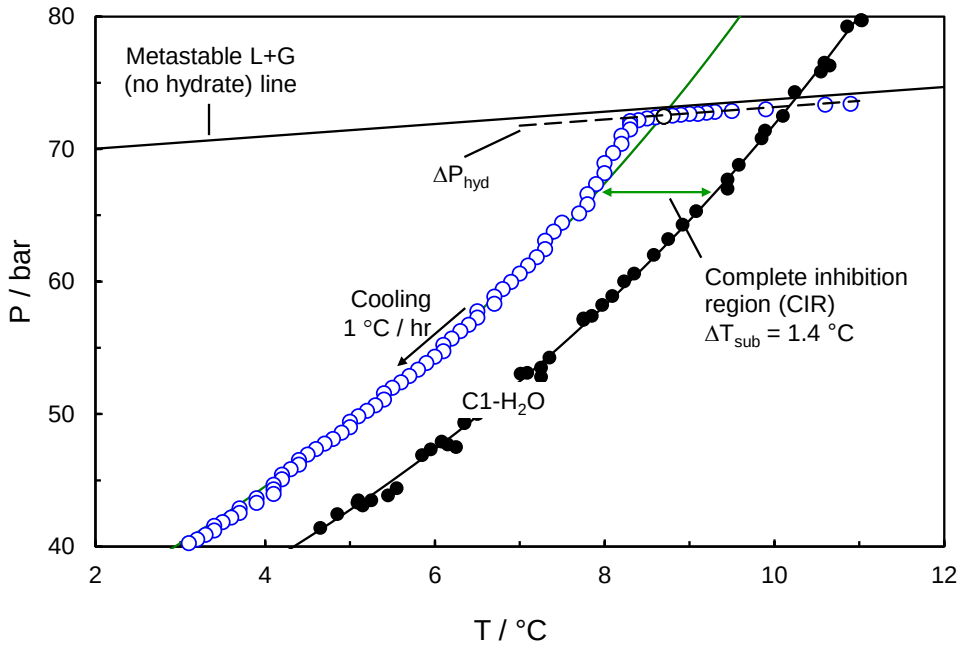

Figure 3-17 PT plot showing cooling curves for determination of complete inhibition (CIR) region boundary line for 0.5 mass% PVP aqueous with hydrate present.

Furthermore, no clear evidence for any slow dissociation region was observed for PVP. This clearly supports the small CIR region observed for and suggests that the strength of PVP adsorption on hydrate crystal surfaces is much weaker than that for PVCap, which would explain the poor performance typically reported for PVP. Moreover, as is evident from the figure, the rapid growth region is also very small at ~−2 °C which again confirms the weak performance of PVP.

Conclusively, similar to Larsen's explanation (Larsen et al., 1998) the reduced performance of PVP can be largely related to the pendant group of PVP being smaller and not having the same stabilizing effect on partial cavities, thus not providing strong enough adsorption. On the other hand, PVCap pendant groups are clearly larger than that for PVP hence can fit better into the open cavities on the surface of hydrate crystals and result in the better performance of this polymer.

3.1.3. PVCap−PVP−Water−Methane System

As found in sections 3.1.1and 3.1.2, for methane systems, PVCap concentrations ≥ 0.5 mass% PVCap gives complete inhibition up to a subcooling of ~−5.2 °C and can reduce growth rates up to a subcooling of ~−9.5 to 10.0 °C. In contrast, for hydrate/history present, PVP can only completely inhibit up to a subcooling of ~−1.4 °C and reduce growth rates to ~−2.0 °C of subcooling. Although it is evident from this that PVCap is a

much better KHI than PVP, due to its poor solubility in water it may experience problem during the production process. Hence in a PVCap based KHI formulation, the addition of PVP with higher solubility can help to diminish this problem. At the same time, this means a reduction in the KHI performance which is not favourable and must be avoided as much as possible. Therefore, it was important to find a suitable combination of PVCap-PVP that would offer a balanced KHI with a reasonable solubility and good performance. In light of this, using the newly developed crystal growth inhibition (CGI) approach KHI performance for a number of PVCap−PVP combinations were studied and are reported in this section.

Like all other experiments detailed in this chapter tests were carried out on high-pressure stirred autoclaves using the CGI method described in Chapter 2. The PVCap used was Luvicap-EG base polymer (K-value = 25-8, average MW = 7000) supplied by BASF, with the ethylene glycol solvent removed by vacuum oven drying and the PVP was PVP-400 (average MW = 400) supplied by Sigma Aldrich. Initial methane hydrate crystal growth inhibition region data were generated for 1 mass% polymer aqueous comprising 0.25/0.75, 0.10/0.90 and 0.05/0.95 PVCap/PVP fractions in a 99.995% pure methane system.

Results and Discussion

Figure 3-18, Figure 3-19 and Figure 3-20 show example CGI method cooling curves for 0.25 mass% PVCap / 0.75 mass% PVP, 0.10 mass% PVCap / 0.90 mass% PVP , 0.05 mass% PVCap / 0.95 mass% PVP with methane respectively. As previously reported (Section 3.1.2), PVP alone performs very poorly with methane, yielding an apparent CIR which is only about −1.4 °C in subcooling extent. Reduced growth rates likewise are only observed up to around −2.0 °C subcooling at most. The addition of small fractions of PVCap however, greatly improves PVP performance, as can be seen from Figure 3-18, Figure 3-19 and Figure 3-20.

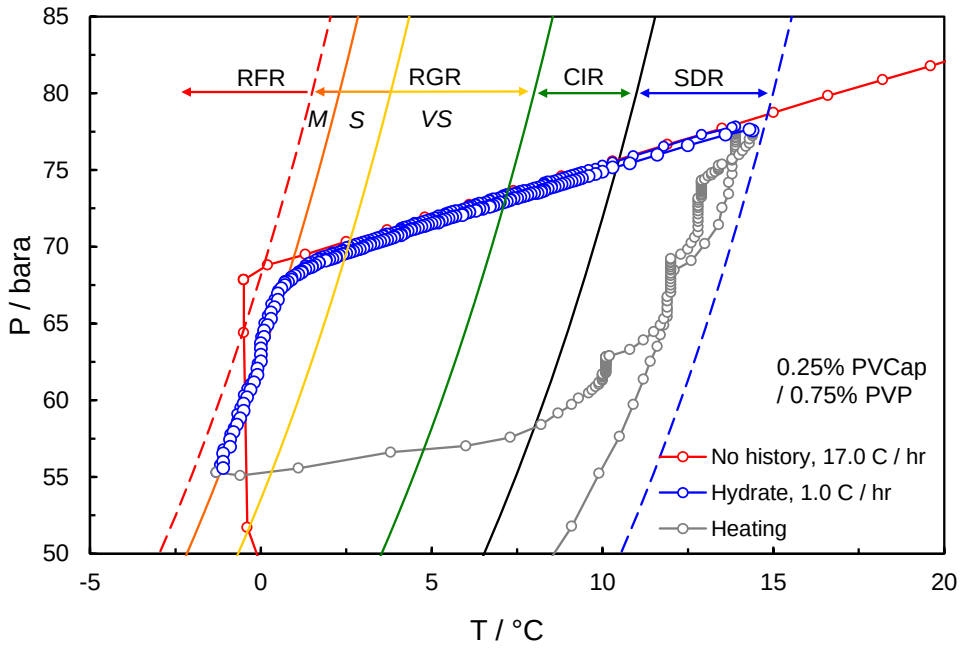

Figure 3-18 Example CGI cooling and heating runs for 0.25 mass% PVCap / 0.75 mass% PVP aqueous with methane.

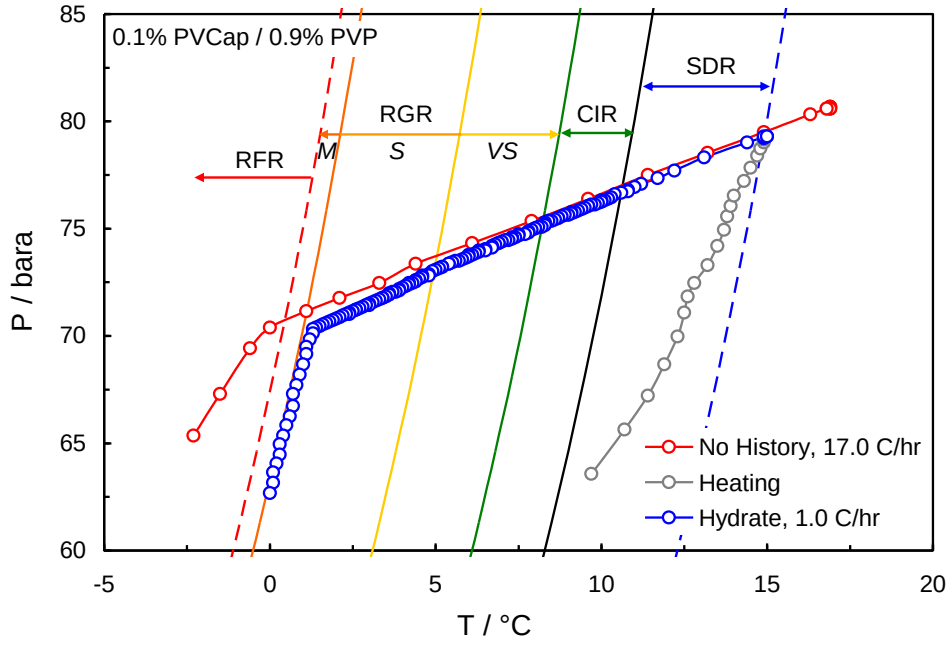

Figure 3-19 Example CGI cooling and heating runs for 0.10 mass% PVCap / 0.90 mass% PVP aqueous with methane.

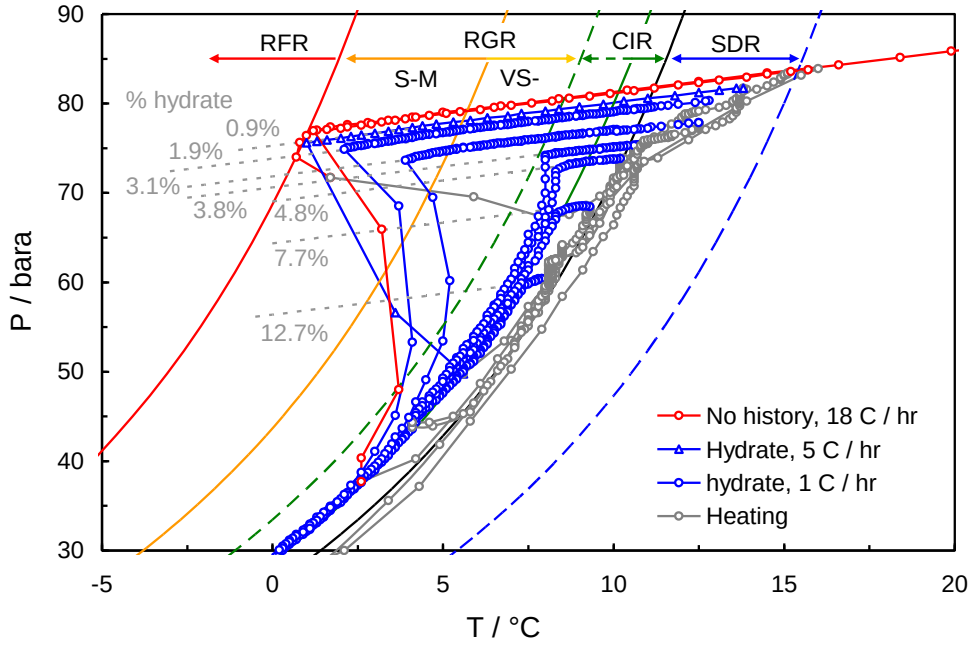

Figure 3-20 Plot of CGI cooling curves for different initial hydrate fractions (mass% of aqueous phase converted) and heating runs for 0.05 mass% PVCap / 0.95 mass% PVP aqueous with methane.

With 0.25% PVCap and 0.75% PVP, the CIR is ~−3.0 °C with the RGR and RFR extending to ~−8.7 °C and ~−9.5 °C of subcooling respectively. Moreover, in a 0.1% PVCap and 0.90% PVP which has an even lower PVCap concentration, the CIR is ~−2.2 °C which is still larger than the CIR in a PVP alone system. The RGR and RFR are also extended to ~−8.5 °C and ~−9.3 °C of subcooling respectively. Also, for a system with very slight amount of PVCap (0.05 mass% PVCap / 0.95 mass% PVP) RGR and RFR are clearly extended to lower subcoolings of ~−5.2 °C and ~−9.3 °C respectively. The extent of CIR in this system will be explained in more detail below.

Figure 3-21 shows subcooling extent of CGI regions as a function of aqueous polymer fraction of PVP with PVCap for a total polymer concentration of 1 mass% aqueous. As can be seen, while the performance of PVP/PVCap mixtures is always poorer than the same concentrations of PVCap, the addition of only a small fraction of PVCap to PVP gives a better performance than would be expected for the same fractions of PVP or PVCap alone. For example, performance with 0.25% PVCap + 0.75% PVP is considerably better than 0.25 mass% PVCap alone (e.g. RGR slow-moderate boundary is ΔT_{sub} = ~−8.7 °C for 0.25 PVCap / 0.75 PVP but only ~−5.2 °C for 0.25 mass% PVCap alone), even though PVP alone is worse than 0.25 mass% PVCap.

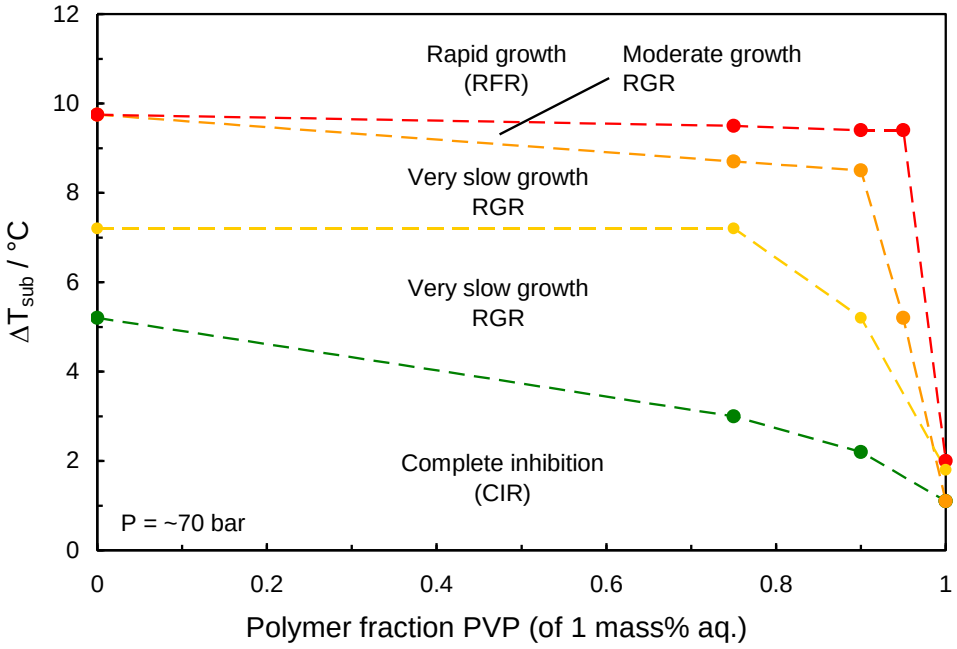

Figure 3-21 Subcooling extent of CGI regions as a function of aqueous polymer fraction of PVP with PVCap. Total polymer fraction is 1 mass% aqueous. Data are preliminary for only one pressure of ~80 bar.

The benefit of PVP is its much greater solubility in water. This results in much higher lower critical solution temperature than PVCap, so reducing the risk of polymer dropout at higher (e.g. wellhead) temperatures. Clearly, there is a sacrifice in substituting PVP for PVCap; the CIR is in particular reduced considerably more than the RGR. However, results show that PVP−PVCap mixtures can perform well and long induction times would be expected for RGR (very slow and slow) growth regions, where even if hydrate formed, growth would be very slow initially.

An interesting feature detected for the combination of PVCap-PVP with low concentrations of PVCap is the tendency to perform well at low hydrate fractions but fail suddenly and often catastrophically with higher hydrate fractions at low subcoolings. Moreover there seems to be two CIRs for these PVCap−PVP mixtures; one which applies to low hydrate fractions at higher subcoolings and one which applies to higher hydrate fractions at low subcoolings.

Figure 3-20 shows a plot of CGI cooling curves for different initial hydrate fractions (mass% of aqueous phase converted) and heating runs for 0.05 mass% PVCap / 0.95 mass% PVP aqueous with methane. For ‘no history’ runs, repeatability is good, with rapid failure consistently occurring at around a subcooling of around −9.4 °C, which is close to that offered by 0.5 mass% PVCap and much higher than might have been

expected for PVP. Relatively fast cooling (5 °C / hr) with hydrate present results in failure at the same CGI boundary.

However, for slower, standard 1 °C / hr cooling runs with hydrate present, as the initial fraction of hydrate is increases, the subcooling to failure reduces dramatically, as shown in Figure 3-20 and Figure 3-22. Up to 1% hydrate, failure occurs at or close the RFR boundary, i.e. up to this fraction of hydrate, the KHI is at optimal performance. However, as the initial hydrate fraction increases to 4 mass% of the aqueous phase, performance is reduced dramatically, and by 8 mass%, failure occurs at only 1 °C of subcooling, which is that for the PVP CIR. For all runs and hydrate fractions of up to 20 mass%, the PVP induced CIR remains, with all cooling curves following this (Figure 3-20). Even where rapid failure has occurred, when PT conditions reach this boundary (e.g. following the exothermal peak), growth stops again abruptly. This is very typical and is seen for PVCap as well.

While it has not been investigated in depth, these findings suggest that modest fractions (e.g. 0.5 to 1 mass% aqueous) of KHI polymers, including PVCap and PVP, can still inhibit fully up to high hydrate fractions of 10 mass% or aqueous or greater, i.e. CGI regions remain intact.

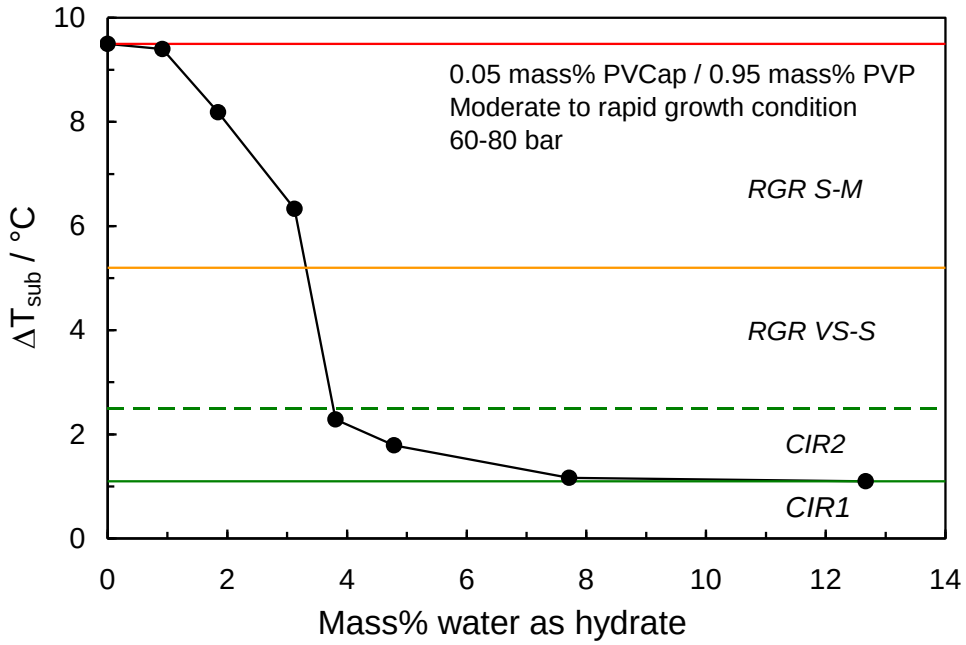

Figure 3-22 Plot of mass% initial water converted to hydrate versus subcooling to moderate/rapid growth for methane with 0.05 mass% PVCap / 0.95 mass% PVCap. CGI regions are for low fractions of hydrate (< 1 mass% converted) apart from CIR1, which applies to high hydrate fractions (> 13 mass% converted).

Clearly, the formation of hydrate uses up the polymer in the aqueous phase; the behaviour seen in Figure 3-20 is testament to this. As to whether a specific hydrate fraction will use up a specific fraction of polymer depends on whether the 'hydratepolymer' complexes that form have any polymer/water stoichiometry. While it might be expected that a hydrate surface area to polymer ratio could be constant, a volumetric ratio may not; i.e. a large, euhedral hydrate crystal (those that are well-formed with sharp, easily-recognised faces and controlled by their own natural crystallographic form) with low surface to volume would be expected to have a lower polymer to water ratio than a dendritic-like needle with very high surface to volume. However, the fact that CGI boundaries – notably the SDR which does not involve growth but metastability/dissociation – are very repeatable suggests some degree of stoichiometry in hydrate–polymer complexes that form.

3.1.4. PEO− Water−Methane System

Poly Ethylene Oxide (PEO) is a polymer made up of repeating ethylene oxide (EO) monomers. Since EO is a structure I hydrate former it was suspected that pendant groups of PEO may be of a suitable size to sit into the open cavities of methane hydrate which is also a SI hydrate. This way PEO may act as an inhibitor by coating the surface of this hydrate and preventing further growth of hydrate crystals. To investigate KHI properties of this polymer, CGI behaviour of it was studied and its different crystal growth inhibition regions were determined.

Same procedure as all other CGI tests mentioned were carried out throughout the experiments for 1mass% PEO with 99.995% pure methane gas. PEO used in these experiments was 99.99% pure and supplied by SIGMA ALDRICH.

Results and Discussion

Figure 3-23 shows an example CGI method cooling curve for 1.0 mass% PEO in methane. As evident from this graph, PEO has very weak inhibition properties and all crystal growth inhibition regions are significantly smaller than that for PVCap at this concentration or even PVP at a smaller polymer concentration (0.5mass% PVP +C1). CIR region is only ~−0.5 °C which is also supported by the negligible SDR region. The RGR in this system is quite similar to the RGR for 0.5mass% PVP in methane sitting at about ~−2 °C subcooling. However, after a small growth of hydrate this region apparently becomes smaller and decrease to about ~−1.2 °C subcooling represented

with the dotted line in the figure. RFR region is also not too large occurring at ~−4.7 °C subcooling from the methane phase boundary.

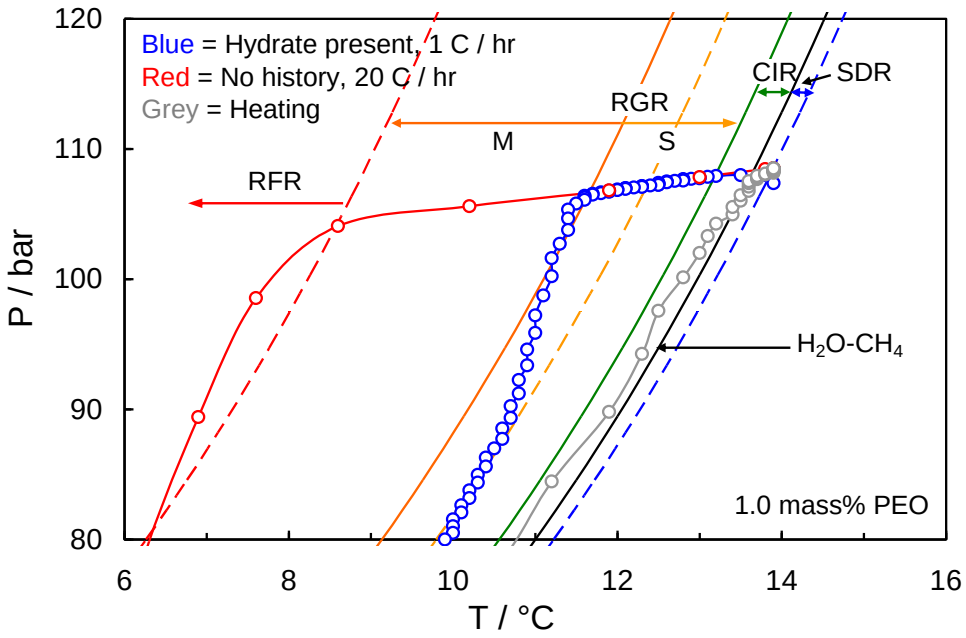

Figure 3-23 Example CGI cooling and heating runs for 1.0 mass% PEO aqueous with methane.

Results suggest that a good KHI polymer is not necessarily made up of monomers of the right size for hydrate formation, but more polymers that have a suitable size pendant group like PVCap. Polymer pendant groups that have a suitable size can fit into the open cavities and form a polymer layer on the surface of the hydrate and through this further growth of hydrate is prevented. If the pendant groups are not the right size, polymer cannot stabilize on this surface hence a stable layer cannot be formed and KHI properties of this polymer will perform very weakly and may not have inhibitor properties in any way. This was the case for PEO polymer in methane.

3.1.5. *T1441*−Water−Methane and *HYTREAT10-588K*−Water−Methane Systems

Measurements of KHI induced CGI regions for PVCap−PVP mixtures, as detailed in Section 3.1.3, showed that while PVP performs poorly on its own, the addition of small fractions of PVCap (e.g. 0.05 mass% PVCap, 0.95 mass% PVP) greatly increases performance.

However, this performance increase is highly susceptible to the fraction of hydrate formed for low PVCap concentrations**;** sudden and rapid failure can occur once a critical hydrate fraction is reached. Furthermore, the combination of 2 polymers gives 2 CIR regions; a higher subcooling one applicable only at low hydrate fractions and a

lower subcooling one which can be sustained even to quite high hydrate fractions (>10 mass% of aqueous phase).

While some commercial KHIs consist of only one type of polymer along with some synergists other may contain a combination of different polymers, a small fraction of a strongly absorbing one such as PVCap, and large fraction of a weakly absorbing one such as PVP. Hence it is suspected that these KHIs may behave similar to PVCap−PVP mixtures having high sensitivity to the fraction of hydrate present and also show two CIRs; one at higher subcoolings for low fractions of hydrate and one at much lower subcoolings. To show the applicability of the developed CGI technique for evaluation of real commercial polymers and confirm its reliability and at the same time understand the behaviour of some of these KHIs, CGI regions for 2 commercial base polymers with methane were examined. The two KHIs used were *T1441* a co-polymer (in water) supplied by Champion Technologies and *HYTREAT 10-588K* in (monoethylene glycol / MEG), supplied by Clarient, Inc. The specific structures of these polymers are unknown but it is known that *T1441* is 0.5 mass % active ingredient dissolved in water hence a concentration of 1.0 mass% polymer solution was used in all test to maintain a 0.5mass% active polymer in the system. Moreover, *HYTREAT 10-588K* is 40 mass% active ingredient dissolve in MEG thus to provide similar polymer concentrations for better comparison of the two commercial KHIs, a concentration of 1.25 mass% KHI solution was used in all tests. Tests were all carried out in methane (99.995% pure) up to 300 bar pressure using the same procedure detailed in Chapter 2. In addition to that, some preliminary atmospheric cloud point measurements were carried to compare precipitation temperatures (for wellhead hot injection) with performance. To perform these tests, exact concentration of KHI solutions were gradually heated in a stepwise manner (~0.5 °C temperature intervals) inside small jacketed beaker illustrated in Figure 3-24. Since the jacket on these reactors is made up of glass the clarity/cloudiness or any precipitation within the solution is easily detectable at each temperature.

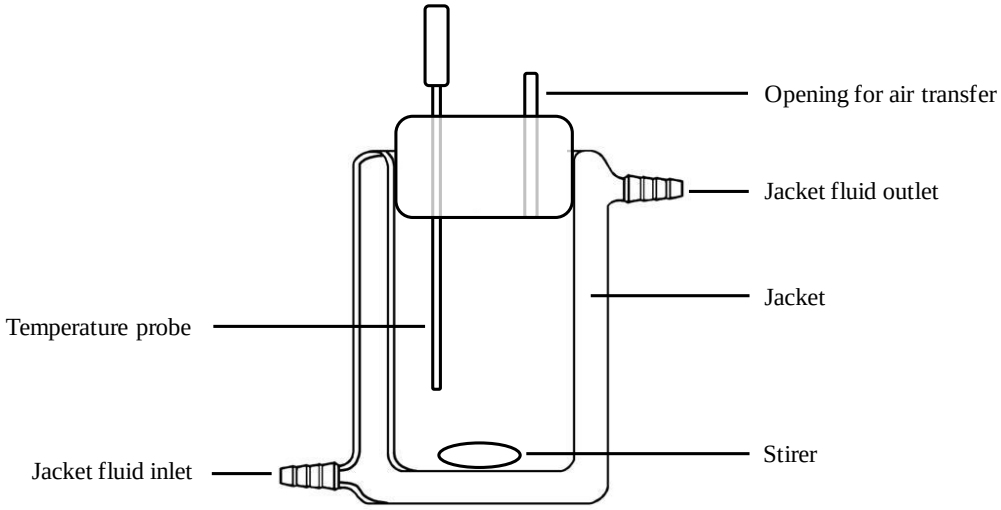

Figure 3-24 Illustration of the jacketed beaker used for polymer cloud point measurements

Results and Discussion

T1441 Co-Polymer Methane CGI Regions

Example 'with hydrate' cooling curves for 0.5 mass% T1441 aqueous with methane along with interpolated boundaries are shown in Figure 3-25. Determined points on CGI region boundaries are reported in Table 3-6.

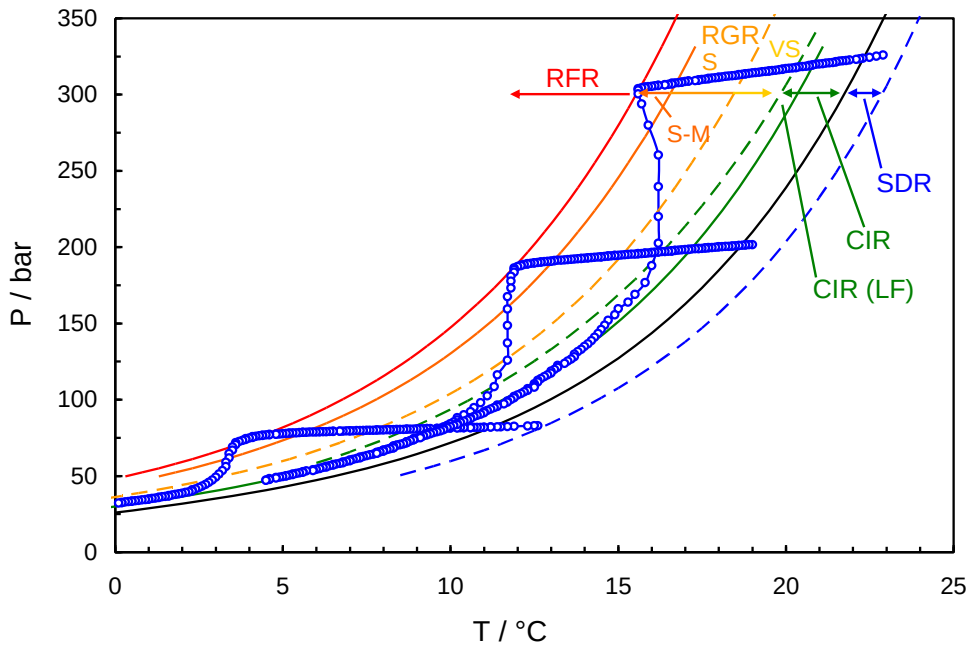

Figure 3-25 Example CGI cooling with hydrate (1 °C/hr) runs for 0.5 mass% T1441 aqueous with methane.

Table 3-6 Experimentally determined points on CGI region boundaries for methane with 0.5 mass% T1441 co-polymer aqueous. See Section 2.3.1 for growth rate definitions.

CGR Boundary	*Growth rate	T / ºC (± 0.5)	P / bar (± 0.2)	ΔT_{s-I} / ºC (± 0.5)
SDR	Slow dissociation	12.9	83.5	1.5
		20.0	203.5	1.2
		23.5	327.6	1.1
CIR-RGR(VS-S)	No Growth	8.8	81.2	−2.3
		16.3	196.7	−2.2
		20.3	317.5	−1.9
RGR(VS-S)-RGR(M)	Very slow to slow	5.6	78.5	−5.2
		13.0	191.5	−5.3
		16.6	303.7	−5.2
RGR(S-M)-RFR	Moderate	3.6	71.7	−6.4
		11.9	185.1	−6.1
		15.6	302.9	−6.2

*Growth rate is for ΔT CGI region preceding the associated boundary

As can be seen in Figure 3-25, the behaviour of T1441 when cooling with a small fraction of hydrate present (>0.5%) was very repeatable, with rapid to moderate growth occurring at a consistently fixed subcooling of ~−6.2 °C. While this is only 1.0 °C less than the subcooling condition where 0.5 mass% PVCap shows moderate growth rates, the behaviour of T1441 is quite different. For 0.5 mass% PVCap, growth PT conditions typically continue to follow the RGR(M) boundary to modest hydrate fractions (few mass% of water converted). In contrast, T1441 shows behaviour more similar to PVCap−PVP mixtures (Section 3.1.3); once a small fraction of hydrate has formed, growth rates increase rapidly, with PT conditions returning to − and following to higher hydrate fractions − a small CIR region comparable to that for PVP with methane. Again similar to PVCap−PVP mixtures, T1441 has 2 CIR regions; one similar to PVP at ΔT_{sub} = ~−1.4 °C and one which applies only at lower initial hydrate fractions (< ~1%) to ΔT_{sub} = ~−2.2 °C. It is not known whether T1441 is a mixture of polymers or purely a co-polymer, however, behaviour is clearly similar to a mixture of strong and weak polymers.

While T1441 is clearly significantly less able to inhibit s-I methane hydrate growth compared to PVCap (T1441 has not been tested for s-II CGI behaviour), it has the advantage of being considerably more soluble in water. With an ambient pressure cloud point temperature of >90 °C at 0.5 mass% aqueous compared to 38−39 °C for 0.5 mass% PVCap (PVCap average MW = 7000, both cloud points measured visually as part of this work), T1441 is likely to be much less potentially problematic with respect

to hot wellhead injection; KHI drop-out and 'gunking' at wellheads being a significant concern to operators.

HYTREAT Polymer Methane CGI Regions

HYTREAT co-polymer was supplied as 40% polymer in monoethylene glycol (MEG) however from in depth work done on MEG−PVCap systems (detailed in Chapter 8), it is not expected that the low concentration of MEG solvent present (0.75%) in the HYTREAT case will have a major effect on measured CGI regions.

Example cooling curves for 0.5 mass% HYTREAT aqueous with methane are shown in Figure 3-26 with interpolated boundaries Determined points on CGI region boundaries are reported in Table 3-7.

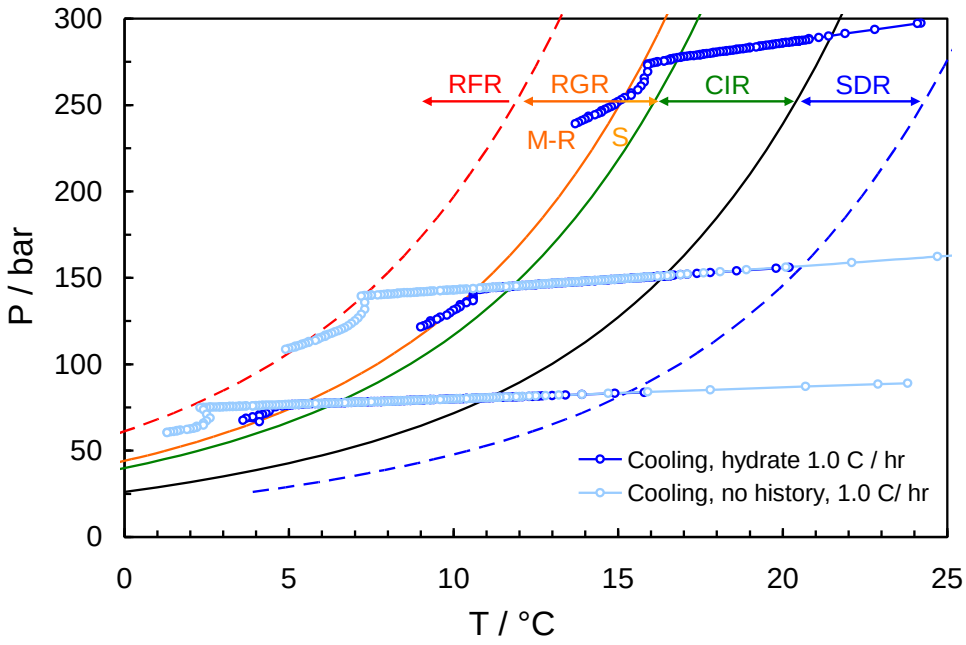

Figure 3-26 Example CGI cooling with hydrate (blue) and no history (light blue) cooling runs (1 °C/hr) for 0.5 mass% HYTREAT aqueous with methane (0.75 mass% MEG solvent present).

As can be seen in Figure 3-26, the behaviour of HYTREAT when cooling with a small fraction of hydrate present (>0.5%) was highly repeatable, with moderate growth occurring a consistently fixed subcooling of ~−5.3 °C; a common subcooling for CGI region changes in s-I methane systems. Step cooling with hydrate present confirms a CIR subcooling of ~−4.4 °C; this is only 0.8 °C less than that of 0.5% PVCap with methane. The significant extent of these CGI regions, combined with consistent rapid failure occurring only at ΔT_{sub} = ~−8.5 °C and no evidence for susceptibility to lose inhibition performance at low hydrate fractions, shows HYTREAT to be a relatively

well performing KHI; regions are overall only ~1.0 °C less than those for PVCap, at least in s-I methane systems. However, while HYTREAT can inhibit hydrate crystal growth more significantly that T1441, it has a lower cloud point comparable with PVCap at ~40 °C (measured visually as part of this work).

Table 3-7 Experimentally determined points on CGI region boundaries for methane with 0.5 mass% HYTREAT co-polymer aqueous (0.75 mass% MEG solvent present). See Section 2.3.1 for growth rate definitions.

CGR Boundary	*Growth rate	T / ºC (± 0.5)	P / bar (± 0.2)	ΔT_{s-I} / ºC (± 0.5)
SDR	Slow dissociation	20.5	156.7	3.8
		15.5	85.6	3.9
CIR-RGR(VS-S)	No Growth	6.3	77.4	−4.4
		11.7	145.0	−4.4
		16.7	275.6	−4.4
RGR(VS-S)-RGR(M)	Very slow to slow	5.3	76.7	−5.3
		10.7	143.6	−5.3
		15.9	273.0	−5.1
RGR(S-M)-RFR	Moderate	7.2	139.4	−8.6
		2.0	75.7	−8.5
		12.2	267.0	−8.6

*Growth rate is for ΔT CGI region preceding the associated boundary

Figure 3-27 shows a comparison of CGI region extents as a function of subcooling for 0.5 mass% aqueous T1441, HYTREAT and PVCap with methane at 70 bar which was explained above.

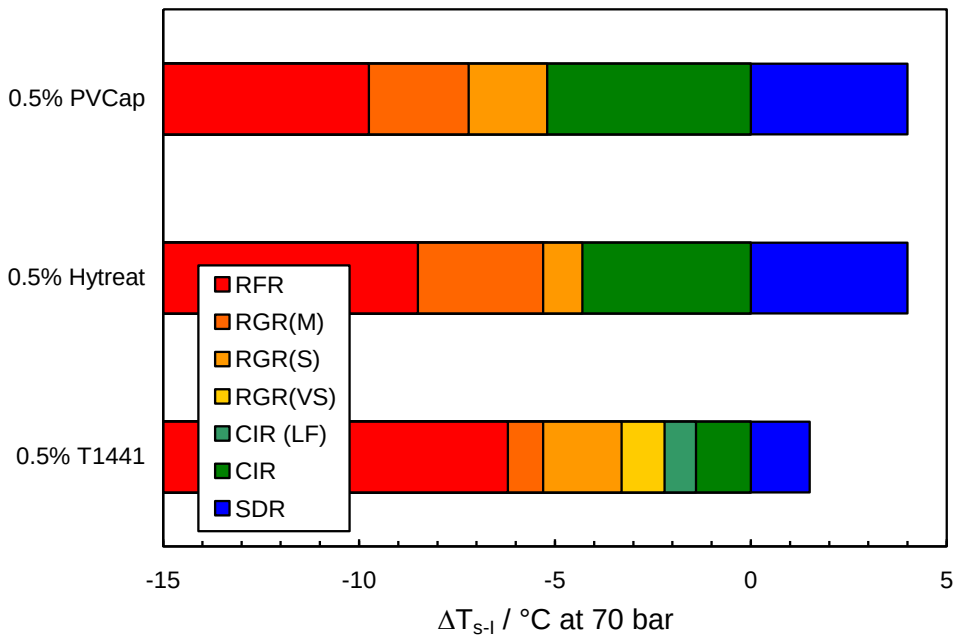

Figure 3-27 Comparison of subcooling extents of CGI regions for PVCap, HYTREAT and T1441 co-polymer at 70 bar pressure. Note that HYTREAT has 0.75 mass% MEG solvent present. CIR LF = CIR applies only at low hydrate fractions (< ~1%).

3.1.6. Luvicap Bio−Water−Methane System

Due to the growing interest in the use of biodegradable based polymers the use of a bio KHI as an inhibitor was evaluated using the new CGI technique. The biodegradable KHI used in these test was Luvicap-Bio base polymer (30mass% active ingredient in water) supplied by BASF. The concentration of the KHI solution used was 1.67 %mass in water to get a final 0.5mass% Luvicap-Bio in total. In addition, in some tests 2-butoxyethanol (ethylene glycol butyl ether / EGBE), was added as a synergist/solvent which was supplied by Sigma-Aldrich at 99.5% pure. The latter tests were carried out both to assess whether Luvicap Bio performance could be enhanced by synergists, and to provide an example for the guide to making CGI measurements provided in Chapter 2; industry testing typically focussing on formulation evaluation rather than the in-depth base polymer studies. These tests were carried out on 0.5 mass% Luvicap Bio / 1.5 mass% 2-butoxethanol to represent a KHI 'formulation' (polymer + synergist/solvent). Experiments were again performed in 99.995% pure methane up to 240 bar pressure using the same procedure detailed in Chapter 2.

Results and Discussion

Figure 3-28 and Figure 3-29 show example CGI method cooling runs and CGI region boundaries for 0.5 mass% Luvicap Bio aqueous with methane. Experimentally determined points and interpolated CGI boundaries for 0.5 mass% Luvicap Bio aqueous with methane are reported in Table 3-8. Figure 3-30 shows example CGI cooling and heating runs for 0.5 mass% Luvicap Bio / 1.5 mass% 2-butoxyethanol aqueous with methane. Figure 3-31 shows a comparison of methane hydrate CGI subcooling extents for 0.5 mass% Luvicap Bio, 0.5 mass% Luvicap Bio / 1.5 mass% 2-butoxyethanol and 0.5 mass% PVCap aqueous.

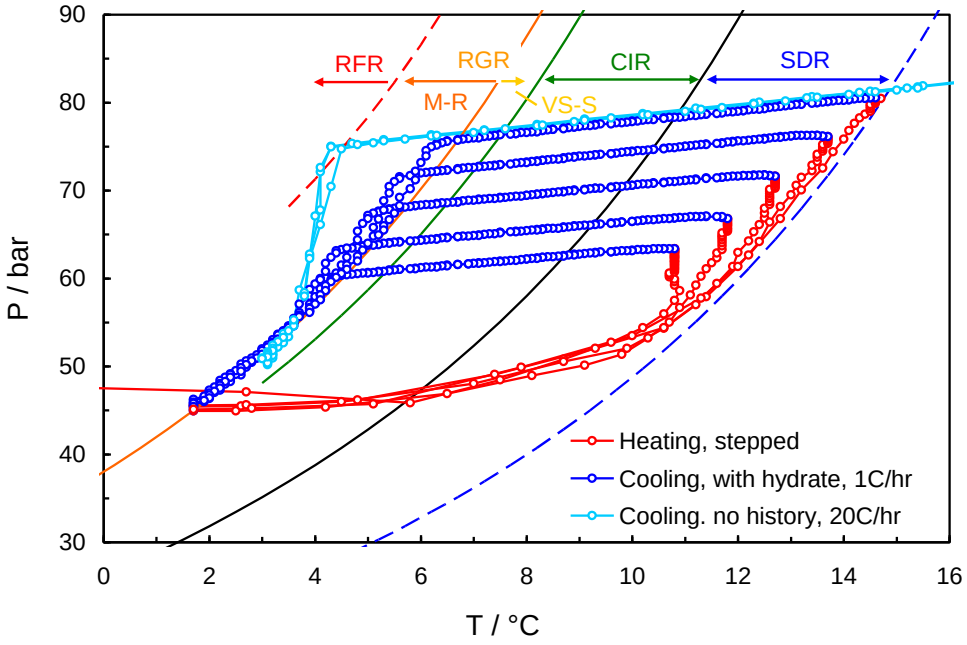

Figure 3-28 Example cooling runs with various fractions of hydrate present for 0.5 mass% Luvicap Bio aqueous with methane. Also shown are fast cooling runs with history eliminated.

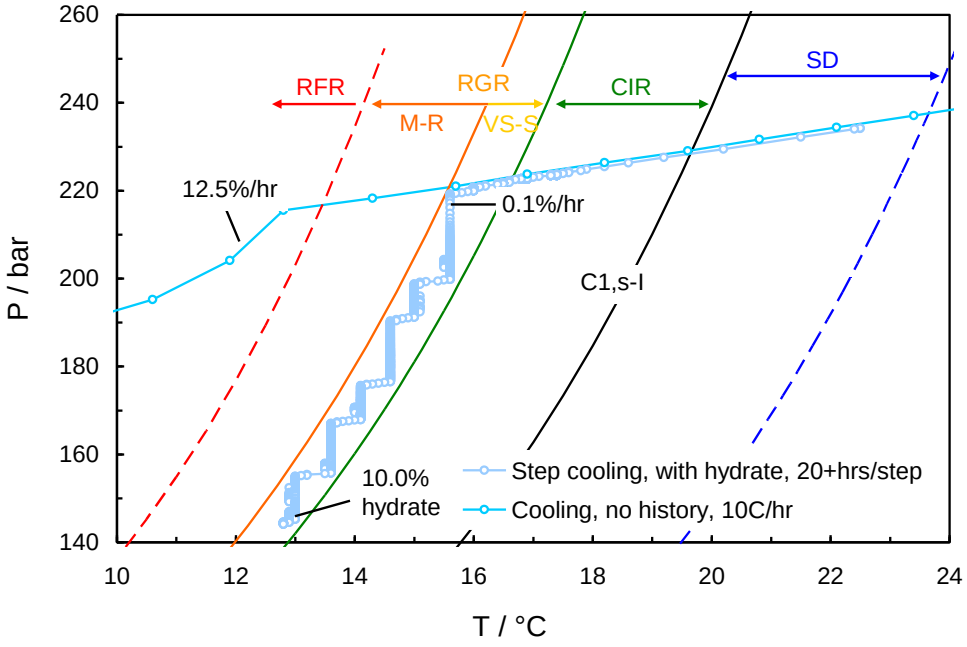

Figure 3-29 Example step-cooling run data for 0.5 mass% Luvicap Bio aqueous with methane.

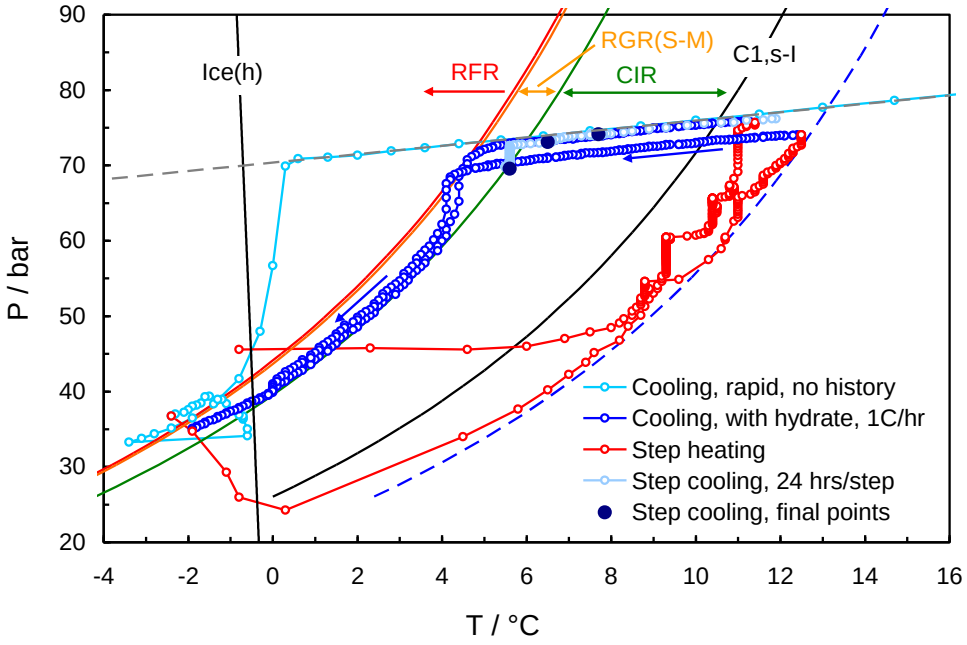

Figure 3-30 Example CGI cooling and heating runs for 0.5 mass% Luvicap Bio / 1.5 mass% 2-butoxyethanol aqueous with methane.

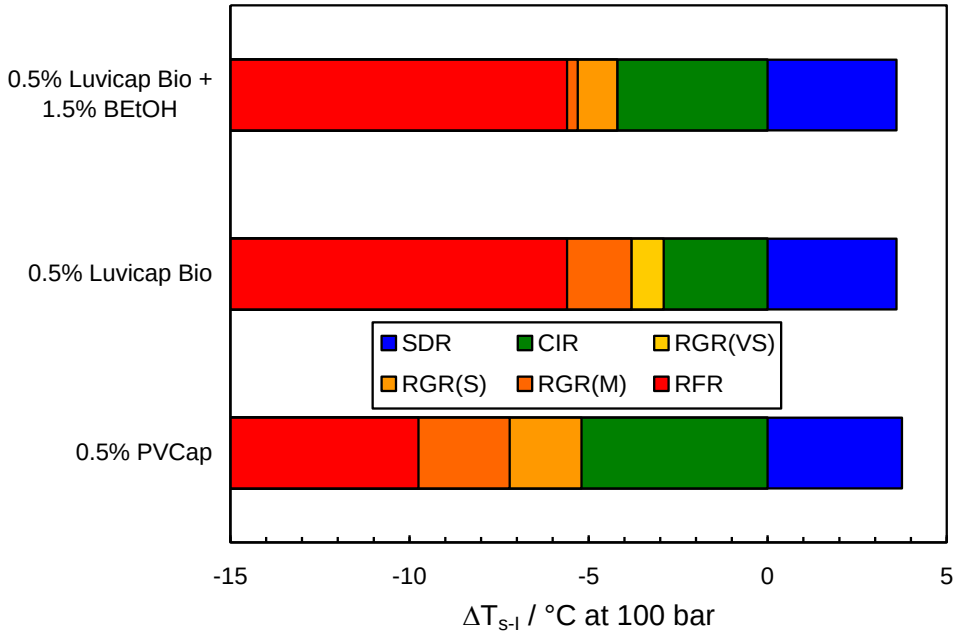

Figure 3-31 Comparison of subcooling extents of CGI regions from the s-I methane phase boundary for 0.5 mass% Luvicap Bio, 0.5 mass% Luvicap Bio / 1.5 mass% 2-butoxyethanol (BEtOH) and 0.5 mass% PVCap aqueous.

Table 3-8 Experimentally determined points on CGI region boundaries for 0.5 mass% Luvicap Bio aqueous with methane. See Section 2.3.1 for growth rate definitions.

CGR boundary	*Growth rate	T / ºC (± 0.5)	P / bar (± 0.2)	ΔT_{s-I} / ºC (± 0.5)
SDR	Slow dissociation	14.7	80.5	3.7
		20.2	151.8	3.7
CIR-RGR(VS)	No growth	7.6	77.0	−3.0
		13.1	143.7	−2.9
		16.6	221.4	−2.8
RGR(VS-M)	Very slow	3.0	50.9	−3.7
		6.5	75.6	−4.0
		12.1	141.0	−3.8
		15.6	221.0	−3.8
RGR(M)-RFR	Moderate	4.5	74.7	−5.9
		10.2	139.8	−5.6
		13.5	218.0	−5.8

*Growth rate is for ΔT CGI region preceding the associated boundary

As can be seen in Figure 3-28 to Figure 3-31, Luvicap Bio shows reasonably good performance as a crystal growth inhibitor for s-I methane hydrates. The pure base polymer induces complete inhibition (CIR) up to a subcooling of ~−2.9 °C and shows significant crystal growth inhibition up to ~−5.6 °C subcooling. As can be seen in Figure 3-29, step cooling over some 6 days within the RGR(VS) region only resulted in the growth of 10% hydrate, demonstrating strong repression of crystal growth.

As shown in Figure 3-30 and Figure 3-31, the addition of the common KHI solvent/synergist 2-butoxethanol improves performance, increasing the subcooling extent of the s-I methane CIR to ~−4.2 °C, although the extent of the RFR remains similar to that for pure base polymer.

Figure 3-32 shows induction time measured data and regions plotted as induction time versus subcooling from the methane phase boundary for 0.5 mass% Luvicap Bio + 1.5 mass% 2-butoxyethanol aqueous. Induction time measurements for this system revealed the *t*i trend to follow the commonly observed relationship to CGI regions in that *t*i drops to zero within a few degrees subcooling into the RFR region, rising rapidly towards infinity as the CIR is approached (explained in detail in section 2.5). In this case, the combination of 0.5 mass% Luvicap Bio + 1.5 mass% 2-butoxyethanol gave *t*i values > 12 hrs at ~−7 °C subcooling and < 50 hours at ~−6.5 °C subcooling, demonstrating good nucleation inhibition in addition to crystal growth suppression.

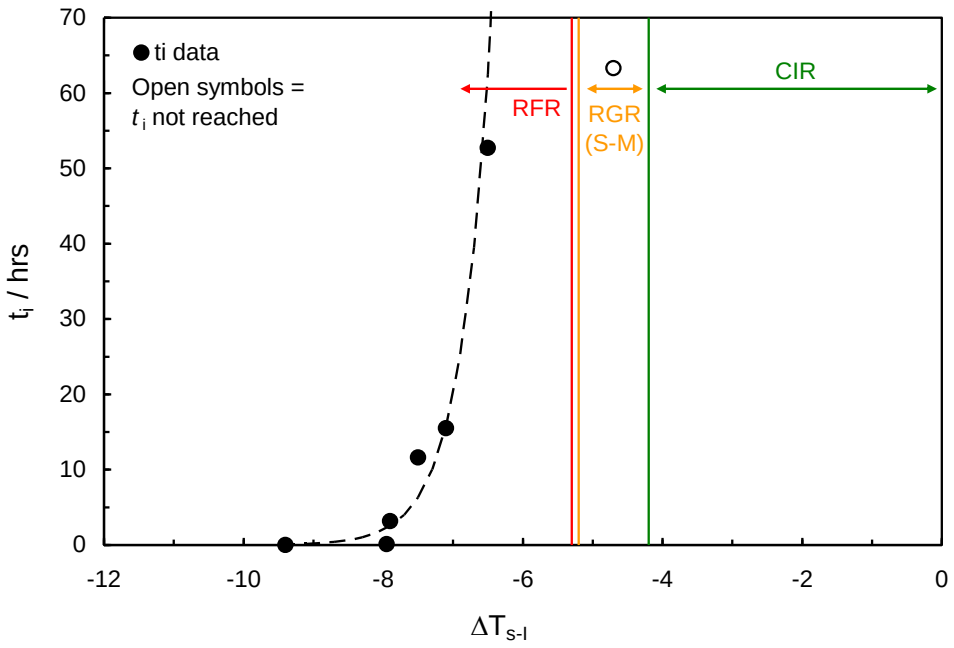

Figure 3-32 Measured *ti* data and CGI regions plotted as induction time versus subcooling from the methane phase boundary for 0.5 mass% Luvicap Bio + 1.5 mass% 2-butoxyethanol aqueous.

3.2. Polymer Molecular Weight

As detailed in Section 3.1 KHI polymer structure can have significant effect on its performance as a crystal growth inhibitor. As detailed, polymers with suitable size and shape pendant groups can absorb more strongly on hydrate surface and act as a strong barriers to further crystal growth. However, it is suspected that molecular mass of polymer molecules can also play some role in their inhibition properties since it is assumed that longer polymer chains will absorb more strongly to the crystal surface while shorter chains can diffuse faster to nucleation sites.

In Habetinova's studies on hydrate dissociation under the influence of low dosage kinetic inhibitors, the effect of polymer molecular weight (K-value) was also investigated. In this research, four PVP polymers with different K-values were tested in THF solution for their dissociation temperature that can then reflect the inhibition strength of the inhibitor. Polymers with higher K-values have higher molecular weight; the carbon chain which makes up the inhibitor is longer. Results revealed that, dissociation temperature for higher molecular weight PVP polymers were slightly higher. However, the dissociation time, the time elapsed after the temperature is raised to the dissociation temperature, clearly increased and also the dissociation rates decreased as the K-value of the polymer increased at the same weight percentages of polymer. The explanation given for this by Habetinova et al. (2002) was that for higher

K-value polymers more molecules are present at the same weight percentage of polymer. Hence, more molecules cover a larger area of the hydrate, and more time is needed before all the molecules are disengaged. Also the liquid around the hydrate consists of more inhibitor molecules, and the chance is greater that some inhibitor molecules diffuse towards the hydrate again. Moreover, for higher molecular weight polymers, the carbon chain, which makes up the inhibitor, is longer, hence when disengaged, more hydrate surface is exposed, and the dissociation can be faster (Habetinova et al., 2002).

More recently, O'Reilly et al. (2011) investigated the effect of polymer molecular weight on growth inhibition properties of PVP, PVCap and PVPip in THF solution. Results indicated that for all three polymers, as the molecular weight of the polymer increases, the concentration of polymer needed to prevent THF hydrate crystal growth decreased at any one subcooling. The explanation given for this was also considered to be that the longer polymer chains, higher molecular weight polymers, can more strongly adsorb onto hydrate crystal surfaces giving better surface coverage and therefore prevents THF hydrate crystal growth better. However, a further study on PVP in real gas hydrate systems (natural gas mixture giving S-II hydrates) showed that low molecular weight PVP gave best results. The reason for this behaviour was given by the fact that for gas hydrate nucleation inhibition, it is the low molecular weight polymer which has the greatest surface to volume ratio. Thus, the low molecular weight polymer perturbs the water structure better than higher molecular weight polymers which may in addition be curled up or entangled with intramolecular hydrogen-bonding, thus being less available to perturb the free water structure (O'Reilly et al., 2011).

In both the above studies, it is assumed that polymer molecular weight can have a clear effect on the polymer inhibition performance. However, the above studies where mainly performed in a THF solution at atmospheric pressure rather than a real gas at high pressure. Moreover, result of the second study showed that molecular weight of the polymer could have diverse effect in a real gas system compared to a THF solution. Therefore, to clearly understand the actual effect of molecular weight of polymer on its performance it was necessary to evaluate this parameter using the CGI technique and determine the CGI boundaries for different molecular weight polymer samples.

For this purpose, two samples of PVCap, (Luvicap-EG base polymer with MEG removed by drying, supplied by Champion Technologies), were used with average

molecular weights in the range of 4000-8000 for the low molecular weight (LMW) PVCap sample and 7000-15000 for high molecular weight (HMW) PVCap sample at concentration of 0.5 mass% PVCap relative to water for both samples. All experiments were carried out on high pressure stirred autoclaves using the CGI method described in Chapter 2 in a 99.995% pure methane system up to ~240 bar pressure.

Results and Discussion

Figure 3-33 and Figure 3-34 show example CGI method cooling curves for high molecular weight (HMW) and low molecular weight (LMW) PVCap methane systems respectively with CGI boundaries illustrated on each diagram. Data points for these boundaries for each of the systems are reported in Table 3-9 and Table 3-10. Also Table 3-11 shows average PVCap induced inhibition regions for each system.

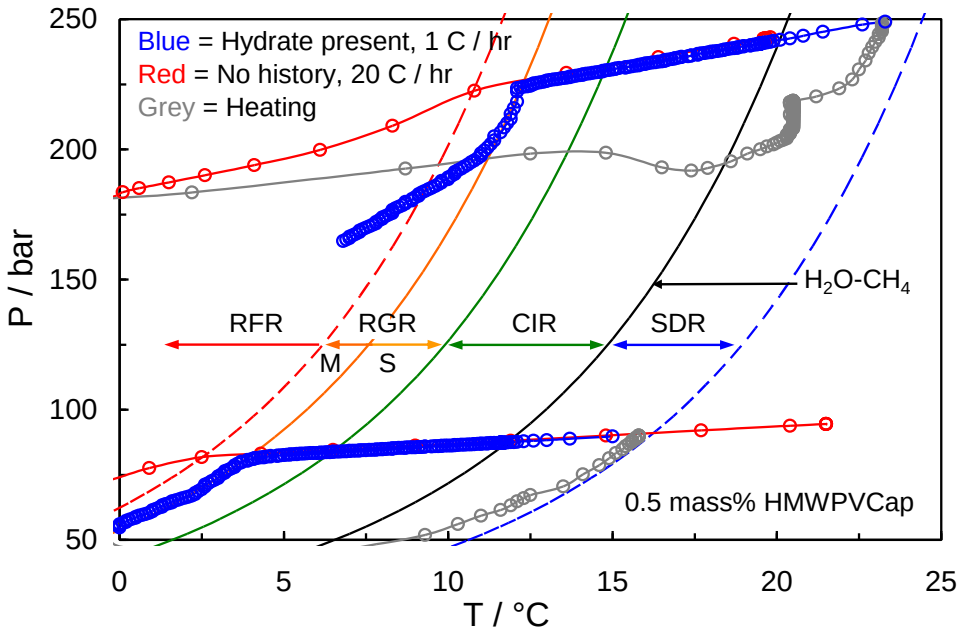

Figure 3-33 Example CGI cooling and heating runs for 0.5 mass% high MW PVCap aqueous with methane

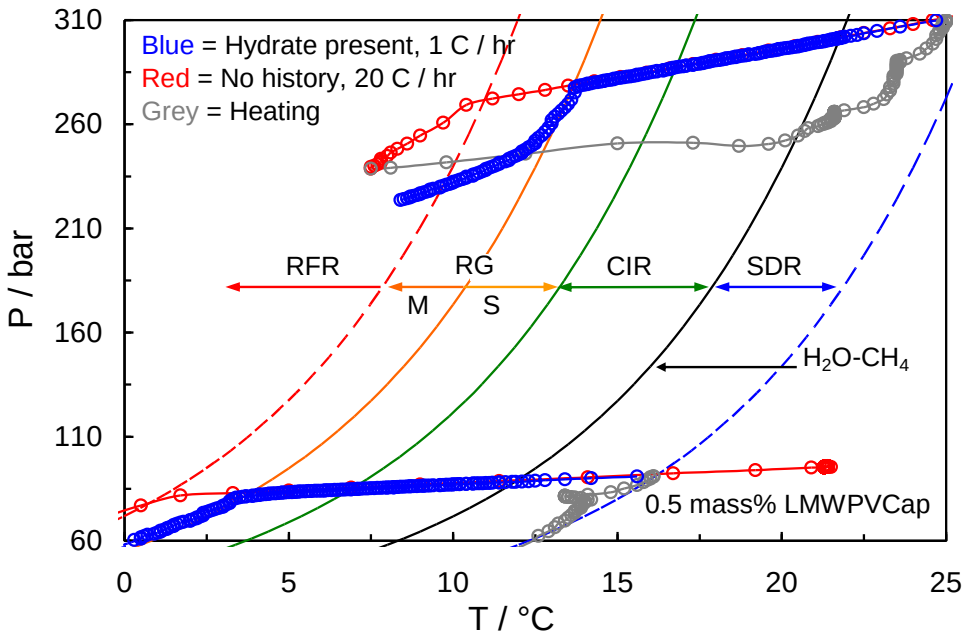

Figure 3-34 Example CGI cooling and heating runs for 0.5 mass% high MW PVCap aqueous with methane

Table 3-9 Experimental methane hydrate CGI region data for 0.5 mass% High MW PVCap aqueous. See Section 2.3.1 for growth rate definitions.

CGR Boundary	*Growth rate	T / ºC (± 0.5)	P / bar (± 0.2)	ΔT_{s-I} / ºC (± 0.5)
SDR	Slow dissociation	16.3	89.3	4.3
		24.3	251.7	3.9
CIR-RGR(S)	No growth	6.3	83.7	−5.1
		14.9	230.8	−4.8
RGR(S-M)	Very slow to slow	3.9	81.1	−7.3
		12.2	222.7	−7.3
RGR(M)-RFR	Moderate	1.7	79.7	−9.3
		9.9	216.2	−9.3

*Growth rate is for ΔT CGI region preceding the associated boundary

Table 3-10 Experimental methane hydrate CGI region data for 0.5 mass% Low MW PVCap aqueous. See Section 2.3.1 for growth rate definitions.

CGR Boundary	*Growth rate	T / ºC (± 0.5)	P / bar (± 0.2)	ΔT_{s-I} / ºC (± 0.5)
SDR	Slow dissociation	16.1	91.1	3.9
		25.4	283.2	4.1
CIR-RGR(S)	No growth	6.5	84.6	−5.0
		16.5	286.3	−4.8
RGR(S-M)	Very slow to slow	3.9	81.6	−7. 6
		12.2	277.9	−7. 4
RGR(M)-RFR	Moderate	1.6	81.6	−9.6
		11.2	271.8	−9.7

*Growth rate is for ΔT CGI region preceding the associated boundary

In both Figure 3-33 and Figure 3-34, different CGI regions can clearly be distinguished from cooling curve data. In agreement with previous tests on PVCap systems (Section 3.1), the presence of 0.5 mass% PVCap induces characteristic CGI complete inhibition (CIR), reduced growth rate (RGR) and rapid growth/failure (RFR) regions.

Results for 0.5 mass% HMW PVCap aqueous and 0.5 mass% and LMW PVCap aqueous show that in both systems CIR (ΔT_{sub} =~−5.0 °C) and SDR (ΔT_{sub} =~+4 °C) remain almost identical. However, there is a minor difference in the RGR and RFR gained from two different molecular weight PVCap systems. In the high molecular weight PVCap system RGR and RFR are ΔT_{sub} =~−7.3 °C and ~−9.3°C respectively which is slightly less than that for low molecular weight PVCap system which has RGR of ΔT_{sub} =~−7.5 °C and RFR of ΔT_{sub} =~−9.7 °C. However, it should be considered that the difference in the RGR of the two experiments lies within experimental error (± 0.5°C).

Table 3-11 Experimental methane hydrate average CGI region data for 0.5 mass% high and low molecular weight PVCap aqueous

	ΔT_{sub} RFR/°C	ΔT_{sub} RGR(M) /°C	ΔT_{sub} CIR /°C	ΔT_{sub} SDR /°C
High Mw PVCap	−9.3	−7.3	−5.0	4.1
Low Mw PVCap	−9.7	−7.5	−4.9	4.0

The fact that CGI behaviour is unchanged between the two different molecular weight PVCap systems is significant. Hence, this unchanged behaviour indicates that the length of PVCap polymer does not really affect its ability in absorption to the hydrate surface, at least for the molecular weights tested (it should be considered that the difference in the molecular weight samples that were used was not very large; both samples being >4000).

3.3. Conclusions

The newly developed Crystal Growth Inhibition technique was applied to a number of KHI polymers in a simple methane system to both prove the validity of the method and evaluate how different KHIs can perform as a crystal growth inhibitor.

Confirming earlier conclusions in the previous chapter; controlled PVT studies using the new approach have revealed that aqueous PVCap induces a number of well-defined

hydrate growth / inhibition / dissociation regions which have been observed for all PVCap concentrations tested to date. These regions include a slow dissociation rate region (SDR) outside the hydrate stability zone, a complete crystal growth inhibition region (CIR) within the HSZ to quite high subcoolings, a following restricted/reduced hydrate growth rate region (RGR), which can be further subdivided based on relative crystal growth rates, and a final rapid/immediate failure region (RFR).

Moreover, evaluating the performance PVCap show a distinct PVCap concentration dependence for the degree of hydrate inhibition offered. For 0.25 mass% PVCap, the CIR and subcooling to the RFR are consistently smaller than for 0.5 and 1.0 mass%, although all concentrations share the common RGR boundary line at ΔT_{sub} = ~−5.2 °C suggesting this is an ubiquitous crystal growth morphology controlled feature.

There is little difference in all measured boundaries for 0.5 and 1.0 mass% PVCap, again indicating that the features likely relate to underlying, subcooling-controlled (driving force) crystal growth patterns which the polymer is exploiting. Data also suggest that the 'optimum' PVCap concentration for methane−water systems is > 0.25 mass% and ≤ 0.5 mass%, at least in terms of CIR subcooling. However, increasing the concentration of PVCap to 1.0 mass% is very beneficial in that it greatly reduces growth rates in the RGR region compared to 0.5 mass% (e.g. rates are 4 times slower in the first 50 hours in the temperature range of ~−7.3-−9.5°C when the concentration is 1.0 mass%). This is even more evident from 5.0 mass% PVCap data in which CIR is again at ~−5.2 °C but growth rates in all other regions are significantly reduced and extended to much higher subcoolings.

Initial tests on PVP confirm its performance is much poorer than PVCap; the CIR for PVP being only ~−1.4 °C, compared to ~−5.2 °C for PVCap, with little or no SDR observed. This suggest the adsorption strength of PVP on hydrate crystal surfaces is much weaker, potentially due to the smaller molecular diameter of the amide pendant group (i.e. its interactions with open hydrate cavities are much weaker).

Due to the good performance of PVCap detected and knowing the higher solubility of PVP, CGI studies were undertaken on a PVCap-PVP mixture sample. Measurement of KHI induced CGI regions for PVCap−PVP mixtures showed that while PVP is very poor when performing on its own, the addition of small fractions of PVCap (e.g. 0.05 mass% PVCap, 0.95 mass% PVP) greatly increases performance. However, this

performance increase is highly susceptible to the fraction of hydrate formed for low PVCap concentrations; sudden and rapid failure can occur once a critical hydrate fraction is reached.

Furthermore, the combination of 2 polymers gives 2 CIR regions; a higher subcooling one applicable only at low hydrate fractions and a lower subcooling one which can be sustained even to quite high hydrate fractions (>10 mass% of aqueous phase).

Thus, it is concluded that care must be taken when applying the new method to inhibitor evaluation, and it is recommended that 'hydrate present' runs be carried out for various initial hydrate fractions to assess the KHI sensitivity to this and ensure results take this into account. Moreover, results clearly demonstrate that polymer performance must not be judged on performance in pure form. While polymers may perform poorly alone, in combination they may have strong synergism.

Examining the effect of PEO revealed that this polymer has very weak inhibition properties and all crystal growth inhibition regions are significantly smaller than that for PVCap at the same concentration or even PVP at a smaller polymer concentration. Hence, results show that although PEO is a polymer made up of monomers that are the right size for taking part in the formation of a hydrate structure, the polymer itself is not necessarily an effective hydrate inhibitor due to the unsuitable size pendant groups which cannot stabilize on the surface of the hydrate. As a result, the pendant group of a polymer plays a major role on the KHI inhibition properties.

Results of CGI studies on two commercial KHI polymers − T1441 co-polymer and HYTREAT− in s-I methane systems showed that each of these commercial polymers clearly have defined CGI boundaries although performing very differently. While T1441 is clearly significantly less able to inhibit s-I methane hydrate growth compared to PVCap, it is considerably more soluble in water, with an ambient pressure cloud point temperature of >90 °C (0.5 mass% aqueous) compared to 38−39 °C for PVCap. T1441 is thus less likely to be problematic with respect to hot injection 'gunking' at wellheads. Significantly, T1441, a co-polymer, shows similar behaviour to weak-strong polymer combinations (e.g. PVCap−PVP) as it is highly sensitive to the fraction of hydrate present in the system; failure conditions reducing dramatically to low subcoolings for only small fractions of hydrate (< 1 mass% of aqueous phase) as well as

having 2 CIR regions for this polymer, with one only applicable at low hydrate fractions (< ~1.0 mass% of aqueous phase).

The significant extent HYTREAT CGI regions (only ~1.0 °C less than PVCap), combined with no evidence for susceptibility to lose inhibition performance at low hydrate fractions, shows HYTREAT to be a relatively good performing KHI. However, while HYTREAT can inhibit hydrate crystal growth more significantly that T1441, it has a low cloud point comparable with PVCap at ~40 °C (measured visually as part of this work).

The on-going problem of balancing polymer solubility with KHI performance is readily apparent; high polymer precipitation temperatures − which offer less potential hot-injection issues − commonly equating to reduced inhibition performance, at least for PVCap and the 2 commercial polymers tested here.

CGI studies of the biodegradable polymer Luvicap Bio (manufactured by BASF) revealed that Luvicap Bio shows reasonably good performance as a KHI, both in terms of crystal growth inhibition and nucleation inhibition. Moreover, its performance can be enhanced by the addition of synergist solvents such as 2-butoxethanol. In light of these findings, good crystal growth inhibition up to subcoolings of ~−10 °C or more is apparently possible for Luvicap Bio base polymer, making it comparable with many existing commercial formulations in performance.

CGI region studies on the effect of polymer molecular weight on inhibition properties of two different molecular weight PVCap (high and low) solutions showed that, PVCap performance does not change noticeably due to PVCap average molecular weight difference at least for the molecular weights tested (4000- 8000 and 7000-15000); both HMW PVCap and LMW PVCap samples studied offer equivalent complete crystal growth inhibition (CIR) regions and show similar SDR regions. Changes in the position of RGR and RFR boundaries are small and within the range of experimental error.

The fact that CGI behaviour is unchanged indicates that the length of PVCap polymer does not really affect its ability in absorption to the hydrate surface, at least for the molecular weights tested. Certainly, benefit of very low molecular weight polymers is increased water solubility and thus a higher critical solution temperature (Kirsh, 1998); an advantage at wellhead temperatures. Therefore, if very low molecular weight PVCap (even lower than PVCap samples tested here) shows similar performance to higher

molecular weight PVCap samples, the former will be a better option as a kinetic hydrate inhibitor.

References

Colle, K. S., R. H. Oelfke, et al., 1999, *"Method for inhibiting hydrate formation"*, U.S. Patent 5,874,660.

Habetinova, E., Lund, A., and Larsen, R., 2002, *"Hydrate Dissociation under the Influence of Low-Dosage Kinetic Inhibitors"*, Proceedings of the 4th International Conference on Gas Hydrates, Yokohama, Japan

Kelland, M. A., 2006, *"History of the Development of Low Dosage Hydrate Inhibitors"*, Energy Fuels, 20, 825-847

Kelland, M. A. and J. E. Iversen., 2010, *"Kinetic hydrate inhibition at pressures up to 760 bar in deep water drilling fluids."* Energy & Fuels 24(5), 3003-3013

Kirsh, Y. E. and I. E. Kirsh, 1998*, "Water soluble poly-N-vinylamides: synthesis and physicochemical properties*", John Wiley & Sons, Chichester

Kumar, R., Lee, J. D., Song, M., and Englezos, P., 2008, *"Kinetic inhibitor effects on methane/propane clathrate hydrate-crystal growth at the gas/water and water/n-heptane interfaces"*, Journal of Crystal Growth, 310, 1154–1166

Larsen, R., Knight, C. A., and Sloan, E. D., 1998, *"Clathrate Hydrate Growth and Inhibition"*, Fluid Phase Equilibria, 150-151, 353-360

Larsen, R., Knight, C. A., Rider, K. T., and Sloan, E. D., 1999, *"Melt Growth and Inhibition of Ethylene Oxide Clathrate Hydrate"*, Journal of Crystal Growth, 204, 376- 381

Lederhos, J., J. Long, et al., 1996, "*Effective kinetic inhibitors for natural gas hydrates.",* Chemical Engineering Science, 51, 1221-1229

Makogon, T. Y., Larsen, R., Knight, C. A., and Sloan, E. D., 1997, *"Melt Growth of Tetrahydrofuran Clathrate Hydrate and its Inhibition: Method and First Results"*, Journal of Crystal Growth, 179, 258-262

O'Reilly, R., Ieong, N. Z., Chua, P. C., and Kelland, M. A., 2011, *"Crystal growth inhibition of tetrahydrofuran hydrate with poly(N-vinyl piperidone) and other poly(N-vinyl lactam) homopolymers"*, Chemical Engineering Science, 66, 6555–6560

Sakaguchi, H., Ohmura, R., and Mori, Y. H., 2003, *"Effects of kinetic inhibitors on the formation and growth of hydrate crystals at a liquid–liquid interface"*, Journal of Crystal Growth, 247, 631–641

Sloan Jr, E. D., 1995, *"Method for controlling clathrate hydrates in fluid systems"*, U.S.Patent 5,432,292

Sloan Jr, E. D., 1995, *"Method for controlling clathrate hydrates in fluid systems"*, U.S.Patent 5,420,370

Sloan Jr, E. D., R. L. Christiansen, et al., 1997, *"Additives and method for controlling clathrate hydrates in fluid systems"*, U.S. Patent 5,639,925

Svartaas, T. M., Gulbrandsen, A. C., Huseboe, S. B. R., and Sandved, O., 2008, *"An experimental study on "un-normal" dissociation properties of structure II hydrates formed in presence of PVCAP at pressures in the region 30 to 175 bars – dissociation by temperature increase"*, Proceedings of the 6th International Conference on Gas Hydrates, Vancouver, Canada

4. EFFECT OF GUEST GAS/HYDRATE STRUCTURE ON CGI REGIONS

The newly developed CGI technique provided the chance to assess the effect of guest gas on KHI-induced hydrate crystal growth inhibition patterns.

Only a few studies have been done on the performance of KHIs in different hydrate structure systems, and most of these studies were performed using semi-clathrate hydrate formers, such as THF and EO, at atmospheric pressure.

Larsen et al. (1998, 1999) studied the effect of PVCap and PVP in both Tetrahydrofuran (THF) and ethylene oxide (EO) aqueous solutions which form hydrate structure II (s-II) and hydrate structure I (s-I) respectively. Results clearly showed that polymers change the morphology of the hydrate in different ways depending on the type of hydrate, s-I or s-II, that the system can form. For instance PVCap has the capability of changing the morphology of the hydrate crystal such that for the same concentration of KHI in both systems THF, s-II, system is inhibited to higher subcoolings than the EO, s-I, system (Larsen et al., 1998; Larsen et al., 1999)

Zhang et al. (2009) investigated the adsorption behaviours of two kinetic inhibitors, PVP and PVCap, on cyclopentane (CP) hydrates which is again a structure II former but slightly different to THF and expected to behave closer to natural gas. His work also proved that both these polymers can inhibit hydrate formation and growth with PVCap being more effective than PVP. However, these studies were again at atmospheric pressure and yet not totally comparable with a real gas system at critical conditions of high pressure and low temperature (Zhang et al., 2009).

Peng et al. (2009) investigated the effect of a different KHI, VC-713, on the nucleation of hydrate by measuring interfacial tensions between methane and aqueous solution at different KHI concentrations. His investigations also found that this KHI definitely inhibits the growth stage of hydrate formation. However, in this study too evaluations are done only on one type of hydrate, methane in this case, and no comparison is done on the performance of this KHI in a different gas/hydrate system (Peng et al., 2009).

As a result, to understand the performance of KHIs in different guest gas/hydrate structure systems, it was required to thoroughly investigate this behaviour using the new CGI technique. By measuring different CGI regions in each system in the presence of the same KHI (PVCap in this case) at an identical concentration (0.5 mass% in aqueous) the effect of guest gas/structure on CGI regions can be inspected. For this purpose several different systems with single, binary and multi component gases were tested. By gradually building up more complex gas systems toward natural gas, the influence of each individual component and its presence with other gases can be better understood. As a result, in a real natural gas system a more precise prediction of the system can be made. Single gas systems that were examined were methane (C1), ethane (C2), propane (C3) and carbon dioxide (CO2) with C1, C2 and CO2 as structure I formers and C3 Structure II former (Sloan et al., 2008).

Binary gas systems examined were methane + ethane (95mole% C1 / 5mole% C2), two different combinations of methane + propane (98mole% C1 / 2mole% C3 and 90mole% C1/ 10mole% C3) and methane + carbon dioxide (85mole% C1 / 15mole% CO2) which all form structure II hydrates (determined through finding dissociation points and hydrate phase boundary). Also, two other binary systems tested in which one of the components was in liquid state were methane + Cyclopentane (cC5) (1:4 cC5 to water volume ratio) which is a structure II hydrate former and methane + Methylcyclohexane (mC6) (1:4 mC6 to water volume ratio) which forms hydrate structure H.

Multi component gas systems that were tested were methane + ethane + propane (93mole% C1 / 5mole% C2 / 2mole% C3), and a standard North Sea natural gas (NG) (gas composition displayed in Table 4-11). In all these systems the stable hydrate structure is s-II.

Due to the good performance of PVCap compared to other simple KHIs and the extensive studies undertaken on evaluating the performance of this polymer (Section 3.1), PVCap was the selected KHI to adopt throughout all the experiments in this chapter. For fairer judgment of all tested systems, the concentration of KHI was taken to be 0.5 mass% PVCap aqueous (PVCap was Luvicap-EG base polymer K-value = 25-8, average MW = 7000, supplied by BASF, with the ethylene glycol solvent removed by vacuum oven drying) which was assumingly the optimum PVCap concentration. (Section 3.1.1)

The technique applied in each experiment was again the CGI approach detailed in Chapter 2. For each system careful, controlled *PVT* studies were undertaken to thoroughly define hydrate growth / inhibition / dissociation regions which, as mentioned before, are:

1. A *slow dissociation rate* region (SDR) outside the hydrate stability zone (HSZ)
2. A *complete crystal growth inhibition* region (CIR) within the HSZ to quite high subcoolings
3. A following *restricted/reduced hydrate growth rate* region (RGR), which can be further subdivided based on relative crystal growth rates
4. And a final rapid/immediate failure region (RFR)

4.1. Effect of Methane on CGI Regions with PVCap

Evaluating the performance of PVCap, or in other words the effect of methane on CGI regions with PVCap, tests were performed in the presence of 99.995% pure methane gas, which forms structure I hydrate, at pressures up to 300 bar (4350 psi). The extensive experiments carried out for determining these CGI regions are explained in Section 3.1.1. For 0.5mass% PVCap crystal growth inhibition regions (SDR, CIR, RGR and RFR) are illustrated in Figure 4-1 with example cooling curves for no history, history and hydrate present. Experimental methane hydrate CGI region data for 0.5 mass% PVCap aqueous are reported in Table 4-1.

Table 4-1 Experimental methane hydrate CGI region data for 0.5 mass% PVCap aqueous. See Section 2.3.1 for growth rate definitions.

CGR Boundary	*Growth rate	T / ºC (± 0.5)	P / bar (± 0.2)	ΔT_{s-I} / ºC (± 0.5)
SDR	Slow dissociation	14.9	77.8	4.2
		20.9	167.3	3.7
		23.4	196.9	4.0
CIR- RGR(S)	No Growth	4.7	71.0	–5.2
		13.6	204.8	–5.2
		16.4	297.6	–5.2
RGR(S-M)	Slow to moderate	2.4	68.3	–7.1
		7.9	129.6	–7.3
		14.2	288.5	–7.2
RGR(M)- RFR	Moderate	0.2	69.2	–9.5
		9.0	196.9	–9.5
		11.6	284.1	–9.7

*Growth rate is for ΔT CGI region preceding the associated boundary

As can be seen from the figure, the SDR region in this system in about ~+4.0 °C outside the thermodynamic stability zone and the CIR extends to ΔT_{sub}=~–5.2 °C for this PVCap concentration; this is clearly defined in the figure where pressure is seen to begin dropping on leaving this region. While 5.2 °C is not a particularly large degree of subcooling for complete inhibition, it is equivalent to the same degree of thermodynamic inhibition offered by ~18.5 mass% MEG, i.e. 0.5 mass% PVCap offers the same degree of complete inhibition as 37 times its mass of MEG (will be discussed in more detail in Chapter 8). This is a very substantial reduction in inhibitor mass/volume, yet still offering time-independent complete aqueous phase hydrate inhibition.

Furthermore as detected from the graph, in this system the temperature range in which crystal growth does happen but is very slow, RGR (S), extends to ΔT_{sub} = ~–7.2 °C, with region of moderate crystal growth, RGR(M), extending to the rapid failure region boundary, RFR, at ΔT_{sub} = ~–9.5 °C. Moreover, it is evident that PT conditions in the RGR closely follow a crystal growth region boundary line. These findings along with others indicated in Section 3.1.1 clearly support the assumption that these features likely relate to underlying, subcooling-controlled (driving force) crystal growth patterns which the polymer is exploiting.

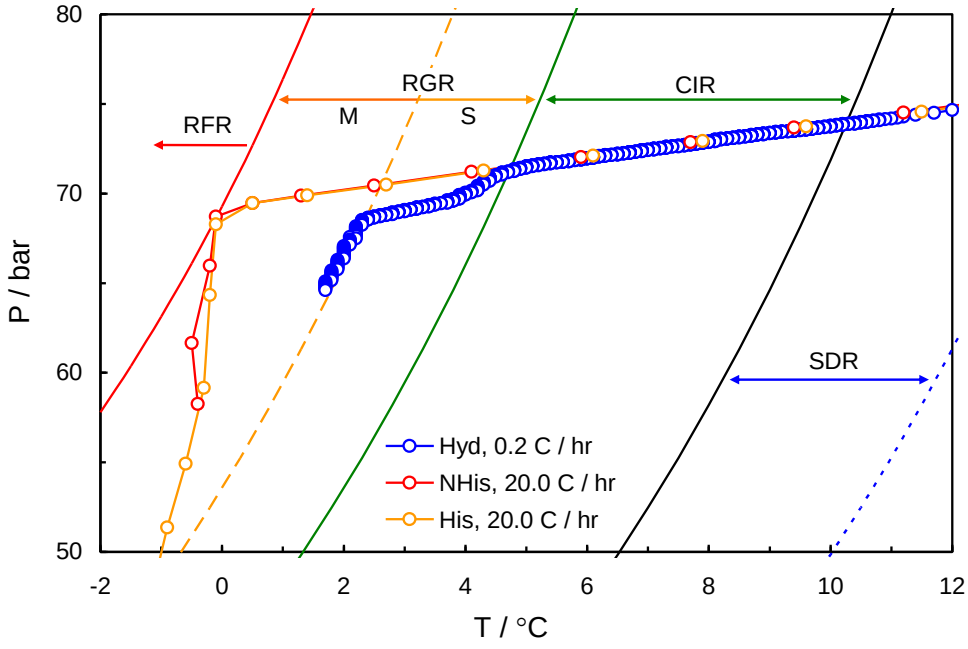

Figure 4-1 PT plot showing cooling curves for determination of complete inhibition (CIR) and reduced growth rate region (RGR) boundary lines for 0.5 mass% PVCap (Luvicap-EG base polymer) aqueous for no history (NHis), history (His) and hydrate (Hyd) present.

4.2. Effect of Ethane on CGI Regions with PVCap

CGI measurements have been made for 0.5 mass% PVCap aqueous with 99.5% pure ethane, a structure I hydrate former, at around ~27 bar(~400 psi) pressure. Experimental ethane hydrate CGI region data for 0.5 mass% PVCap aqueous are reported in Table 4-2. Also, Figure 4-2 shows an example cooling curve used to determine CGI regions for this system.

Table 4-2 Experimental ethane hydrate CGI region data for 0.5 mass% PVCap aqueous. See Section 2.3.1 for growth rate definitions.

CGR Boundary	*Growth rate	T / ºC (± 0.5)	P / bar (± 0.2)	ΔT_{s-I} / ºC (± 0.5)
SDR	Slow dissociation	16.9	28.0	3.3
CIR-RGR(VS)	No growth	7.8	26.1	−5.2
RGR(VS-S)	Very slow to slow	5.8	25.6	−7.2
RGR(S)-RFR	Moderate	3.1	25.0	−9.7

*Growth rate is for ΔT CGI region preceding the associated boundary

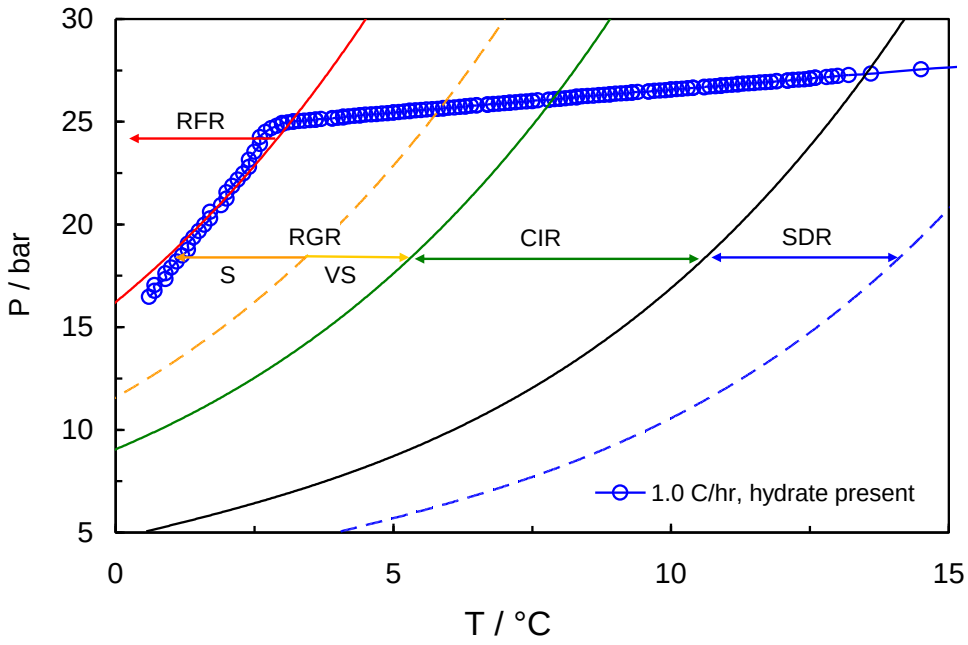

Figure 4-2 Example cooling curves for determination of CGI regions for 0.5 mass% PVCap aqueous with ethane. With hydrate present, growth is very slow at ΔT_{sub} > ~−5.2 °C (RGR(VS)), increasing slowly before moderate growth finally occurs at ΔT_{sub} = ~−9.5 °C (RGR(S)-RFR boundary).

As can be seen, while the s-I ethane hydrate system shares the same CGI boundaries as for s-I methane (which supports the current assumption that underlying crystal growth patterns as a function of subcooling have a major influence on behaviour), hydrate

growth rates are much greater in the RGR in the case of methane, i.e. PVCap is able to inhibit the growth of ethane hydrates much more effectively than it can methane.

Given that both methane and ethane have very low aqueous solubility their dissolution in the aqueous phase would not be intuitively expected to affect PVCap performance. Therefore an alternative explanation as to why the PVCap performance varies so significantly between systems when both gases are s-I formers is required. One possibility is guest cage occupancies; ethane hydrates only require the filling of large ($5^{12}6^2$) cavities for stability. In contrast, methane hydrate requires complete occupancy of large and ~90% occupancy of small (5^{12}) cages for stability. If PVCap pendant groups are adsorbing into partially open large cavities on the hydrate surface, then maybe the fact that accompanying open small cavity filling is not required in the case of ethane favours the formation of a more stable PVCap-hydrate complex, increasing performance. In the case of methane hydrate, the inability of PVCap to satisfy the requirement for small cavity filling could encourage breakdown of the PVCap-hydrate complex and hydrate growth on certain crystal faces. This is of course highly speculative, but certainly the influence of guest gas is an important one.

4.3. Effect of Propane on CGI Regions with PVCap

In addition to examining the performance of PVCap in a structure I hydrate system it is necessary to evaluate this behaviour in an s-II forming system. For this purpose crystal growth inhibition region data have been generated for 1.0 mass% PVCap with propane, a larger molecules than methane and ethane, which occupies the $5^{12}6^4$ cavity and forms s-II (Sloan et al., 2008). Propane used in these experiments was 99.99% pure and supplied from BOC Gases.

Figure 4-3 shows example CGI method cooling curves with and without hydrate for a propane–water–PVCap system. As shown in simple propane–water–PVCap systems, it was impossible to grow s-II C3 hydrates in the H+L+G region; PVCap apparently indefinitely inhibiting crystal growth down to the ice point (+8 °C subcooling). The only way to induce hydrate formation in this system was to cool it down into the ice region, form ice and since PVCap cannot prevent the ice to hydrate transition consequently convert ice to hydrate. Therefore, the growth of ice and subsequent conversion of ice to hydrate facilitated hydrate growth when the temperature was raised

back above the ice point. The very large SIR region illustrated on the graph (~ 13 °C outside phase boundary) confirms the presence of the large CIR region in this system.

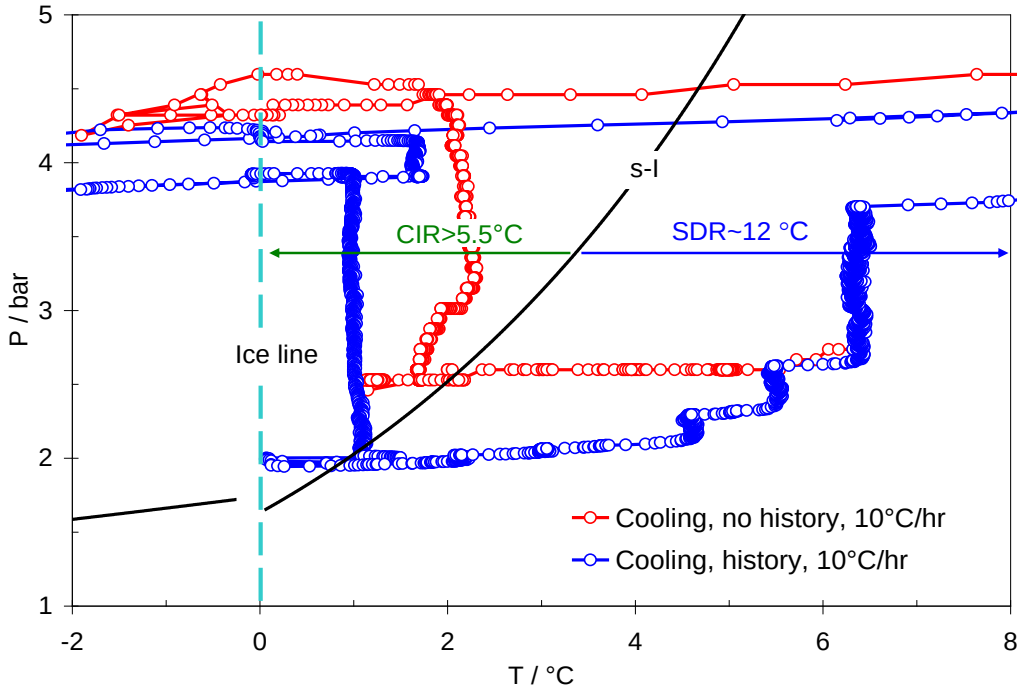

Figure 4-3 CGI regions determined for a propane system with 1.0 mass% PVCap aqueous.

Results suggest that PVCap performs much better in an s-II forming system almost indefinitely inhibiting structure II hydrate. However for this to be confirmed further investigations were required which will be presented in the following sections of this chapter.

4.4. Effect of Carbon Dioxide on CGI Regions with PVCap

Evaluating the effect of CO_2 which is a structure I hydrate former is particularly important due to the presence of CO_2 in natural gases. Crystal growth inhibition region studies have been performed 0.5 mass% PVCap with CO_2 in which the CO_2 was 99.99% pure and supplied from Air Products. Figure 4-4 illustrates example CGI method cooling curves with and without hydrate for a CO_2–water–PVCap system and also the interpolated CGI boundaries for this system.

As evident from the graph PVCap performance is considerably reduced in pure CO_2 (s-I) systems. The complete inhibition region in this system has considerably reduced to only about ~2.1 °C subcooling from the s-I boundary. The reduced growth rate region in this system lies almost on the same boundary (~2.2 °C) beyond which growth rates increase markedly, indicating a significant reduction in the ability of the polymer to

inhibit crystal growth. The RFR boundary is also only up to ΔT_{s-I} = ~–5.2 °C which is again very small compared to the simple methane system.

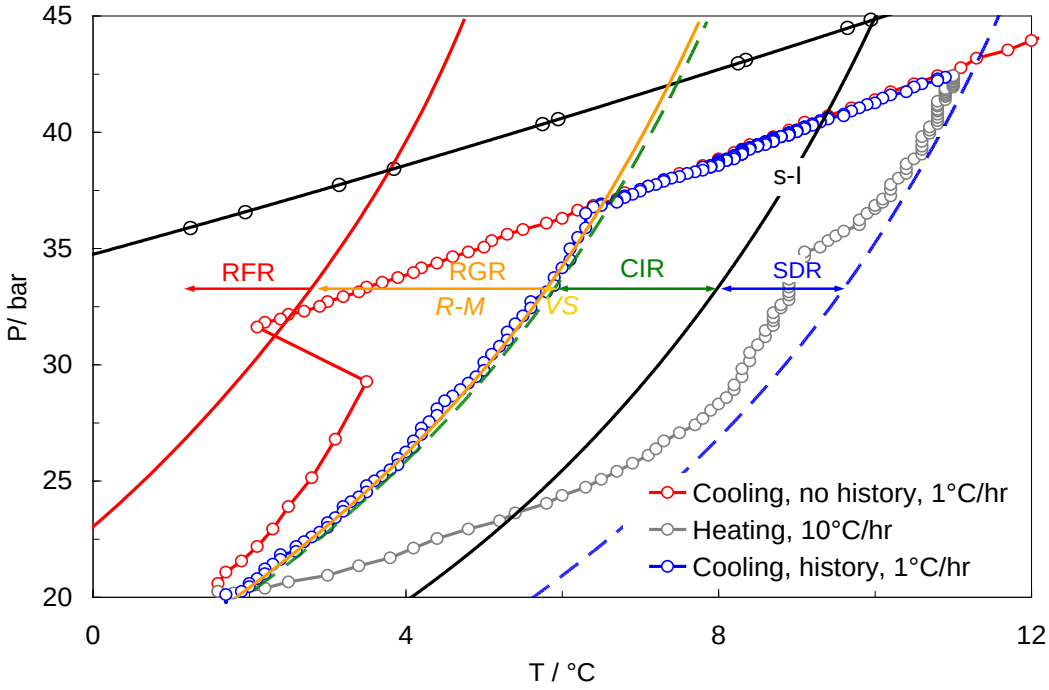

Figure 4-4 CGI regions determined for a CO_2 system with 0.5 mass% PVCap aqueous.

In conclusion the presence of CO_2 in natural gases is expected to cause a negative effect and reduce PVCap performance in such systems. To conclude on this behaviour, other CO2 present systems have been evaluated in Sections 4.8 and 4.9 (methane–CO_2 and NG systems).

4.5. Effect of Methane + Propane on CGI Regions with PVCap

As discussed in Section 4.3, in studies on simple propane–water–PVCap systems, it was impossible to grow s-II C3 hydrates in the H+L+G region; PVCap apparently indefinitely inhibiting crystal growth down to the ice point (8 °C+ subcooling). Hence, to apply the new CGI method on a system where structure II is the most stable structure, growth inhibition regions for methane–propane–water systems in the presence of aqueous PVCap were determined. For this purpose, two different gas compositions of C1-C3 (90 mole% C1 / 10 mole% C3 and 98 mole% C1 / 2 mole% C3) were tested. Results of each set of experiments are reported individually.

4.5.1. Effect of (90 mole% C1 / 10 mole% C3) Regions with PVCap

CGI Regions for a 10 Mole% Propane 90 Mole% Methane System

Crystal growth inhibition region data have been generated for 0.5 and 1.0 mass% PVCap aqueous with 90 mole% C1 / 10 mole% C3 gas mixture at pressures up to 300 bar (4350 psi). The high C3 content of the gas (10 mole%) used was chosen as it would allow a large degree of subcooling to be achieved before ice or s-I methane hydrate phase boundaries were surpassed; i.e. the aim being to avoid the formation of these, whereby ideally permitting PVCap-induced inhibition regions for s-II hydrates to be clearly distinguished. As reported in Section 4.3 due to s-II hydrate inhibition all the way down to the ice point (formation of ice at +8 °C subcooling) in the presence of PVCap at this concentration, CGI studies were not possible to perform appropriately. The high propane content of the gas used here (10%) would allow some +17 °C subcooling (at 50 bar) to be achieved before the ice point. Likewise, this propane content would give at least 12 °C subcooling before the methane hydrate stability region was entered.

Crystal growth inhibition regions are illustrated in Figure 4-5 and Figure 4-6 for 0.5 and 1.0 mass% PVCap aqueous respectively.

Table 4-3 details the average subcooling range and observed relative growth rates for each region. Experimental points for region boundaries, as determined from changes in relative growth rates for both continuous and step-cooling runs, are reported in Table 4-4 and Table 4-5.

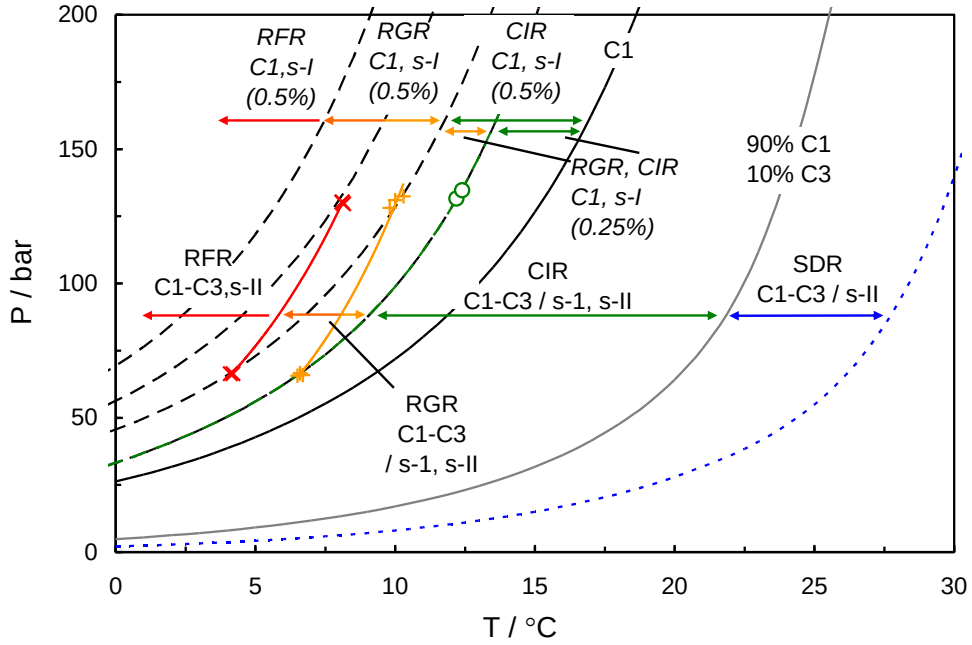

Figure 4-5 PT plot showing measured experimental points delineating the various crystal growth inhibition regions for 0.5 mass% PVCap with a 90 mole% C1 / 10 mole% C3 mixture (coloured lines) and 0.25 , 0.5 and 1.0 mass% PVCap with C1 (black dotted lines)

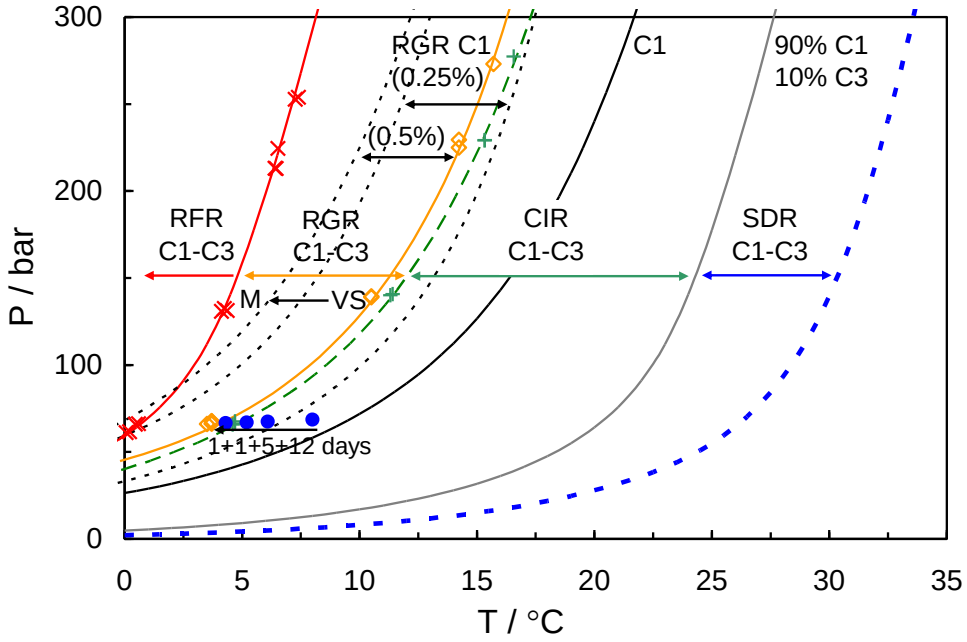

Figure 4-6 PT plot showing measured experimental points delineating the various crystal growth inhibition regions for 1.0 mass% PVCap with a 90 mole% C1 / 10 mole% C3 mixture (red points / lines) and methane (black lines, 0.25, 0.5 and 1.0 mass% PVCap). Blue points are cooling steps for experiment detailed in Figure 4-7

Two important features of inhibition regions for the C1-C3 mix can be observed in Figure 4-5 and Figure 4-6: (1) the considerable size of the CIR in terms of subcooling, and (2) the apparent strong correlation between some C1-C3 s-II forming mixture inhibition/polymer controlled growth regions with those for s-I methane systems.

Table 4-3 Experimentally determined hydrate growth inhibition regions for PVCap-water-methane-propane systems. The gas used was 90 mole% C1 / 10 mole% C3. Growth rates are relative. For comparison, approximations to convert initial 1% of aqueous phase to hydrates are as follows: very slow = 48 hours+, slow = 24-48 hours, moderate = 1-24 hours, fast = <1 hour. ΔT_{sub} ranges are average values.

Mass% PVCap	0.5	1.0
CIR ΔT_{sub} range / ºC (± 0.5) Growth Rate	0.0 − 11.5-13.6* Zero	10.6-15.6 Zero
RGR ΔT_{sub} range / ºC (± 0.5) Growth Rate	11.5-13.6 − 15.5-16.1* Slow − moderate	10.6-15.5− 19.5 Very slow − moderate
RFR ΔT_{sub} range / ºC (± 0.5) Growth Rate	~15.5-16.1+* Fast	19.5+ Fast

* ΔT_{sub} range / ºC (± 0.5 ºC) for 60 to 130 bar

Table 4-4 Experimentally determined points on crystal growth inhibition region boundary lines for 0.5 mass% PVCap (Luvicap-EG base polymer) aqueous with a 90mole% methane / 10 mole% propane gas mixture.

CGR Boundary	*Growth rate	T / ºC (± 0.5)	P / bar (± 0.2)	ΔT_{s-I} / ºC (± 0.5)	ΔT_{s-II} / ºC (± 0.5)
CIR–RGR(S)	No growth	6.5	65.8	–2.7	–13.6
		12.2	131.5	–3.1	–11.5
RGR(S-M) (s-I independent)	Slow growth	6.5	65.7	–2.7	–13.6
		10.3	132.4	–5.1	–13.5
RGR(M)-RFR (s-I independent)	Moderate to rapid	4.2	66.4	–5.1	–16.0
		8.1	130.3	–7.1	–15.6

*Growth rate is for ΔT CGI region preceding the associated boundary

Table 4-5 Experimentally determined points on crystal growth inhibition region boundary lines for 1.0 mass% PVCap (Luvicap-EG base polymer) aqueous with a 90mole% methane / 10 mole% propane gas mixture

CGR Boundary	*Growth rate	T / ºC (± 0.5)	P / bar (± 0. 2)	ΔT_{s-I} / ºC (± 0.5)	ΔT_{s-II} / ºC (± 0.5)
CIR–RGR(S)	No growth	4.7	66.2	–4.5	–15.5
		11.4	140.7	–4.5	–12.6
		16.6	277.3	–4.5	–10.6
RGR(S–M) (s-II independent)	Slow growth	3.7	66.2	–5.5	–16.5
		10.5	139.4	–5.3	–13.5
		14.2	229.5	–5.4	–12.0
RGR(M)-RFR (s-I independent)	Moderate to rapid	0.1	61.1	–8.4	–19.6
		4.1	130.8	–11.2	–19.6
		6.5	224.5	–12.7	–19.5
		7.3	252.7	–13.1	–19.4

*Growth rate is for ΔT CGI region preceding the

In a recent comprehensive review, Kelland (2006) surmised that KHI use would most likely have to remain restricted to systems with subcoolings < 10 °C due to their inability to prevent hydrate growth at higher values. However, Figure 4-6 shows that the complete crystal growth inhibition region for 1 mass% PVCap with 90%C1/10%C3 extends to over 15.5 °C subcooling at lower pressures (60 bar) relative to structure II phase boundary. As discussed, in this region (CIR) hydrate growth is apparently indefinitely inhibited; even if hydrate is already present in the system it does not grow.

Figure 4-7 shows an example plot of pressure change due to hydrate growth and subcooling for a stepped cooling run through the CIR region for 1 mass% PVCap with 90% C1 / 10% C3. PT conditions for each step and number of days at that condition are shown in Figure 4-6. As can be seen, even with a small fraction of hydrate present in the system, essentially no detectable growth (pressure drop) is seen at high subcoolings (12-15.2 °C) in the CIR for 19 days. Only when the temperature is reduced (i.e., subcooling is increased) a fraction of a degree further into the RGR(VS) region does hydrate growth begin very slowly before becoming faster in RGR(M) (at 20 days).

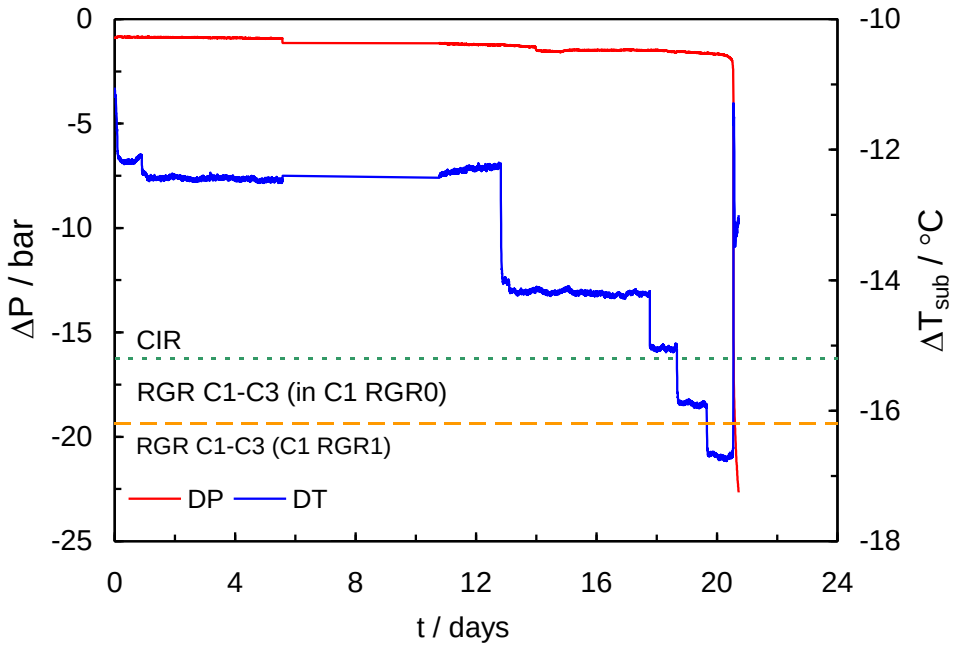

Figure 4-7 Example plot of pressure change due to hydrate growth (ΔP) and subcooling (ΔT_{sub}) for a stepped cooling run through the CIR region for 1 mass% PVCap with 90% C1 / 10% C3. PT conditions for each step and number of days at that condition are shown in Figure 4-6

Based on results, it is speculated that higher propane contents could yield even higher effective CIR subcoolings (Examined and reported in Section 4.5.2). In this sense, while regions clearly are a function of subcooling (e.g. see Section 3.1.1 for methane systems), the maximum subcooling that can be achieved before KHI failure is not

around 10-12 °C as commonly postulated (Kelland, 2006), but rather can be considerably greater and is clearly related to the gas composition/phase boundary; for hydrates which have a high thermal stability (e.g. large component of s-II forming guests), the CIR can be very large as seen here. It is speculated that this subcooling could be even greater if PVCap could more effectively inhibit structure-I hydrate formation, as is discussed below.

As shown in Figure 4-5 and Figure 4-6, there appears to be a very close association with hydrate growth/inhibition boundaries for the C1-C3 mixture with those for methane. Figure 4-8 shows cooling curves to determine inhibition regions for 0.5 mass% PVCap with the 90 mole% C1 / 10 mole% C3 mixture at about 60 bar. Runs are for no history, history, and hydrate present at various cooling rates. As can be seen, for hydrate history and hydrate present, the initial hydrate growth begins at a subcooling of $\Delta T_{s\text{-}I}$=~–2.7 which is a commonly seen region boundary line in methane systems (Section 3.1.1). This line appears to be almost identical to the CIR boundary line for 0.25 mass% PVCap with methane.

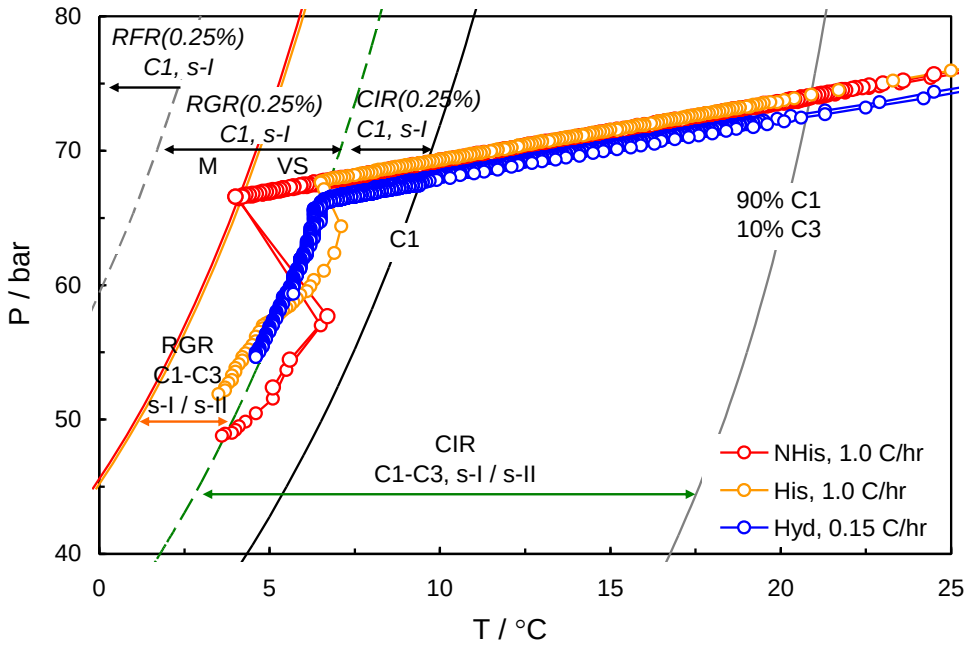

Figure 4-8 PT plot showing example cooling curves to determine inhibition regions for 0.5 mass% PVCap with the 90 mole% C1 / 10 mole% C3 mixture. Runs are for no history (NHis), history (His) and hydrate (Hyd) present. Also demonstrated are methane hydrate (s-I) growth/inhibition regions for 0.25 mass% PVCap

In hydrate history and hydrate present runs the rapid growth region measured at this pressure was found to occur at the same subcooling as the CIR relative to s-I phase boundary. However, at the higher pressure this region had a larger subcooling from s-I

phase boundary. Although both these points where found to be at a subcooling of ~–13.6 from s-II phase boundary.

For a no history run at this pressure and also the higher pressure tested as shown in Figure 4-5, growth begins suddenly and rapidly at a fixed system boundary line at a subcooling of ~–15.6 relative to s-II hydrate phase boundary. This result indicates that for 0.5wt% PVCap with 90 mole% C1 / 10 mole% C3 mixture similar to RGR the RFR boundary is clearly related to structure-II phase boundary.

Thus data for 0.5 mass% PVCap with the C1-C3 mix suggest that the CIR region appears to be related to the formation of s-I methane hydrates. However, it is known that PVCap is incapable of inhibiting the liquid- liquid transition of s-I hydrates to s-II hydrates hence after passing the CIR s-II hydrates may also be present in the system. As a result, as it is found that other KHI failure/hydrate growth boundaries seem related to s-II phase boundary; this failure may be related to the inability for PVCap to prevent or slowdown the growth of s-II methane hydrates.

Figure 4-9 and Figure 4-10 show example cooling curves to determine inhibition regions for 1.0 mass% PVCap with the 90 mole% C1 / 10 mole% C3 mixture for no history, history and hydrate present at various cooling rates. Methane hydrate growth/inhibition boundaries are shown for comparison.

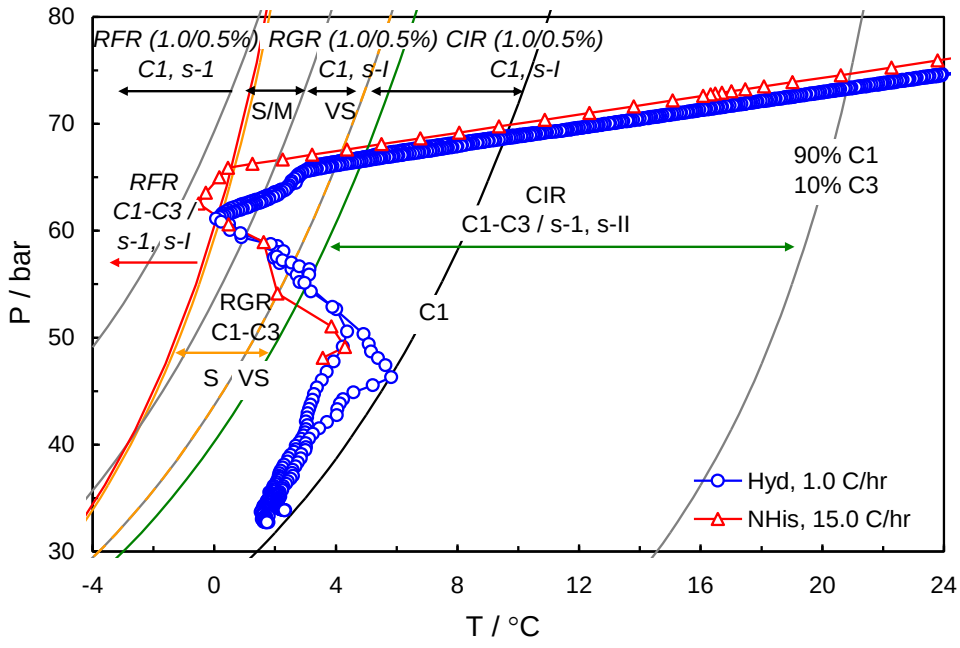

Figure 4-9 PT plot showing example cooling curves to determine inhibition regions for 1.0 mass% PVCap with the 90 mole% C1 / 10 mole% C3 mixture. Runs are for no history (NHis) and hydrate (Hyd) present at various cooling rates. Coloured and black lines are C1-C3 mix and methane hydrate (s-I) inhibition regions for 1.0/0.5 mass% PVCap respectively.

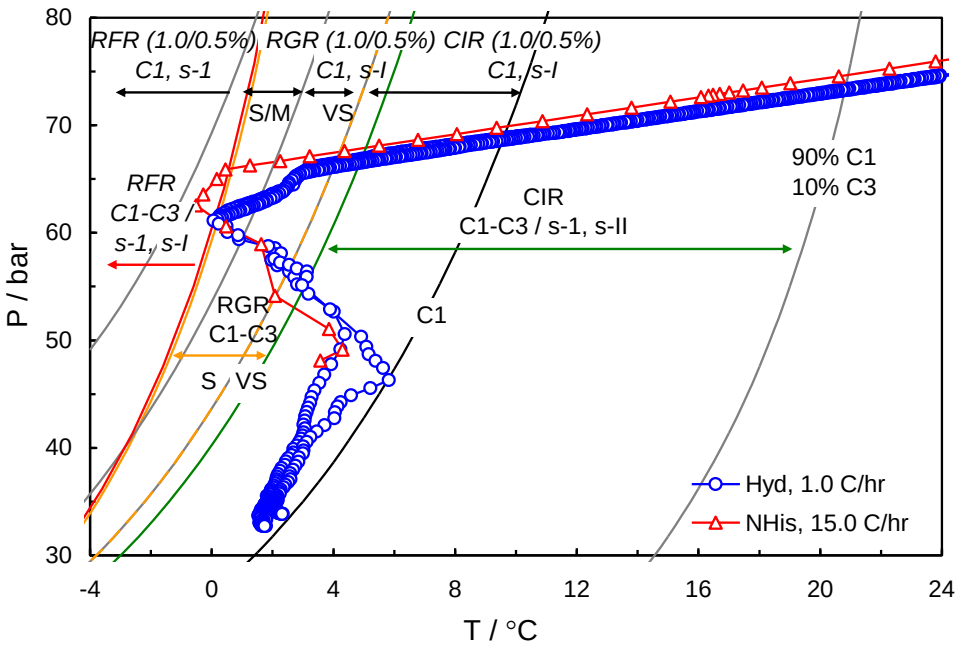

Figure 4-10 PT plot showing example cooling curves to determine inhibition regions for 1.0 mass% PVCap with the 90 mole% C1 / 10 mole% C3 mixture. Runs are for no history (NHis) and hydrate (Hyd) present at various cooling rates. Coloured and black lines are C1-C3 mix and methane hydrate (s-I) inhibition regions for 1.0/0.5 mass% PVCap respectively.

At 1 mass% PVCap hydrate growth conditions in the C1-C3 system seem to be closely related to those for structure-I methane hydrate. For hydrate present, runs are highly repeatable; no growth/dissociation occurs on cooling to the methane hydrate boundary. As the methane hydrate boundary is passed at ΔT_{sub} = > ~10 °C, dissociation commonly begins (e.g. Figure 4-9); as indicated by a reduction in pressure drop. Growth finally begins in earnest, albeit very slowly at the C1-C3 CIR boundary. This boundary lies within the region where growth can occur in methane systems at low PVCap concentrations (e.g. ΔT_{sub} = >~–3.0 °C for 0.25 mass% PVCap). Upon crossing the CIR boundary line for 1.0/0.5 mass% PVCap with methane (ΔT_{sub} = ~–5.2 °C from methane hydrate phase boundary) in the C1 RGR(M) region, growth rates for hydrate present runs with the C1-C3 mix increase, but are still relatively slow. This behaviour is very similar to that for methane systems (Section 3.1.1). As can be seen in Figure 4-6, Figure 4-9 and Figure 4-10, this behaviour was observed for all pressures tested up to 300 bar. Thus data for 1.0 mass% PVCap with the C1-C3 show that at this higher concentration of PVCap inhibition growth regions seem closely related to structure-I methane behaviour, strongly suggesting that at higher KHI concentrations where there is sufficient polymer present for hydrate inhibition, 'failure' in s-II systems is very likely due to their inability to inhibit s-I hydrates as effectively as s-II.

One feature of data for the 90% C1 / 10% C3 mix with 1.0 mass% PVCap which is apparently unrelated to s-I regions is the RFR (Rapid Failure Region) boundary line, similar to 0.5 mass% PVCap. As shown in Figure 4-6, Figure 4-9 and Figure 4-10, unlike all other boundaries which show fixed subcoolings relative to the methane hydrate phase boundary, the C1-C3 mix RFR line is at fixed subcooling (ΔT_{sub} = ~–19.6 °C) from the s-II phase boundary for the mixture. Points on this line were most readily achieved when fast cooling rates (e.g. > 10 °C / hr) were used and no history was present, as shown in Figure 4-10. With history present (Figure 4-10, higher pressure run), even if cooling rates were fast, moderate growth begun before the RFR line, with failure similarly occurring rapidly when it was reached. The fact that this line parallels the C1-C3 mix phase boundary and does not relate to methane growth/inhibition regions suggests that it is likely a purely s-II feature; i.e. it may represent the conditions where PVCap can no longer prevent s-II growth, with boundaries at lower subcoolings being related to the influence of s-I formation.

The C1-C3 RFR line, like the s-I methane RFR, appears to delineate the maximum subcooling to which the polymer can significantly control crystal growth rates; exceeding this results in rapid, largely uncontrolled hydrate growth within minutes. This line could thus be considered as representing the point where induction time is effectively zero.

Gas Phase Analyses During Hydrate Growth in C1-C3 systems

The above results demonstrated that for a 10 mole% propane / 90 mole% methane gas mixture, CGI region boundaries (CIR, RGR) seem closely related to those expected for s-I methane hydrates and it is thus speculated that failure in s-II systems is predominantly due to the inability of PVCap to prevent s-I growth.

In light of this, to gain a better understanding as to which structure was being formed, the gas phase composition of a PVCap inhibited system during initial hydrate formation was monitored. Thus test carried out, involved monitoring of the gas composition during hydrate formation for systems with PVCap and a structure II hydrate forming synthetic mixture (90mole% methane / 10 mole% propane); the aim being to investigate if any s-I hydrate is initially formed during the failure of the system, which would suggest that hydrates form due to the weakness of the PVCap to inhibit s-I hydrates.

The apparatus used for online gas sampling, as shown in Figure 4-11was based on a static-analytic method with fluid phase sampling. Phase equilibrium was achieved in a 80 ml cylindrical hastelloy cell which can operate up to 400 bar between –30°C and +100 °C. The cell was immersed in a constant–temperature liquid bath that controlled and maintained the desired temperature. In order to perform accurate temperature measurements in the equilibrium cell, temperature was measured directly inside the cell with uncertainty within ± 0.05 °C. Pressure was measured by means of a *Druck* pressure transducer. The pressure transducer was calibrated against a deadweight tester and the measurement uncertainties were estimated to be within ± 0.08 bar in the 1 to 400 bar range.

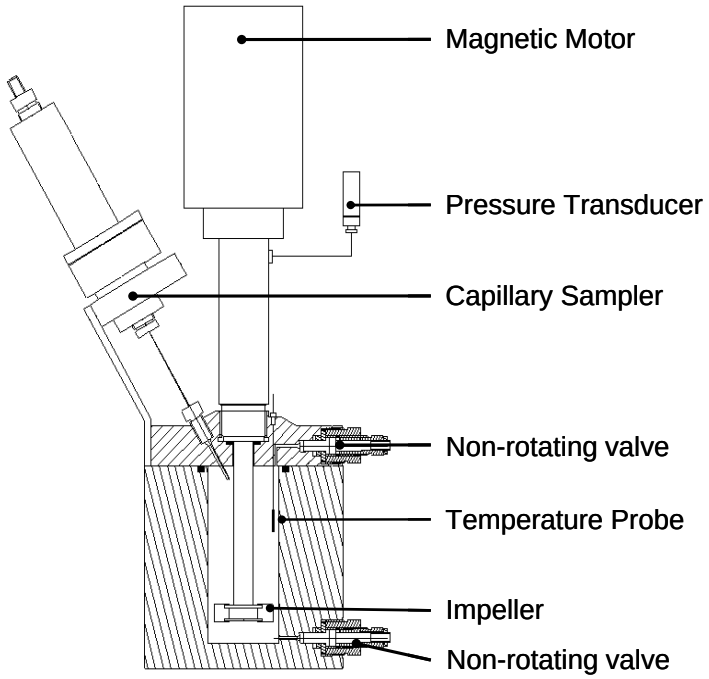

Figure 4-11 Schematic illustration of the autoclave capillary sampling cell.

Fluid sampling was carried out using a capillary sampler injector, which was connected to the top of the cell through 0.1 mm internal diameter capillary tube. The withdrawn samples were swept into a Varian 3800 gas chromatograph for analysis through heated lines (T = 180 °C, Figure 4-12). The capillary inlet of the sampler was directly in contact with the vapour phase and the outlet of the capillary was closed by a movable micro-stem operated by a pneumatic bellows. When the bellows was open the outlet of the capillary was also open, then the sample could flow inside the expansion room which was flushed with the carrier gas. The carrier gas swept the sample to the GC column for analysis. The sampler allowed direct sampling at the working pressure without disturbing the cell equilibrium due to the relatively small size of the sample.

The mass of samples could be adjusted continuously from 0.01 to several mg by an electronic timer. The expansion room of the sampler was heated independently from the equilibrium cell to allow the samples to remain in vapour state. The GC was equipped with a Flame Ionisation Detector (FID) and a Thermal Conductivity Detector. The FID was used to detect methane and propane.

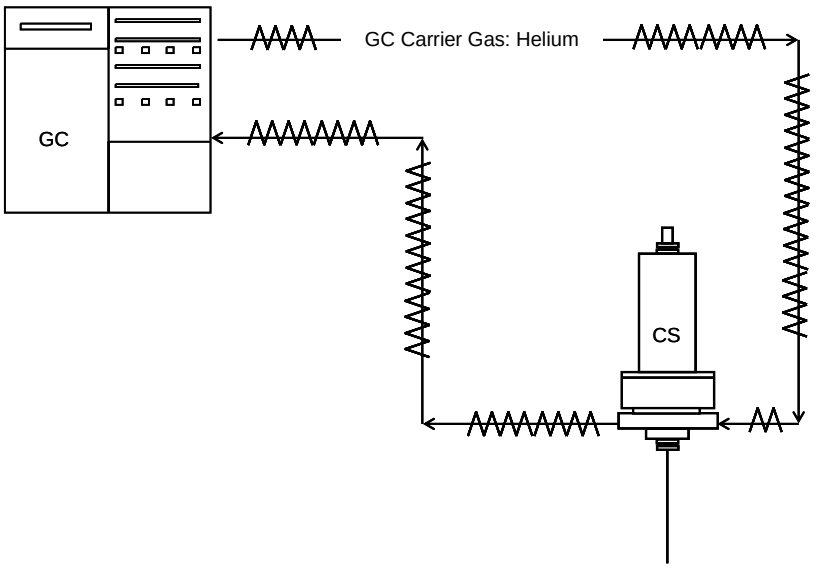

Figure 4-12 Flow diagram of apparatus for on-line compositional analysis (GC: Gas Chromatograph, CS: Capillary sampler).

For PVCap gas analyses experiments, the equilibrium cell and its loading lines were vacuumed prior to introduction of ~75 ml of a 1mass% PVCap solution. Then, the synthetic gas was introduced into the cell directly from a pressurised cylinder. After introduction of gas into the cell, efficient stirring was started, and pressure was stabilized within a few minutes. The temperature was then lowered to form hydrates well inside the hydrate stability zone, i.e. ~ 0 °C. The system was then heated a few degrees outside the hydrate stability zone to dissociate initial hydrates before re-cooling with only a very small fraction of hydrates remaining; i.e. following the standard CGI method detailed in Chapter 2.

The first test was carried out at ~1500 psia / 103 bar (Figure 4-13). During the initial stage of hydrate formation (Figure 4-14), a decrease in methane (s-I) / increase in propane (s-II) concentration in the gas phase was first observed, supporting the formation of s-I methane hydrates. The growth occurred at a subcooling greater than the s-I methane hydrate CIR.

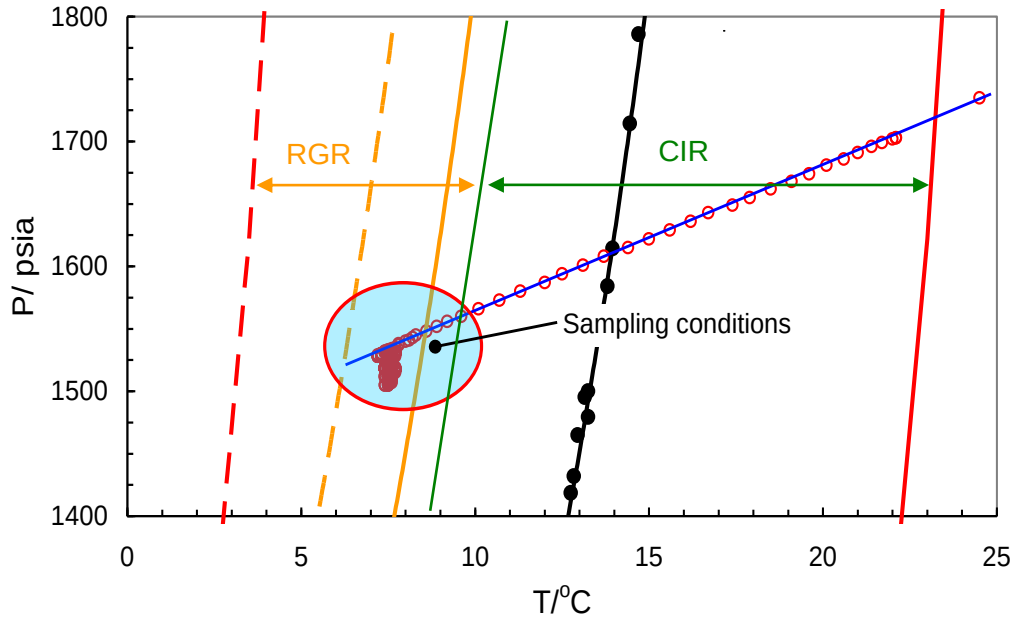

Figure 4-13 Test 1 experimental condition of the gas analyses during hydrate formation in 10 mole% C3 / 90 mole% C1 system

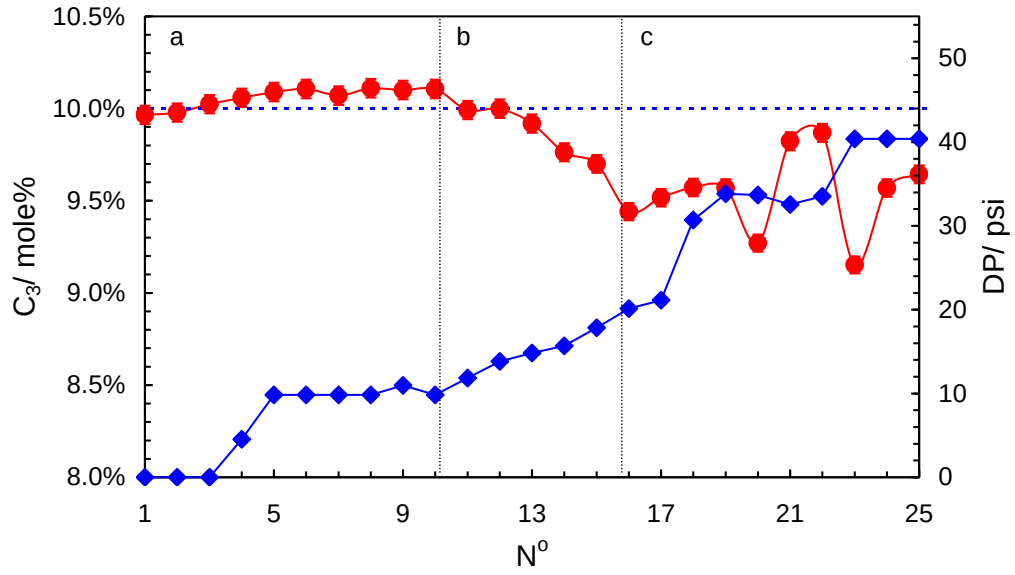

Figure 4-14 Test 1 online compositional analysis of vapour phase propane content (red points) and pressure drop due to hydrate growth (blue points) in the highlighted region of Figure 4-12. Samples/points are every 2.5 minutes.

Following the initial rise in propane contents, as growth rates increased, so the propane content decreased, then climbed and fell through time, suggesting s-II was growing (possibly through solid-solid conversion of s-I) then dissociating periodically.

The second test was carried out at ~1000 psia / 68.9 bar (Figure 4-15). In this test the initial decrease in methane (s-I) / increase in propane(s-II) concentration in the gas phase during early growth was not completely detectable (Figure 4-16). However, after this initial fluctuation in methane / increase in propane content, a rapid decrease in

pressure and propane concentration was observed suggesting final s-II formation and KHI failure.

Thus one suggestion would be that that initial growth in s-II systems is related to the formation of s-I hydrates. The formation of these s-I hydrates could promote subsequent s-II formation, potentially by s-I to s-II conversion. However, for a final conclusion further in depth studies are required.

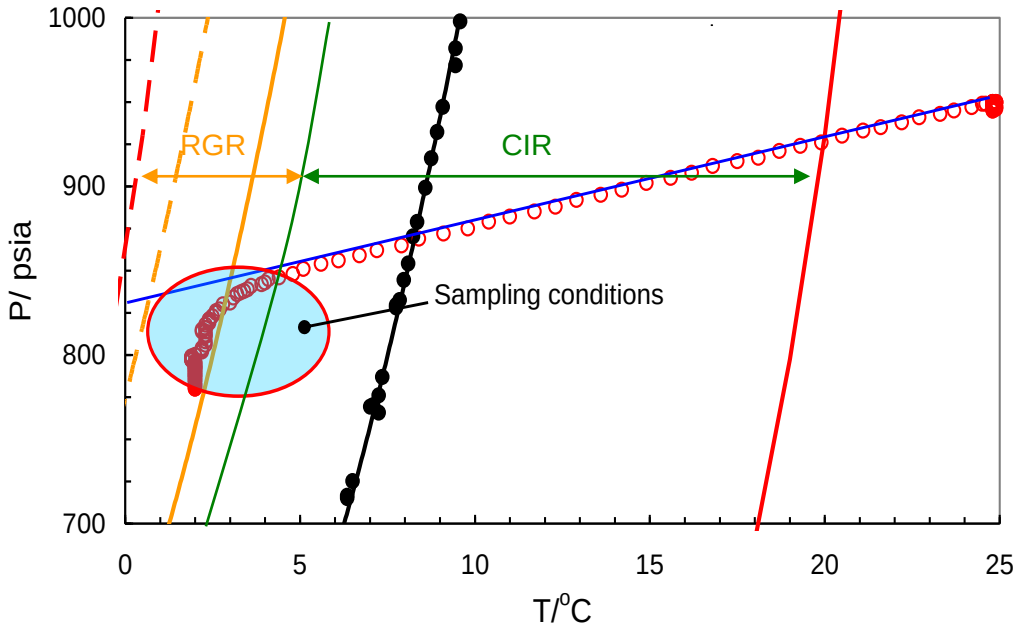

Figure 4-15 Test 2 experimental conditions of the gas analyses during hydrate formation in 10 mole% C3 / 90 mole% C1 system.

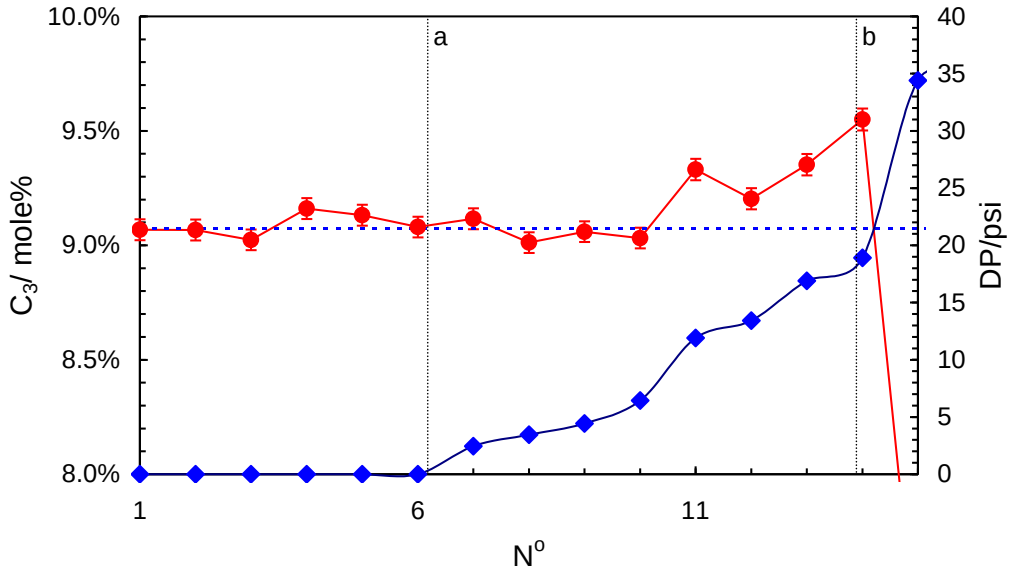

Figure 4-16 Test 2 online compositional analysis of vapour phase propane content (red points) and pressure drop due to hydrate growth (blue points) in the highlighted region of Figure 4-14. Samples/points are every 2.5 minutes.

4.5.2. Effect of (98 mole% C1 / 2 mole% C3) Regions with PVCap

CGI Regions for a 2 Mole% Propane 98 Mole% Methane System

Based on the above results, it was speculated that if failure in a C1-C3 system is related to s-I formation, then varying the propane content should not result in a change in CGI region boundaries as these are related to subcooling from the s-I methane phase boundary, not the s-II boundary.

Figure 4-17 shows example cooling curves for determination of CGI regions for 0.5 mass% PVCap aqueous with 2 mole% propane / 98 mole% methane at initial test pressures of ~80-90 bar. Also shown are CGI region boundaries for 10 mole% methane / 90 mole% propane (tested previously for 1 mass% PVCap). Interpretation of cooling curves for 2 mole% propane show CGI regions to be essentially identical to those for 10 mole% propane. On fast cooling with no history, rapid failure for 2 mole% propane occurs at the same CGI region boundary as for 10 mole%. The same applies for CIR and RGR regions; changes in growth rates as a function of subcooling are the same for 10 and 2 mole% propane, with these CGI boundaries being more closely related in terms of subcooling to the s-I boundary (note the RFR boundary is related in subcooling to the s-II boundary, providing evidence for eventual PVCap failure to prevent s-II at very high subcoolings).

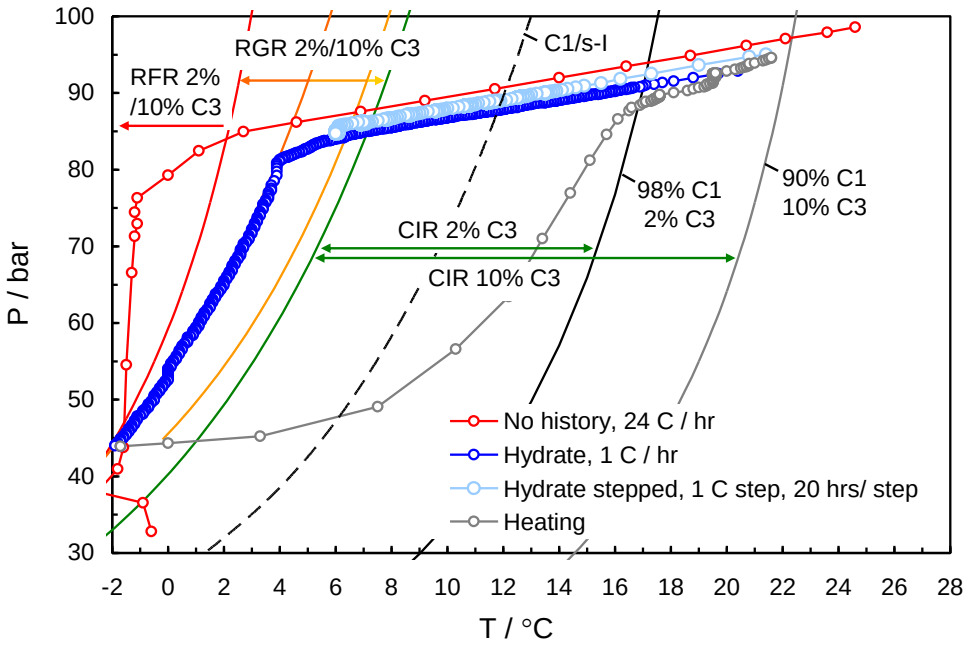

Figure 4-17 Example cooling curves for determination of CGI regions for 0.5 mass% PVCap aqueous with 2 mole% propane / 98 mole% methane. CGI regions region boundaries are those for 10 mole% methane / 90 mole% propane; these are apparently identical for 2 mole% propane.

Moreover, CGI region data have been generated for the 2 mole% propane / 98 mole% methane mixture at pressures up to ~300 bar. Example 'with hydrate' cooling curves and interpolated CGI region boundaries are shown in Figure 4-18. Determined points on CGI region boundaries are reported in Table 4-6. As can be seen in Figure 4-18 CGI region boundary positions effectively mirror those for pure methane with 0.5 mass% PVCap, supporting the theory that failure of PVCap in s-I/s-II systems is due to s-I formation. Notably however, performance is slightly enhanced at low pressures.

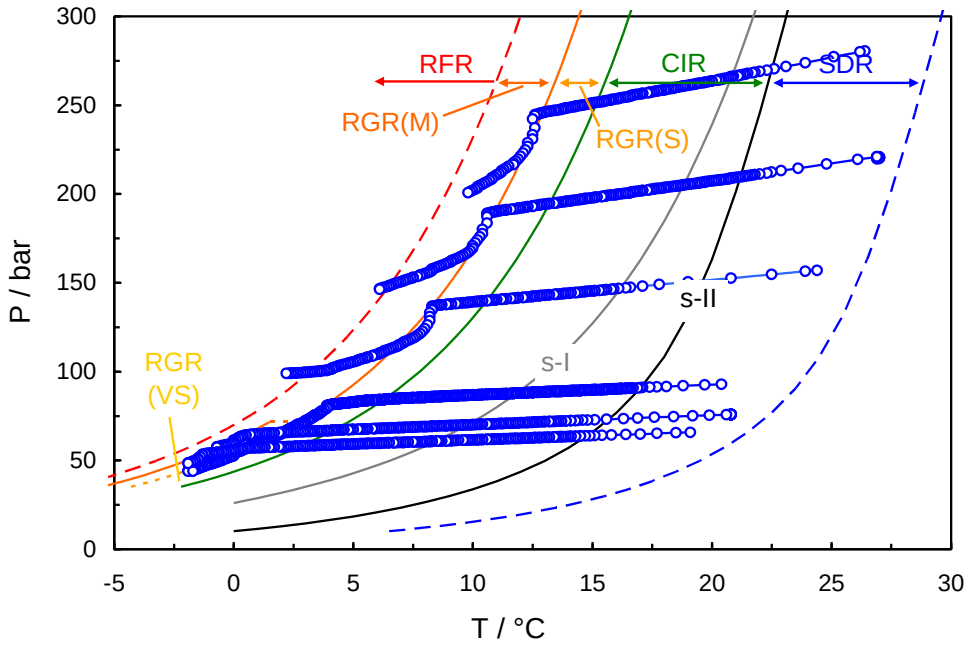

Figure 4-18 Example cooling curves for determination of CGI regions for 0.5 mass% PVCap aqueous with 2 mole% propane / 98 mole% methane.

As can be seen, at low pressures, while rapid failure conditions appear to be largely the same, the subcooling at which moderate growth occurs is measurably higher and a small region of very slow growth appears, at least for low (< 0.5%) hydrate fractions. This contrasts the behaviour for natural gas (as will be presented in Section 4.9) where a reduction in PVCap performance was observed for the same pressure range.

The origins of these changes in performance at low pressures are not clear, however they could be related differences in driving force versus subcooling, and/or gas cage occupancy patterns as will be presented in more detail in the analysis of natural gas behaviour in Section 4.9.

Certainly, these results show gas composition plays a major role in KHI performance / CGI behaviour. It is not uncommon that methane–propane mixtures are used as a simple natural gas substitute in KHI testing for benchmark purposes. Findings presented here,

which will be compared to those for natural gas later in this chapter, show that this may not be actually very representative of real natural gases.

Table 4-6 Experimentally determined points on CGI region boundaries for a 2 mole% methane / 98 mole% propane gas mixture with 0.5 mass% PVCap aqueous.

CGR boundary	*Growth rate	T / ºC (± 0.5)	P / bar (± 0.2)	ΔT_{s-I} / ºC (± 0.5)	ΔT_{s-II} / ºC (± 0.5)
SDR	Slow dissociation	20.6	57.4	-	6.5
		21.6	67.7	-	6.5
		26.3	160.4	-	6.5
		28.2	224.6	-	6.6
		29.3	299.0	-	6.3
CIR-RGR(S)	No growth	0.8	48.5	–5.5	–12.9
		2.7	57.9	–5.3	–12.2
		6.1	84.8	–5.4	–11.2
		10.7	139.1	–5.0	–9.1
		13.1	194.0	–5.3	–8.3
		15.1	255.2	–5.4	–7.6
RGR(S-M)	Slow growth	–1.3	53.4	–8.5	–15.7
		0.5	64.0	–8.4	–15.1
		3.9	82.4	–7.4	–13.3
		8.3	136.4	–7.3	–11.4
		10.9	190.0	–7.3	–10.3
		12.7	245.0	–7.5	–9.8
RGR(M)-RFR	Moderate to Rapid	1.7	84.3	–9.8	–15.6
		5.6	135.2	–9.9	–14.1
		10.8	249.0	–9.6	–11.9

*Growth rate is for ΔT CGI region preceding the associated boundary

4.6. Effect of Methane + Ethane on CGI Regions with PVCap

As noted in Section 4.2, given the apparent good performance of PVCap in simple ethane systems (compared to methane), it was speculated that ethane may play an important role in KHI crystal growth inhibition behaviour. Certainly, ethane is somewhat unique in that it can stabilise the large cavity of both s-I and s-II hydrates (propane, butane and larger molecular weight hydrocarbons only form s-II as their molecular diameters are too large for the s-I $5^{12}6^2$ cage) , and this may be a factor in CGI patterns. In light of this, PVCap induced CGI behaviour in 5 mole% ethane / 95 mole% methane gas mixture, was examined at several pressures up to around 300 bar.

4.6.1. Dissociation Point Measurements

In the past, as in simple (single guest) systems both ethane and methane form s-I hydrates, it was commonly assumed that in binary mixtures of these gases s-I would also be the more stable structure. However, ethane is able to stabilise the large cavity of both s-I and s-II, meaning in mixtures with smaller 'help' gases which can enter the smaller 5^{12} cavity (e.g. methane), either structure can potentially be formed. This is supported by thermodynamic model predictions (e.g. HydraFLASH® 2.2 developed by Hydrafact) and experimental studies (e.g. Subramanian et al., 2000) which show that for a range of lower molar fractions of ethane, s-II is the more stable structure.

To confirm model predictions and structural relations for the ethane–methane mixture, dissociation point measurements were carried out without PVCap present system using the isochoric step-heating method of Tohidi et al. (2000) detailed in Section 2.3.1.

Figure 4-19 shows raw PT data, determined equilibrium heating curve points and interpolations for dissociation conditions for the 5 mole% ethane / 95 mole% methane gas mixture. Phase boundaries (HydraFLASH® predictions) for methane and 5 mole% ethane in methane are shown for comparison. As can be seen, due to the fact that ethane-methane mixtures can form both s-I and s-II hydrates, the complete heating curve is very complex in this case and, due to preferential ethane uptake during hydrate formation, results in apparently 4 distinct dissociation points which include 2 structural transitions from s-II to s-I and back again as the s-I/s-II locus (the line representing the intersection of s-I/s-II phase boundaries for different ethane concentrations – ethane fraction in the gas being progressively reduced/increased as more hydrate is formed/dissociated respectively) is crossed. These structural transitions are evident in raw PT cooling curve data; the reduction in growth rates associated with solid-solid transitions being obvious is the clustering of points, as illustrated in Figure 4-19. With respect to CGI measurements however, heating curve data are in agreement with model predictions in that at 5 mole% ethane / 95 mole% methane, s-II is consistently the more stable structure up to ~300 bar. The final s-II dissociation point determined for the system is reported in Table 4-7. As can be seen in Figure 4-19, this and the model prediction are in excellent agreement with phase boundary data from the literature.

Table 4-7 Experimentally determined final (phase boundary) s-II dissociation point for the 5 mole% ethane 95 mole% methane gas mixture.

T / °C (± 0.2)	P / bar (± 0.2)
20.6	224.0

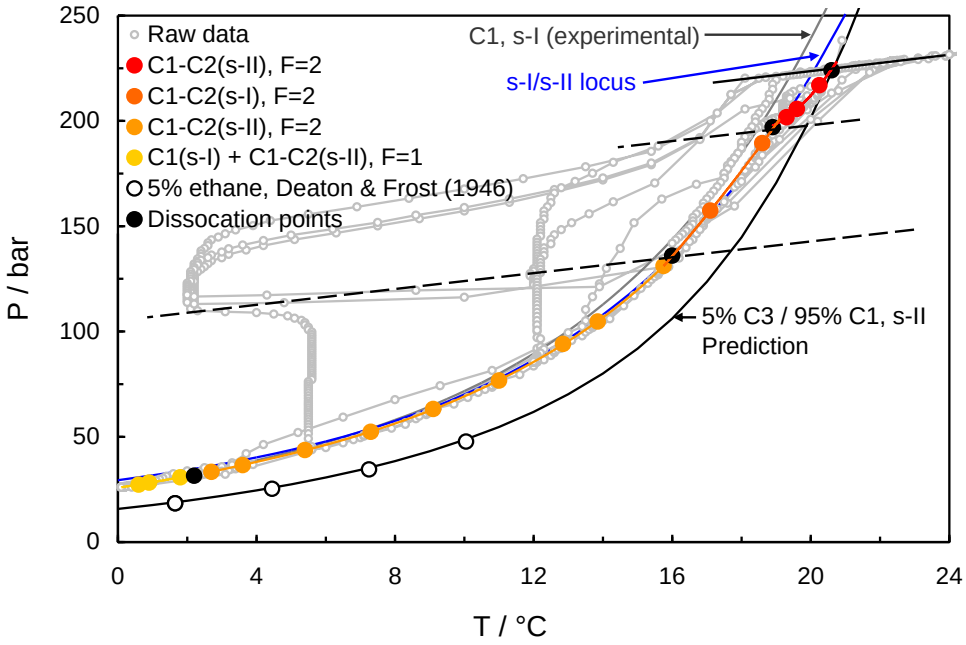

Figure 4-19 Raw PT data (points every 5 minutes), determined equilibrium heating curve points and interpolations for dissociation conditions for the 5 mole% ethane / 95 mole% methane gas mixture. Phase boundaries (HydraFLASH® predictions) for methane (s-I) and 5 mole% ethane in methane (s-II) are shown for comparison, along with literature data for this gas mixture.

4.6.2. Effect of (95 mole% C1 / 5 mole% C2) Regions with PVCap

Figure 4-20 shows example cooling 'with hydrate' present curves for the 5 mole% ethane / 95 mole% methane gas mixture with 0.5 mass% PVCap aqueous present and also interpolated CGI boundaries for this system. Interpreted points on CGI boundaries are also reported in Table 4-8.

Evident from Figure 4-20, the ethane–methane mixture shows, as for methane–propane (at higher pressures) and methane systems, that CGI regions are typical in extent for 0.5 mass% PVCap and appear related through subcooling to the s-I boundary for the system. Thus, consistent with C_1-C_3, in the ethane–methane system, while s-II is the more stable structure, hydrate growth appears to be the results of s-I formation; PVCap performance being poorer for s-I.

Table 4-8 Experimentally determined points on CGI region boundaries for the 5 mole% ethane / 95 mole% methane gas mixture with 0.5 mass% PVCap aqueous.

CGR boundary	*Growth rate	T / °C (± 0.5)	P / bar (± 0.2)	$\Delta T_{s\text{-}I}$ / °C (± 0.5)	$\Delta T_{s\text{-}II}$ / °C (± 0.5)
SDR	Slow dissociation	20.5	91.8	-	5.5
		23.8	156.7	-	5.3
		26.5	244.0	-	5.3
CIR-RGR (VS)	No growth	7.8	83.4	–5.2	–6.5
		11.6	139.2	–5.3	–6.1
		14.5	208.7	–5.3	–5.7
		16.8	289.9	–5.4	–5.5
RGR(VS-M)	Very slow	5.3	82.5	–7.6	–8.9
		9.2	133.8	–7.5	–8.3
		9.3	135.7	–7.5	–8.3
		12.6	211.4	–7.3	–7.7
		14.7	288.4	–7.4	–7.5
RGR(M)-RFR	Slow to moderate	3.3	80.3	–9.4	–10.7
		7.4	136.1	–9.4	–10.2
		10.2	209.9	–9.7	–10.1
		12.5	294.0	–9.8	–9.8

*Growth rate is for ΔT CGI region preceding the associated boundary

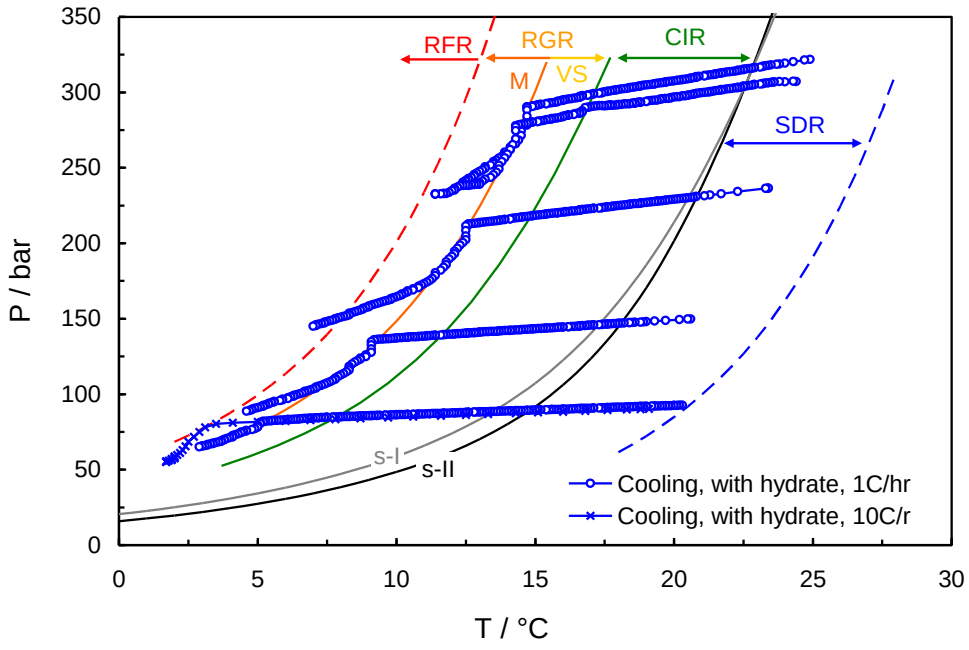

Figure 4-20 Example cooling 'with hydrate' present curves for the 5 mole% ethane / 95 mole% methane gas mixture with 0.5 mass% PVCap aqueous. Interpreted CGI boundaries are shown for reference.

As for methane and C_1-C_3 systems, the complete inhibition region for 5% ethane / 95% methane extends to ~–5.3 °C subcooling from the s-I boundary. This is followed by a

reduced growth rate region which, again in common with C_1 and C_1-C_3 systems, extends to ΔT_{s-I} = ~–9.6 °C, beyond which growth rates increase markedly, indicating a significant reduction in the ability of the polymer to inhibit crystal growth. Again in common with C_1 and C_1-C_3 systems, the RGR for the ethane–methane system can be subdivided into two regions, namely a very slow growth region (RGR(VS)) which extends from the CIR to ΔT_{s-I} =~–7.5 °C, before growth rates increase to moderate as the RFR boundary is approached.

As will be discussed in Section 4.9, given that PVCap performance is apparently enhanced in simple ethane systems, it has been speculated that the presence of ethane may be a factor in the observed improved PVCap CGI performance for NG systems compared to C_1-C_3 systems at higher pressures (>100 bar). From data presented above, whilst CGI boundaries (relative to the s-I phase boundary) for the 5 mole% ethane / 95 mole% methane system are comparable in subcooling to those for methane and the C_1-C_3 at higher pressures, ethane does apparently more significantly reduce the rate of hydrate growth within the RGR, i.e. RGR(S) follows the CIR in the C_1-C_3 (>100 bar) and C_1 systems, but in the C_1-C_2 system, this is RGR(VS).

Significantly, unlike C_1-C_3 system, CGI regions in the C_1-C_2 system do not show the abrupt change in subcooling extent below ~100 bar. This would suggest that this behaviour which will also be seen in NG (Section 4.9) is therefore more related to the presence of propane and the influence this has on hydrate structure/stability/cage occupancy patterns with pressure. Thus, while C_1-C_2 data do not offer direct support to the theory that ethane alone enhances PVCap performance in natural gases (will be detailed in Section 4.9) at higher pressures, this cannot be ruled as the presence of a small fraction of ethane (5 mole%) does appear to improve PVCap performance compared to pure methane systems.

4.7. Effect of Methane + Ethane+ Propane CGI Regions with PVCap

Given the apparent good performance of PVCap in simple ethane systems (compared to methane), and the improved performance in ethane containing natural gas systems (detailed in Section 4.9) compared to binary methane–propane systems, it was speculated that ethane may play an important role in KHI crystal growth inhibition behaviour. In light of the above, it was decided to progress this section of the work programme examine PVCap induced CGI behaviour in methane–ethane–propane

systems; i.e. working in steps towards the composition of a real natural gas. For this purpose, CGI studies of 0.5 mass% PVCap aqueous with a 93 mole% methane / 5 mole% ethane / 2 mole% propane were carried out up to around 300 bar pressure.

Figure 4-21 shows various example CGI method cooling curves and the interpolated CGI boundaries for the 93 mole% methane / 5 mole% ethane / 2 mole% propane gas mixture with 0.5 mass% PVCap aqueous present. These CGI boundaries are also reported in Table 4-9.

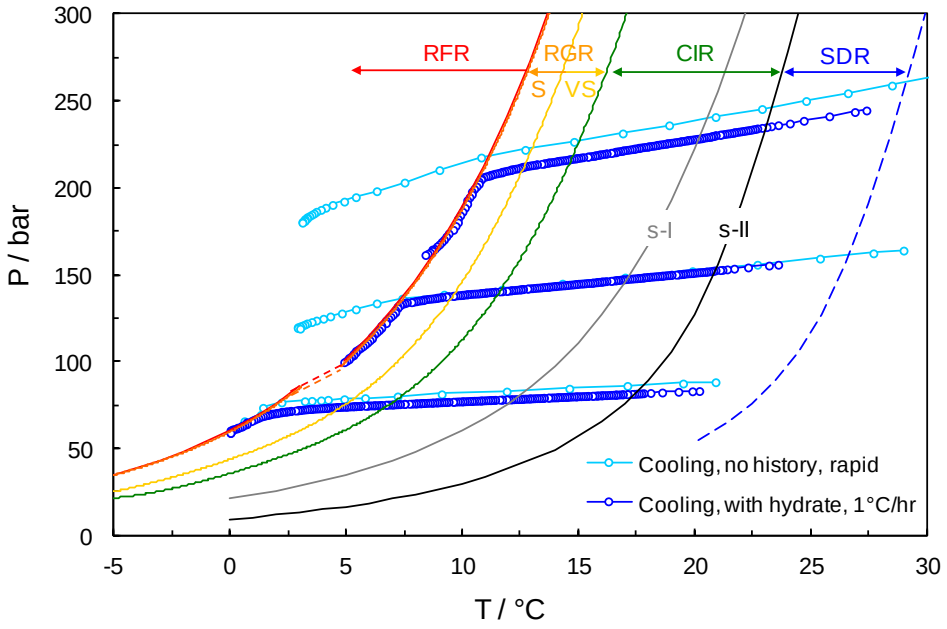

Figure 4-21 Example cooling 'no history' and 'with hydrate' present curves for the 93 mole% methane / 5 mole% ethane / 2 mole% propane ternary gas mixture with 0.5 mass% PVCap aqueous.

As shown in Figure 4-21 data for the C_1–C_2–C_3 mixture shows that, consistent with C_1-C_2 and C_1-C_3, while s-II is the more stable structure, CGI boundaries are related primarily though subcooling to the s-I phase boundary for the gas, i.e. hydrate growth appears to be the result of initial s-I formation; PVCap performance being poorer for s-I compared to s-II.

As for C1, C1-C2 and C1-C3 systems, the complete inhibition region (CIR) for 93% methane / 5% ethane / 2% propane extends to ~5.2 °C subcooling from the s-I boundary. This is followed by a reduced growth rate region which – again in common with C1, C1-C2 and C1-C3 – extends to $\Delta T_{s\text{-}I}$ = ~–9.9 °C at pressures < 70 bar. However, in contrast to C1, C1-C2 and C1-C3 systems, in the C1–C2–C3 mixture the RGR region is reduced slightly at pressures > 100 bar to $\Delta T_{s\text{-}I}$ = ~–9.1 °C, i.e. performance is slightly poorer at higher pressures. Again in common with C1, C1-C2

and C1-C3 systems, the RGR in the C1–C2–C3 system is subdivided by a CGI boundary at ΔT_{s-I} = ~–7.2 °C, in this case being RGR(VS) to (S).

Table 4-9 Experimentally determined points on CGI region boundaries for the 5 mole% ethane / 95 mole% methane gas mixture with 0.5 mass% PVCap aqueous

CGR boundary	*Growth rate	T / °C (± 0.5)	P / bar (± 0.2)	ΔT_{s-I} / °C (± 0.5)	ΔT_{s-II} / °C (± 0.5)
SDR	Slow dissociation	23.6	90.3	-	5.5
		26.6	159.5	-	5.5
		29.1	261.2	-	5.5
CIR-RGR (VS)	No growth	6.9	76.0	–5.1	–10.1
		11.5	140.1	–5.2	–9.0
		14.7	215.9	–5.1	–7.9
RGR(VS)-(S)	Very slow	5.3	76.0	–6.7	–11.7
		9.4	137.2	–7.2	–11.0
		12.5	211.0	–7.1	–10.0
RGR(S)-(M)-RFR	Slow	1.3	68.3	–9.8	–15.0
		7.2	132.4	–9.1	–13.0
		10.7	203.7	–8.7	–11.6

*Growth rate is for ΔT CGI region preceding the associated boundary

As discussed previously, given that PVCap performance is apparently enhanced in simple ethane systems (Section 4.2) , it has been speculated that the presence of ethane may be a factor in the observed improved PVCap CGI performance for NG systems (described in Section 4.9) compared to C1-C3 systems at higher pressures (> 100 bar). However, at lower pressures (< 70 bar), the total extent of CGI regions for the C1–C2–C3 system are comparable to C1-C3, with only a slight reduction in RGR growth rates for the former. Likewise, at higher pressures (> 100 bar), the total extent of the CGI regions are reduced for the C1–C2–C3 mixture compared to C1-C3. This suggests that while ethane is beneficial (e.g. compared to C1 alone), it is not the sole cause of the strong performance of PVCap with natural gas at > 100 bar, nor does it appear related to the clear reduction in performance at lower pressures (< 70 bar) which will be seen in NG systems (detailed in Section 4.9).

4.8. Effect of Methane–CO_2 on CGI Regions with PVCap

As found in Section 4.5 PVCap performance is considerably reduced in pure CO_2 (s-I) systems. However, it is not totally clear whether this negative effect will show itself in a CO_2-methane mixture. Evaluating CO_2 effect is particularly important due to the

presence of CO_2 in natural gases. Hence, PVCap performance in methane–CO_2 systems were studied using the CGI method to both examine the effect of high CO_2 contents and to assess what influence CO_2 might have generally in real natural gases. For this purpose CGI studies were performed for 15 mole% CO_2 / 85 mole% methane gas mixture with 0.5 mass% PVCap aqueous present up to around 260 bar pressure.

Figure 4-22 shows example CGI method cooling curves at different pressures and interpreted CGI boundaries for the this system. Interpreted points on CGI boundaries are reported in Table 4-10 .

Table 4-10 Experimentally determined points on CGI region boundaries for the 15 mole% CO_2 / 85 mole% methane binary gas mixture with 0.5 mass% PVCap aqueous.

CGR boundary	*Growth rate	T / °C (± 0.5)	P / bar (± 0.2)	$\Delta T_{s\text{-}I,C1}$ / °C (± 0.5)	$\Delta T_{s\text{-}I,C1\text{-}CO2}$ / °C (± 0.5)
SDR	Slow dissociation	9.7	43.9	4.4	3.7
		14.8	91.6	2.6	2.3
		20.1	177.5	2.4	2.7
		22.7	250.0	2.4	2.9
CIR-RGR (VS)	No growth	1.8	38.8	–2.2	–3.0
		2.2	61.1	–6.3	–6.9
		4.9	83.6	–6.5	–6.8
		10.7	162.8	–6.3	–6.1
		13.3	230.5	–6.4	–5.9
RGR(VS)-(S)	Very slow	0.5	38.8	–3.5	–4.3
		4.3	84.6	–7.2	–7.5
		9.7	162.8	–7.3	–7.1
		12.4	228.2	–7.2	–6.8
RGR(S)-(M)	Slow	–3.8	33.5	–6.3	–7.2
		0.7	59.4	–7.5	–8.1
		1.9	80.0	–9.1	–9.5
		7.5	153.4	–9.0	–8.9
		10.4	224.1	–9.1	–8.6
RGR(M)-RFR	Moderate	–4.6	40.74	–9.1	–9.9
		0.6	77.4	–10.1	–10.5
		7.0	159.7	–9.9	–9.7
		9.3	219.6	–10.0	–9.6

*Growth rate is for ΔT CGI region preceding the associated boundary

As shown in Figure 4-22, at pressures > 100 bar, the total CGI region subcooling extent is ~–10 °C from the s-II phase boundary. Moreover the CIR region in this system larger

than the normal CIR being ~–6.3 °C from the s-I phase boundary at higher pressures (CIR is typically ~–5.2 °C from s-I boundary for C_1, C_1-C_2, C_1-C_2-C_3 at 0.5% PVCap). From both these behaviours it was observed that at high pressures (> 100 bar) PVCap performance for the C_1-CO_2 mixture is most closely comparable to that for natural gas (detailed in Section 4.9). On the contrary, at lower pressures (beginning below ~70 bar with full impact by ~40 bar) in the C_1–CO_2 system the performance of PVCap is greatly reduced; the CIR is only ~−2.2 °C in subcooling extent with moderate growth occurring by only ~−6.3 °C subcooling. Out of the gas mixtures studied and presented in this Chapter, only NG show a similar clear reduction in PVCap performance at lower pressures. This strongly suggests that CO_2 is the cause of this behaviour in natural gas systems.

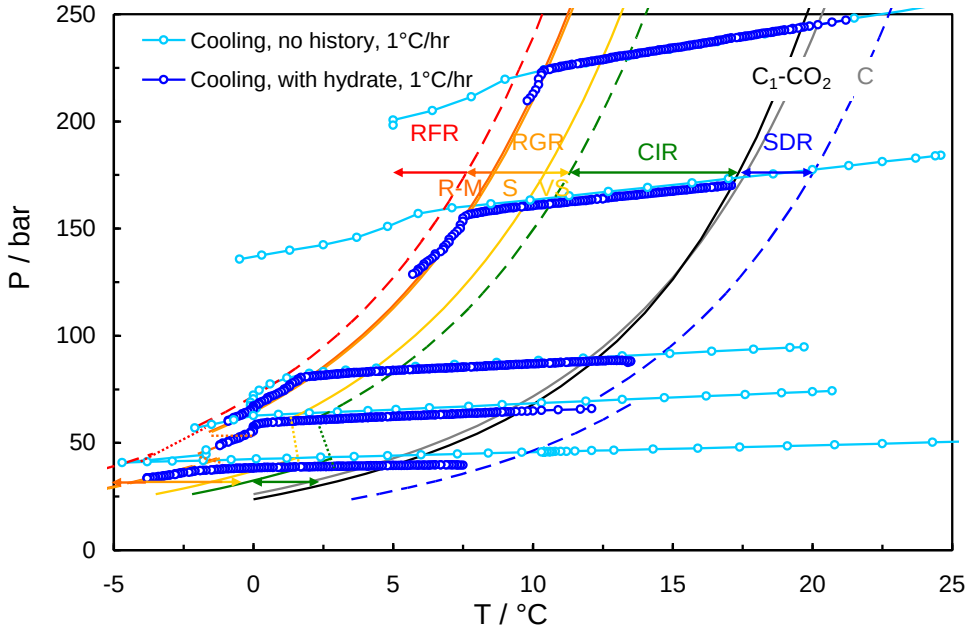

Figure 4-22 Example cooling 'no history' and 'with hydrate' present curves for the 15 mole% CO2 / 85 mole% methane binary gas mixture with 0.5 mass% PVCap aqueous.

4.9. Effect of Natural Gas on CGI Regions with PVCap

Having worked towards a natural gas system in this chapter a 0.5 mass% PVCap aqueous with a standard North Sea natural gas (NG) was examined to evaluate the behaviour/effect of guest gases for a real s-II forming system, with particular focus on an apparent abrupt change in CGI region trends at lower pressures. For this purpose a North Sea natural gas (NG) (composition in Table 4-11) with 0.5 mass% PVCap has been tested at five different pressures.

Table 4-11 Composition (from GC analysis) of the North Sea natural gas used in CGI experiments with 0.5 mass% PVCap aqueous.

Component	Mole%
Methane	89.41
Ethane	5.08
Propane	1.45
i-Butane	0.18
n-Butane	0.26
i-Pentane	0.06
CO2	1.55
Nitrogen	1.93
n-Pentane	0.06
n-Hexane	0.02

Figure 4-23 shows example cooling curves for the North Sea natural gas with 0.5 mass% PVCap at different pressures and interpreted CGI boundaries for the this system. Interpreted points on CGI boundaries are reported in Table 4-12.

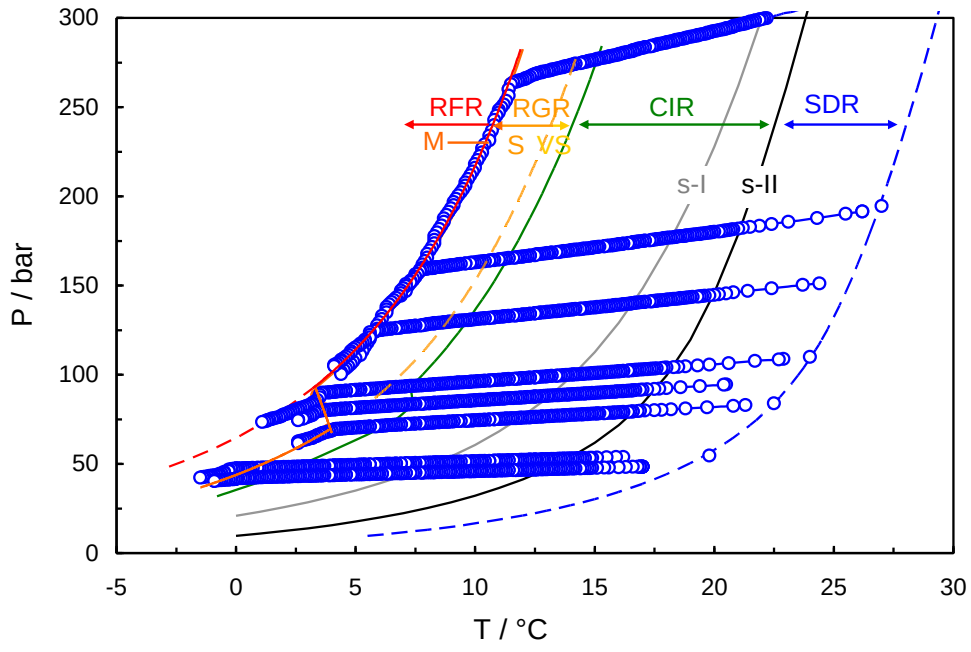

Figure 4-23 CGI regions and example cooling curves with hydrate present (<0.5% of aqueous phase as hydrate initially) for the North Sea Natural gas with 0.5 mass% PVCap aqueous. An abrupt reduction in the subcooling extent of KHI induced crystal growth inhibition regions at pressures below 90 bar is clearly evident.

As can be seen, at pressures >90 bar, moderate growth is consistently observed once conditions reach a CGI boundary at around $\Delta T_{s\text{-}I}$ = ~–9.7 °C; with *PT* conditions commonly closely following this as cooling continues/growth progresses. However, at

pressures below 90 bar, moderate growth occurs at measurably lower subcoolings. Likewise, an abrupt reduction in the extent of PVCap-induced crystal growth inhibition regions is clearly apparent at pressures below 100 bar; both the CIR and RGR shift to lower subcoolings.

Table 4-12 Experimentally determined points on CGI region boundaries for the North Sea natural gas (composition given in Table 2.1) with 0.5 mass% PVCap aqueous.

CGR boundary	*Growth rate	T / ºC (± 0.5)	P / bar (± 0.2)	ΔT_{s-I} / ºC (± 0.5)	ΔT_{s-II} / ºC (± 0.5)
SDR	Slow dissociation	19.8	54.7	-	5.6
		22.5	84.0	-	5.5
		24.0	109.9	-	5.5
		27.0	194.6	-	5.6
		29.7	328.2	-	5.3
CIR-RGR(VS)	No growth	–0.8	31.8	–4.9	–10.7
		1.6	42.6	–5.2	–10.6
		3.0	48.7	–5.1	–10.3
		6.2	71.1	–5.2	–9.8
		7.4	83.2	–5.2	–9.5
		7.3	93.1	–6.2	–10.3
		11.4	165.8	–6.4	–9.2
		15.1	276.5	–6.3	–8.2
RGR(VS-S)	Very slow	6.3	92.5	–7.2	–11.3
		8.7	129.0	–7.3	–10.7
		14.1	273.2	–7.2	–9.2
RGR(S-M)-RFR	Slow to moderate	–1.5	36.2	–6.8	–12.4
		–0.8	40.4	–7.1	–12.6
		0.7	47.8	–7.2	–12.4
		1.8	54.3	–7.2	–12.2
		4.0	68.8	–7.1	–11.7
		3.7	80.5	–8.7	–13.0
		3.5	89.1	–9.7	–13.8
		5.6	121.9	–10.0	–13.5
		7.7	158.1	–9.8	–12.7
		7.7	158.2	–9.8	–12.7
		11.5	262.9	–9.5	–11.5

*Growth rate is for ΔT CGI region preceding the associated boundary

At pressures below 70 bar, the subcooling where rapid failure occurs remains largely the same. However, while at >100 bar, this was proceeded by a slow growth region, at < 70 bar growth rates are moderate for the same subcooling range. Likewise, at >100 bar, the

extent of the CIR is apparently greater and very slow growth extends to ΔT_{s-I} = ~–7.2 °C; at < 70 bar, slow growth only occurs up to this subcooling. Thus it is quite clear that the performance of PVCap is moderately reduced at lower pressures.

The origin of this reduction in performance is unclear though it is speculated that it might be related to the fact that driving force (–ΔG/RT) commonly deviates from its normal relationship to subcooling (ΔT_{sub}) in this pressure range in natural gases (Figure 4-24 Arjmandi et al., 2005).

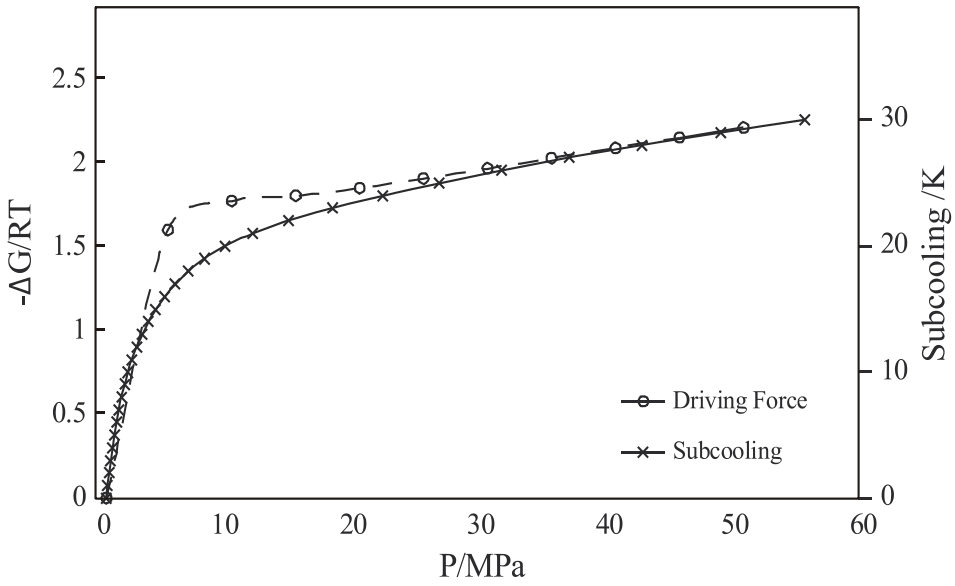

Figure 4-24 Plot of driving force (–ΔG/RT) and subcooling versus pressure for a standard natural gas. From Arjmandi et al. (2005).

The change also marks the pressure condition where ethane (and methane) begins to dominate large s-II cage occupancy as pressure increases. As shown in section 4.2, PVCap performance is enhanced in pure ethane systems, hence it is assumed that increasing ethane cage occupancy may be playing a role. However as seen in section 4.5, the same behaviour does not occur in methane–propane systems. While a similar apparent change in performance occurred at low pressures for 2 mole% propane / 98 mole% methane, this change was positive rather than negative, with CGI region extent seemingly expanding at lower pressures rather than reducing as they do in the natural gas system.

Figure 4-25 shows a comparison of subcooling extent of CGI regions from the s-I phase boundary for the North Sea natural gas, C1 (Section 4.14.1), CO_2 (Section 4.4), 95 mole% C1 / 5 mole% C2 mixture (Section 4.6), 98 mole% C1 / 2 mole% C3 mixture

(Section 4.5), 85 mole% C1 / 15 mole% CO_2 mixture (Section 4.8) and 93 mole% C1 / 5 mole% C2/ 2 mole% C3 mixture (Section 4.7) at < 70 and > 100 bar pressure.

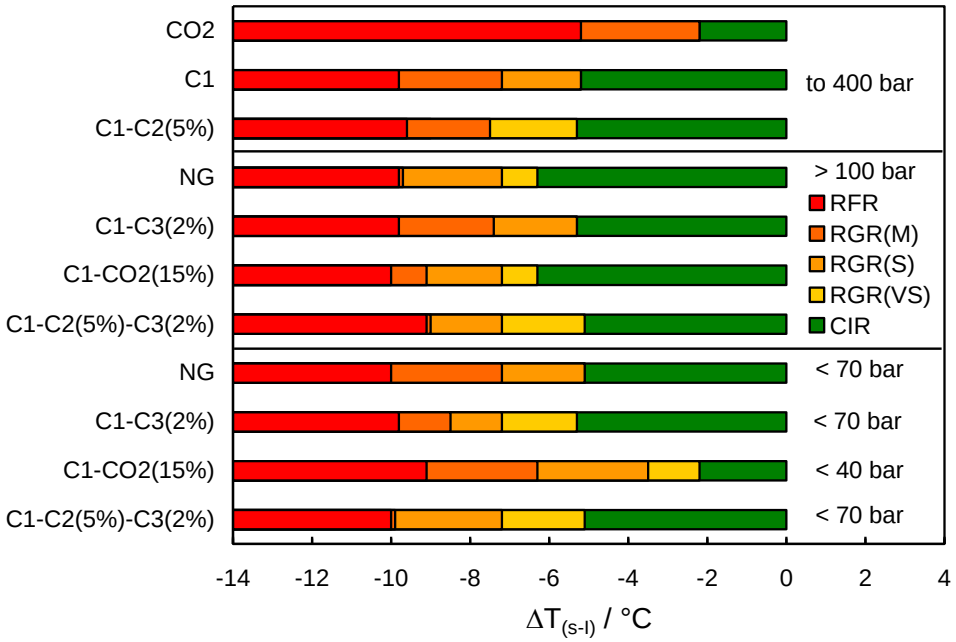

Figure 4-25 Comparison of subcooling extent of CGI regions from the s-I phase boundary for various single, binary, ternary and multicomponent gas mixtures with 0.5 mass% PVCap aqueous at different pressures.

For all systems, CGI regions appear closely related to the s-I phase boundary and share many common subcooling positions. This supports the working theory that for PVCap, failure is apparently because of s-I growth. As can be seen for the North Sea Natural gas, at pressures above ~90 bar, moderate growth occurs (where conditions commonly follow the RGR(M) CGI boundary, as seen in Figure 4-23) at $\Delta T_{s\text{-}I}$ = ~–9.7 °C and at higher subcoolings, rapid growth occurs. This subcooling CGI boundary is shared, within experimental error, with most of the other systems shown in Figure 4-25, typically marking the change to rapid, polymer-uncontrolled growth.

As discussed earlier in this chapter, due to the enhanced PVCap performance in the presence of ethane, this component may be a factor in the observed improved PVCap CGI performance for NG systems. This is further supported by the reduction of hydrate growth rate within the RGR in C_1-C_2 system in comparison to C_1 and C_1-C_3 systems which have comparable RGR boundaries. However, as can be seen in Figure 4-25, NG has an abrupt change in subcooling extent below ~100 bar which is not seen in either C2 and C_1-C_2 systems. Hence, while ethane is beneficial (e.g. compared to C_1 alone) it is clearly not controlling PVCap behaviour in NG system alone.

On the other hand, the sudden reduction in PVCap performance at lower pressures is clearly seen for C_1-C_3 and C1-C2-C3 systems with only a slight reduction in RGR growth rates for the latter. Hence this behaviour can be related to the presence of propane and the influence this has on hydrate structure/stability/cage occupancy patterns with pressure. Moreover, the most closely comparable behaviour to NG at pressures > 100 bar is the C_1-CO_2 mixture with a larger CIR than C1 alone. Furthermore, out of all gas mixtures studied, only NG and C_1-CO_2 show the clear reduction in PVCap performance at lower pressures (beginning below ~70 bar with full impact by ~40 bar for C_1-CO_2). Hence, results strongly suggest that CO_2 is the cause of this behaviour in natural gas systems.

Thus, in conclusion, while ethane does have a positive effect, results for the various systems suggest it is a CO_2+C_2(+C_1) combination in NG that gives good performance at higher pressures, although contrastingly, CO_2 is at the same time apparently responsible for the significant reduction in PVCap performance at lower pressures in NG systems.

4.10. Effect of Cyclopentane–Methane on CGI Regions with PVCap

From results presented earlier in this chapter, seemingly PVCap can strongly inhibit structure II hydrate up and the system only fails when the structure I can potentially form and the system has reached higher subcoolings than structure I inhibition regions. Therefore KHI failure in s-II systems can be the result of s-I growth. However, it is important to understand to what extent can PVCap inhibit hydrate structure II formation and whether it is can be inhibited indefinitely.

Cyclopentane (cC5) can form a very stable s-II hydrate (complete large $5^{12}6^4$ cavity occupancy) that dissociates at ~8 °C at 1 bar (Sloan and Koh, 2008). The presence of methane further stabilises this hydrate though occupancy of small 5^{12} cavities, giving dissociation temperatures in excess of 20 °C at only 25 bar (Tohidi et al., 1997). Due to the high stability of structure II hydrate in a cC5-C1 system there is a very large temperature difference between s-I and s-II phase boundaries. This leaves a large degree of subcooling for PVCap to show its inhibition performance on s-II hydrate before reaching a boundary in which s-I can form.

To examine this property, cyclopentane–methane hydrate crystal growth inhibition regions (CGI) have been investigated for 0.5 mass% PVCap aqueous with a 1 to 4

cyclopentane to water volume ratio at pressures up to 70 bar. The cyclopentane (cC5) used for this purpose was 98% pure and supplied from Sigma-Aldrich.

Example heating/cooling curves with derived CGI region boundary points, including data as a function of time, are shown in Figure 4-26, Figure 4-27 and Figure 4-28. Measured points on CGI boundaries are reported in Table 4-13.

Table 4-13 Experimental CGI region data for 0.5 mass% PVCap aqueous with cyclopentane and methane (1:4 cC5 to water volume ratio). See Section 1.3.3 for growth rate definitions.

CGI boundary	*Growth rate	T / °C (± 0.5)	P / bar (± 0.2)	$\Delta T_{s\text{-}II}$/°C (± 0.5)	$\Delta T_{s\text{-}I}$/°C (± 0.5)
SDR	Slow dissociation	28.1	23.6	8.5	-
		31.9	43.6	8.5	-
		34.9	68.0	8.5	-
CIR-RGR (S-M)	No growth	6.9	20.0	–11.6	-
		11.0	37.8	–11.6	-
		14.2	62.1	–11.6	-
RGR(VS-S)-RGR(M)	Very slow to slow growth	4.2	56.4	–21.0	–3.5
RGR(M)-RFR	Moderate to fast growth	2.8	58.0	–22.5	–5.2†

*Growth rate is for ΔT_{sub} CGI region preceding the associated boundary

†Subcooling from s-I boundary is equal to CIR subcooling for methane-PVCap and cyclopentane. Cyclopentane to water ratio is 1:4. C1-cC5 data from Tohidi et al. (1997).

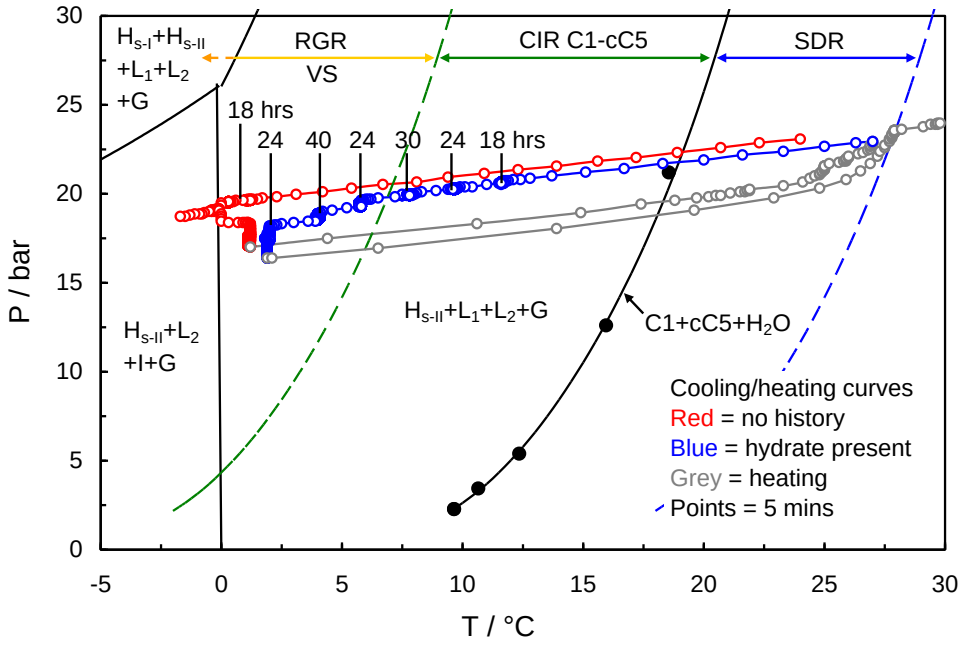

Figure 4-26 Example cooling and heating curves for 0.5 mass% PVCap with methane and cyclopentane. Cyclopentane to water ratio is 1:4. C1-cC5 data from Tohidi et al. (1996). On the initial cooling run with no history, cooling to form ice was required before hydrate formation began.

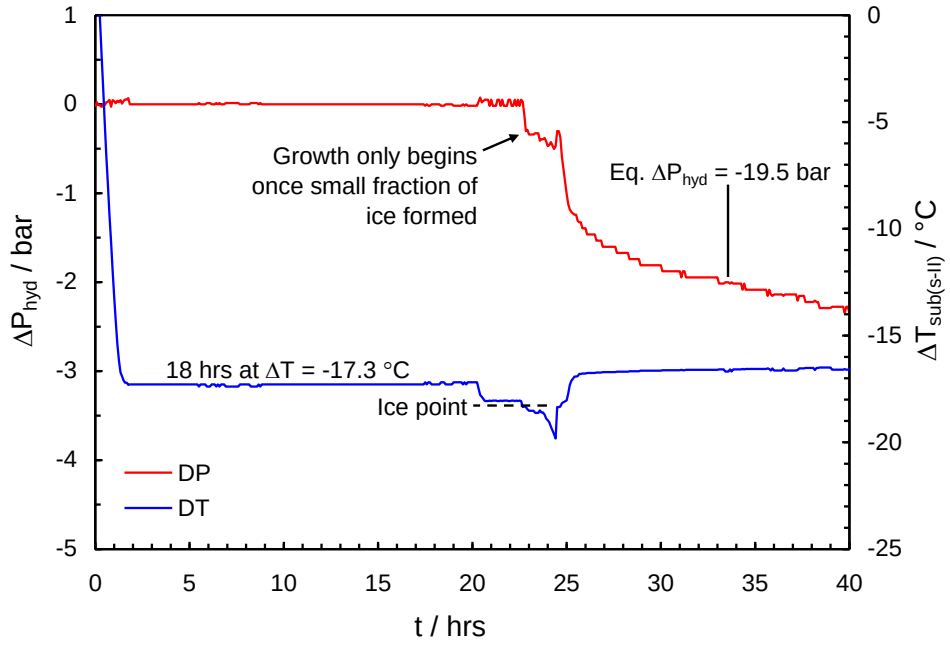

Figure 4-27 Example cooling curves data for 0.5 mass% PVCap with methane and cyclopentane as a function of time at ~17.5 bar. Cyclopentane to water ratio is 1:4.

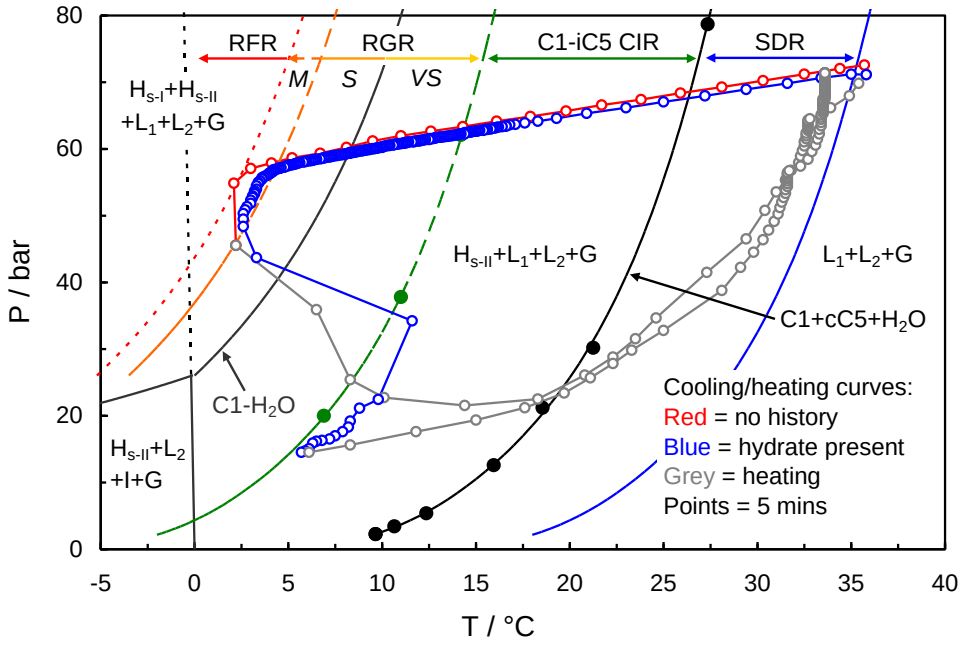

Figure 4-28 Example cooling and heating curves for 0.5 mass% PVCap with methane and cyclopentane at ~ 60 bars. Cyclopentane to water ratio is 1:4. C1-cC5 data from Tohidi et al. (1996). The rapid failure region boundary appears to coincide with the subcooling from the s-I (methane) phase boundary where the CIR ends in methane-PVCap systems.

The most obvious effect of PVCap is the very large CGI regions it generates, even at only 0.5 mass%. The CIR extends to ~−11.6 °C of subcooling from the s-II phase boundary, with PVCap actively reducing growth rates up to a $\Delta T_{sub(s\text{-}II)}$ of ~–22.5 °C. A very large SDR of $\Delta T_{sub(s\text{-}II)}$ = ~+8.5 °C is also present. This supports previous findings for methane–propane systems (Section 4.5) which disprove the widespread belief that KHIs are largely ineffective beyond ~−10 °C of subcooling (Kelland, 2006); clearly,

performance is in fact highly guest/structure dependent with much greater subcoolings possible.

The high performance of PVCap in this system was evident on the first cooling run with no history. As shown in Figure 4-26 and Figure 4-27, following 18 hours at $\Delta T_{sub(s\text{-}II)}$ = ~–17.3 °C, hydrate did not form. Even though the system was highly agitated (stirrer rpm > 750), to induce hydrate formation, cooling into the ice region was required. The growth of ice and subsequent conversion of ice to hydrate (previous work on PVCap–propane systems presented in Section 4.3 showed that PVCap cannot prevent the ice to hydrate transition) facilitated hydrate growth when the temperature was raised back above the ice point.

However, even at this high subcooling ($\Delta T_{sub(s\text{-}II)}$ = ~–16.5 °C), hydrate growth rates were extremely slow. As shown in Figure 4-27, ΔP_{hyd} reached only ~–2.5 bar in 17 hours compared to an equilibrium value of ~–19.5 bar, meaning only a relatively small fraction of the water phase (calculated as ~ < 0.5 mass%) was converted to hydrate during this period.

Similar behaviour was seen on subsequent stepped 'with hydrate' runs to determine the CIR, as shown in Figure 4-26. When growth does occur in the RGR region, it is extremely slow; over 3 steps totalling 88 hours within the RGR, again < 0.5 mass% of the aqueous phase was converted to hydrate.

Due to inevitable ice formation at lower temperatures, the limits of the RGR region could not be determined at lower pressures. For higher pressure tests at 60-70 bar (Figure 4-28), due to the increasing subcooling range before the ice point, the extent of the RGR/RFR boundary could be evaluated.

As shown in Figure 4-28, rapid failure was observed to occur, even on cooling runs with no hydrate/history present, at a subcooling from the s-II phase boundary of ~–22.5 °C. Significantly, this corresponds to a subcooling from the s-I (methane) phase boundary of ~–5.2 °C. This is the subcooling where the CIR ends in methane–PVCap systems at this PVCap concentrations (Section 4.1) and CGI boundaries commonly occur at this same condition (relative to the s-I boundary) in commercial formulations (Section 3.1.5) . Likewise the onset of moderate growth occurs at $\Delta T_{sub(s\text{-}II)}$ = ~–3.5 °C; a change in

growth rates at this subcooling from the s-I phase boundary also commonly occurs in commercial KHI systems.

Certainly, the fact that the rapid failure boundary occurs at $\Delta T_{sub(s\text{-}I)}$ = ~–5.2°C supports the current theory that KHI failure in s-II systems can be the result of s-I growth, although clearly in this case s-II hydrates can grow without s-I formation at lower subcoolings, at least between the s-I phase boundary s-II CIR boundary. Likewise, the appearance of CGI region boundaries at similar subcooling conditions in different systems supports the theory that CGI patterns are strongly influenced by underlying crystal growth patterns.

4.11. Effect of Methylcyclohexane–Methane on CGI Regions with PVCap

To examine whether s-I formation is also the cause of PVCap failure in mixed s-I/s-H systems, CGI region studies were carried out on 0.5 mass% PVCap aqueous with methane and methylcyclohexane – an s-H former. Methylcyclohexane used in the experiments was 99% pure supplied from Sigma-Aldrich.

Figure 4-29 shows example cooling and heating curves with interpolated CGI region boundaries. As can be seen behaviour is effectively that for methane with 0.5 mass% PVCap. CGI regions are largely unchanged with the exception of an apparent increase in very slow to slow RGR growth conditions, at least initially at low hydrate fractions, with moderate growth then proceeding to return to lower subcoolings, following the common $\Delta T_{s\text{-}I}$= ~–7.2 °C RGR boundary (Figure 4-29).

Thus, as for s-II systems, data suggest that PVCap failure in s-H systems is due to the formation of s-I hydrates. However, in s-II/s-I systems, the common appearance of an s-II related slow dissociation region suggests s-II does eventually form, possibly by conversion of s-I to s-II following s-I growth. However, in the case of methane–methylcyclohexane, it appears no s-H formed at all; complete dissociation occurred consistently within the s-H thermodynamic stability region, although slowly as this was the SDR of the pure methane hydrates which apparently formed.

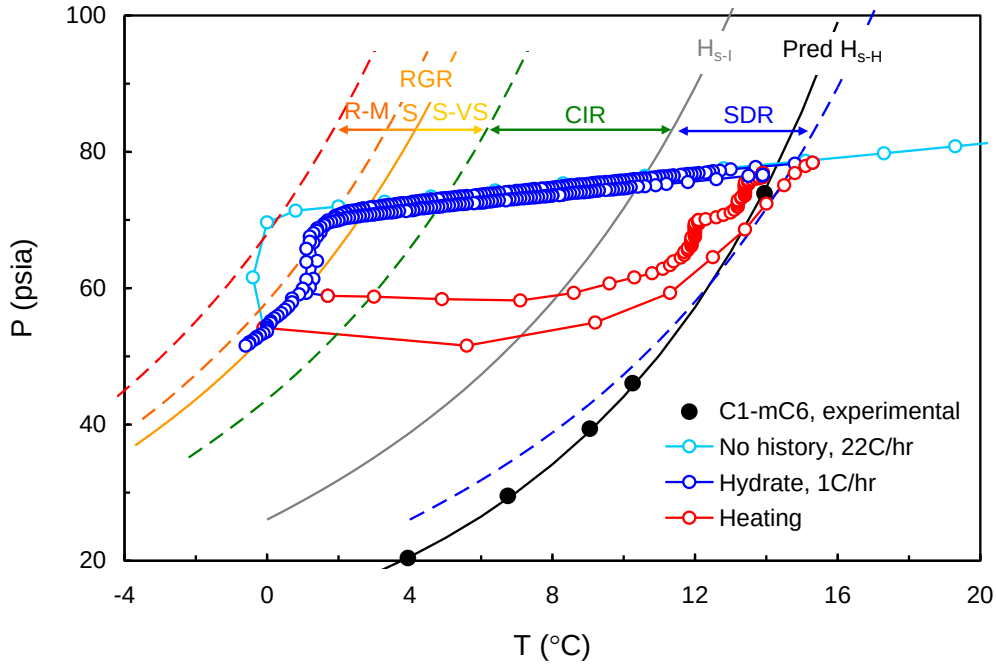

Figure 4-29 CGI regions determined for a methane–methylcyclohexane (mC6) system with 0.5 mass% PVCap aqueous. C1–mC6 data from Tohidi et al. (1996).

While only for one pressure, data do suggest that PVCap is able to completely inhibit the formation of s-H hydrates, at least for the conditions tested. This could be due to PVCap adsorbing more strongly on s-H crystal nuclei, possibly as the large caprolactam pendant group fits better into the s-H large ($5^{12}6^8$) cavity which has a greater diameter (5.71Å) than s-I and s-II large cages (4.73Å for s-II large $5^{12}6^4$ and 4.33 Å for s-I large $5^{12}6^2$).

4.12. Conclusions

The newly developed CGI technique provided the chance to assess the effect of guest gas on KHI-induced hydrate crystal growth inhibition patterns. To understand this behaviour a number of different guest gas/hydrate structure systems (C1, C2, C3, CO_2, C1–C2, C1–C3, C1–C2 –C3, C1–CO_2 and NG, cC5 and mC6) were tested using the new technique.

Controlled PVT studies using the new approach for PVCap-methane system revealed that aqueous PVCap induces a number of well-defined hydrate growth / inhibition / dissociation regions. Moreover, methane hydrate data suggest an optimum PVCap concentration for complete inhibition which is > 0.25 mass% and ≤ 0.5 mass%, at least in terms of CIR subcooling.; the benefit of adding further PVCap being primarily to reduce growth rates at higher subcoolings (RGR region).

While the s-I ethane hydrate system shares the same CGI boundaries as for s-I methane (which supported the assumption that underlying crystal growth patterns as a function of subcooling have a major influence on behaviour) PVCap was able to inhibit the growth of ethane hydrates much more effectively than it could in methane.

CO_2, an s-I former, has a distinctly negative effect on PVCap performance, with a remarkably reduced CIR/RGR compared to methane and ethane. This is important in natural gas systems due to the presence of CO_2 in these systems. However tests show that small fractions of CO_2 (e.g. 1.6%) in natural gases does not appear to have any significant and obvious negative effect.

PVCap performance is considerably superior in s-II forming systems (both simple s-II and binary s-I/-s-II) compared to s-I forming systems (e.g. methane), supporting stronger polymer adsorption on s-II hydrate crystal surfaces:

- PVCap performs much better in the presence of propane, an s-II former, almost indefinitely inhibiting the structure II hydrate.
- In C1-C3, C1–C2 and C1–C2–C3 systems which are all structure II formers, both the CIR and RFR extend to much greater subcoolings compared to s-I formers like methane or ethane. This further supported the established belief that PVCap is more effective at inhibiting s-II clathrates due to stronger crystal surface absorption.
- Natural gas data support previous findings in that PVCap fails due to s-I growth in mixed s-I/s-II forming systems. Results also indicate guest/cage occupancy plays an important role.

In binary and multicomponent s-I/s-II forming systems (e.g. natural gas), PVCap ‘failure’ appears predominantly due to the formation of s-I hydrates, with CGI regions commonly related in subcooling extent to the s-I phase boundary for the system:

- Hydrate growth/KHI ‘failure’ in mixed C1-C3 systems may be in a large part due to the formation of structure-I hydrates; region boundaries for the C1-C3 s-II system being closely correlated with those for s-I methane systems.
- CGI boundaries for C1-C3 mixtures appear to be largely independent on the propane fraction, at least for lower (< 10 mole%) C3 contents, with hydrate growth conditions related (through subcooling) to the s-I methane phase boundary, supporting the growing consensus that KHI failure is commonly

associated with failure to stop s-I formation. CGI regions appear to grow in extent somewhat at low pressures in C1-C3 systems, although the cause of this is not clear.

- Data for the C1-C2 system strongly suggest s-I growth is the primary cause of PVCap failure, even though s-II is the more stable structure; at 5 mole% ethane, dissociation point measurements indicate s-II is the more stable hydrate structure, as predicted by thermodynamic modelling and in agreement with literature studies.
- CGI boundary positions (relative to s-I stability) for the C1–C2, are comparable in subcooling to those for methane and the C1-C3 (at higher pressures) which further supports the inhibition failure due to s-I formation. Moreover, data shows that ethane does apparently more significantly reduce the rate of hydrate growth within the RGR.
- For the C1–C2–C3 mixture, CGI region boundaries are – as for other s-I/s-II forming mixtures – related to subcooling to the s-I boundary for the system, consistent with the theory that it is the initial formation of s-I hydrate which causes PVCap 'failure'

PVCap performance in s-I/s-II forming natural gas systems is superior to that in binary s-I/s-II forming methane–propane systems at pressures > 100 bar. At pressures below 70 bar in natural gas systems, PVCap performance is moderately reduced. It is speculated and supported through CGI tests that this may be related to driving force and/or propane/ethane cage occupancy patterns as a function of pressure.

Thus, while data cannot offer strong support that ethane enhances PVCap performance in natural gases, the presence of a small fraction of ethane (5 mole%) in C1–C2 system does appear to improve PVCap performance compared to pure methane systems, meaning this cannot be ruled out as a factor.

PVCap performance in NG systems is better than for C1-C3 systems – possibly due to the presence of ethane – although there is an abrupt, but moderate reduction in the extent of CGI regions at pressures below 100 bar. This reduction could be attributed to differences in driving force as a function of subcooling and/or cage occupancy patterns; the change in CGI boundary coinciding with a change from C3-C4 to C2-C1 dominance in large s-II cavities

In the C1–C2–C3, while the addition of ethane to the methane-propane mix causes a modest improvement in PVCap induced crystal growth inhibition, it alone cannot apparently explain the good performance of PVCap in NG systems

Instead, it is the CO_2+C_2(+C_1) combination in NG that seems to give good PVCap performance at higher pressures, although CO_2 is at the same time apparently responsible for the significant reduction in PVCap performance observed at lower pressures in NG systems.

To understand the extent of PVCap inhibition for s-II hydrate a cyclopentane–methane system was tested which showed that PVCap performance is very efficient in this system; it can still significantly inhibit cC5-C1 hydrate growth at over 22 °C of subcooling.

- As a rule of thumb from all above results the more stable the s-II hydrate former (i.e. the better it stabilises the large $5^{12}6^4$ cavity), the more effective PVCap is at inhibiting growth
- While some CGI regions (e.g. the CIR) for C1-cC5 are entirely related to s-II hydrate formation, those at higher subcoolings (e.g. RGR-RFR) may be influenced by s-I growth, as observed for a variety of KHI systems (e.g. methane–propane)
- The appearance of CGI region boundaries at similar subcooling conditions in different systems supports the theory that CGI patterns are strongly influenced by underlying crystal growth patterns

As for s-II/s-I forming systems with PVCap, the formation of s-I hydrates appears to be the reason for PVCap failure in s-H/s-I systems, as evidenced by CGI data for a methane–methylcyclohexane system. In this case, it appeared the formation of s-H hydrates was completely inhibited and only s-I methane hydrate formation occurred. This could be due to the fact that PVCap absorbs more strongly on s-H crystal nuclei, possibly as the caprolactam pendant group fits better into the s-H large cavity which has a greater diameter than s-I and s-II large cages.

References

Arjmandi, M., Tohidi, B., Danesh, A., and Todd, A. C., 2005, *"Is Subcooling the Right Driving Force for Testing Low-Dosage Hydrate Inhibitors?"*, Chemical Engineering Science, 60, 1313-1321

Deaton, W. M., and Frost, E. M., 1946, *"Gas Hydrate Composition and Equilibrium Data"*, Oil and Gas Journal, 45, 170-178

Kelland, M. A., 2006, *"History of the Development of Low Dosage Hydrate Inhibitors"*, Energy and Fuels, 20, 825–847

Larsen, R., Knight, C. A., and Sloan, E. D., 1998, *"Clathrate Hydrate Growth and Inhibition"*, Fluid Phase Equilibria, 150-151, 353-360

Larsen, R., Knight, C. A., Rider, K. T., and Sloan, E. D., 1999, *"Melt Growth and Inhibition of Ethylene Oxide Clathrate Hydrate"*, Journal of Crystal Growth, 204, 376- 381

Peng, B-Z., Sun, C-Y., Peng, L., Liu, Y-T., Chen, J., and Chen, G-J., 2009, *"Interfacial properties of methane/aqueous VC-713 solution under hydrate formation conditions"*, Journal of Colloid and Interface Science, 336 , 738–742

Sloan Jr, E. D. and C. Koh, 2007, *"Clathrate Hydrates of Natural Gases"*, Third Edition, CRC Press, New York.

Subramanian, S., Ballard, A. L., Kini, R. A., Dec, S. F. and Sloan, E. D., 2000, *"Structural Transitions in Methane+Ethane Gas Hydrates — Part I: Upper Transition Point and Applications"*, Chemical Engineering Science, 55, 5763-5771

Tohidi, B., Danesh, A., Todd, A. C., Burgass, R. W., and Todd, A. C., 1996, *"Hydrate Equilibrium Data and Thermodynamic Modelling of Methylcyclopentane and Methylcyclohexane"*, Proceedings of the 2nd International Conference on Gas Hydrates, Toulouse, France

Zhang, J. S., Lo, J. S., Couzis, A., Somasundaran, P., Wu, J., and Lee, J. W., 2009, *"Adsorption of Kinetic Inhibitors on Clathrate Hydrates"*, The Journal of Physical Chemistry C, 113, 17418–17420

5. EFFECT OF LIQUID HYDROCARBONS ON KHI-INDUCED HYDRATE CRYSTAL GROWTH PATTERNS

Investigating the effect of various components present in reservoir fluids on the performance of kinetic hydrate inhibitors is very challenging (mainly due to the multitude of components present in real fluids). While the performance of inhibitors may be enhanced in some heavy oil systems, the performance of the same inhibitors may be worsened in lighter condensate systems. Accordingly, these phenomena are of concern to those using, developing and testing these inhibitors. Research on the effect of hydrocarbons on KHI performance previously carried at the Institute of Petroleum Engineering at Heriot Watt University (2006-2009) consists of both induction time and polymer solubility studies. Throughout this research, induction time studies concluded that while n-heptane has a negative effect on the performance of PVCap in methane−water systems, real condensate apparently has a positive effect in these systems. On the other hand, both n-alkanes and real condensate have a negative effect on the performance of PVCap in natural gas systems (Heriot Watt, 2009).

Moreover, PVCap solubility studies concluded that very little or no PVCap/synergist transfer to the hydrocarbon phase occurs (Progress Report, October 2006), thus the negative effect of a liquid hydrocarbon phase on the performance of KHIs is not likely to be the result of partitioning of inhibitor into the liquid hydrocarbon.

While all results clearly point to the liquid hydrocarbon phase having an important effect on KHI performance, the precise mechanisms by which this occurs are unclear. Also, while data for single alkanes such as n-heptane all suggest a negative effect, contrasting data has been found for real condensate depending on whether the gas is methane (positive effect) or a natural gas (negative effect).

In light of the above, in this section the new crystal growth inhibition (CGI) approach was applied to systems with a liquid hydrocarbon phase present to see if this method could yield more definitive information on the role of the latter. Moreover, to confirm a

further possible mechanism by which polymer concentration might be reduced in the aqueous phase, simple hydrocarbon−water polymer partitioning tests were carried out.

In Section 4.10, CGI regions were studied on cyclopentane, a hydrate forming liquid hydrocarbon phase, for a different purpose. As these studies showed CGI technique gave a good understanding of the behaviour of an s-II hydrate forming liquid hydrocarbon in the presence of PVCap; PVCap performance was very efficient in a system with cyclopentane present.

In this section, for a clear understanding of PVCap behaviour in a simple s-I forming hydrocarbon−methane system crystal growth/inhibition regions were investigated using the new approach for a methane−n-heptane−water system (n-heptane to water volumetric ratio = 1:4) with 0.5 mass% PVCap aqueous at pressures up to 200 bar. Furthermore, experiments were carried out to examine whether the ratio of n-heptane to water had a significant influence on PVCap performance and for this purpose CGI regions were determined for 1.0 mass% PVCap with a high n-heptane to water ratio (4 n-heptane to 1 water).

In addition to experimental investigations with simple known hydrocarbon systems, work concentrated on the study of PVCap performance in the presence of a real condensate phase (for which the composition is well established and presented in Table 5-3). For the real condensate−methane hydrate, crystal growth inhibition regions (CGI) have been investigated for 0.5 mass% PVCap aqueous with a 1 to 4 condensate to water volume ratio at pressures up to 300 bar.

5.1. Effect of Heptane on CGI Regions with PVCap

5.1.1. Crystal Growth/Inhibition Regions

Crystal growth/inhibition regions have been investigated using the new approach for a methane−n-heptane−water system (n-heptane to water volumetric ratio = 1:4 and provided from SIGMA ALDRICH.) with 0.5 mass% PVCap aqueous at pressures up to 200 bar. Figure 5-1 shows example cooling curves and determined inhibition regions for 0.5 mass% PVCap with methane and n-heptane for no history and history present. Also, subcooling range and relative growth rates for each region are outlined in Table 5-1.

Table 5-1 Experimentally determined hydrate growth inhibition regions for a water-methane-n-heptane system with 0.5 mass% PVCap (n-heptane to water volumetric ratio = 1:4). Growth rates are relative. For comparison, approximations to convert initial 1% of aqueous phase to hydrates are as follows: very slow = 48 hours+, slow = 24-48 hours, moderate = 1-24 hours, fast = <1 hour. ΔT_{sub} ranges are average values.

Mass% PVCap	0.50
CIR ΔT_{sub} range / °C (± 0.5) Growth Rate	0.0 − 4.8 Zero
RGR(VS-S) ΔT_{sub} range / °C (± 0.5) Growth Rate	4.8 − 6.9-7.2 Very slow
RGR(M) ΔT_{sub} range / °C (± 0.5) Growth Rate	6.9-7.2 − 9.0 Moderate
RFR ΔT_{sub} range / °C (± 0.5) Growth Rate	9.0+ Fast

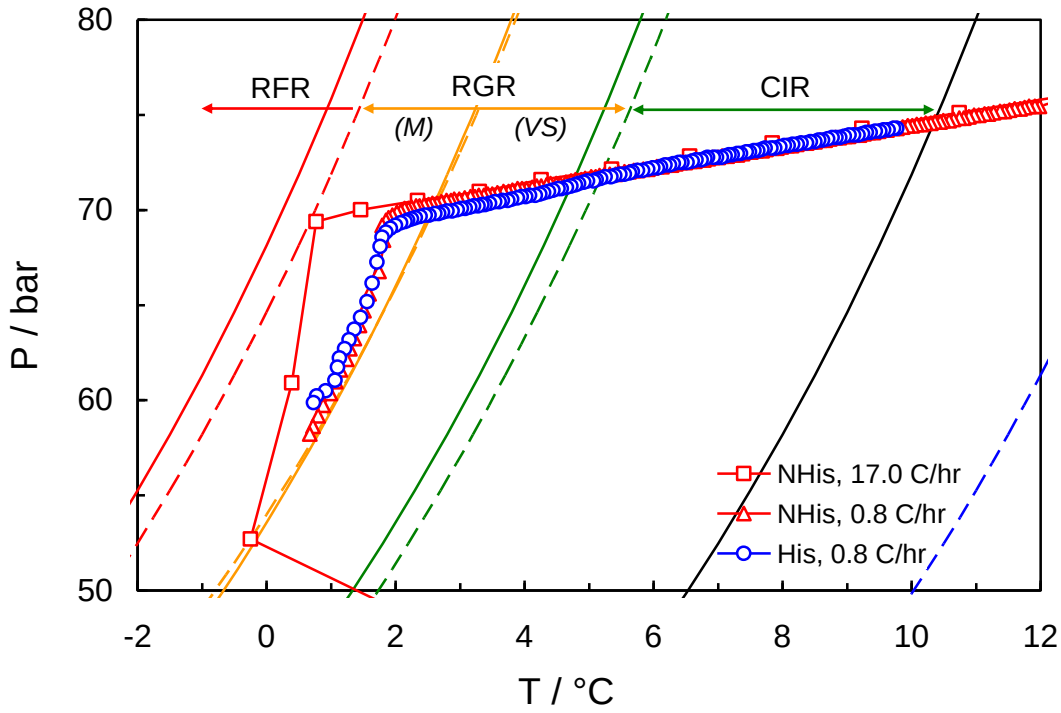

Figure 5-1 PT plot showing example cooling curves to determine inhibition regions for 0.5 mass% PVCap with methane and n-heptane (n-heptane to aqueous phase volume ratio = 1:4). Runs are for no history (NHis) and history (His) present. Solid lines are regions for methane alone, dotted lines are for n-heptane present.

As can be seen in Figure 5-1, all regions (CIR, RGR and RFR) observed in methane−water systems with 0.5 mass% PVCap are also present when n-heptane is added (see Chapter 2 for details on methane regions). However, results suggest that

n-heptane has a mildly negative effect, reducing the subcooling to all region boundaries by up to 0.5 °C. Moreover, it is clear from the history present (typically near identical behaviour to hydrate present) run, that hydrate growth (as indicated by pressure drop) begins at a lower subcooling (compared to that for methane alone) when n-heptane is present (this behaviour was consistent at all pressures). Likewise, rapid failure points which delineate the RFR boundary were generally at lower subcoolings with n-heptane present, as shown in the Figure for the rapid (cooling rate, 17 °C/hr) no history run. These were also more scattered (± 0.5 °C), hence the RFR line is tentative (based on average of 2-3 runs at each pressure). For no history runs at low cooling rates (e.g. 0.8 °C/hr), behaviour was commonly similar to history present runs in that moderate growth rates occurred in a 'subdued' RGR(M) (for methane alone) region, as shown in Figure 5-1. Similar behaviour is observed in methane systems; rapid cooling rates typically being required to avoid significant growth in RGR(M), whereby allowing rapid failure on the RFR boundary line to be observed. As can be seen in the Figure, in hydrate present runs hydrate starts to grow very gently once the RGR region is entered/CIR exited on cooling. On reaching the RGR(VS-M) boundary, moderate growth rates are observed, with PT conditions following the (at slightly lower subcooling) RGR(VS-M) boundary line in the early stages, as is typical for methane-water systems without n-heptane present.

5.1.2. Polymer Partitioning Between Phases

The reason for the negative effect of n-heptane on KHI performance observed in the CGI tests was not totally clear although it was considered that it may be some kind of concentration reduction that results in this behaviour. Since polymer does not significantly partition into n-heptane (Heriot Watt, 2009), it was speculated that the cause of this may be an interfacial partitioning of the polymer between the water and liquid hydrocarbon phase. For the polymer concentration in the aqueous phase to be reduced, it does not have to partition into another phase (e.g. the liquid hydrocarbon); instead it could concentrate at water-hydrocarbon interfaces. Two mechanisms could induce this: (1) that PVCap has surfactant-like properties and (2) disturbance of the water structural organisation at the water hydrocarbon interface which reduces (the rather tenuous) PVCap solubility.

PVCap molecules comprise of a hydrophobic hydrocarbon chain backbone and a mildly hydrophilic pendant amide ring; the amide oxygen offering hydrogen bonding

opportunities and so facilitating solubility in water and other polar solvents such as alcohols/glycols (e.g. Kirsh, 1998). This hydrophobic/hydrophilic combination could potentially give the polymer surfactant-like properties.

To test this hypothesis, a 0.5 mass% PVCap aqueous solution was mixed with a similar volume of n-heptane at room temperature and pressure. Mixing readily yielded an emulsion with moderate stability, as shown in Figure 5-2. This emulsion took around 1 hour to completely separate, compared to < 1 minute when PVCap was not present. Furthermore, following demulsification, a white, solid-like particulate film was observed to remain at the water−n-heptane interface (Figure 5-2). As no other obvious explanation can be found to explain the origins of this film, it is assumed that it is PVCap; i.e. the polymer is congregating at the water-hydrocarbon interface. This observation would agree with the surfactant-like properties observed and could readily explain the reduced inhibition performance in the presence of n-heptane; polymer partitioning to the interface reducing the concentration in the aqueous phase. While PVCap and other poly-n-vinyl amides are soluble in water, this solubility is very tenuous, with most polymers having a low critical solution temperature (Kirsh, 1998). While n-heptane has a very low solubility in water, its addition to the aqueous phase could potentially disturb the water structural organisation which permits such a large polymer hydrophobic hydrocarbon backbone chain to be accommodated. The fact that the ‘film’ observed between the aqueous and hydrocarbon phase appears to comprise of visible particles suggests that a fraction of the polymer has been precipitated out of solution. Certainly, for the polymer to precipitate when it would normally be soluble suggests that polymer molecules have been directed and displaced towards the water heptane interface. From a purely electrostatic point of view, because of the intermolecular forces, the approach of an ion (or in this case polymer molecule with a hydrophilic end) to the interface of water and a nonpolar fluid is unfavourable. However, work relating to streaming potential at water/oil interfaces have shown that when a dielectric phase (solid or fluid) is placed in contact with polar liquid, such as water, the interface gets charged due to either specific adsorption of ions initially dissolved in the polar liquid (e.g. HO- ions in the boundary water molecules), or dissociation of surface ionisable groups (e.g. depletion of H+ ions in the boundary layer). The final result of these two processes is the formation of an electrical layer which contains concentration of charged materials (Birdi, 2002). In this case, this electrical layer is concentrated with polymer molecules and hence due to the relatively

weak solubility of polymers in water some of these molecules have precipitated out of the solution.

A.

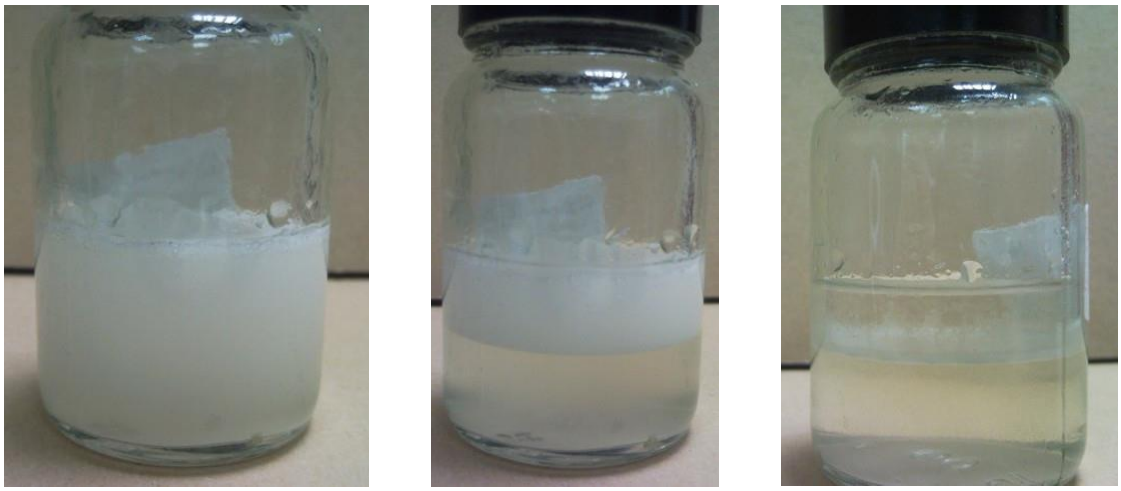

0 mins 5 mins 60 mins

B.

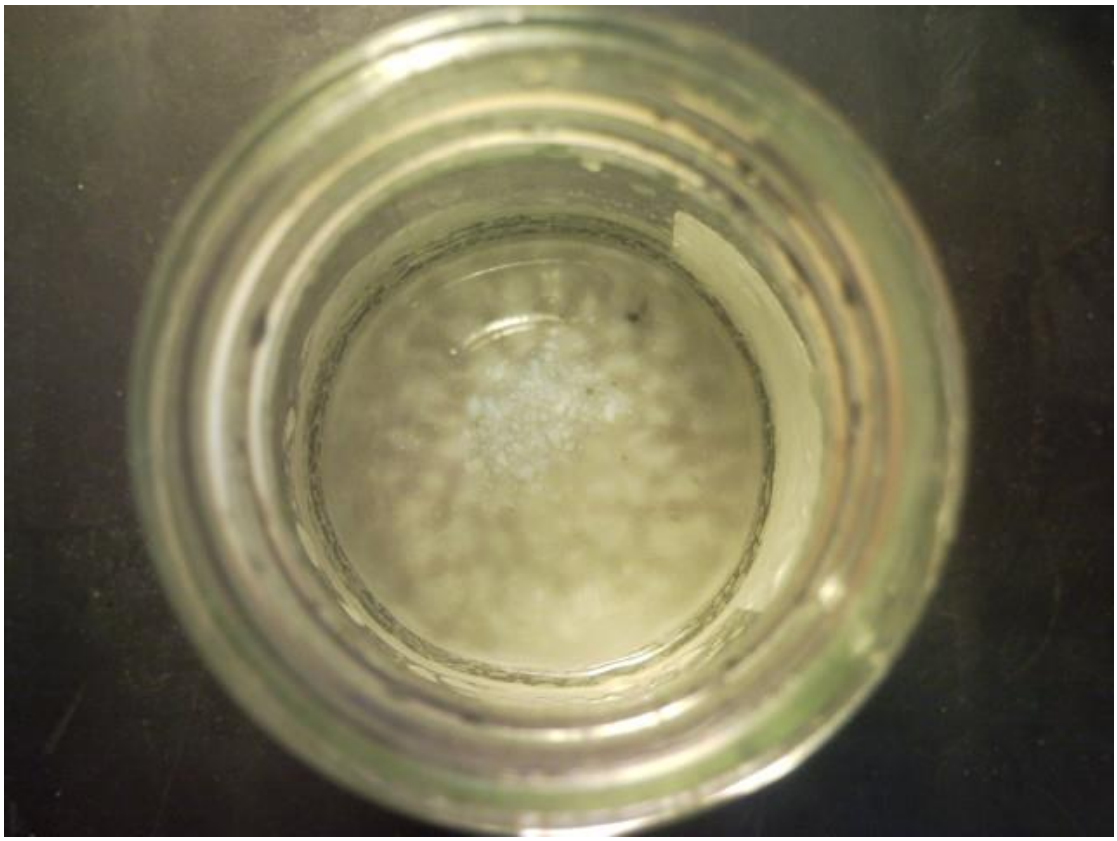

Figure 5-2 A: Images of water−n-heptane−PVCap emulsion (0.5 mass% PVCap aqueous) just after vigorous mixing (0 mins), during (5 mins) and after (60 mins) demulsification at static conditions (5 mins). B: Looking down through the overlying n-heptane at the white, solid-like particulate film which gathers at the water-hydrocarbon interface.

5.1.3. High n-Heptane to Water Ratio

As shown above CGI studies revealed that for a 1 heptane to 4 water volume ratio, heptane had only a minor negative effect on the performance of PVCap at 0.5 mass% aqueous; methane hydrate CGI regions being reduced to lower subcoolings by ~0.5 °C at most from those for systems with no heptane present. This was speculatively attributed to partial precipitation of PVCap at the heptane-water interface in the presence of heptane; this presumably reducing the concentration in the aqueous phase and thus performance.

To examine whether the ratio of n-heptane to water had a significant influence on PVCap performance, measurement of PVCap CGI regions for a high n-heptane to water ratio (4 heptane to 1 water) were checked for 1.0 mass% PVCap aqueous. Example cooling curves and determined CGI region boundary points are shown in Figure 5-3 in comparison with CGI boundary lines for no heptane present (methane−water−0.5/1.0 mass% PVCap aqueous; boundaries for 1.0 and 0.5 mass% being essentially identical for methane systems). CGI boundary points are reported in Table 5-2.

Table 5-2 Experimental methane hydrate CGI region data for 1.0 mass% PVCap aqueous with n-heptane (4:1 heptane to water volume ratio). See Section 2.3.1 for growth rate definitions.

CGI boundary	*Growth rate	T / ºC (± 0.5)	P / bar (± 0.2)	ΔT_{s-l} / ºC (± 0.5)
SDR	Slow dissociation	13.9	74.9	3.5
CIR-RGR(VS)	No growth	4.7	71.3	–5.2
		4.8	71.3	–5.1
RGR(VS-M)	Very slow to slow growth	2.6	70.1	–7.2
		2.6	70.3	–7.2
RGR(M)-RFR	Moderate to fast growth	-1.0	66.4	–10.2
		-1.0	67.1	–10.3
		-0.9	68.3	–10.4

*Growth rate is for ΔT CGI region preceding the associated boundary

As shown in Figure 5-3, CGI regions and hydrate growth rates for a high n-heptane to water volume ratio with 1 mass% PVCap are essentially identical to those for no heptane present. Thus, in agreement with findings for 0.5 mass% PVCap with a low n-heptane volume fraction (1 heptane to 4 water), the presence of a (non-hydrate forming) liquid hydrocarbon phase has little effect on CGI regions; only at lower PVCap concentrations does the partial precipitation of polymer at water-hydrocarbon interfaces reduce performance.

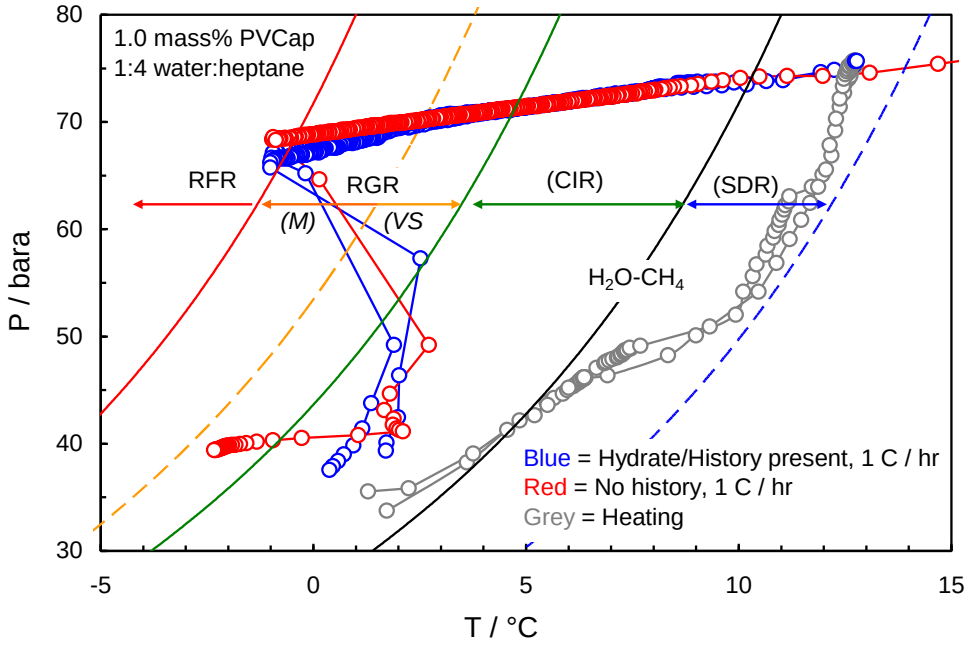

Figure 5-3 Example cooling curves for determination of CGI regions for 1.0 mass% PVCap aqueous with methane and n-heptane (n-heptane to aqueous phase volume = 4:1). CGI boundary lines are those for no heptane present (methane−water−0.5/1.0 mass% PVCap).

5.2. Effect of Real Condensate on CGI Regions with PVCap

After experimenting with simple known hydrocarbon system, n-heptane, work concentrated on the investigation of real condensate−methane hydrate crystal growth inhibition regions (CGI) have been investigated for 0.5 mass% PVCap aqueous with a 1 to 4 condensate (composition is presented in Table 5-3) to water volume ratio at pressures up to 300 bar.

Example heating/cooling curves with derived CGI region boundaries are shown in Figure 5-4. Measured points on CGI boundaries are reported in Table 5-4

As can be seen in Figure 5-1, all regions (CIR, RGR and RFR) observed in methane−water systems with 0.5 mass% PVCap are also present when a real condensate is added. However, results suggest that, unlike n-heptane, the presence of condensate has both a slightly positive and a mildly negative effect. Like n-heptane, in the presence of condensate, the complete inhibition region is reduced; in this case by almost 1 °C, compared to only ~0.4 °C for n-heptane. A reduction in the extent of the SDR is also apparent, changing from ~ 4 °C to ~3.2 °C.

Table 5-3 Composition the real condensate used in experiments

Component	Molar fraction
iC4	0.0014
nC5	0.0058
iC5	0.0116
C5	0.0143
C6	0.0600
C7	0.1228
C8	0.1812
C9	0.1459
C10	0.1239
C11	0.0936
C12	0.0647
C13	0.0517
C14	0.0364
C15	0.0258
C16	0.0178
C17	0.0133
C18	0.0103
C19	0.0073
C20	0.0122

Table 5-4 Experimental methane hydrate CGI region data for 0.5 mass% PVCap aqueous with methane and condensate. Condensate to water ratio is 1:4.

CGR boundary	*Growth rate	T / ºC (± 0.5)	P / bar (± 0.2)	ΔT_{s-I} / ºC (± 0.5)
SDR	Slow dissociation	14.5	79.3	3.5
		21.2	184.1	3.2
		24.7	304.2	2.9
CIR-RGR(S)	No growth	6.5	74.7	–3.9
		12.8	172.5	–4.7
		17.1	288.1	–4.3
RGR(S-M)	Slow to moderate (dotted region)	0.35	55.7	-7.2
		8.9	144.1	-7.2
		12.3	217.2	-6.9
RGR(S-M)	Slow to moderate	2.2	72.5	–7.9
		9.5	165.8	–7.7
		13.0	277.4	–8.1
RGR(M)-RFR	Moderate	1.0	72.6	–9.1
		9.4	167.2	–7.9
		11.2	275.8	–9.8

*Growth rate is for ΔT CGI region preceding the associated boundary

However, while in this condensate–water–PVCap system, the extent of the CIR is reduced, the extent of RGR actually is increased slightly; ΔT_{sub} shifted about –0.6°C in average, changing it from ~–7.3 °C (PVCap–water) to ~–7.9 °C

(condensate–water–PVCap). It is interesting to point that in an n-heptane–water–PVCap system RGR had remained largely constant.

In spite of this, although the RGR has increased in condensate–water–PVCap system, from hydrate present cooling curves in Figure 5-4 it is notable that after some small growth of hydrate in the system, this boundary move back and follow a similar trend to RGR boundary in water–PVCap system (hydrate continues to grow at a subcooling of around ΔT_{sub} =~–7.1 °C, illustrated with a dotted line on the graph), thus the positive effect seen apparently only applies at lower hydrate fractions.

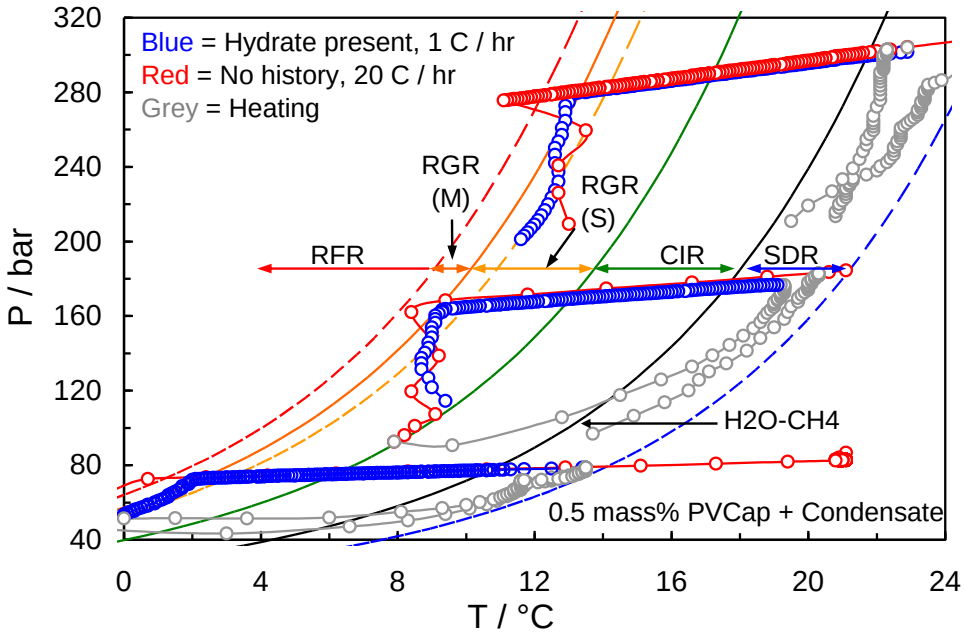

Figure 5-4 Example cooling and heating curves for 0.5 mass% PVCap with methane and condensate. Condensate to water ratio is 1:4.

In addition, RFR in the condensate–water–PVCap system changed in a similar manner to the CIR. It is again evident that RGR with ΔT_{sub} =~–8.9 °C has had a slight reduction in this system compared to that for a PVCap–water system with ΔT_{sub}=~–9.6 °C. This behaviour is also similar to an n-heptane–water–PVCap system where the ΔT_{sub} for RFR changed to ~–9°C.

Average PVCap induced inhibition regions for all three systems (water–PVCap, n-heptane–water–PVCap and condensate–water–PVCap) are reported in Table 5-5.

For better interpretation and comparison of the effect condensate and n-heptane on PVCap performance, this data is also illustrated in Figure 5-5.

Table 5-5 Experimental methane hydrate average CGI region data for 0.5 mass% PVCap aqueous, 0.5 mass% PVCap aqueous with n-heptane (n-heptane to water ratio is 1:4) and 0.5 mass% PVCap aqueous with condensate (condensate to water ratio is 1:4).

	ΔT_{sub} RFR/°C	ΔT_{sub} RGR(S) /°C	ΔT_{sub} CIR /°C	ΔT_{sub} SDR /°C
Real condensate	–8.9	–7.9	–4.3	3.2
n-heptane	–9.0	–7.2	–4.8	3.5
No liquid hydrocarbon	–9.6	–7.3	–5.2	4.0

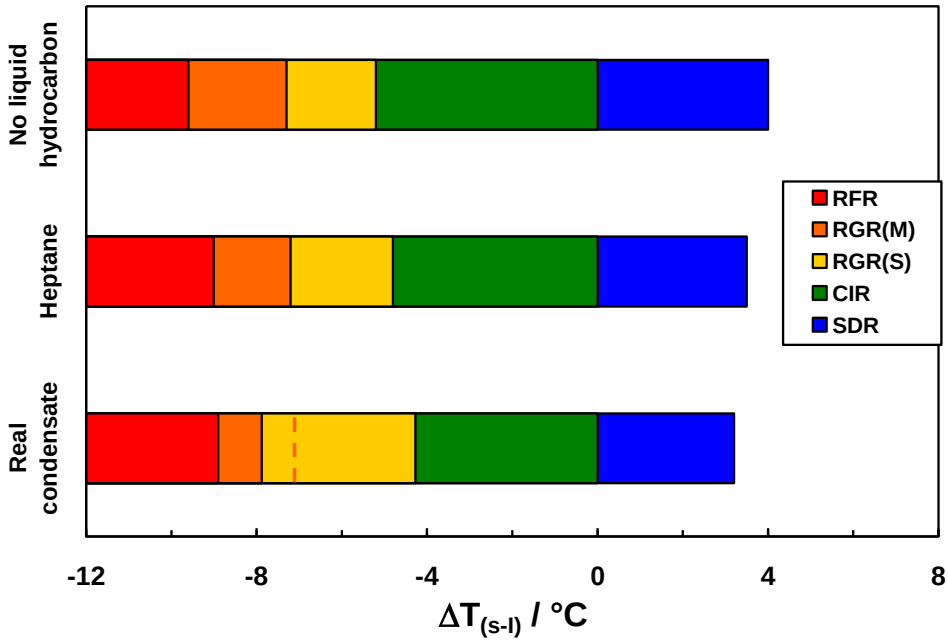

Figure 5-5 Experimental methane hydrate average CGI region data for 0.5 mass% PVCap aqueous, 0.5 mass% PVCap aqueous with n-heptane (n-heptane to water ratio is 1:4) and 0.5 mass% PVCap aqueous with real condensate (condensate to water ratio is 1:4).

5.3. Conclusions

Results of work applying the new approach to methane−n-heptane−water−PVCap systems revealed that for a 1 heptane to 4 water volume ratio, heptane had only a minor negative effect on the performance of PVCap (Luvicap EG base polymer) at 0.5 mass% aqueous; methane hydrate CGI regions being reduced to lower subcoolings by ~0.5 °C at most from those for systems with no heptane present.

Simple visual observation of n-heptane−water−PVCap behaviour at room temperature and pressure suggest that this negative effect could be related to polymer partitioning at the water−hydrocarbon interface, reducing the aqueous phase concentration. Certainly, a reduction in aqueous polymer concentration has been shown to reduce the subcooling to different region boundaries (CIR, RGR, RFR) for methane systems. Thus a reduction

in aqueous concentration due to polymer interface partitioning would be expected to have the effect observed in the n-heptane system as discussed. Consequently, it can be concluded that the negative effect is apparently more significant at lower PVCap concentrations where polymer precipitation at water-hydrocarbon interfaces results in a more significant relative reduction in the aqueous phase concentration

Testing 1.0 mass% PVCap with a high n-heptane to water ratio (4 n-heptane to 1 water) for evaluation of the effect of n-heptane to water ratio showed that results were consistent with those for a low n-heptane to water ratio. It was again proved that a non-hydrate forming liquid hydrocarbon phase had only a limited negative effect on PVCap CGI regions.

In a condensate system, similar to an n-heptane system, PVCap performance has been deteriorated slightly; slow dissociation, complete inhibition and rapid failure regions are clearly reduced to lower subcoolings in the presence of condensate. However, the RGR(S) shows a slight increase in subcooling extent, at least at lower hydrate fractions, before returning to its normal (methane−water−PVCap) trend as hydrate fraction increases. The explanation for this negative effect of condensate could be similar to that presumed for n-heptane which was related to polymer partitioning at the water−hydrocarbon interface, reducing the aqueous phase concentration.

Overall condensate acts slightly more negative than n-heptane; possibly due to the presence some hydrate forming compounds in the real condensate (e.g. iso-butane, iso-pentane). However, these may also be having a positive effect in the RGR similar to that for ethane (Section4.2). Clearly the hydrocarbon composition, which determines cage occupancy, has an important role to play.

References

Birdi. K. S., 2002, *"Handbook of Surface and Colloid Chemistry"*, Second Edition, CRC Press, New York

Kirsh, Y. E. and I. E. Kirsh, 1998, *"Water soluble poly-N-vinyl amides: synthesis and physicochemical properties",* Wiley, New York

Heriot-Watt Institute of Petroleum Engineering, 2009, *Flow Assurance: Micro and Macro-Scale Evaluation of Low Dosage Hydrate Inhibitors 2006-2009 Program*, Edinburgh, Heriot-Watt Institute of Petroleum Engineering

6. EFFECT OF SALTS ON KHI-INDUCED HYDRATE CRYSTAL GROWTH PATTERNS

Reservoir produced waters commonly contain varying concentrations of dissolved salts. Typically, the salinity of produced waters increases during field life as water is stripped by the gas phase.

Sloan et al. (1998), has previously found that sodium chloride has a generally positive effect on the performance of PVCap increasing the subcooling to formation on cooling at a constant rate (analogous to points in the RFR region using the CGI method). In this research for 0.5 wt % PVCap and salt concentrations from 0 to 7.0 wt %, it was shown that at low concentrations of salt, there was little or no effect on the high molecular weight PVCap. However, the lowest molecular weight of PVCap (Mn = 900 g/gmol) showed a significant subcooling decrease at lower salt concentrations. On the other hand, at higher salt concentrations (above 5.0 wt % salt), all molecular weight PVCap tested showed an improved subcooling. Sloan et al. (1998) speculated that although it is not clear why salt affect the subcooling of PVCap, it seems likely that the addition of salt could change PVCap's conformation in solution and possibly decrease the ability of PVCap to adsorb to the hydrate surface. It should be noted that because longer chain lengths are associated with higher molecular weight PVCap, the conformation in solution may be different for polymers of different chain lengths (Sloan et al., 1998).

In contrast, it should be considered that although results showed positive behaviour of NaCl, higher salt concentrations commonly reduce polymer (e.g. PVCap) solubility in aqueous solutions, causing solid polymer precipitation, which poses problems for KHI use in systems with highly saline brines.

In a different study by Yang et al. (2004), visual observations were made on the effect of NaCl on gas hydrate growth at the pore scale. In this study it was found that due to the ionic interfacial absorption of NaCl molecules, independent of test temperature the presence of this salt changed the morphology of hydrates formed. Similar to an anti-agglomerant, instead of massive hydrate crystals and crusts covering the gas bubbles, NaCl caused hydrate crystals to form thin flakes and separate tiny grains. In addition to that, Yang et al. (2004) found that if salt was added to a system with hydrate history, the

effect of salt on hydrate morphology became much weaker suggesting that the influence of salt absorption is most effective at the hydrate nucleation stage rather than later stages of hydrate growth.

To gain better understanding on the effect of NaCl on PVCap performance it was necessary to study CGI regions for NaCl plus PVCap system with methane. For this purpose methane hydrate crystal growth inhibition regions (CGI) have been measured for 0.5 mass% PVCap aqueous with 5 mass% NaCl (relative to water + PVCap) at pressures up to ~250 bar. The NaCl used in all test was 99.5% pure supplied from Fisher Scientific.

Clearly results for NaCl would not necessarily apply for all other salts particularly carbonate salts that have a completely different structure. In light of this, some preliminary tests on the effect of K_2CO_3 – a carbonate salt – on PVCap performance were also conducted using the crystal growth inhibition technique. For this purpose, methane hydrate crystal growth inhibition regions (CGI) were measured for 0.5 mass% PVCap aqueous with 2.0 mass% K_2CO_3 (relative to water + PVCap) at pressures up to ~220 bar. The K_2CO_3 used in these tests was 99.5% pure supplied from BDH Laboratory Supplies and the salt concentration of 2.0 mass% was chosen as polymer precipitation occurs at higher concentrations.

6.1. Effect of NaCl on CGI Regions with PVCap

As mentioned above methane hydrate crystal growth inhibition regions (CGI) were measured for 0.5 mass% PVCap aqueous with 5.0 mass% NaCl (relative to water + PVCap) at pressures up to 250 bar. Example cooling curves for determination of CGI region boundaries and the determined CGI region boundaries are shown in Figure 6-1. Experimental points on CGI region boundaries are reported in Table 6-1. Data are compared with those for distilled water−PVCap−methane systems in Figure 6-3.

As seen in Figure 6-1, as for methane–water–PVCap systems, CGI regions in the presence of salt are clearly distinguishable and repeatable. As shown in Figure 6-3, the complete inhibition region (CIR) for salt is the same as for distilled water at ~–5 °C subcooling. In contrast, the RGR is larger with salt present, slow-very slow growth extending to ΔT_{sub} =~–8.1 °C instead of ~–7.2 °C for distilled water, with the RFR boundary at ΔT_{sub} =~–11.4 °C compared with ~–9.7 °C for distilled water. The SDR is

also slightly larger for 5 mass% NaCl which confirms the slight extension of RGR in this system. Overall, as can be seen from the figures, NaCl has a positive effect on PVCap performance preserving the CIR while extending slow and moderate growth regions to higher subcoolings.

Table 6-1 Experimental CGI region data for 0.5 mass% PVCap aqueous with 5 mass% NaCl (relative to water + PVCap). See Section 2.3.1 for growth rate definitions.

CGI boundary	*Growth rate	T / ºC (± 0.5)	P / bar (± 0.2)	ΔT_{sub} / ºC (± 0.5)
SDR	Slow dissociation	12.7	71.9	4.5
		18.5	150.7	3.9
		21.6	238.5	3.5
CIR-RGR(S)	No growth	2.6	68.1	–5.1
		2.7	67.6	–4.9
		9.3	142.9	–4.9
		12.4	220.0	–5.1
RGR(S-M)	Very slow to slow growth	–0.9	65.3	–8.2
		–0.8	65.5	–8.1
		5.6	138.8	–8.4
		5.6	137.7	–8.2
		9.1	211.9	–8.1
		9.2	212.3	–8.1
RGR(M)-RFR	Moderate to fast growth	–4.2	65.5	–11.5
		–4.3	64.4	–11.5
		2.4	135.4	–11.3
		2.4	135.5	–11.3
		5.6	205.0	–11.4

*Growth rate is for ΔT CGI region preceding the associated boundary

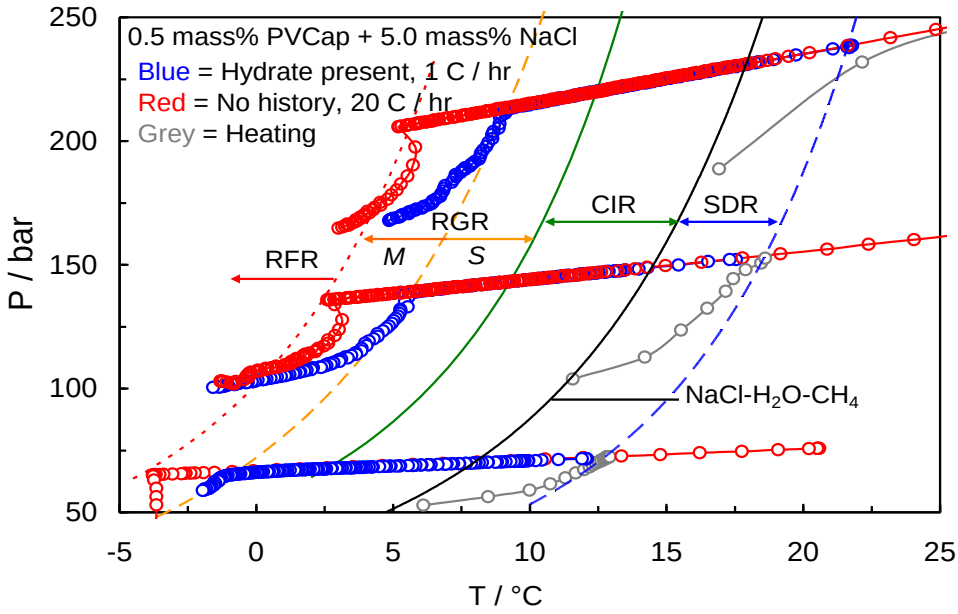

Figure 6-1 Example CGI region determination cooling and heating runs for 0.5 mass% PVCap / 5 mass% NaCl aqueous with methane. Both 'no history' runs and 'hydrate present' runs are for a 1 °C/hour cooling rate (in the HSZ).

6.2. Effect of K_2CO_3 on CGI Regions with PVCap

As mentioned above methane hydrate crystal growth inhibition regions (CGI) were measured for 0.5 mass% PVCap aqueous with 2.0 mass% K_2CO_3 (relative to water + PVCap) at pressures up to ~220 bar.

Example cooling and heating curve data for determination of CGI region boundaries and the determined CGI region boundaries are shown in Figure 6-2. Experimental points on CGI region boundaries are reported in Table 6-2. CGI region extents of distilled water, 5.0 mass% NaCl and 2.0 mass% K_2CO_3 aqueous with 0.5 mass% PVCap and methane are compared in Figure 6-3.

Table 6-2 Experimental methane hydrate CGI region data 0.5 mass% PVCap / 2 mass% K_2CO_3 aqueous

CGR boundary	*Growth rate	T / ºC (± 0.5)	P / bar (± 0.2)	ΔT_{s-I} / ºC (± 0.5)
SDR	Slow dissociation	15.7	88.3	4.8
		20.5	171.2	3.9
		22.8	231.8	3.8
CIR-RGR(S)	No growth	4.9	82.7	–5.4
		11.1	160.1	–4.9
		13.6	223.3	–5.1
RGR(S-M)	Slow to moderate	2.7	72.7	–6.4
		9.7	158.2	–6.2
		12	207.7	–6.2
RGR(M)-RFR	Moderate	2.9	79.2	–7.0
		9.1	157.0	–6.8
		10.8	202.5	–7.2

*Growth rate is for ΔT CGI region preceding the associated boundary

As shown in Figure 6-2, CGI regions in the presence of K_2CO_3 are clearly distinguishable and results readily repeatable. This figure shows that the complete inhibition region (CIR) in this system is very similar to that for distilled water and 5 mass% NaCl at ~–5.2 °C subcooling. Likewise the SDR at around ~+4.2 °C greater than the phase boundary is comparable to these systems. However, the RGR region is apparently reduced when compared to the distilled water system, in contrast to 5 mass% NaCl where it was larger. For 2 mass% K_2CO_3, the RGR-RFR boundary is reduced ΔT_{sub} = ~–7.2 °C compared to ΔT_{sub} = ~–9.5 °C for distilled water and ~–11.5 °C for 5 mass% NaCl aqueous. Thus even though CIR and SDR are preserved in this system other CGI regions are clearly reduced, hence the overall effect of K_2CO_3 on PVCap performance is moderately negative.

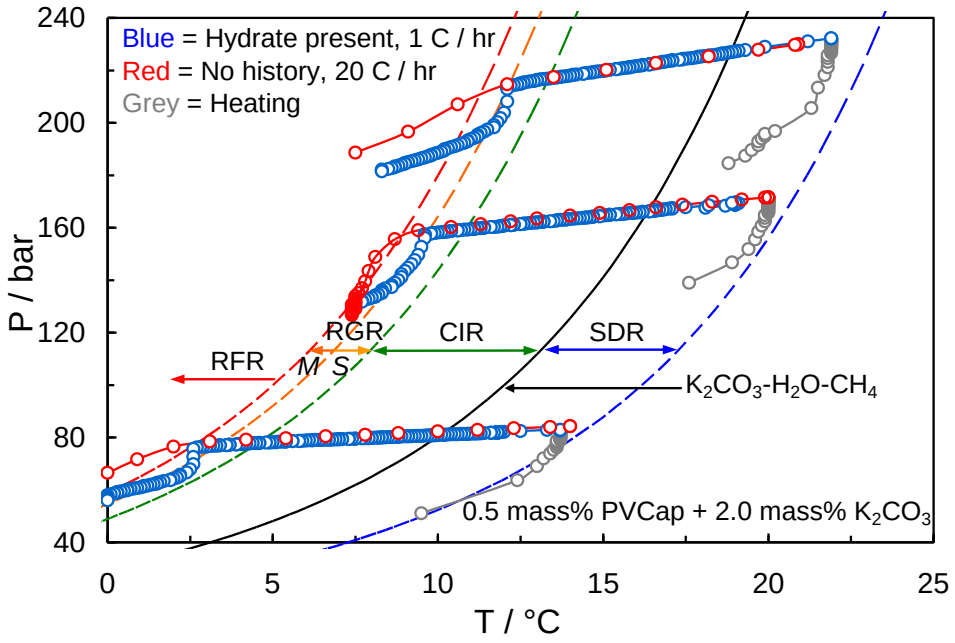

Figure 6-2 Example CGI method cooling and heating curve data for 0.5 mass% PVCap / 2.0 mass% K_2CO_3 aqueous with methane.

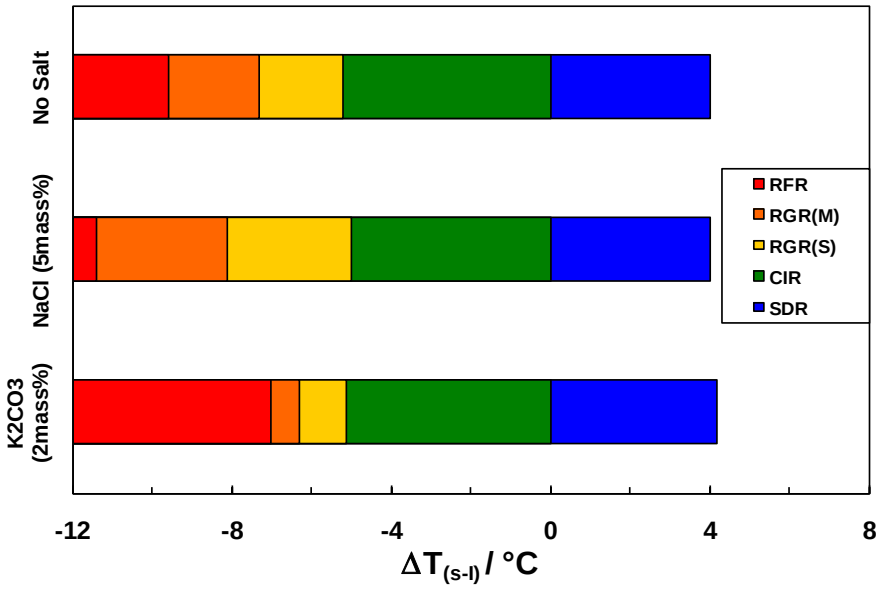

Figure 6-3 Comparison of subcooling extent of CGI regions from the s-I phase boundary for distilled water, 5.0 mass% NaCl and 2.0 mass% K_2CO_3.

6.3. Conclusions

CGI region studies on NaCl−PVCap−water systems with methane at 0.5 mass% PVCap and 5 mass% NaCl showed that NaCl at this concentration has a positive effect on PVCap performance. It can be further explained that NaCl is apparently a 'top-up' thermodynamic inhibitor at lower concentrations; crystal growth inhibition regions remain at similar (e.g. CIR) or extend to greater (RGR) subcoolings in the presence of 5

mass% aqueous sodium chloride. Moreover, the slow dissociation region is larger with salt present which confirms the positive behaviour observed.

The positive behaviour of NaCl can be explained through Yang et al.'s (2004) finding in that the large ionic absorption of sodium chloride at the interface clearly changes the morphology of hydrates. This morphology change is most possibly in favour of the polymer pendant group stabilization on the surface of the hydrate. As a result, PVCap can inhibit hydrate formation and growth more effectively in the presence of this salt.

At higher salt concentrations CGI regions may grow even further, although this was not confirmed as higher sodium chloride concentrations (e.g. 10 mass%) caused polymer precipitation and 0.5 mass% PVCap was no longer soluble and partially precipitated at those concentrations.

CGI region studies on a K_2CO_3−PVCap−water system with methane at 0.5 mass% PVCap and 2 mass% K_2CO_3 showed that K_2CO_3 at this concentration has a generally negative effect PVCap performance. Unlike NaCl, K_2CO_3 is apparently not a complete 'top-up' thermodynamic inhibitor; at the concentration tested the CIR is maintained but the RGR is reduced in subcooling extent compared with distilled water. This behaviour suggests that this carbonate salt does not influence the hydrate morphology towards causing a more effective adsorption of polymer on the hydrate surface. However, confirming this theory requires visual observation.

At higher K_2CO_3 concentrations (>2 mass%), 0.5 mass% PVCap was no longer soluble and partial precipitation occurred therefore could not be tested.

The fact that K_2CO_3, in contrast to NaCl, had a slightly negative effect on PVCap performance shows that the effects of salts may be more complex and that salt structure (carbonate or non-carbonate) can play an important role on the effect it has on PVCap performance; probably due to changes that they cause to the morphology of the hydrate which can affect the adsorption of polymer on the hydrate surface. Therefore, for prediction of system behaviour knowing the type of salt is essential.

References

Sloan, E. D., Subramanian, S., Matthews, P. N., Lederhos, J. P., and Khokhar, A. A., 1998, "*Quantifying Hydrate Formation and Kinetic Inhibition*", Industrial and Engineering Chemistry Research, 37, 3124-3132

Yang, J., Tohidi, B., Anderson, R., 2004, *"Visual Observation of Hydrate Growth from Pure Water and Aqueous Salt Solutions in Synthetic Pore Micromodels"*, The 32th International Geological Congress, Florence, Italy.

7. EFFECT OF ALCOHOLS ON KHI-INDUCED HYDRATE CRYSTAL GROWTH PATTERNS

Thermodynamic hydrate inhibitors such as methanol and ethylene glycol are commonly used as solvents in KHI formulations and as a 'top-up' inhibitor to increase the subcooling to which KHIs can be used. Likewise, KHIs offer a potential means to reduce the amount of thermodynamic inhibitor required for high subcooling operations. Hence the performance of the combination of a thermodynamic inhibitor and a KHI can be of high importance.

Previously, Sloan et al. (1998) showed that methanol (MeOH) has a detrimental effect on the performance of PVCap, reducing the subcooling to formation on cooling at a constant rate (analogous to points in the RFR region using the CGI method). Testing 0.5 wt % PVCap with methanol at concentrations from 0 to 15.0 wt % he showed that subcooling decreased in linear proportion to the concentration of methanol, indicating that PVCap was less effective in the presence of methanol. Also it was observed that lower molecular weights of PVCap were more negatively affected by the presence of increased methanol concentrations. The reason for this was not clear, however it was speculated that the addition of methanol could change PVCap's conformation in solution and possibly decrease the ability of PVCap to adsorb to the hydrate surface. (Sloan et al., 1998)

In addition to that, Budd et al. (2004) discovered a strong synergistic effect between a certain ratio of methanol and a low molecular weight oligomer type LDHI. In their studies Budd et al. (2004) came up with a formulation of an effective hydrate inhibitor (combination of methanol and LDHI) that they claimed to reduce up to 80% of the original and often insufficient methanol dosage. (Budd et al., 2004)

In another study by, Wu et al. (2006) the effect of methanol and a kinetic hydrate inhibitor (VC-713) were tested separately and in combination. In this research it was uncovered that although each of these inhibitors perform well separately, in practice, the combination of thermodynamic inhibitors and kinetic inhibitors gives better results. Hence, it is better to use thermodynamic inhibitors together with the kinetic inhibitors. (Wu et al., 2006)

Furthermore, in the study on uncovering a dual nature of polyether amines hydrate inhibitors by Pakulski et al. (2005), it was confirmed that there is a synergy between MeOH and polyether amine (PEA) as a kinetic inhibitor. At intermediate PEA to MeOH ratios the initial gas to hydrate conversion took longer periods to happen and also conversion rates were much smaller at these PEA to MeOH ratios (Pakulski et al., 2005).

To understand the effect of different alcohols which are commonly used in KHI formulations on the performance of these KHIs, it is necessary to investigate CGI behaviour for the combination of these thermodynamic inhibitors and kinetic hydrate inhibitors (PVCap). The most common thermodynamic inhibitor amongst alcohols is methanol. Researchers have shown that although methanol is an effective thermodynamic hydrate inhibitor when added in sufficient quantities, it actually enhances the rate of hydrate formation when added at low concentrations to water (Yousif, 1998). Hence understanding the effect of this inhibitor on PVCap performance requires in depth investigations. For this purpose, methanol CGI behaviour and boundaries were tested and measured at different concentrations in a range of pressures.

Moreover, given that ethanol is seeing increasing use as a hydrate inhibitor due to its good environmental credentials, extended investigations were undertaken on the effect of this alcohol at different concentrations. Also, ethanol has similar properties/molecular structures to methanol, the difference only lying in the carbon number of the alkyl ‘tail’. Hence, testing this alcohol can help in understanding the influence of this factor on KHI performance. Furthermore, similar to methanol although ethanol is known as a thermodynamic inhibitor, it has been found that it can in fact form clathrate hydrates at conditions pertinent to offshore operations (Anderson et al., 2009). Hence, it was speculated that this parameter could also affect the influence of ethanol on PVCap performance and required exploration.

In addition to ethanol, n-propanol and n-butanol which have similar properties/molecular structures to methanol with the only different in the number of carbons in the alkyl ‘tail’ were also tested to further investigate the effect of alkyl ‘tail’ carbon number of alcohols on their effect on PVCap performance.

In addition to that, i-propanol, which has the same molecular formula but different structure to n-propanol, was also tested to better distinguish the potential role of alcohol alkyl 'tail' on PVCap performance.

All experiments were carried out using high pressure stirred autoclaves and the CGI technique. In all the experiments alcohols were testes with 0.5mass% PVCap aqueous with methane. All the alcohols were tested at least at one similar molar concentration (0.76 mole%) for a fairer comparison of their performance relative to one another. These alcohols were supplied by Fisher Scientific and the purity of each alcohol was as follows; Methanol 99.5%, Ethanol 99.5%, n-propanol 99.9%, i-propanol 99.0% and n-butanol 99.4%.

7.1. Effect of MeOH on CGI Regions with PVCap

Methane hydrate crystal growth inhibition region data have been generated for 0.5 mass% PVCap aqueous with 2.5, 5, 10, 20 and 50 mass% methanol (relative to water + PVCap) at pressures up to ~300 bar for some.

Figure 7-1 to Figure 7-5 show example CGI method cooling curves and CGI boundary data points for different methanol concentration systems of methanol−PVCap−methane systems. CGI boundary data points of each system are reported in Table 7-1 to Table 7-5. Figure 7-6 shows PVCap induced inhibition regions as a function of aqueous (relative to water) methanol concentration. Figure 7-7 shows combined methanol (thermodynamic) + PVCap induced inhibition regions as a function of aqueous (relative to water) methanol concentration.

As shown in Figure 7-1 to Figure 7-5 CGI regions are clearly discernible from cooling curve data. For all methanol concentrations tested, the presence of 0.5 mass% PVCap induced the presence of characteristic complete inhibition (CIR), reduced growth rate (RGR) and rapid growth/failure (RFR) regions. However, methanol overall had a detrimental effect on the subcooling extent of all regions at all concentrations tested.

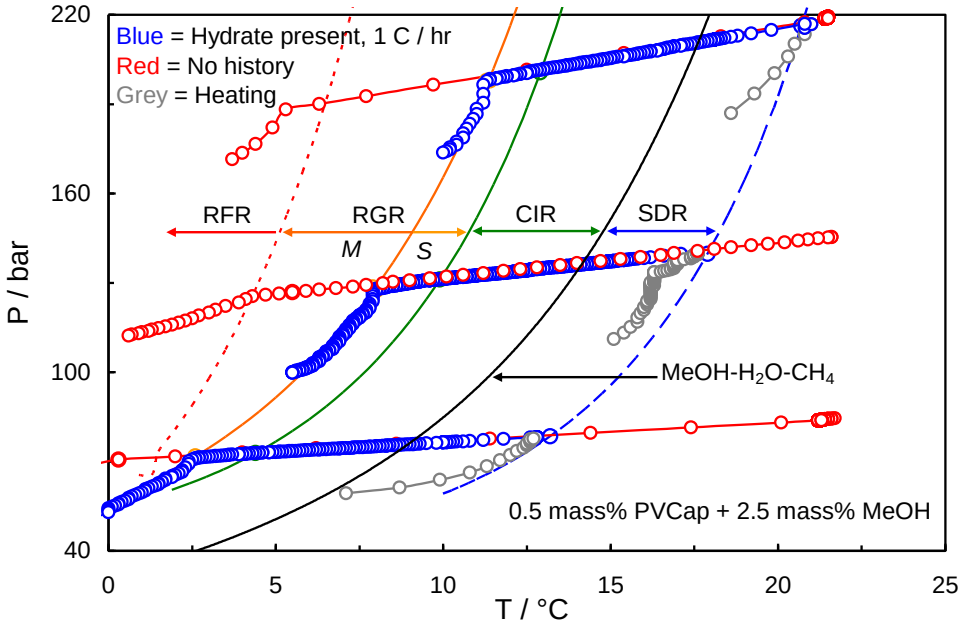

Figure 7-1 Example CGI cooling and heating runs for 0.5 mass% PVCap / 2.5 mass% methanol aqueous with methane also showing CGI regions determined from changes in relative hydrate growth rates.

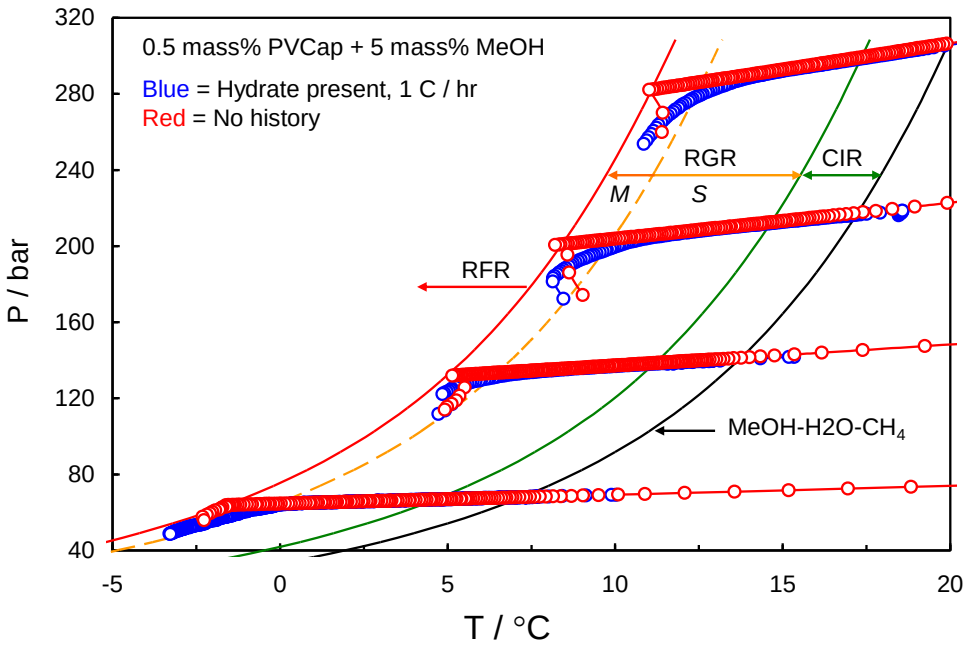

Figure 7-2 Example CGI cooling and heating runs for 0.5 mass% PVCap / 5.0 mass% methanol aqueous with methane also showing CGI regions determined from changes in relative hydrate growth rates.

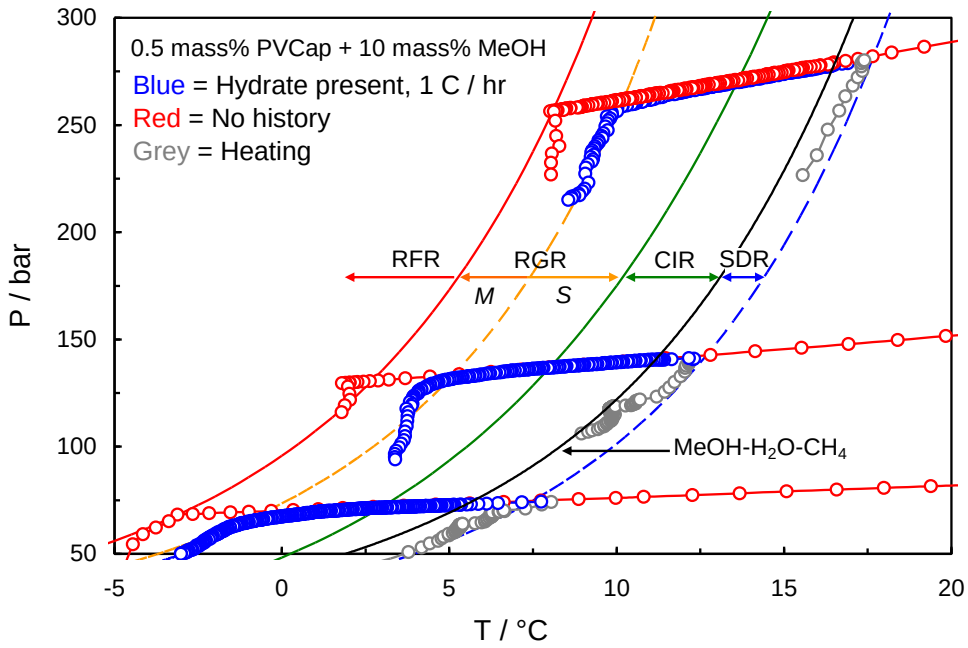

Figure 7-3 Example CGI cooling and heating runs for 0.5 mass% PVCap / 10.0 mass% methanol aqueous with methane also showing CGI regions determined from changes in relative hydrate growth rates.

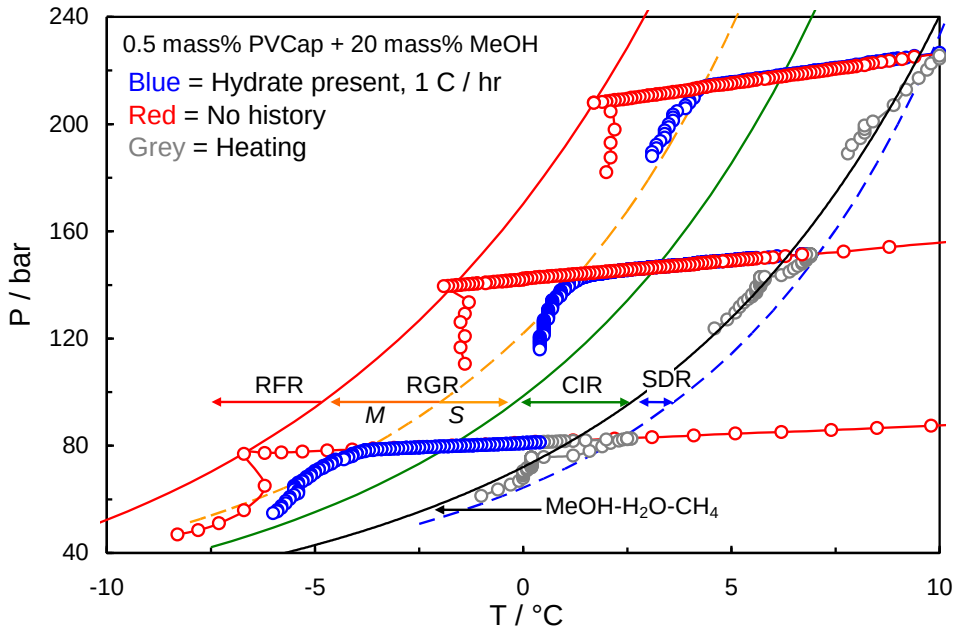

Figure 7-4 Example CGI cooling and heating runs for 0.5 mass% PVCap / 20.0 mass% methanol aqueous with methane also showing CGI regions determined from changes in relative hydrate growth rates.

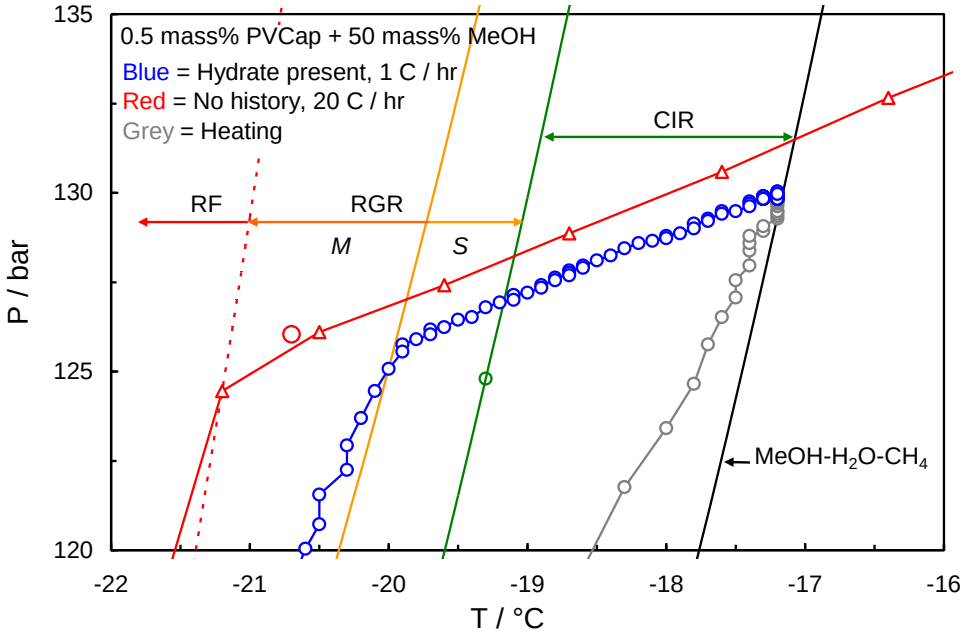

Figure 7-5 Example CGI cooling and heating runs for 0.5 mass% PVCap / 50.0 mass% methanol aqueous with methane also showing CGI regions determined from changes in relative hydrate growth rates.

Table 7-1 Experimental methane hydrate CGI region data for 0.5 mass% PVCap aqueous with 2.5 mass% methanol (relative to water + PVCap).

CGR boundary	*Growth rate	T / °C (± 0.5)	P / bar (± 0.2)	ΔT_{s-I} / °C (± 0.5)
SDR	Slow dissociation	13.2	78.5	3.9
		17.9	139.8	3.5
		20.7	216.2	2.9
CIR-RGR (S)	No growth	4.4	72.8	–4.2
		9.9	131.1	–3.9
		12.9	200.6	–4.3
RGR (S-M)	Very slow to slow	2.6	71.7	–5.8
		7.9	128.4	–5.7
		11.3	197.8	–5.8
RGR(M)-RFR	Moderate	5.5	126.9	–8.0
		0.3	70.6	–8.0

*Growth rate is for ΔT CGI region preceding the associated boundary

Table 7-2 Experimental methane hydrate CGI region data for 0.5 mass% PVCap aqueous with 5 mass% methanol (relative to water + PVCap). See Section 2.3.1 for growth rate definitions.

CGI boundary	*Growth rate	T / ºC (± 0.5)	P / bar (± 0.2)	ΔT_{s-I} / ºC (± 0.5)
SDR	Slow dissociation	9.9	69.3	2.7
		16.1	143.7	2.6
		19.4	220.1	2.5
		21.8	311.6	2.2
CIR-RGR(S)	No growth	4.5	66.4	–2.4
		16.8	296.9	–2.4
		14.1	209.8	–2.4
RGR(S-M)	Very slow to slow	–0.7	63.3	–7.0
		5.2	122.1	–7.0
		8.6	186.4	–7.0
		11.4	265.0	–6.9
RGR(M)-RFR	Moderate	–1.3	64.0	–7.8
		5.2	132.0	–7.7
		8.4	201.0	–7.8
		11.0	282.0	–7.8

*Growth rate is for ΔT CGI region preceding the associated boundary

Table 7-3 Experimental methane hydrate CGI region data for 0.5 mass% PVCap aqueous with 10 mass% methanol (relative to water + PVCap).

CGI boundary	*Growth rate	T / ºC (± 0.5)	P / bar (± 0.2)	ΔT_{s-I} / ºC (± 0.5)
SDR	Slow dissociation	7.4	74.1	1.7
		12.7	141.5	1.3
		17.7	281.1	0.9
CIR-RGR(S)	No growth	2.9	70.7	–2.4
		7.9	135.7	–3.1
		13.6	270.5	–2.9
RGR(S-M)	Very slow to slow	–0.9	67.4	–5.7
		5.2	132.7	–5.6
		10.1	258.5	–6.1
RGR(M)-RFR	Moderate	–3.1	68.3	–8.0
		2.7	130.6	–8.0
		8.2	256.2	–7.9

*Growth rate is for ΔT CGI region preceding the associated boundary

Table 7-4 Experimental methane hydrate CGI region data for 0.5 mass% PVCap aqueous with 20 mass% methanol (relative to water + PVCap).

CGI boundary	*Growth rate	T / ºC (± 0.5)	P / bar (± 0.2)	ΔT_{s-I} / ºC (± 0.5)
SDR	Slow dissociation	2.3	82.4	1.1
		7.1	151.6	0.7
		9.8	225.9	0.3
CIR-RGR(S)	No growth	–1.8	79.5	–2.7
		3.2	146.7	–2.9
		6.2	217.4	–3.0
RGR(S-M)	Very slow to slow	–4.1	76.1	–4.6
		1.3	143.1	–4.6
		4.2	210.8	–4.8
RGR(M)-RFR	Moderate	–6.7	76.9	–7.3
		–1.7	139.5	–7.4
		1.7	207.9	–7.2

*Growth rate is for ΔT CGI region preceding the associated boundary

Table 7-5 Experimental methane hydrate CGI region data for 0.5 mass% PVCap aqueous with 50 mass% methanol (relative to water + PVCap).

CGR boundary	*Growth rate	T / ºC (± 0.5)	P / bar (± 0.2)	ΔT_{s-I} / ºC (± 0.5)
SDR	Slow dissociation	–17.1	129.7	0.0
		–14.2	195.4	0.0
		–12.0	268.5	0.0
CIR-RG R(S)	No growth	–19.3	124.8	–1.8
		–16.3	187.4	–1.8
		–14.0	258.9	–1.8
RGR (S-M)	Very slow to slow	–20.0	125.1	–2.5
		–16.7	190.0	–2.2
		–14.6	252.3	–2.2
RGR-RFR	Moderate	–15.7	254.1	–3.4
		–20.7	126.0	–3.4

*Growth rate is for ΔT CGI region preceding the associated boundary

For water-PVCap alone, as previously found and shown in Figure 7-6, the complete inhibition region extends to ΔT_{sub} = ~–5.2 °C. However, data for 5 different concentrations of methanol tested show that that methanol has a consistently negative effect on the performance of PVCap; the extent of CGI region subcoolings reducing as methanol concentration increases. For example, the complete inhibition (for water–PVCap) region reduces from ΔT_{sub} = ~–5.2 °C to ~–4.1 °C, ~–2.4 °C, ~–2.8°C, ~–2.9°C and ~–1.8°C respectively at 2.5 mass%, 5.0 mass%, 10.0 mass%, 20.0 mass% and 50.0 mass% MeOH. This is in direct contrast to ethylene glycol systems where the CIR is preserved, even up to 50 mass% (Chapter 8). Similarly, the reduced growth rate

region and rapid failure region are reduced to lower subcoolings as a function of methanol concentration (this is in agreement with Yousif's 1998 finding in that presence of methanol in water actually enhances the rate of hydrate formation).

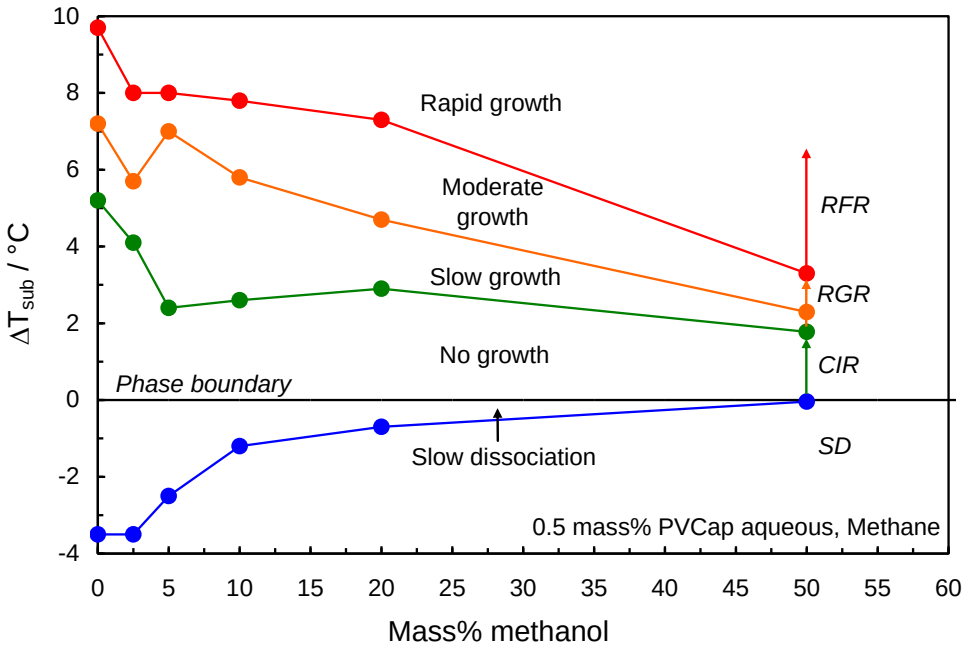

Figure 7-6 Average (50 to 300 bar) PVCap induced CGI regions for 0.5 mass% PVCap aqueous as a function of mass% methanol (relative to water + PVCap).

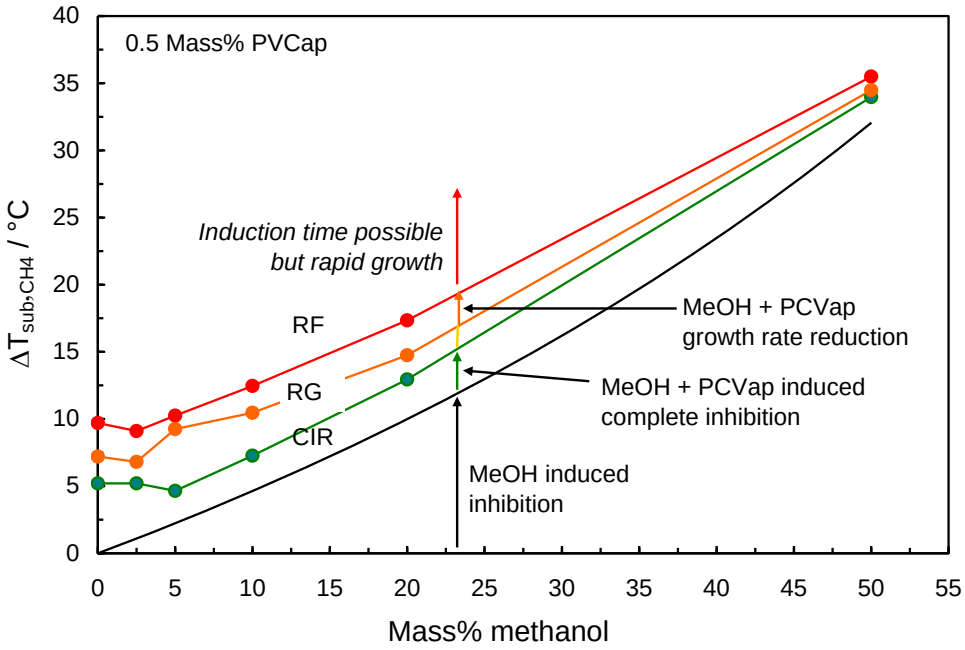

Figure 7-7 Total methane hydrate inhibition offered through the combination of methanol and 0.5 mass% PVCap. While methanol reduces the complete inhibition region offered by PVCap, the combination does offer more inhibition than methanol alone.

For very low methanol concentrations (< 5 mass %), the RGR slow growth region reduces rapidly as methanol concentration increases (ΔT_{sub} = ~–5.2 °C at 2.5 mass% MeOH), before rising again slightly to a peak (ΔT_{sub} = ~–7.0 °C) at ~5 mass% MeOH (Figure 7-6), beyond which it steadily reduces in subcooling extent again (decreasing all the way down to ~2.3 °C at 50 mass% MeOH). The reasons for this peak are unknown, although it is speculated that lower concentrations of methanol might be encouraging nucleation; methanol is known to form s-II hydrates at cryogenic temperatures.

Furthermore, as evident from Figure 7-1 to Figure 7-5 and clearly illustrated in Figure 7-6 the slow dissociation region consistently reduces to lower subcoolings with MeOH concentration increase which confirms the reduced PVCap performance with increase of MeOH content of the system.

Although the presence of MeOH has negative effect on PVCap performance in the system and reduces the extent of all CGI regions, as Figure 7-7 clearly illustrates the combination of methanol and PVCap does still offer better inhibition by mass inhibitor than methanol alone. However, 0.5 mass% PVCap offers equivalent complete inhibition to around 0.5 mass% PVCap plus 5 mass% methanol. It should also be noted that 0.5 mass% PVCap offers the equivalent of 12 mass% methanol when used without the latter.

7.2. Effect of EtOH on CGI Regions with PVCap

Ethanol hydrate crystal growth inhibition region data have been generated for 0.5 mass% PVCap aqueous with 1.7, 2.5, 11.4 and 50 mass% ethanol (relative to water + PVCap) at pressures up to ~150 bar for some (1.7mass% EtOH = 0.76mole% EtOH).

Figure 7-8 to Figure 7-11 show example CGI method cooling curves and CGI boundary data points for PVCap−ethanol−methane systems with 1.7, 2.5, 11.4 and 50 mass% ethanol in 0.5 mass% PVCap aqueous respectively. CGI boundary data points for each of the systems are reported in Table 7-6 to Table 7-9. Figure 7-12 shows PVCap induced inhibition regions as a function of aqueous (relative to water) ethanol concentration.

Table 7-6 Experimental methane hydrate CGI region data for 0.5 mass% PVCap and 1.7 mass% (0.76 mole %) ethanol (both relative to water) aqueous.

CGR boundary	*Growth rate	T / °C (± 0.5)	P / bar (± 0.2)	ΔT_{s-I} / °C (± 0.5)
SDR	Slow dissociation	13.75	88.4	2.5
CIR-RGR(VS)	No growth	7	86.6	–4.1
RGR(VS-S)	Very slow	4.5	84.4	–6.4
RGR(S-M)	Slow	3.2	82.8	–7.5
RGR(M)-RFR	Moderate	2.5	84.7	–8.4

*Growth rate is for ΔT CGI region preceding the associated boundary

Table 7-7 Experimental methane hydrate CGI region data for 0.5 mass% PVCap aqueous with 2.5 mass% ethanol (relative to water + PVCap).

CGR boundary	*Growth rate	T / ºC (± 0.5)	P / bar (± 0.2)	ΔT_{s-I} / ºC (± 0.5)
SDR	Slow dissociation	12.5	79.7	2.2
		17.6	147.7	1.8
CIR-RGR(S)	No growth	6.3	77.2	–3.8
		11.4	140.3	–4.1
RGR(S-M)	Very slow to slow	1.0	66.2	–7.6
		7.0	125.9	–7.5
RGR(M)-RFR	Moderate	0.3	74.1	–9.4
		5.6	130.6	–9.2

*Growth rate is for ΔT CGI region preceding the associated boundary

Table 7-8 Experimental methane hydrate CGI region data for 0.5 mass% PVCap aqueous (relative to water) with 11.4 mass % ethanol (relative to water + PVCap).

CGR boundary	*Growth rate	T / ºC (± 0.5)	P / bar (± 0.2)	ΔT_{s-I} / ºC (± 0.5)
SDR	Slow dissociation	3.3	48.8	1.0
		7.1	74.2	0.7
		10.4	107.6	0.7
CIR-RGR(S)	No growth	1.1	47.8	–1.0
		5.25	74.9	–1.2
		8.4	107.4	–1.3
RGR(S-M)	Slow to moderate	–3.9	44.4	–5.3
		0.3	66.8	–5.1
		4.4	102.3	–4.9
RGR(M)-RFR	Moderate	–6.8	40.1	–7.2
		–1.5	71.5	–7.5
		1.3	95.8	–7.4

*Growth rate is for ΔT CGI region preceding the associated boundary

Table 7-9 Experimental methane hydrate CGI region data for 0.5 mass% PVCap aqueous (relative to water) with 50 mass % ethanol (relative to water + PVCap).

CGR boundary	*Growth rate	T / °C (± 0.5)	P / bar (± 0.2)	$\Delta T_{s\text{-}I}$ / °C (± 0.5)
SDR	Slow dissociation	–5.7	78.1	0.3
RGR(S-M)	Slow	–7.2	77.6	–1.2
RGR(M)-RFR	Moderate	–7.7	77.1	–1.6

*Growth rate is for ΔT CGI region preceding the associated boundary

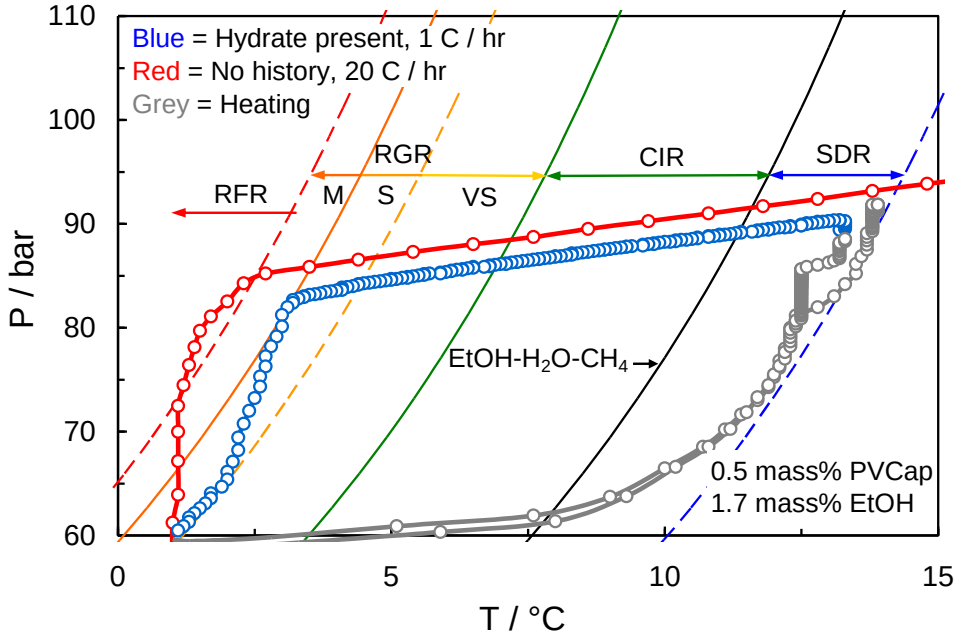

Figure 7-8 Example CGI cooling and heating runs for 0.5 mass% PVCap / 1.7 mass% (0.76 mole %) ethanol (both relative to water) aqueous with methane also showing CGI regions determined from changes in relative hydrate growth rates.

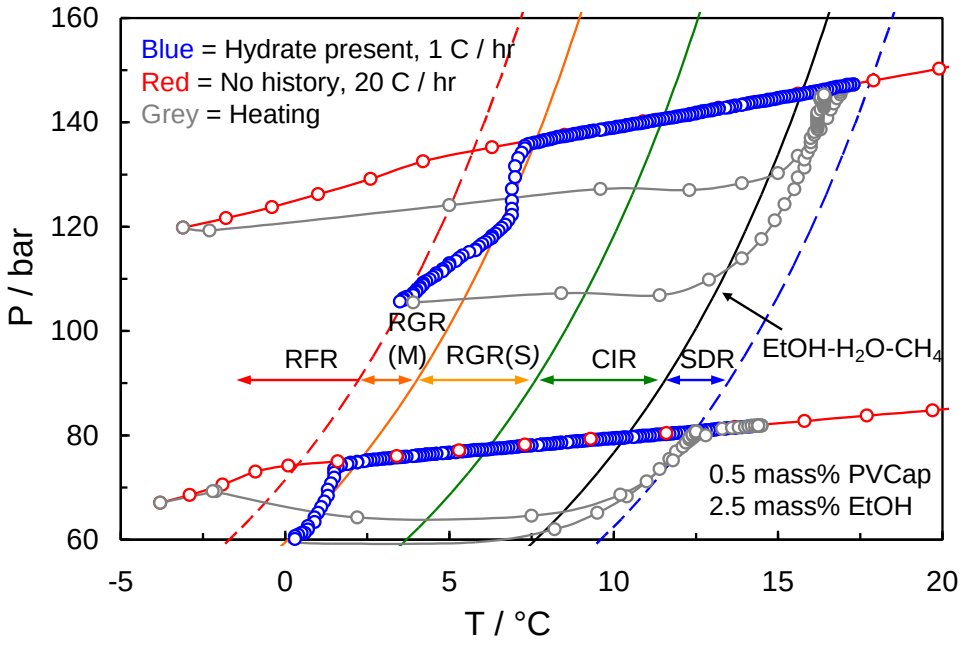

Figure 7-9 Example CGI cooling and heating runs for 0.5 mass% PVCap / 2.5 mass% ethanol aqueous with methane also showing CGI regions determined from changes in relative hydrate growth rates.

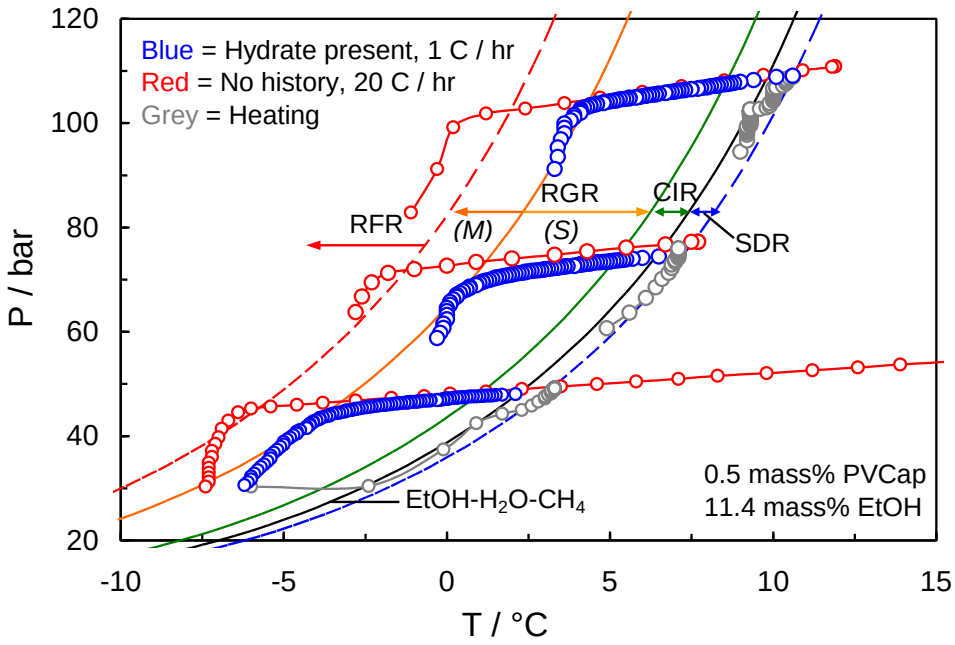

Figure 7-10 Example CGI method cooling and heating curves for 0.5 mass% PVCap / 11.4 mass % ethanol aqueous with methane also showing CGI regions determined from changes in relative hydrate growth rates.

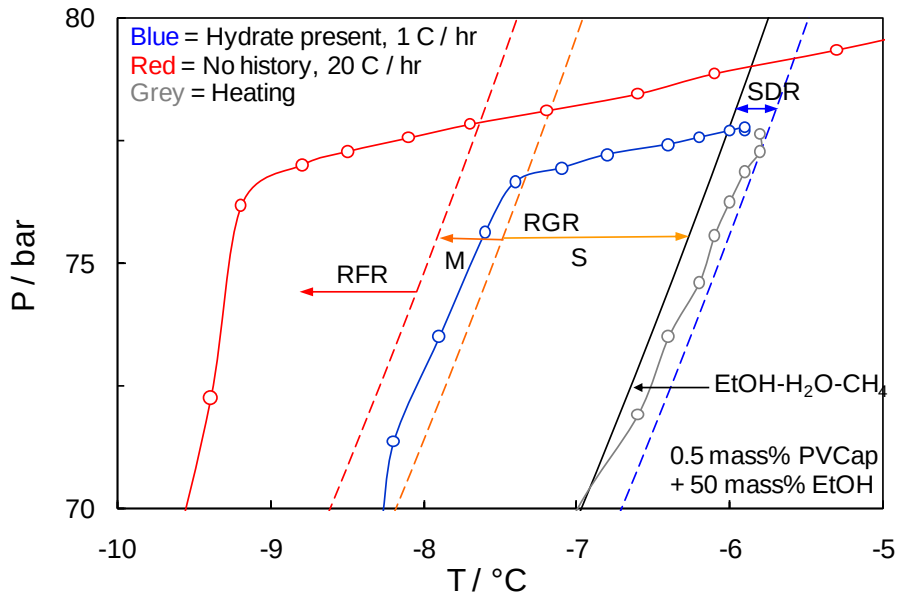

Figure 7-11 Example CGI method cooling and heating curves for 0.5 mass% PVCap / 50 mass % ethanol aqueous with methane also showing CGI regions determined from changes in relative hydrate growth rates.

As shown in Figure 7-8 to Figure 7-11 CGI regions are clearly distinguishable from cooling curve data. For all ethanol concentrations tested, similar to methanol, the presence of 0.5 mass% PVCap induced the presence of characteristic complete inhibition (CIR), reduced growth rate (RGR) and rapid growth/failure (RFR) regions. However, ethanol overall had a detrimental effect on the subcooling extent of all regions at all concentrations tested although being less negative in comparison to methanol.

Results for 0.5 mass% PVCap with 1.7 mass% ethanol with methane showed that, in this system the extent of the RGR(M) (moderate growth begins) at ΔT_{sub} =~–7.5 °C which is similar to water–PVCap systems (ΔT_{sub} =~–7.3 °C). However, from hydrate present cooling curves in Figure 7-8, it is notable that after growth of a small fraction of hydrate in the system, PT conditions retreat and follow a boundary with a lower ΔT of around ΔT_{sub} =~–6.4 °C, as illustrated. Thus the presence of EtOH apparently causes a slight negative effect on the RGR at higher hydrate fractions. In addition to that, in the water–ethanol–PVCap system, the complete inhibition and rapid failure region boundaries decrease by ~1°C from ΔT_{sub} =~–5.2 °C and ~–9.6 °C (for water–PVCap) to ΔT_{sub} =~–4.1 °C and ~–8.4 °C (for water–ethanol–PVCap) respectively.

Likewise as illustrated in Figure 7-9, results for 0.5 mass% PVCap and 2.5 mass% ethanol with methane show that ethanol has a generally negative effect on the performance of PVCap. For example, while in a water–ethanol–PVCap system the beginning of reduced growth region (moderate growth) and rapid failure regions (ΔT_{sub} =~–7.5 °C and ~–9.3 °C respectively) remain very much similar to a water–PVCap system (ΔT_{sub} =~–7.3 °C and ~–9.6 °C respectively), the complete inhibition region reduces from ΔT_{sub} =~–5.2 °C (for water–PVCap) to ~–3.9 °C (for water–ethanol–PVCap). So although the presence of ethanol does not notably affect the reduced growth rate region and rapid failure region, the complete inhibition region is reduced to lower subcoolings which results in an overall negative behaviour.

Furthermore, results for tests on 0.5 mass% PVCap and 11.4 mass% ethanol support the above findings in that ethanol has a negative effect on PVCap performance (Figure 7-10). At this intermediate concentration of ethanol, the complete inhibition region has been reduced to only ΔT_{sub} =~–1.2 °C. Similarly, the reduced growth rate region (RGR) and rapid failure region (RFR) are reduced to lower subcoolings being only ΔT_{sub} =~–5.1 °C and –7.3 °C respectively. This reduction in performance agrees with there only being a very small SDR at ΔT_{sub} =~+0.8 °C; i.e. polymer adsorption on crystal surfaces is presumably very weak.

Correspondingly, tests on 0.5 mass% PVCap and 50 mass% ethanol with methane show that very high ethanol concentrations (50 mass%) greatly deteriorate the performance of PVCap. At 50 mass% ethanol, it is apparent that the complete inhibition region has been completely lost, with only a small RGR region extending to ΔT_{sub} =~–1.6 °C; 1.2 C of

this comprising RGR(S) and the remainder RGR(M). Again like previous results this reduction in performance agrees with their only being a very small SDR at ΔT_{sub} =~+0.3 °C, illustrated in Figure 7-11.

As evident from data for 5 different concentrations of ethanol, similar to the findings for methanol, ethanol has a consistently negative effect on the performance of PVCap; the extent of CGI region subcoolings reduced as ethanol concentration increased. As illustrated in Figure 7-12 it is evident that the higher the EtOH concentration the smaller the CIR region becomes up to a point where CIR region is completely lost at 50mass% EtOH. Similarly, the reduced growth rate region and rapid failure region are reduced to lower subcoolings as a function of ethanol concentration.

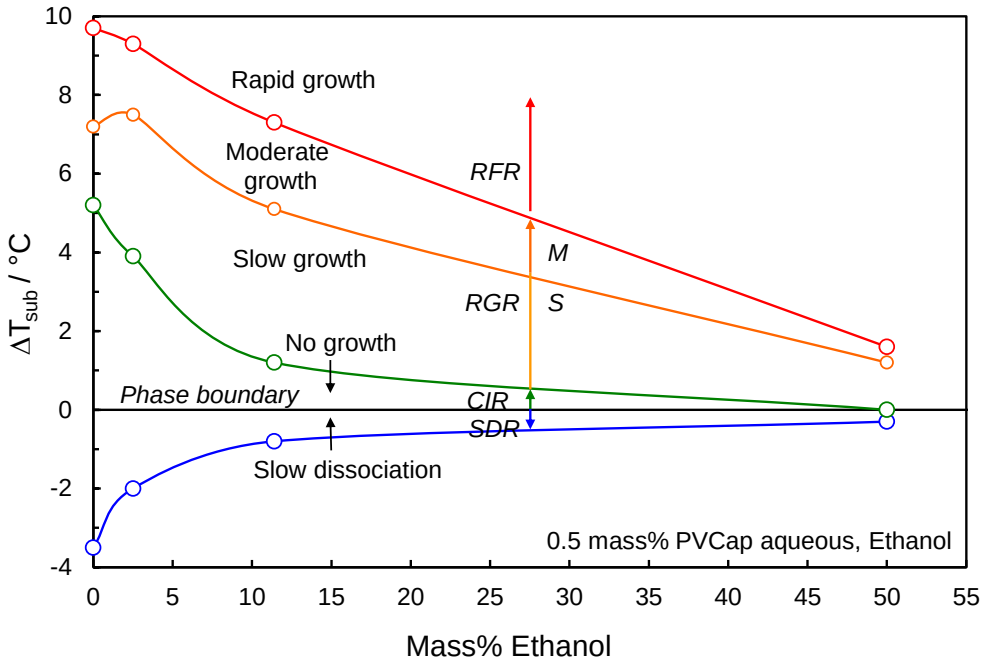

Figure 7-12 Average (40 to 120 bar) PVCap induced CGI regions for 0.5 mass% PVCap aqueous as a function of mass% ethanol (relative to water + PVCap).

Furthermore, comparable to methanol, at very low ethanol concentrations (< 2.5 mass %), the RGR slow growth region rises to a peak (ΔT_{sub} = ~–7.5 °C) beyond which it steadily reduces in subcooling extent as the EtOH concentration increases (Figure 7-12). The reasons for this peak are unknown, although like methanol it is speculated that lower concentrations of ethanol might be encouraging nucleation; ethanol can in fact form clathrate hydrates at conditions pertinent to offshore operations (Anderson et al., 2009). Moreover, the growth rate after the CIR is very slow at low ethanol concentrations (< 2.5 mass %), compared to the slow growth rate in the RGR at higher concentrations. This again confirms the fact that PVCap performance deteriorates further at higher ethanol concentrations.

Although the presence of EtOH has negative effect on PVCap performance in the system and reduces the extent of all CGI regions, the combination of ethanol and PVCap does still offer better inhibition by mass inhibitor than ethanol alone.

7.3. Effect of POH on CGI Regions with PVCap

Propanol hydrate crystal growth inhibition region data have been generated for 0.5 mass% PVCap aqueous with 2.5 mass% propanol (relative to water + PVCap) with methane at pressures up to ~160 bar (2.5 mass% POH = 0.76mole% POH).

Figure 7-13 shows example CGI method cooling curves and CGI boundary data points for the mentioned PVCap−propanol−methane system. CGI boundary data points for this system are reported in Table 7-10.

Table 7-10 Experimental methane hydrate CGI region data for 0.5 mass% PVCap aqueous with 2.5 mass% n-propanol (relative to water + PVCap).

CGR boundary	*Growth rate	T / ºC (± 0.5)	P / bar (± 0.2)	ΔT_{s-I} / ºC (± 0.5)
SDR	Slow dissociation	13.3	76.3	3.3
		19.6	161.4	3.1
CIR-RGR(S)	No growth	5.2	71.9	–4.2
		12.0	151.1	–4.0
RGR(S-M)	Very slow to slow	2.5	69.9	–6.6
		8.9	146.8	–6.9
RGR(M)-RFR	Moderate	–1.1	68.3	–10.0
		6.6	139.2	–9.4

*Growth rate is for ΔT CGI region preceding the associated boundary

As can be detected from Figure 7-13, 0.5 mass% PVCap and 2.5 mass% n-propanol shows both negative and positive effects on the performance of PVCap. Results illustrate that similar to ethanol, a water–n-propanol–PVCap system reduces the complete inhibition region from ΔT_{sub} = ~–5.2 °C (for water–PVCap) to ~–4.1 °C (for water–n-propanol–PVCap). In contrast, the reduced growth region has been extended to higher subcoolings, e.g. RGR has increased from ΔT_{sub} =~–7.3 °C (for water–PVCap) to ~–8.7 °C (for water–n-propanol–PVCap). However, in the water–n-propanol–PVCap system RFR has remained largely similar to that in a water–PVCap system (ΔT_{sub} =~–9.7 °C and ~–9.6 °C respectively). Consequently, while the presence of n-propanol has had a negative effect on CIR it has shifted both RGR conditions to higher subcoolings while RFR has remained unchanged.

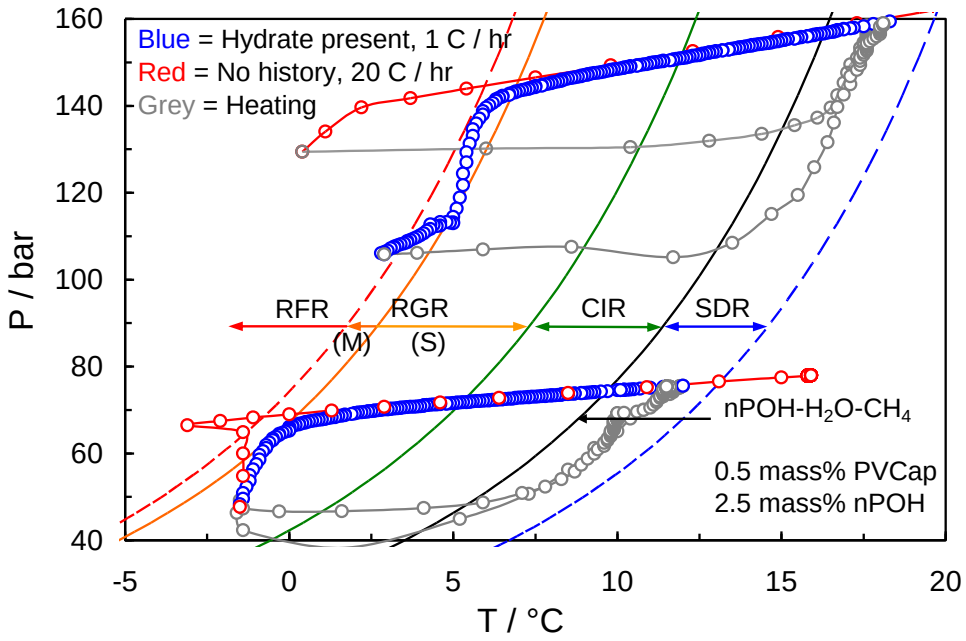

Figure 7-13 Example CGI cooling and heating runs for 0.5 mass% PVCap / 2.5 mass% n-propanol aqueous with methane also showing CGI regions determined from changes in relative hydrate growth rates.

7.4. Effect of i-POH on CGI Regions with PVCap

As mentioned earlier in this chapter iso-propanol which has a similar molecular weight and formula but different structure to n-propanol, was also tested to better understand the potential role that the alcohol alkyl 'tail' could have on PVCap performance. For this purpose hydrate crystal growth inhibition region data have been generated for 0.5 mass% PVCap aqueous with 2.5 mass% i-propanol (relative to water + PVCap) with methane at pressures up to ~160 bar (2.5 mass% i-POH = 0.76mole% POH).

Figure 7-14 shows example CGI method cooling curves and CGI boundary data points for the mentioned PVCap−i-propanol−methane system. CGI boundary data points for this system are reported in Figure 7-11.

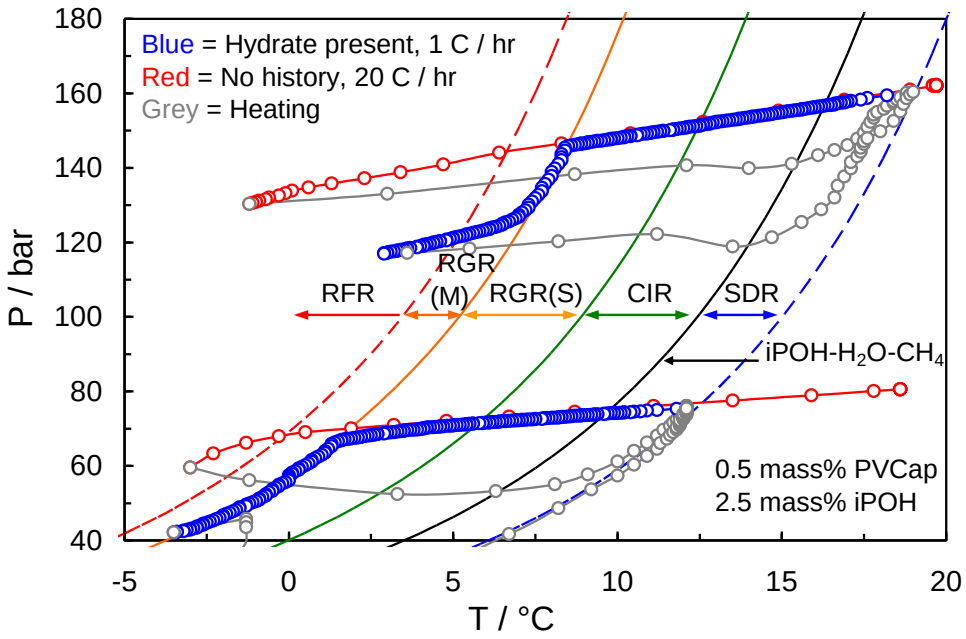

Figure 7-14 Example CGI cooling and heating runs for 0.5 mass% PVCap / 2.5 mass% i-propanol aqueous with methane also showing CGI regions determined from changes in relative hydrate growth rates.

Table 7-11 Experimental methane hydrate CGI region data for 0.5 mass% PVCap aqueous with 2.5 mass% iso-propanol (relative to water + PVCap).

CGR boundary	*Growth rate	T / ºC (± 0.5)	P / bar (± 0.2)	ΔT_{s-I} / ºC (± 0.5)
SDR	Slow dissociation	12.6	76.3	2.7
		19.0	161.0	2.5
CIR-RGR(S)	No growth	6.3	72.1	–3.1
		12.0	150.7	–4.0
RGR(S-M)	Slow	1.5	66.7	–7.2
		8.2	143.4	–7.3
RGR(M)-RFR	Moderate	0.1	68.2	–8.8
		6.4	144.1	–9.2

*Growth rate is for ΔT CGI region preceding the associated boundary

As Figure 7-14 shows, in contrast to n-propanol, 2.5 mass% i-propanol has an overall negative effect on PVCap performance. Similar to the water–ethanol–PVCap system, in a water–i-propanol–PVCap system, although the performance of PVCap remains largely unchanged in the reduced growth rate region and rapid failure region (ΔT_{sub} =~–7.2 °C and ~–9.0 °C respectively), the complete inhibition region considerably reduces from ΔT_{sub}=~–5.2 °C (for water–PVCap) to ~–3.5 °C (for water–i-propanol–PVCap). The smaller SDR region (ΔT_{sub} =~+2.6°C) confirms these findings.

7.5. Effect of BOH on CGI Regions with PVCap

For a more comprehensive evaluation of the role of molecular structure of alcohols on PVCap performance, n-butanol with a longer alcohol alkyl 'tail' was also examined. Butanol hydrate crystal growth inhibition region data have been generated for 0.5 mass% PVCap aqueous with 1 and 3.1 mass% butanol (relative to water + PVCap) at pressures up to ~120 bar (3.1mass% BOH = 0.76mole% BOH).

Figure 7-15 and Figure 7-16 show example CGI method cooling curves and CGI boundary data points for PVCap−Butanol−methane systems with 1 mass% butanol in 1.0 mass% PVCap aqueous and 3.1 mass% butanol in 0.5 mass% PVCap aqueous respectively. CGI boundary data points for each of the systems are reported in Table 7-12 and Table 7-13.

Table 7-12 Experimental methane hydrate CGI region data for 1.0 mass% PVCap aqueous with 1.0 mass% butanol (relative to water + PVCap).

CGR boundary	*Growth rate	T / ºC (± 0.5)	P / bar (± 0.2)	ΔT_{s-I} / ºC (± 0.5)
SDR	Slow dissociation	18.3	125.8	3.4
CIR-RGR(VS)	No growth	9.1	118.5	–5.4
RGR(VS-S)	Very slow	6.8	115.7	–7.5
RGR(S-M)	Slow	3.4	108.5	–10.3
RGR(M)-RFR	Moderate	1.1	106.7	–12.5

*Growth rate is for ΔT CGI region preceding the associated boundary

Table 7-13 Experimental methane hydrate CGI region data for 0.5 mass% PVCap and 0.76 mole % n-butanol (both relative to water) aqueous.

CGR boundary	*Growth rate	T / °C (± 0.5)	P / bar (± 0.2)	ΔT_{s-I} / °C (± 0.5)
SDR	Slow dissociation	15.2	92.5	3.5
CIR-RGR(VS)	No growth	5.7	85.2	–5.3
RGR(VS-S)	Very slow	3.8	84.2	–7.0
RGR(S-M)	Slow	–0.1	79.4	–10.3
RGR(M)-RFR	Moderate	–1.6	81.1	–12.1

*Growth rate is for ΔT CGI region preceding the associated boundary

Both Figure 7-15 and Figure 7-16 illustrate that in contrast to the other three alcohols tested, n-butanol has an overall positive synergistic effect on PVCap hydrate crystal growth inhibition properties, at least at tested concentrations.

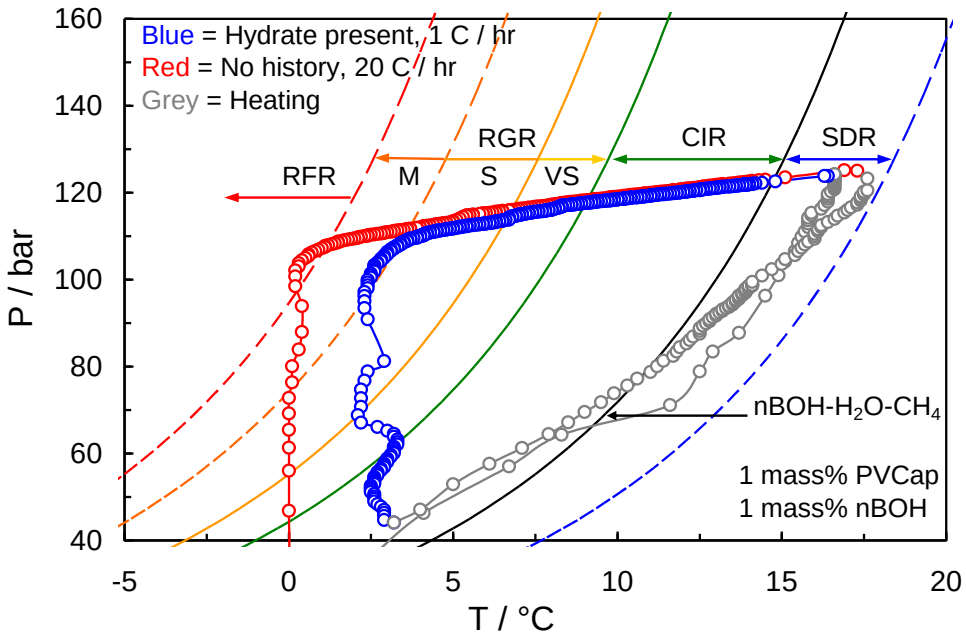

Figure 7-15 Example CGI cooling and heating runs for 1mass% PVCap / 1 mass% butanol aqueous with methane also showing CGI regions determined from changes in relative hydrate growth rates.

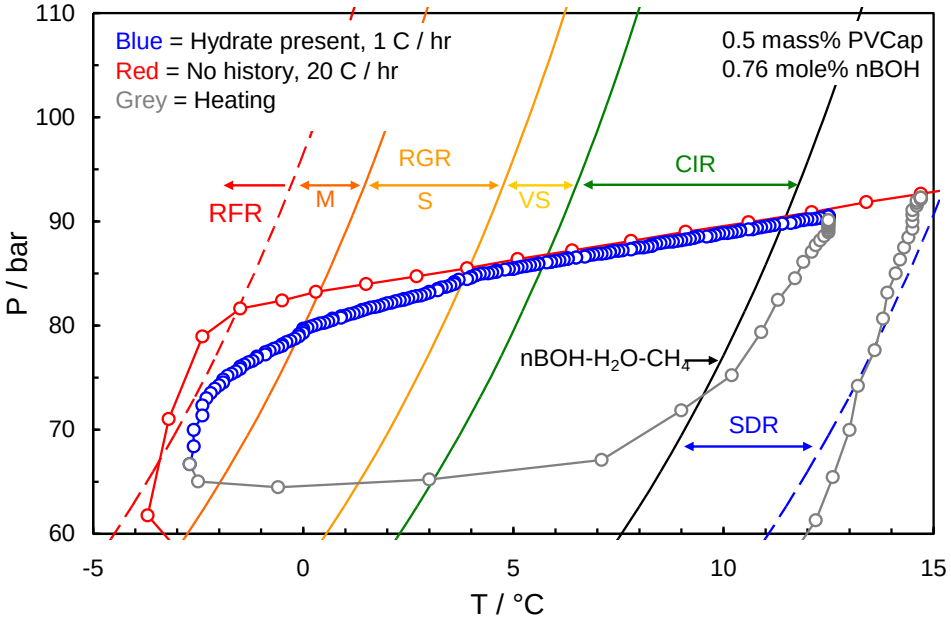

Figure 7-16 Example CGI cooling and heating runs for 0.5 mass% PVCap / 3.1 mass% n-butanol aqueous with methane also showing CGI regions determined from changes in relative hydrate growth rates.

Results of the 1.0 mass% PVCap and 1.0 mass% n-butanol system show that the complete inhibition region is very well preserved in this system remaining largely comparable to a water–PVCap system at ΔT_{sub} =~–5.4 °C. In addition, in this system, as for propanol systems, both reduced growth and rapid failure regions have been extended to higher subcoolings, e.g. Both RGR and RFR in water–n-butanol–PVCap

system at the mentioned concentrations have increased about 3 °C extending to ΔT_{sub} =~–10.3 °C and ~–12.5 °C respectively (Figure 7-15

Supporting the above findings, results for 0.5 mass% PVCap and 3.1mass% n-butanol aqueous with methane show that the complete inhibition region is again preserved at ΔT_{sub} =~–5.3 °C. Moreover, the PVCap−Butanol−methane system at this concentration also extends the RGR region to higher subcoolings, in this case to ΔT_{sub}= ~–12.1 °C (Figure 7-16).

More interestingly, in both above PVCap−Butanol−methane systems the RGR region is subdivided into three sub-regions. In the first region, RGR(VS), hydrate growth rate is incredibly slow in comparison to all other tested alcohol present systems and even an alcohol free water–PVCap system. The presence of this very slow growth rate region again supports the positive synergistic effect of BOH on PVCap performance.

7.6. Comparison of the effect of 4 tested alcohols on CGI Regions with PVCap

To better evaluate the effect of molecular structures of alcohols, carbon number of the alkyl ‘tail’ in particular, results of all five alcohols (methanol, ethanol, propanol, iso-propanol and butanol) are summarized and compared in this section.

For a fairer evaluation of result all alcohols are compared at the same molar concentration. Figure 7-17 illustrates the comparison of average PVCap induced inhibition regions for all tested alcohols (MeOH, EtOH, n-POH, i-POH and n-BOH) at 0.76 mole % alcohol aqueous for 0.5mass% PVCap solutions with methane (Data for 0.76 mole % MeOH is not experimental and is interpreted from the trend of changes of PVCap induced CGI regions for 0.5 mass% PVCap aqueous as a function of mass% MeOH shown in Figure 7-6). The average CGI data for each alcohol is also shown in Table 7-14.

Results indicate that overall the longer the alkyl ‘tail’ of an alcohol, the further the hydrate crystal growth inhibition becomes. However, it is clear that neither of these alcohols are ‘top-up’ inhibitors for a PVCap + water system; while the effect of n-butanol is very positive at low concentrations, it is insoluble in water at higher aqueous fractions. However, this low solubility may be in part responsible for the synergistic

effect; the presence of n-butanol making it more difficult for the water structure to accommodate PVCap, thus encouraging polymer absorption on hydrate crystal surfaces.

Table 7-14 Experimental methane hydrate average CGI region data for 0.5 mass% PVCap with 0.76 mole% methanol, ethanol, n-propanol, iso-propanol and n-butanol (both relative to water) aqueous.

	ΔT_{sub} RFR/°C	ΔT_{sub} RGR(M) /°C	ΔT_{sub} RGR(S) /°C	ΔT_{sub} CIR/°C	ΔT_{sub} SDR/°C
n-BOH	–12.1	–10.3	–7.0	–5.3	3.5
i-POH	–8.5	–7.2	—	–3.5	2.6
n-POH	–9.7	–8.7	—	–4.1	3.2
EtOH	–8.4	–7.5	–6.4	–4.1	2.5
MeOH	–8.6	–5.7	—	–4.1	3.5
PVCap	–9.6	–7.3	—	–5.2	3.5

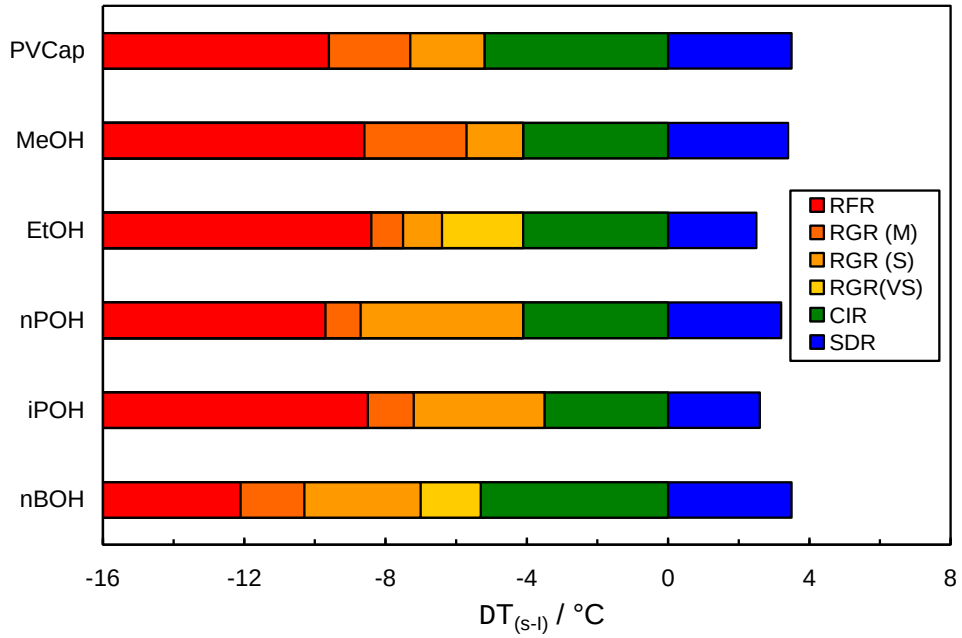

Figure 7-17 Experimental methane hydrate average CGI region extents for 0.5 mass% PVCap with 0.76 mole% methanol, ethanol, n-propanol and i-propanol and n-butanol (both PVCap and alcohol concentrations relative to water) aqueous.

Similar to methanol, both ethanol and propanol reduce the CIR around 1.1 °C leaving a subcooling of about ΔT_{sub}=~–4 °C in all three cases. It should be mentioned that unlike methanol, ethanol and both propanol isomers can form clathrate hydrates at conditions pertinent to offshore operations (Østergaard et al., 2002; Chapoy et al., 2008; Anderson et al., 2009). This could possibly explain the reason for this earlier hydrate growth which causes a reduction in the CIR. Furthermore, i-propanol, although very similar to propanol in physical properties, decreased the CIR even further to a subcooling of

ΔT_{sub}=~–3.5 °C. Considering that under specific conditions i-propanol may take part in structure II hydrate formation, occupying the large cavity of the hydrate structure, this could again explain the observed behaviour of this alcohol. Unlike all other four alcohols, n-butanol which does not form hydrates however maintains the CIR at ΔT_{sub}=~–5.3 °C which is just as it would be in a >0.5% mass% PVCap + water system. All these findings are also confirmed by the changes evident in SDR for different alcohols. It perceived that while SDR is reduced in the presence of methanol, ethanol, n-propanol and i-propanol, it is largely kept constant in the presence of n-butanol.

Conversely, these alcohols have a different impact on reduced growth and rapid failure regions. While methanol clearly reduces both RGR and RFR, ethanol preserves both these regions. Furthermore, it is interesting to note that i-propanol shows similar behaviour to ethanol in that both these regions are kept almost constant in the presence of i-propanol at this concentration at least. On the other hand, it is evident that both n-propanol and n-butanol extend the RGR to higher subcoolings while n-propanol preserves the RFR and n-butanol increases the subcooling of this region. Also it is apparent that n-butanol performs even better by reducing hydrate growth rate in both these regions. Consequently, from Figure 7-17 it is observed that while alcohol molecular weight alone does not seem to have much of an effect on PVCap performance, alkyl tail length is apparently important. Accordingly, the longer the alkyl tail, the higher subcooling obtained for RGR and RFR hence the less negative/more positive/synergistic the effect on PVCap performance is. However, as noted increasing alkyl tail length results in increasingly lower water solubility of alcohols.

7.7. Conclusions

CGI region studies on alcohol (MeOH, EtOH, n-POH, i-POH and n-BOH)-PVCap-water systems at tested concentrations of alcohols with methane at 0.5 mass% PVCap showed that none of the above alcohols act as a ‘top-up’ thermodynamic inhibitor; complete inhibition regions are consistently reduced to lower subcoolings in the presence of methanol, ethanol, propanol and i-propanol, although this it is preserved in the presence of n-butanol.

The reasons why methanol, ethanol, i-propanol and n-propanol have negative effect on CIR are unclear, although it is known that the former alcohol (MeOH) can form clathrate hydrates at low temperatures and the latter three alcohols can form clathrate

hydrates at conditions pertinent to offshore operations, thus they may be encouraging growth by competing with polymer pendant amide groups for partial enclathration into open cages.

On the other hand, while all the above alcohols (except n-butanol) reduce the CIR, their impact on RGR and RFR are different; methanol reduces both RGR and RFR, ethanol and i-propanol preserve both these regions, n-propanol and n-butanol both extend RGR to higher subcoolings. However, while n-propanol only preserves the RFR, n-butanol significantly extends this region to even higher subcoolings and reduces the growth rate in both RGR and RFR, acting as a synergist for PVCap.

Although four of the alcohols (MeOH, EtOH, n-POH and i-POH) clearly deteriorate the performance of PVCap, the combination of alcohol plus PVCap does still offer better inhibition by mass of inhibitor than any of the alcohols alone. Hence, it can be concluded that KHIs offer a potential means to reduce the amount of thermodynamic inhibitor required for high subcooling operations.

As evidenced by results for n-propanol and i-propanol, molecular weight alone is not apparently the controlling factor while solubility parameters may play a role on the influence that alcohol could have on PVCap performance.

In addition to that, alcohol alkyl 'tail' length apparently plays a role in PVCap hydrate crystal growth inhibition properties; the longer the alkyl tail, the higher subcooling obtained for RGR and RFR, with increasing preservation of the CIR (e.g. n-butanol).

Results of testing the effect of MeOH and EtOH concentration on the extent on CGI region boundaries proved that these alcohols had a consistently negative effect on the performance of PVCap; the extent of CGI region subcoolings reducing as the alcohol concentration increases.

References

Anderson, R., Chapoy, A., Haghighi, H., and Tohidi, B., 2009, *"Binary Ethanol−Methane Clathrate Hydrate Formation in the System CH_4-C_2H_5OH-H_2O: Phase Equilibria and Compositional Analyses"*, Journal of Physical Chemistry C, 113, 12602–12607

Budd, D., Hurd, D., Pakulski, M., Schaffer, T. D., 2004, *"Enhanced Hydrate Inhibition in Alberta Gas Field*", Proceedings of the SPE Annual Technical Conference and Exhibition, U.S.A, Texas, Houston

Chapoy, A., Anderson, R., Haghighi, H., Edwards, T., and Tohidi, B., 2008, *"Can n-Propanol Form Hydrate "*, Industrial and Engineering Chemistry Research, 47, 1689–1694

Pakulski, M., Hurd, D., 2005, *"Uncovering a Dual Nature of Polyether Amines Hydrate Inhibitors*", Proceedings of the Fifth International Conference on Gas Hydrates, Trondheim, Norway

Sloan, E. D., Subramanian, S., Matthews, P. N., Lederhos, J. P., and Khokhar, A. A., 1998, *"Quantifying Hydrate Formation and Kinetic Inhibition"*, Industrial and Engineering Chemistry Research, 37, 3124-3132

Wu, M., Wang, S., Lui, H., 2007, *"A Study on Inhibitors for the Prevention of Hydrate Formation in Gas"*, Journal of Natural Gas Chemistry, 16, 81-85

Yousif, M.H., 1998, *"Effect of Underinhibition with Methanol and Ethylene Glycol on the Hydrate-Control Process"*, Proceedings of the Offshore Technology Conference, U.S.A, Texas, Houston, 184-189

Østergaard, K. K., Tohidi, B., Anderson, R., Todd, A.C., and Danesh, A., 2002, *"Can 2-Propanol Form Clathrate Hydrate?"*, Industrial and Engineering Chemistry Research, 41, 2064-2068

8. EFFECT OF GLYCOLS ON KHI-INDUCED HYDRATE CRYSTAL GROWTH PATTERNS

Methanol (MeOH) and ethylene glycol (EG) are the most widely used thermodynamic inhibitors for hydrate inhibition in gas and gas-condensate pipelines. These chemicals are normally injected at the wellhead by small diameter umbilical that extend from the platform to the wellhead (Yousif, 1998). However, the use of these traditional thermodynamic inhibitors has the dis-advantage that large quantity of inhibitor is required for the prevention of hydrate formation. In addition to that, huge storage and injection equipment are required for the use of these chemicals as well as causing environmental pollution. Hence, as already mentioned in Chapter 2 kinetic hydrate inhibitors have become a potential alternative to these inhibitors. However, as mentioned in Chapter 7, it is common to use these thermodynamic hydrate inhibitors (e.g. methanol and ethylene glycol) in KHI formulations to increase the subcooling to which KHIs can be used by acting as a 'top-up' inhibitor. As was found in the previous Chapter (Chapter7), although methanol (and other tested alcohols) have negative effect on PVCap performance, the combination of KHIs and alcohols as thermodynamic inhibitors offer better inhibition by mass of inhibitor than any of the tested alcohols alone. Hence, the use of KHIs can potentially reduce the amount of thermodynamic inhibitor required for high subcooling operations. However in addition to alcohols, other popular thermodynamic inhibitors like glycols (e.g. mono ethylene glycol (MEG)) need to be tested to better understand the performance of the combination of KHIs and thermodynamic inhibitors.

Apparently, very limited research has been undertaken on the performance of combination of glycols and KIHs as hydrate inhibitors. In one study by Wu et al. (2006) the inhibitory performance of mono-ethylene-glycol (MEG) and a kinetic hydrate inhibitor (VC-713) were tested individually and together. From the results of testing MEG as the inhibitors in a pipeline it was concluded that using 10% inhibitors for the pipeline could restrict the hydrate formation. On the other hand, the result of applying VC-713 in the field showed that polymer inhibitors had better efficiency and good application prospect. However, it was found that the combination of thermodynamic inhibitors and kinetic inhibitors had an overall better performance (Wu et al., 2006).

Similar to experiments undertaken for understanding of the behaviour of alcohols, it is necessary to examine crystal growth inhibition behaviour for a number of different glycols with a KHI (PVCap, the typical KHI used in most other experiments throughout this research), to investigate the effect of these thermodynamic inhibitors on KHI performance.

The most common thermodynamic inhibitor amongst glycols is mono-ethylene-glycol. A study by Yousif, 1998 on the hydrate control process with ethylene glycol has shown that although ethylene glycol is known to suppress hydrates when added in adequate amounts to water, it tends to enhance the rate and amount of hydrate formation when present in small concentrations. Taking this study into consideration, it is important to study the effect of this inhibitor in more detail and determine CGI behaviour and boundaries for a range of MEG concentrations and at a number of different pressures.

In addition to mono-ethylene-glycol, it is of interest and importance to investigate whether other diols – namely 1,3-propanediol (HO-$[CH2]_3$-OH) and 1,4-butanediol (HO-$[CH2]_4$-OH) (which have similar properties/molecular structures to MEG and only differ by additional carbons in the central alkyl chain) – show similar performance to MEG. These findings can help us conclude more comprehensively on the performance of glycols and suggest a more reliable explanation for any behaviour observed.

All experiments were carried out on high pressure stirred autoclaves using the CGI technique. In all the experiments glycols were testes with 0.5 or 1.0 mass% PVCap aqueous with methane. MEG was tested at a range of concentrations while 1,3-propanediol and 1,4-butanediol were tested at one similar molar concentration (0.76 mole%) for a fairer comparison of their performance relative to one another and also relative to the tested alcohols in Chapter7. Purity and supplier of each alcohol was as follows; Mono-ethylene-glycol 99.5% supplied by SIGMA ALDRICH, 1,3-propanediol 99.0% supplied by Fluka Analytical and 1,4-butanediol 99.0% supplied by SIGMA ALDRICH.

8.1. Effect of MEG on CGI Regions with PVCap

Methane hydrate crystal growth inhibition region data have been generated for 1.0 mass% PVCap aqueous with 5, 20 and 50 mass% MEG (relative to water + PVCap) at pressures up to ~300 bar.

Figure 8-1 to Figure 8-3 show example CGI method cooling curves and CGI boundary data points for different mono-ethylene-glycol concentration systems of MEG−PVCap−methane systems. CGI boundary data points of each system are reported in Table 8-1 to Table 8-3. Figure 8-4 shows PVCap induced inhibition regions as a function of aqueous (relative to water) MEG concentration. Figure 8-5 shows combined MEG (thermodynamic) + PVCap induced inhibition regions as a function of aqueous (relative to water) MEG concentration.

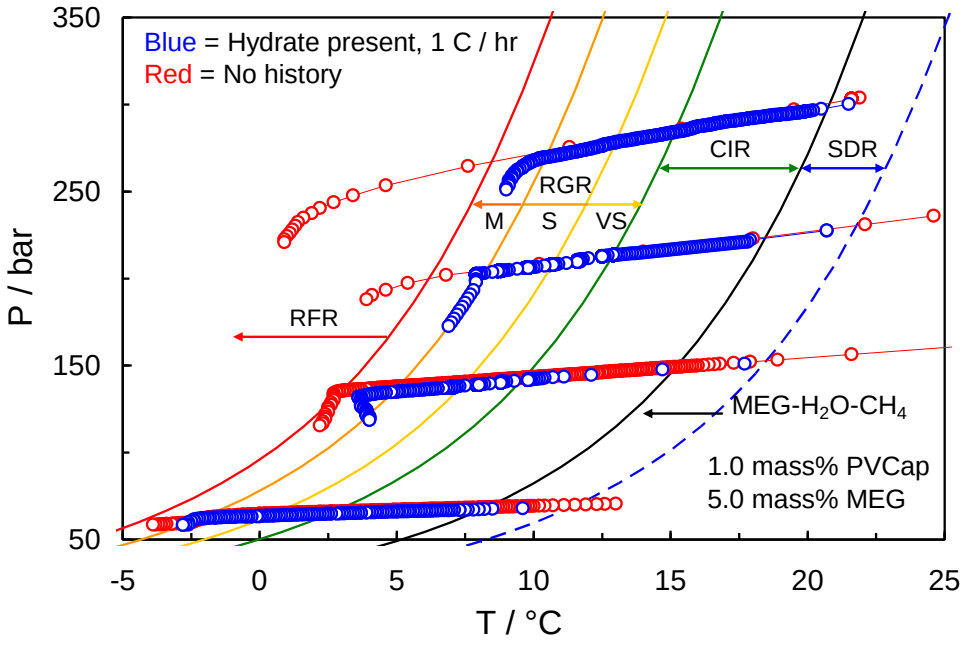

Figure 8-1 Example CGI cooling and heating runs for 1.0 mass% PVCap / 5 mass% mono-ethylene-glycol (both relative to water) aqueous with methane. Points are every 5 minutes.

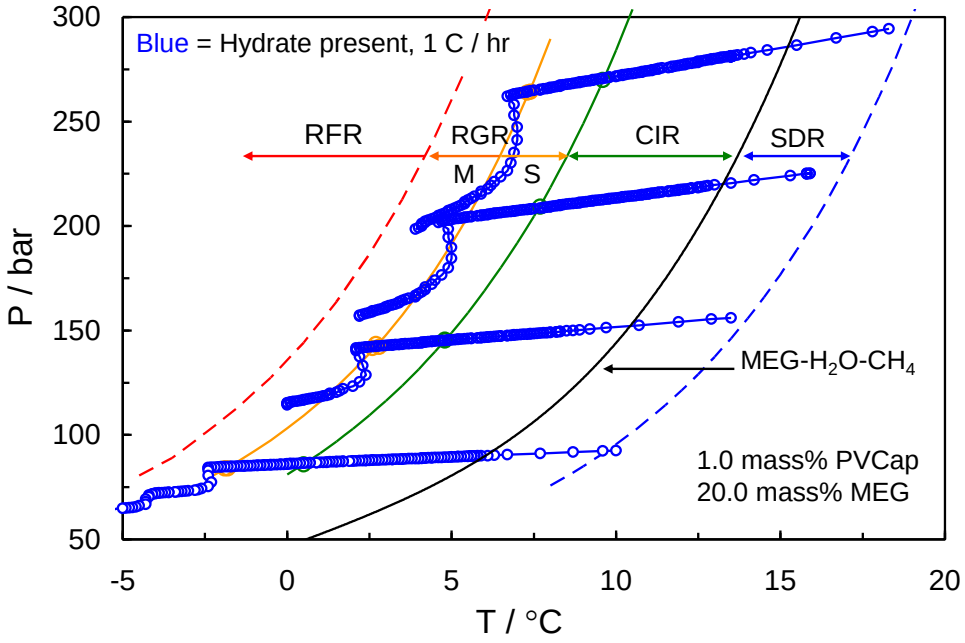

Figure 8-2 Example CGI cooling and heating runs for 1.0 mass% PVCap / 20 mass% mono-ethylene-glycol (both relative to water) aqueous with methane. Points are every 5 minutes.

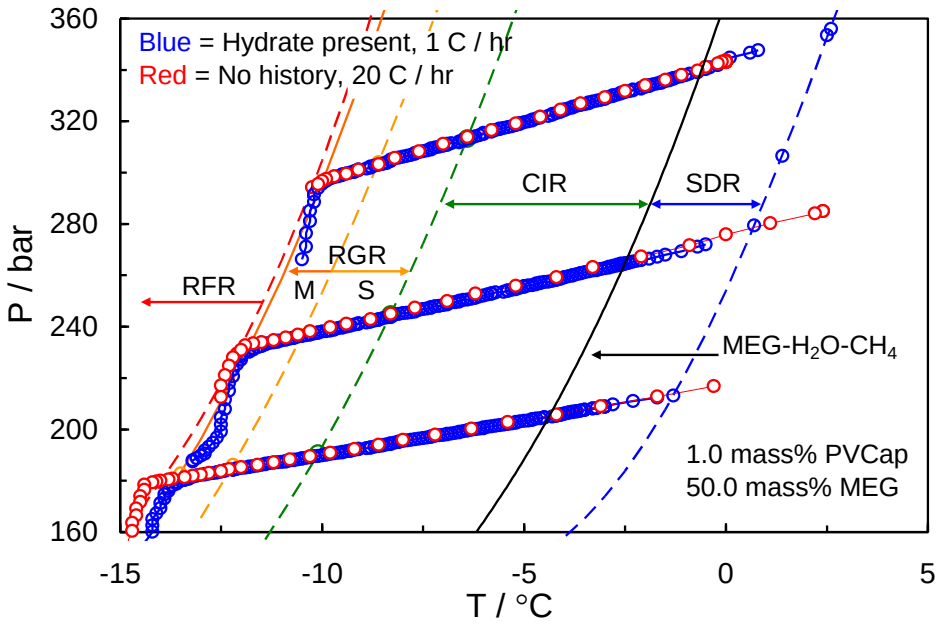

Figure 8-3 Example CGI cooling and heating runs for 1.0 mass% PVCap / 50 mass% mono-ethylene-glycol (both relative to water) aqueous with methane. Points are every 5 minutes.

Table 8-1 Experimental methane hydrate CGI region data for 1.0 mass% PVCap aqueous with 5.0 mass% MEG (relative to water + PVCap).

CGR boundary	*Growth rate	T / °C (± 0.5)	P / bar (± 0.2)	ΔT_{s-I} / °C (± 0.5)
SDR	Slow dissociation	11.7	67.2	3.6
		17.2	129.1	3.2
		21.5	229.5	2.8
		22.3	262.1	2.6
CIR-RGR (S)	No growth	2.5	64.5	–5.2
		9.6	142.5	–5.2
		12.8	210.7	–5.2
RGR (VS-S)	Very slow to slow	0.2	63.5	–7.3
		7.2	138.0	–7.4
		10.6	207.0	–7.3
		12.9	277.9	–7.3
RGR (S-M)	Slow to moderate	–2.2	62.1	–9.5
		4.8	134.6	–9.6
		8.2	204.9	–9.6
		10.4	269.4	–9.6
RGR(M)-RFR	Moderate	–4.2	61.6	–11.4
		2.9	134.7	–11.5
		6.2	200.5	–11.4
		8.5	268	–11.4

*Growth rate is for ΔT CGI region preceding the associated boundary

Table 8-2 Experimental methane hydrate CGI region data for 1.0 mass% PVCap aqueous with 20 mass% MEG (relative to water + PVCap).

CGI boundary	*Growth rate	T / ºC (± 0.5)	P / bar (± 0.2)	ΔT_{s-I} / ºC (± 0.5)
SDR	Slow dissociation	9.7	92.1	–3.5
		14.1	158.3	–3.4
		16.6	216.2	–3.5
		18.9	296.2	–3.4
CIR-RGR(S)	No growth	0.5	86.0	5.1
		4.8	145.2	5.2
		7.7	209.3	5.2
		9.6	269.9	5.2
RGR(S-M)	Very slow to slow	–1.9	84.0	7.3
		2.7	143.5	7.3
		7.3	263.8	7.3
RGR(M)-RFR	Moderate	Indistinct		9.5

*Growth rate is for ΔT CGI region preceding the associated boundary

Table 8-3 Experimental methane hydrate CGI region data for 1.0 mass% PVCap aqueous with 50 mass% MEG (relative to water + PVCap).

CGI boundary	*Growth rate	T / ºC (± 0.5)	P / bar (± 0.2)	ΔT_{s-I} / ºC (± 0.5)
SDR	Slow dissociation	–1.3	213.1	2.7
		0.7	279.4	2.8
		2.5	353.6	2.8
CIR-RGR(VS)	No growth	–10.1	190.5	–5.2
		–8.3	244.8	–5.3
		–6.4	313.2	–5.2
RGR(VS-S)	Very slow to slow	–12.2	186.2	–7.2
		–10.5	236.7	–7.2
		–8.6	304.0	–7.2
RGR(S-M)	Slow-moderate	–13.5	182.8	–8.3
		–11.8	231.9	–8.4
		–10.0	296.1	–8.4
RGR(M)-RFR	Moderate	–14.0	179.5	–8.7
		–12.1	229.5	–8.6
		–10.3	294.3	–8.6

*Growth rate is for ΔT CGI region preceding the associated boundary

As shown in Figure 8-1 to Figure 8-3 CGI regions are clearly discernable from cooling curve data. For all MEG concentrations tested, the presence of 1.0 mass% PVCap will results in the characteristic complete inhibition (CIR), reduced growth rate (RGR) and

rapid growth/failure (RFR) regions. Results from the extent of CGI regions demonstrate that ethylene glycol has a positive, synergistic effect on PVCap hydrate crystal growth inhibition properties, at least at up 50 mass% aqueous. As shown in Figure 8-4 to Figure 8-5, MEG generally acts as a 'top-up' inhibitor for PVCap for the concentrations tested; MEG shifts the PVCap-induced hydrate growth/inhibition regions by a subcooling equivalent to the degree of thermodynamic inhibition offered by that MEG aqueous mass fraction of MEG. Hence as observed, the PVCap-induced CIR remains constant at ΔT_{sub} = ~–5.2 °C (same as the CIR for water-PVCap alone) even up to concentrations as high as 50mass% MEG. This behaviour is quite the opposite of methanol/ethanol systems where the CIR was clearly reduced to lower subcoolings (Chapter 7). In addition to acting as a 'top-up' inhibitor it seems that for all tested MEG concentrations, the characteristic change from very slow/slow to moderate growth at the RGR(VS-S) boundary and the onset of rapid growth at the RFR boundary are extend to higher subcoolings.

For low MEG concentrations (5 mass %) as shown in Figure 8-1 in addition to acting as a as a 'top-up' inhibitor, presence of MEG appears to add an additional reduced growth rate region ,RGR(M), which is not observed for 1.0 mass% PVCap with methane alone (Chapter 2). In the latter case, rapid hydrate growth is observed at the RFR boundary line at ΔT_{sub}= ~9.5 °C. While data for 5 mass% MEG show a clear boundary line at the same subcooling, only moderate growth rates are observed when it is passed, rather than rapid failure. Hydrate growth for a system with no history only begins to occur when the system has reached a subcooling of ~11.4 °C or in other words, the RGR(M)-RFR boundary line has been extended to ΔT_{sub}= ~–11.4 °C. Moreover, it is observed that in the presence of 5 mass% MEG as well as higher subcooling of the RGR regions, growth rates in specific growth/inhibition regions have been greatly reduced when compared to 1 mass% PVCap alone which again supports the positive synergistic effect of MEG on PVCap performance.

On the other hand, Figure 8-2 shows that in 20 mass% MEG system in addition to the preserved CIR at ΔT_{sub} = ~–5.2 °C, all other CGI regions are at values similar to those for PVCap alone with RGR boundary at ΔT_{sub} = ~–7.2 °C . However, presence of MEG still enhances hydrate inhibition as it is found to consistently reduce the rate of hydrate formation at a given subcooled condition compared to PVCap alone. At this

concentration the RFR was unfortunately not very well distinguishable from the performed runs.

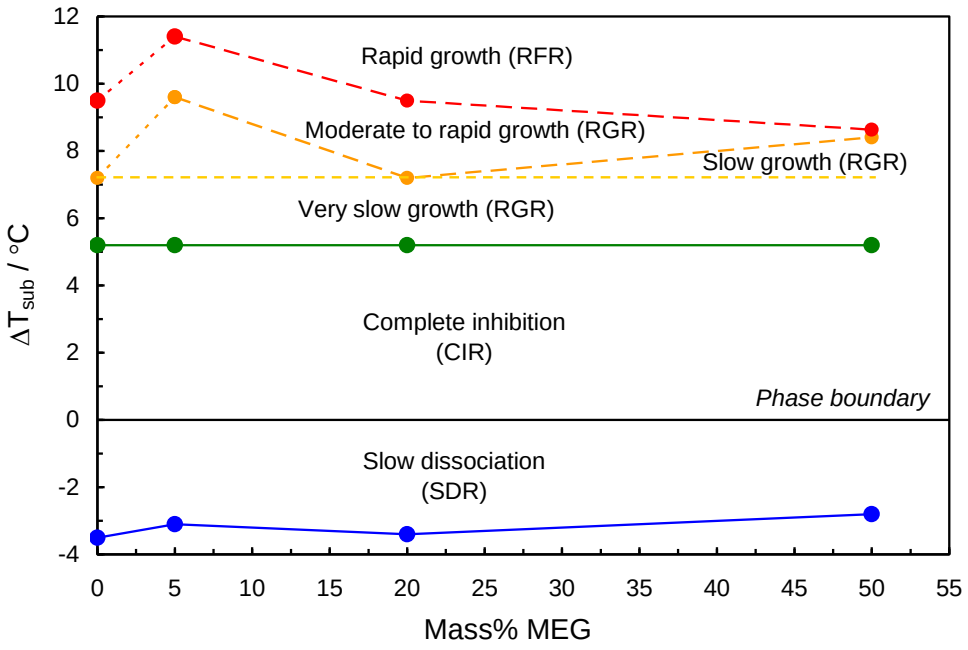

Figure 8-4 Average (50 to 300 bar) PVCap induced CGI regions for 1.0 mass% PVCap aqueous as a function of mass% MEG (relative to water + PVCap).

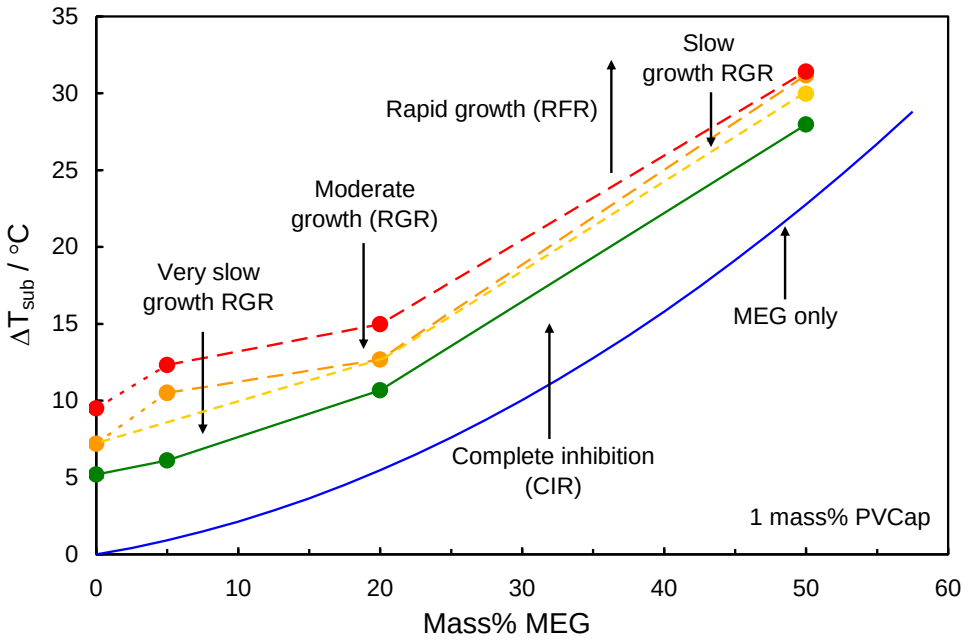

Figure 8-5 Total methane hydrate inhibition offered through the combination of MEG and 1.0 mass% PVCap.

However, as illustrated in Figure 8-3, data for 50mass% MEG aqueous reveals that at very high MEG concentrations, the RGR region is extended to higher subcoolings (ΔT_{sub} = ~–8.4 °C) when compared to 1 mass% PVCap alone, although it is still smaller than that for 5mass% MEG aqueous. In the RGR(VS) region at 50 mass% MEG, growth rates were so slow that they were hardly detectable on reasonable timescales

(days). In that sense, the very slow growth RGR was almost an extension of the CIR. Above this, RGR(S) region could only be defined if cooling rates were slow enough, with detectable growth occurring with hydrate present. Likewise, similar to the other two concentrations mentioned, in addition to increasing the extent of KHI induced inhibition regions, 50mass% MEG consistently reduces the rate of hydrate formation at a given subcooled condition compared to PVCap alone.

Figure 8-4 clearly illustrate that the presence of MEG has a significantly positive effect on PVCap performance. Moreover, Figure 8-5 shows the considerable positive hydrate inhibition properties of PVCap compared to MEG. As can be seen, 1 mass% PVCap offers complete crystal growth inhibition (CIR region) equivalent to the thermodynamic inhibition offered by ~20 mass% MEG; a significant inhibitor volume reduction. Moreover, the combination of MEG + PVCap offers far better inhibition by mass/volume inhibitor than MEG alone. As MEG acts as a 'top-up' inhibitor up to 50 mass% with PVCap, at least in terms of the CIR, then it could in theory be used to extend the subcooling of KHIs and/or significantly reduce MEG thermodynamic inhibitor volumes. Note that MEG volume reductions should be even higher for s-II natural gas hydrates as the PVCap-inducted CIR should include both the ~–5.2°C subcooling from the s-I boundary and the additional few degrees of subcooling which lies between the s-I and s-II boundaries.

8.2. Effect of 1,3-propanediol on CGI Regions with PVCap

Methane hydrate crystal growth inhibition region data have been generated for 0.5 mass% PVCap aqueous with 3.1mass% 1,3-propanediol, equivalent to 0.76 mole % 1,3-propanediol, (relative to water + PVCap) at pressures up to ~250 bar.

Figure 8-6 shows example CGI method cooling curves and CGI boundary data points for the tested 1,3-propanediol−PVCap−methane system. CGI boundary data points are reported in Table 8-4.

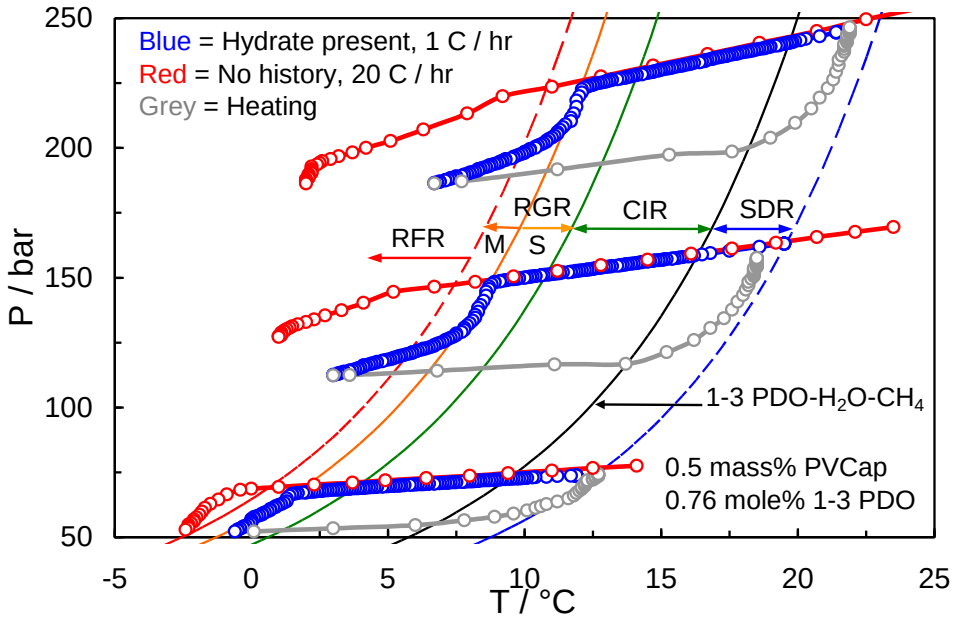

Figure 8-6 Example CGI cooling and heating runs for 0.5 mass% PVCap / 3.1 mass% (0.76 mole%) 1,3-propanediol (both relative to water) aqueous with methane. Points are every 5 minutes.

Table 8-4 Experimental methane hydrate CGI region data for 0.5 mass% PVCap with 3.1 mass% (0.76 mole %) 1,3-propanediol (both relative to water) aqueous.

CGR boundary	*Growth rate	T / °C (± 0.5)	P / bar (± 0.2)	ΔT_{s-I} / °C (± 0.5)
SDR	Slow dissociation	13.2	75.8	3.4
		19.5	161.1	3.0
		22.1	234.6	2.6
CIR-RGR (S)	No growth	4.2	70.5	–4.9
		10.6	148.1	–5.2
		13.9	227.1	–5.3
RGR (S-M)	Very slow to slow	1.8	69.7	–7.3
		8.9	148.2	–6.9
		12.1	223.5	–7.0
RGR(M)-RFR	Moderate	0.2	65.5	–8.2
		7.6	144.6	–8.0
		10.9	220.9	–8.1

*Growth rate is for ΔT CGI region preceding the associated boundary

As shown in Figure 8-6, CGI regions can clearly be distinguished from CGI cooling curve data for 1,3-propanediol–PVCap systems. However, there are some differences in the extent of regions and growth rates in comparison to MEG.

Results for 0.5 mass% PVCap and 3.1 mass% (0.76mole%) 1,3-propanediol show that this diol has little impact on the performance of PVCap, at least at this concentration. Findings suggest that the complete inhibition region is preserved, remaining largely comparable to a water–PVCap system at ΔT_{sub} =~–5.1 °C. Likewise, the slow growth

rate region/moderate growth rate initiation is largely unchanged at ΔT_{sub} =~–7.0 °C. Moreover, growth rates in each region do not seem quite similar to growth rates in a simple 0.5mass% PVCap system. Thus, at this concentration, 1,3-propanediol generally seems to act as a 'top-up' inhibitor for PVCap but, unlike MEG, does not clearly enhance performance.

8.3. Effect of 1,4-butanediol on CGI Regions with PVCap

Methane hydrate crystal growth inhibition region data have been generated for 0.5 mass% PVCap aqueous with 3.7mass% 1,4-butanediol, equivalent to 0.76 mole % 1,4-butanediol, (relative to water + PVCap) at pressures up to ~250 bar.

Figure 8-7 shows example CGI method cooling curves and CGI boundary data points for the tested 1,4-butanediol−PVCap−methane system. CGI boundary data points are reported Table 8-5.

Results for 0.5 mass% PVCap with 3.7mass% (0.76mole%) 1,4-butanediol suggest that this diol has a generally negative effect on PVCap performance, with CGI regions apparently reduced, e.g. CIR and RGR(S)/RGR(M) are ~0.5 °C lower in subcooling extent being at ΔT_{sub} =~–4.6 °C and ΔT_{sub} =~–6.6 °C respectively. Thus, unlike MEG and 1,3-propanediol, 1,4-butanediol is not a top-up inhibitor at this concentration and is somewhat negative.

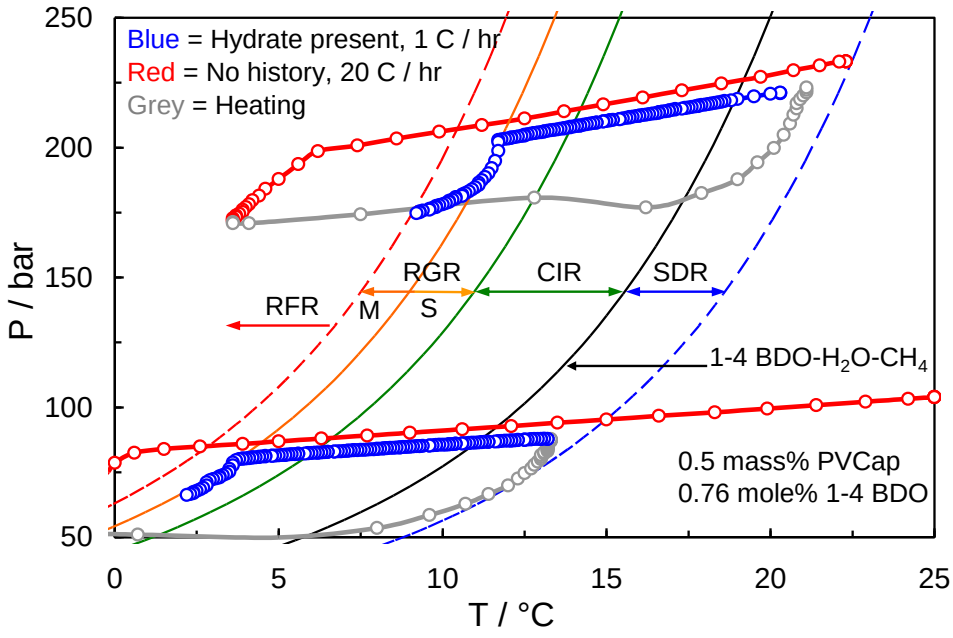

Figure 8-7 Example CGI cooling and heating runs for 0.5 mass% PVCap / 3.7 mass% (0.76 mole %) 1,4-butanediol (both relative to water) aqueous with methane. Points are every 5 minutes.

Table 8-5 Experimental methane hydrate CGI region data for 0.5 mass% PVCap aqueous with (3.7mass%) 0.76 mole % 1,4-butanediol (both relative to water) aqueous.

CGR boundary	*Growth rate	T / ºC (± 0.5)	P / bar (± 0.2)	ΔT_{s-I} / °C (± 0.5)
SDR	Slow dissociation	15.1	94.0	3.3
		21.8	220.1	2.8
CIR-RGR(S)	No growth	6.5	88.0	–4.8
		14.4	214.6	–4.4
RGR(S-M)	Very slow to slow	3.9	81.9	–6.6
		12.1	209.2	–6.5
RGR(M)-RFR	Moderate	2.7	81.3	–7.8
		10.1	202.4	–8.3

*Growth rate is for ΔT CGI region preceding the associated boundary

8.4. Comparison of the effect of 3 tested diols on CGI Regions with PVCap

To better evaluate the effect of molecular structures of diols, carbon number of the alkyl 'tail' in particular, results of all three diols (mono-ethylene-glycol, 1,3-propanediol and 1,4-butanediol) are summarized and compared in this section.

For a fairer evaluation of result all diols are compared at the same molar concentration. Figure 8-8 illustrates the comparison of average PVCap induced inhibition regions for all tested diols (MEG, 1,3-PDO and 1,4-BDO) at 0.76 mole % diol aqueous for 0.5 and 1.0 mass% PVCap solutions with methane (Data for 0.76 mole % MEG is not experimental and is interpreted from the trend of changes of PVCap induced CGI regions for 0.5 mass% PVCap aqueous as a function of mass% MEG shown in Figure 8-4). The average CGI data for each diol is also shown in Table 8-6.

Table 8-6 Experimental methane hydrate average CGI region data for 0.5 mass% PVCap with 0.76 mole% 1,4-butanediol, 1,3-propanediol and 1.0 mass% PVCap with 0.76 mole% MEG (glycol and PVCap concentrations both relative to water) aqueous.

	ΔT_{sub} RFR/°C	ΔT_{sub} RGR(M) /°C	ΔT_{sub} RGR(S) /°C	ΔT_{sub} CIR /°C	ΔT_{sub} SDR /°C
PVCap	–9.3	–7.2	—	–5.2	3.5
MEG	–10.8	–8.7	–7.2	–5.2	3.3
1,3-propanediol	–8.3	–7.0	—	–5.1	3.0
1,4-butanediol	–8.0	–6.6	—	–4.6	3.1

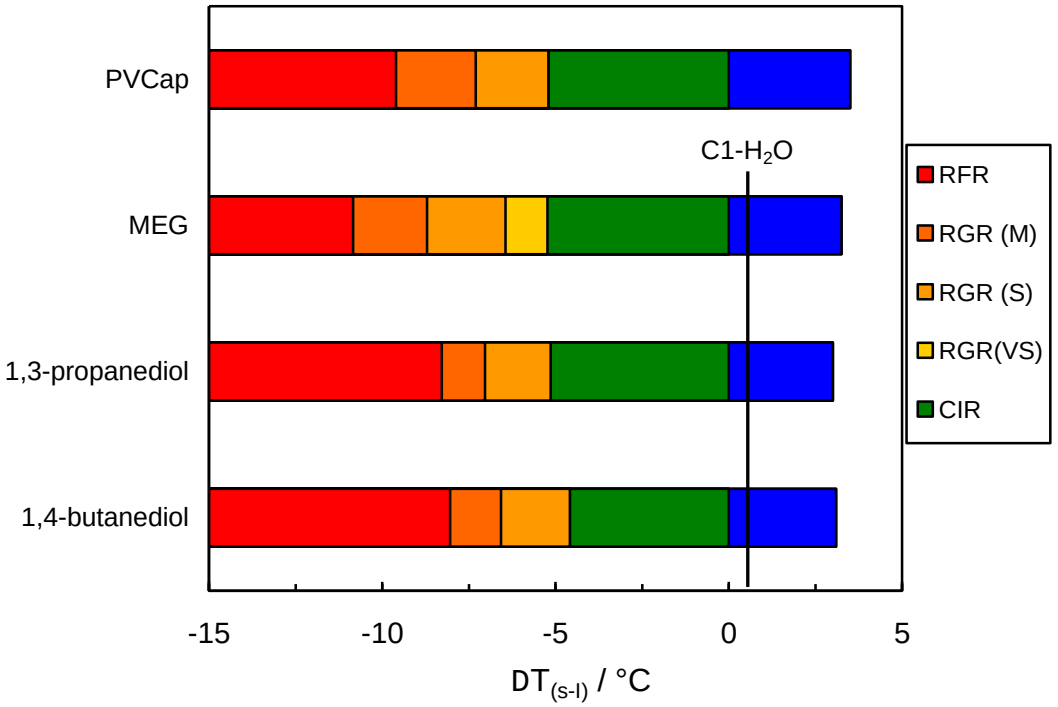

Figure 8-8 Experimental methane hydrate average CGI region data for 0.5 mass% PVCap with 0.76 mole% 1,4-butanediol, 1,3-propanediol and 1.0 mass% PVCap with 0.76 mole% MEG (both PVCap and diol relative to water) aqueous

As Figure 8-8 shows while investigations have not been particularly extensive, results do suggest that increasing the central alkyl chain length of the diol progressively eliminates top-up properties. Likewise, MEG has a significantly positive effect being a top-up inhibitor as well as extending RGR boundaries in which the hydrate growth rate is decreased compared to a simple 1.0 mass% PVCap system. Moreover, 1,3-propanediol is only a to-pup inhibitor (preserving the CIR) with somewhat smaller RGR and RFR regions. While unlike the other two diols, 1,4-butanediol has decreased CGI regions compared to 0.5 mass% PVCap showing that this diol with longer central alkyl chain has a slightly negative effect on PVCap performance.

8.5. Conclusions

Results from application of the new CGI method to methane−PVCap−ethylene glycol−water systems showed that MEG is generally a 'top-up' thermodynamic inhibitor; crystal growth inhibition regions are larger or equal to those for PVCap alone, at least up to concentrations of 50 mass% MEG. Furthermore, compared to PVCap alone, the addition of MEG greatly reduces hydrate growth rates where growth can occur.

Moreover, the combination of MEG + PVCap offers far better inhibition by mass/volume inhibitor than MEG alone; 1 mass% MEG offers complete crystal growth inhibition (CIR region) equivalent to the thermodynamic inhibition offered by ~20 mass% MEG.

The reasons why MEG, unlike methanol, has positive effect are unclear, although data strongly suggest MEG causes an increase in the strength of polymer adsorption on hydrate crystal surfaces, as evidenced by the increase in CGI region subcoolings, and maintenance of SDR region at ~3.3 °C higher than the phase boundary. Furthermore, it is evident that PVCap is highly soluble in both MEG and methanol, thus a simple explanation for negative methanol behaviour in that PVCap-solvent interactions in solution take preference over crystal surface absorption, does not apparently hold for MEG.

Comparable to MEG, CGI studies on methane−PVCap−1,3-propanediol−water have revealed that for the concentration tested, 1,3-propanediol has little observable impact on PVCap performance and acts as 'top-up' thermodynamic inhibitor, with crystal growth inhibition regions generally equal to those for PVCap alone.

In contrast to the other two tested diols, at the same concentration, 1,4-butanediol does not act as 'top-up' thermodynamic inhibitor; CGI regions are consistently reduced to lower subcoolings in its presence.

Neither 1,3-propanediol nor 1,4-butanediol seemingly offer the same good synergism as MEG, indicating that the favourable properties of the latter are not ubiquitous to all diols, and that increasing central alkyl chain length progressively eliminates top-up properties.

References

Wu, M., Wang, S., Lui, H., 2007, *"A Study on Inhibitors for the Prevention of Hydrate Formation in Gas"*, Journal of Natural Gas Chemistry, 16, 81-85

Yousif, M.H., 1998, *"Effect of Underinhibition with Methanol and Ethylene Glycol on the Hydrate-Control Process"*, SPE Production & Facilities, 13, 184-189

9. CONCLUSIONS AND RECOMMENDATIONS

9.1. Conclusions

As mentioned in the early chapters of this thesis, due to nucleation being a stochastic property in nature, the traditionally used induction time, *ti*, method is usually a very problematic and time consuming technique for KHI evaluation. Therefore, the primary aim of this work was to generate a new KHI evaluation method that yields reliable, repeatable and transferable data which is also in agreement and can also help better understand measurements from the previously used techniques.

Chapter 2 of this thesis concentrated on the development of a crystal growth inhibition (CGI) based approach to KHI evaluation in which gas hydrate growth and dissociation patterns in the presence of KHI polymers were carefully inspected. Work done throughout this chapter showed that through simple, carefully controlled isochoric PT tests without any specific equipment, some repeatable and transferable regions of polymer-controlled hydrate crystal growth inhibition can be readily identified from changes in crystal growth rates. Results indicated within a specific subcooling from the hydrate phase boundary, called the complete inhibition region (CIR), it is apparently impossible to grow hydrates even with hydrate crystals already present in the system (at least within tested periods). Moreover, beyond this region and up to another subcooling from the hydrate phase boundary a reduced growth rate region (RGR) is defined in which whether there is history or hydrate present in the system, pressure drop on cooling is observed, indicating hydrate growth. Growth rates in this region depend on both the degree of subcooling and the fraction of hydrate already present in the system. Finally, beyond the RGR a third crystal growth inhibition region is defined called the rapid failure region (RFR). In this region no matter whether there is hydrate/ history present or not, hydrate crystals form and grow rapidly and catastrophically until the RGR/CIR are re-entered. Through carefully determining these boundaries and measuring the extent of each region, hydrate inhibition behaviour of different KHI systems can be well evaluated and better understood.

In addition to that it was observed that the induction times/nucleation inhibition patterns are primary related to underlying CGI regions detected from the new CGI technique. The correlation between the two methods showed that a true induction time can only be

measured for a relatively short range of subcooling within the RGR and the RFR. Likewise, hydrate nucleation induction time is impossible to measure in the CIR, supporting CGI studies which show that hydrate growth is completely/indefinitely inhibited in this subcooling range.

Subsequently, in the following chapters of this thesis, work concentrated on applying the new approach to various KHI systems to gain a good understanding of the real behaviour and effect of KHIs on hydrate forming systems through reliable, repeatable and transferable results. In addition, to that the influence of different factors on KHI performance was evaluated with the application of this method.

In Chapter 3 this newly developed Crystal Growth Inhibition technique was applied to a number of KHI polymers in a simple methane system to both prove and confirm the validity of the method and evaluate how different types of KHIs perform as a crystal growth inhibitor. Results of tests of PVCap polymer in this chapter support distinct polymer concentration dependence for the degree of hydrate inhibition offered by this KHI. Data show that the higher the PVCap concentration, the further hydrate formation and growth is prevented by the KHI. However, results suggest that an 'optimum' PVCap concentration for methane−water systems is present at > 0.25 mass% and ≤ 0.5 mass%, at least in terms of CIR subcooling. It is shown that increasing PVCap concentration above this amount greatly reduces hydrate growth rates in the RGR region as well as extending this region to higher subcoolings. In addition to that, studies on the effect of PVCap molecular weight indicated that PVCap performance does not change noticeably due to PVCap average molecular weight (the length of PVCap polymer) difference at least for the molecular weights tested (4000- 8000 and 7000-15000. Therefore, if very low molecular weight PVCap which has higher water solubility and higher critical solution temperature, shows similar performance to higher molecular weight PVCap samples, the former will be a better option as a kinetic hydrate inhibitor.

Furthermore, initial tests on PVP confirm that its performance is much poorer than PVCap. This suggest the adsorption strength of PVP on hydrate crystal surfaces is much weaker, potentially due to the smaller molecular diameter of the amide pendant group (i.e. its interactions with open hydrate cavities are much weaker).

Due to the good performance of PVCap and the higher solubility of PVP, CGI studies were undertaken on a PVCap-PVP mixture sample. Results show the addition of a small fractions of PVCap to a PVP solution (e.g. 0.05 mass% PVCap, 0.95 mass% PVP) greatly increases hydrate inhibition performance. As a result, while polymers may perform poorly alone, in combination they may have strong synergism thus polymer performance must not be judged on performance in pure form. Moreover, it was found that this enhanced performance is highly susceptible to the fraction of hydrate formed for such low PVCap concentrations. Furthermore, the combination of 2 polymers gives 2 CIR regions depending of the initial hydrate fraction in the system, Thus, it is recommended that in all KHI evaluation tests 'hydrate present' runs be carried out for various initial hydrate fractions to assess the KHI sensitivity to this and ensure results take this into account.

Examining the effect of PEO revealed that this polymer has very weak inhibition properties and all crystal growth inhibition regions are significantly smaller than that for PVCap at the same concentration or even PVP at a smaller polymer concentration. This clearly proves that the pendant group of a polymer plays a major role on the KHI inhibition properties.

To show the applicability of the newly developed technique on real commercial KHI polymers, CGI studies on two of these KHIs − T1441 co-polymer and HYTREAT− in s-I methane systems were performed. Results showed that each of these commercial polymers clearly have defined CGI boundaries although performing very differently. While T1441 is clearly significantly less able to inhibit s-I methane hydrate growth, it is considerably more soluble in water especially at higher temperatures compared to HYTREAT with large CGI regions. Studies on PVCap and the 2 commercial polymers tested here support the on-going problem of balancing polymer solubility with KHI performance. It is evident that at least for the tested polymers, apparently ones with higher precipitation temperatures commonly reduce inhibition performance of the polymer. Hence, addressing this problem in the industry is very important.

Finally in this chapter, the performance of a biodegradable polymer which to date is becoming increasingly important was investigated. CGI studies of the biodegradable polymer Luvicap Bio revealed that this polymer shows reasonably good performance as a KHI, both in terms of crystal growth inhibition and nucleation inhibition. Moreover, its performance can be enhanced by the addition of synergist solvents such as 2-

butoxethanol. Hence, working on the enhancement of this type of polymer can result in the making formulations comparable with many existing commercial KHI in performance.

In Chapter 4 the performance of KHIs was investigated in different guest gas/hydrate structure systems using the new CGI technique. By understanding the KHI behaviour in each different hydrate structure forming gas the mechanism of hydrate inhibition or surface adsorption was also briefly evaluated. Results of this chapter indicate that guest/cage occupancy plays an important role in hydrate inhibition.

Comparison of three different simple s-I hydrate formers (C_1, C_2 and CO_2) individually with PVCap showed contrasting results. Data proved that PVCap was able to inhibit the growth of ethane hydrates much more effectively than it could inhibit methane hydrates. Contrastingly, CO_2 has a distinctly negative effect on PVCap performance, with remarkably reduced CGI regions compared to methane and ethane. However tests show that small fractions of CO_2 (e.g. 1.6%) in natural gases does not appear to have any significant and obvious negative effect.

On the other hand, PVCap performance was considerably superior in s-II forming systems (both simple s-II and binary s-I/-s-II) compared to s-I forming systems (e.g. methane), supporting stronger polymer adsorption on s-II hydrate crystal surfaces. PVCap almost indefinitely inhibits propane hydrate, an s-II former. Furthermore, PVCap performs much better in C1-C3, C1–C2 and C1–C2–C3 systems compared to simple s-I formers like methane or ethane.

In binary and multicomponent s-I/s-II forming systems (e.g. natural gas), PVCap 'failure' appeared predominantly due to the formation of s-I hydrates, with CGI regions commonly related in subcooling extent to the s-I phase boundary for the system. This behaviour was clearly observed for all binary and multicomponent s-I/s-II forming gases (C1-C3, C1–C2, C1–C2–C3, and NG) tested in this chapter. In addition to measuring of CGI regions, this hypothesis was further supported through gas analyses of C1-C3 mixture during initial hydrate; propane content of the vapour phase increased in concentration during initial growth supporting s-I formation at this stage of growth.

PVCap performance in s-I/s-II forming natural gas systems is superior to that in binary s-I/s-II forming methane–propane systems at pressures > 100 bar. At pressures below 70 bar in natural gas systems, PVCap performance is moderately reduced. It is

speculated and supported through CGI tests that this may be related to driving force and/or propane/ethane cage occupancy patterns as a function of pressure. At pressures above 100 bar, the better performance of PVCap in NG was speculated to be somewhat related to the presence of a small fraction of ethane although it alone cannot apparently explain this enhanced performance. On the other hand, CO_2 is considered to be responsible for the significant reduction in PVCap performance observed at lower pressures in NG systems.

In addition to all systems mentioned above, findings from cyclopentane–methane system, an s-II former, verified that as a rule of thumb the more stable the s-II hydrate former (i.e. the better it stabilises the large $5^{12}6^4$ cavity), the more effective PVCap is at inhibiting growth. Moreover, from the fact that some CGI regions (e.g. the CIR) for C1-cC5 are entirely related to s-II hydrate formation while those at higher subcoolings (e.g. RGR-RFR) may be influenced by s-I growth, as observed for a variety of KHI systems (e.g. methane–propane) supports the theory that CGI patterns are strongly influenced by underlying crystal growth patterns

Other than all above findings for s-II/s-I forming systems with PVCap, CGI data for a methane–methylcyclohexane system showed that the formation of s-I hydrates appears to be the reason for PVCap failure in s-H/s-I systems. In this case, it appeared the formation of s-H hydrates was completely inhibited and only s-I methane hydrate formation occurred. This could be due to the fact that PVCap absorbs more strongly on s-H crystal nuclei, possibly as the caprolactam pendant group fits better into the s-H large cavity which has a greater diameter than s-I and s-II large cages.

In Chapter 0 the new crystal growth inhibition (CGI) approach was applied to systems with PVCap and a liquid hydrocarbon phase present to assess the effect that these components can have on PVCap hydrate inhibition performance. Moreover, to confirm a further possible mechanism by which polymer concentration might be reduced in the aqueous phase, simple hydrocarbon–water polymer partitioning tests were carried.

Results of work applying the new approach to methane–n-heptane–water–PVCap systems revealed that independent from the liquid hydrocarbon volume ratio, heptane had only a minor negative effect on the performance of PVCap. Simple visual observation of n-heptane–water–PVCap behaviour at room temperature and pressure

suggest that this negative effect could be related to polymer partitioning at the water−hydrocarbon interface, reducing the aqueous phase concentration.

Likewise, in a condensate system, PVCap performance was slightly deteriorated. The explanation for this negative effect of condensate could be similar to that presumed for n-heptane which was related to polymer partitioning at the water−hydrocarbon interface, reducing the aqueous phase concentration. In addition to that, condensate acted slightly more negative than n-heptane; possibly due to the presence some hydrate forming compounds in the real condensate (e.g. iso-butane, iso-pentane). Clearly the hydrocarbon composition, which determines cage occupancy, has an important role to play.

Chapter 0 concentrated on evaluating the performance of PVCap in the presence of salts that commonly exist in produced waters using the new CGI approach. The most common salt in produced waters is NaCl hence the influence of this salt on PVCap was primarily examined. However, clearly results for NaCl would not necessarily apply for all other salts particularly carbonate salts that have a completely different structure. In light of this, methane hydrate crystal growth inhibition regions (CGI) were also measured for PVCap with K_2CO_3 – a carbonate salt.

CGI region studies on NaCl−PVCap−water systems with methane showed that at lower NaCl concentrations (5mass%) it had a positive effect on PVCap performance or in other words NaCl is apparently a ‘top-up’ thermodynamic inhibitor at lower concentrations. At higher salt concentrations CGI regions were speculated to grow even further, although this was not confirmed as higher sodium chloride concentrations (e.g. 10 mass%) caused polymer precipitation. One possible explanation for this behaviour was the hydrate morphology change due to NaCl presence which can enhance PVCap stabilization on hydrate surface.

Conversely, CGI region studies on a K_2CO_3−PVCap−water system with methane showed that K_2CO_3 at the tested concentration (2 mass%) had a generally negative effect on PVCap performance. Unlike NaCl, K_2CO_3 is apparently not a complete ‘top-up’ thermodynamic inhibitor at this concentration. Moreover, at higher K_2CO_3 concentrations (>2 mass%), PVCap was no longer soluble (at 0.5 mass%) and partial precipitation occurred.

As a result, it is evident that the effects of salts on PVCap performance may be more complex and that salt structure (carbonate or non-carbonate) can play an important role on its influence; probably due to the different impact of each salt on hydrate morphology. Hence, for prediction of system behaviour knowing the type of salt is essential.

In Chapter 7, KHI (PVCap) performance was evaluated in the presence of different alcohols. A number of alcohols such as methanol and ethanol are most commonly alcohols used as thermodynamic inhibitors for hydrate inhibition processes. Moreover, such alcohols are commonly used in KHI formulations hence it is highly important to investigate CGI behaviour for the combination of these thermodynamic inhibitors and kinetic hydrate inhibitors (PVCap). In this chapter in addition to testing methanol, the most popular alcohol thermodynamic inhibitor, and ethanol which is seeing increasing use as a hydrate inhibitor due to its good environmental credentials, a number of other alcohols such as n-propanol and n-butanol which have similar properties/molecular structures to methanol and ethanol with the only different in number of carbons in the alkyl 'tail' were also tested to further investigate the effect of alkyl 'tail' carbon number of alcohols on their effect on PVCap performance. Furthermore to better evaluate the effect of this parameter, i-propanol with the same molecular formula but different structure to n-propanol, was also tested.

CGI region studies on alcohol (MeOH, EtOH, n-POH, i-POH and n-BOH)-PVCap-water systems at tested concentrations of alcohols with methane at 0.5 mass% PVCap showed that none of the above alcohols act as a 'top-up' thermodynamic inhibitor although the combination of alcohol plus PVCap does still offer better inhibition by mass of inhibitor than any of the alcohols alone.

All tested alcohols except n-butanol had negative effect on CIR which although unclear but was supposedly related to the fact that the former alcohol (MeOH) can form clathrate hydrates at low temperatures and the latter three alcohols (EtOH, n-POH and i-POH) can form clathrate hydrates at conditions pertinent to offshore operations, thus they may be encouraging growth by competing with polymer pendant amide groups for partial enclathration into open cages.

Moreover, it was concluded that the longer the alkyl tail of the alcohol the less negative effect it has on PVCap performance. Also, molecular weight alone is not apparently the

controlling factor whereas solubility parameters may play a role on the influence that alcohol could have on PVCap performance.

Chapter 8 looked at the performance of the combination of KHIs (PVCap) and another popular type of thermodynamic inhibitor, glycols. CGI behaviour and boundaries for PVCap in presence of a range of mono ethylene glycol (MEG) concentrations, one of the most widely used thermodynamic inhibitors, with methane were determined. In addition to mono-ethylene-glycol which is very much similar to ethanol but has an additional OH group attached to one end, two other diols, 1,3-propanediol and 1,4-butanediol, which have similar properties/molecular structures to MEG and only differ by additional carbons in the central alkyl chain were also examined to evaluate their influence of PVCap performance. These studies helped conclude more comprehensively on the performance of glycols and suggest a more reliable explanation for any behaviour observed.

Results from application of the new CGI method to methane–PVCap–ethylene glycol–water systems showed that MEG is generally a 'top-up' thermodynamic inhibitor. Also, compared to PVCap alone, the addition of MEG greatly reduces hydrate growth rates where growth can occur. The reasons why MEG, unlike methanol, has positive effect were unclear, although data strongly suggest MEG causes an increase in the strength of polymer adsorption on hydrate crystal surfaces, as evidenced by the increase in CGI region subcoolings. Furthermore, it is evident that PVCap is highly soluble in both MEG and methanol, thus a simple explanation for negative methanol behaviour in that PVCap-solvent interactions in solution take preference over crystal surface absorption, does not apparently hold for MEG.

Studies on two other glycols tested showed that neither 1,3-propanediol nor 1,4-butanediol seemingly offer the same good synergism as MEG. While 1,3-propanediol has little observable impact on PVCap performance and acts as 'top-up' thermodynamic inhibitor, with crystal growth inhibition regions generally equal to those for PVCap alone, 1,4-butanediol does not act as 'top-up' thermodynamic inhibitor and reduces CGI regions to lower subcoolings. Findings indicate that the favourable properties of the latter are not ubiquitous to all diols, and that increasing central alkyl chain length of glycols progressively eliminates top-up properties.

9.2. Recommendations

Although the general understanding is that hydrate structure is very important to KHI performance and that KHIs work well with structure-II hydrates (e.g. standard natural gas containing modest propane, butane etc.) but more poorly with s-I hydrates (e.g. very lean gases), this work has concluded that this interpretation − while correct in principle – is overly simplistic. As mentioned earlier in this chapter studies proved that the formation of structure-I hydrates in structure-II forming systems is commonly the cause of KHI 'failure'; the KHI being better able to prevent growth of the latter, but not the former if subcooling is sufficient to allow formation. Furthermore, as mentioned earlier in this chapter studies of single component, binary, ternary and multicomponent gas mixtures have shown that KHI performance can vary significantly as a function of gas composition and over relatively small pressure changes, particularly up to 150 bar; the pressure range of interest in terms of KHI usage. It was concluded that this behaviour could most likely be related to cage occupancy patterns, hence for an enhanced understanding of this, in addition to the already tested components it would be of great use to gradually work towards more complex systems (e.g. C_1-C_2-C3-CO_2, C_1-C_2-C_3-C_4, C_1-C_2-C_3-N_2 etc.) to build towards a real natural gas system and understand the effect of each component individually and in conjunction with other components on the performance of PVCap. In addition to this, one of the components that is suspected to play an important part on the performance of KHIs in natural gases is H_2S. This sour gas is both a hydrate former and has a similar size and cage occupancy to CO_2 which was detected to have great influence on hydrate formation patterns. Hence, testing this gas can provide good evidence towards a better understanding of the influence gas composition and cage occupancy on KHI performance. However, it should be considered that since this gas is classified as very toxic and dangerous for the environment it should only be tested in a fully equipped H_2S laboratory with great care taken when working with it.

So far there have been some relations and good trends found between already gathered results. Thus if further consistency is found amongst results of the above suggested experiment and previous findings, reviewing all this data combined with modelling studies (particularly hydrate compositions) can assist in better understanding of any changes in occupancy from low to high pressures.

As noted above, gas CO_2 content has been found to play an important role in KHI performance. While as discussed this could partly be related to cage occupancy patterns/polymer adsorption strength on hydrate surfaces, pH could also be an important factor as it is known to play a role in polymer conformation/coiling in solution. Hence, assessing the effect of pH in hydrate forming systems can be of great importance in understanding KHI behaviour and performance in different systems. However, it should be considered that the evaluation of this factor will have its own difficulties as the pH of a solution can change during experiments upon contact with natural gases due to the dissolution of acid components such as CO_2 and H_2S in these gases.

Generally laboratory data are obtained under 'ideal / clean' test conditions, but in reality pipelines contain various solid fine particles such as iron oxides, sulphides, sand fines etc. The presence of these particles can possibly encourage hydrate nucleation/ growth by acting as seeds. Therefore, studying the performance of KHIs in the presence of such particles can give an understanding of the impact of various common pipeline particles/fines on both CGI and *t*i results in these systems.

Thermodynamic inhibitors are often added to produced water which commonly contain significant amounts dissolved salts, either as a solvent/carrier for KHI polymers, or in an attempt to increase the degree of hydrate inhibition offered at higher subcoolings, i.e. as a 'top-up'. As mentioned in Chapters 0, 7 and 8, in this work the effect of a number of salts and aqueous organic inhibitors on PVCap performance have been investigated, principally for s-I methane systems. K_2CO_3 has been found to be negative while NaCl has a generally positive effect, albeit it should be considered that at higher aqueous concentrations it causes polymer drop out. It has also been found that methanol has a generally negative and increasing its concentration in the aqueous phase reduces the subcooling extent of PVCap induced hydrate growth inhibition. In contrast, MEG was found to be an excellent synergist for PVCap, acting as both a 'top-up' inhibitor and improving efficiency by reducing hydrate growth rates. For a more comprehensive conclusion further investigation of these parameters (e.g. for MeOH, MEG, NaCl) in natural gas systems and comparison of data with methane systems can be very helpful. Moreover, examining mixed salt-organic inhibitor systems, e.g. examining whether the positive effect of salts can offset the negative effects of methanol on KHI performance, can be of great importance.

While the performance of one KHI may be enhanced in some heavy oil systems, the performance of the same inhibitors may be worsened in lighter condensate systems. Various studies have been carried out and explained in Chapter 0 on the effects of condensate/liquid hydrocarbons on KHI performance. Results showed that both condensate and the tested liquid hydrocarbon (n-heptane) have slightly negative effects. However, it is speculated that the effect of condensate can apparently vary greatly between different condensates. This could be due to changes of KHI solubility in the liquid hydrocarbon phase as a result of different fractions of long alkyl chains and aromatic components (e.g. toluene, o-xylene and benzene which is an aromatic and a hydrate former) and/or possibly due to the presence some hydrate forming compounds in the real condensate (e.g. iso-butane, iso-pentane). Hence, testing each of these compounds individually and comparing the results can give a good understanding of the effect of each component and a relatively good prediction of how a real condensate with a known composition will perform.

With the development of the new Crystal Growth Inhibition Technique, KHI performance and the effect of different parameters on their performance can be examined reliably with repeatable, consistent results gained. Hence with the application of the new method, KHI evaluation can be performed on many more different systems so that in addition to understanding the effect of different components, the method can yield in better interpretation of the actual mechanism of KHI inhibition and molecular behaviours.